The process of alite hydration:
Implications from quantitative phase analysis of Calcium-Silicate-Hydrate during hydration and from acceleration of the hydration reaction by mechanical activation

Der Ablauf der Hydratation von Alit:

Schlussfolgerungen aus der quantitativen Analyse von Calcium-Silikat-Hydraten während der Hydratation und der Reaktionsbeschleunigung durch mechanische Aktivierung

Der Naturwissenschaftlichen Fakultät

der Friedrich-Alexander-Universität

Erlangen-Nürnberg

zur

Erlangung des Doktorgrades Dr. rer. nat.

vorgelegt von

Sebastian Tobias Bergold

aus Erlangen

Als Dissertation genehmigt
von der Naturwissenschaftlichen Fakultät
der Friedrich-Alexander-Universität Erlangen-Nürnberg
Tag der mündlichen Prüfung: 22.04.2016

Vorsitzender des Promotionsorgans: Prof. Dr. Jörn Wilms

Gutachter/in: Prof. Dr. Jürgen Neubauer
Prof. Dr. Friedlinde Götz-Neunhoeffer

Danksagung

Ich danke Prof. Dr. Jürgen Neubauer für die Möglichkeit dieses spannende Thema im Rahmen einer Promotion zu bearbeiten. Seine Tür stand immer offen und die Diskussionen mit ihm bereicherten diese Arbeit sehr. Vielen Dank für die ausgezeichnete fachliche Betreuung.

Ebenso danke ich Prof. Dr. Friedlinde Götz-Neunhoeffer für die Unterstützung, Diskussionsbereitschaft und das Einbringen von anderen Sichtweisen und Aspekten in die Arbeit.

Ich bedanke mich bei Prof. Dr. Matthias Göbbels dafür, dass er mein Interesse an der Mineralogie geweckt und mir immer wieder neue Seiten dieses Faches gezeigt hat.

Dem Werkstattmeister der Mineralogie Bernd Schleifer möchte ich sehr herzlich danken. Er hatte für jedes technische Problem eine passende Lösung. Ohne seine freundschaftliche Unterstützung wären viele Experimente nicht möglich gewesen.

Dem Werksattmeister der Geologie Konrad Kunz möchte ich danken, da er für technische Probleme meist unkomplizierte und schnelle Lösung fand.

Ich danke den Sekretärinnen der Mineralogie, Bianca Klotsche und Jasmin Weiß, die mir viele Verwaltungstätigkeiten durch ihre tatkräftige Unterstützung erspart haben.

Kerstin Kress und Christian Abe möchte ich für ihre Unterstützung bei der Durchführung von Experimenten danken. Ebenso möchte ich allen Studenten danken, die mir durch ihre Tätigkeit als Hilfswissenschaftler den nötigen Freiraum für die experimentelle Arbeit geschaffen haben: Natalia Illenseer, Matthias Köhler, Anna Windmüller, Philipp Münkel, Markus Schedel, Aaron Roth und Stefan Seitz.

Ich dürfte im Laufe der Arbeit meinen Arbeitsplatz mit Dr. Sebastian Dittrich, Jörg Nehring, Florian Hüller und Kerstin Kress teilen. Ihn en gilt mein besonderer Dank für die gute, kollegiale Atmosphäre und freundliche Duldung der kreativen Ordnung meines Schreibtisches. Bastey, ich danke Dir für den Spitznamen Toni und eine gute Zeit.

Ich danke allen Mineralogen, die mich während dieser Arbeit freundschaftlich begleitet, mich durch fachliche Diskussionen unterstützt und mir Lust gemacht haben auf die Arbeit zu gehen: Dr. Sebastian Dittrich, Dr. Daniel Jansen, Dr. Sebastian Klaus, Dr. Sebastian Seufert, Dr. Andreas Richter, Christopher Stabler, Dominique Ectors, Christina Breunig, Jörg Nehring, Christoph Naber, Florian Hüller. Für besondere Momente sorgten immer wieder ausgedehnte Spieleabende, die Paddeltouren und ähnliche Aktivitäten.

Den Erlanger Homiez, meiner Schwarzen Auge Truppe, meiner Schwester Kathi, ihrer Frau Caro und meinen weiteren Freunden danke ich sehr.

Ich bedanke mich besonders bei Marion für die große Unterstützung und ihren Beistand während dieser Arbeit. Ihr und unserer Tochter Emma danke ich für die vielen schönen Momente.

Meinen Eltern Renate und Wolfgang danke ich für Ihre Unterstützung und insbesondere für die häufige und liebevolle Betreuung von Emma.

Abstract

In this thesis, the hydration of alite, mechanically activated alites, and reduced synthetic white Portland cements is examined in order to test existing theories of alite hydration.

A presented phase model allows the quantitative analysis of the poorly crystalline Calcium-Silicate-Hydrate (C-S-H) phases precipitating in cementitious pastes using in-situ XRD. The coherently scattering domain size of the XRD detectable "long-range ordered" C-S-H (C-S-H_{lro}) remains on a few nanometers during the early hydration. This demonstrates that C-S-H_{lro} precipitates in a continuous nucleation and aggregation process instead of nucleation and subsequent growth in crystallite size.

The alite hydration reaction can be described very well by the measured alite dissolution and the assumption of a synchronous dissolution and precipitation process. However, the start of the precipitation of XRD detectable C-S-H_{lro} is delayed in comparison to the dissolution of alite. Before C-S-H_{lro} precipitates, the formation of XRD amorphous C-S-H phases is indicated. The latter transform into C-S-H_{lro} during the further hydration. It is suggested that the precipitation of XRD amorphous C-S-H, which contains only monomeric silicate tetrahedra, is not able to accelerate the hydration reaction. The precipitation of a XRD amorphous C-S-H, which contains dimeric silicate tetrahedra, is able to slowly increase the hydration rate. However, higher hydration rates and the accelerated dissolution of alite are always related to the precipitation of C-S-H_{lro}. The acceleration of the main hydration period is driven by the enlargement of the reactive substrate surface area of C-S-H_{lro}. In low sulfated synthetic cements, the alite hydration reaction can be partially interrupted when AFm phases precipitate rapidly. The reactive surface of C-S-H_{lro} is partially blocked by precipitating AFm phases. Consequently, the alite hydration rate decelerates.

Mechanical activation of alite results in considerably accelerated and intensified hydration kinetics. The crystalline part of the alite powders exhibits small crystallite sizes and high lattice distortions. This leads to a complete reaction turnover within 24 h. The amorphous "alite" in activated alite powders obviously possesses a higher solubility than crystalline alite. Amorphous "alite" is able to dissolve considerably without the formation of C-S-H_{lro}. Instead, a significantly higher amount of XRD amorphous C-S-H is indicated in pastes of activated alites compared to pastes of pure crystalline alite. Amorphous "alite" reacts prior to crystalline alite during the initial or early acceleration period. The time of the dissolution depends on the concentration and reactivity of the amorphous "alite".

The diminution of small particles and the consequential decrease in alite surface is responsible for the transition into the deceleration period for mechanically activated alites. The mean coherently scattering domain size of the remaining crystalline alite increases during the acceleration period and decreases during the deceleration period. It is suggested that the reduction of alite surface is the trigger also for the start of the deceleration in non-activated alite pastes.

The reaction turnover up to the start of the deceleration period of the same alite sample strongly depends on the hydration kinetics. It is suggested that a higher undersaturation of the solution with respect to alite in the first hours of hydration can lead to a higher surface area of alite by opening of etch pits. This leads to an enlargement of the initial reactive alite surface resulting in a higher reaction turnover during the acceleration period. A higher reaction turnover can be detected when the highly reactive amorphous "alite" in activated alite is

passivated. Additionally, higher temperatures and the consecutive faster C-S-H precipitation increase the reaction turnover. The examination of synthetic cements demonstrates that the initial precipitation of very fine (nano-)ettringite should be the trigger for an enhanced precipitation of C-S-H and a higher reaction turnover in the synthetic cement pastes compared to pure alite pastes in spite of the usage of the same alite sample. Therefore, the initial precipitation of ettringite seems to be an intrinsic accelerator in Portland cements.

Zusammenfassung

In dieser Studie werden gängige Theorien zum Hydratationsprozess von Alit überprüft und erweitert. Hierfür wird die Hydratation von Alit, von mechanisch aktivierten Aliten und von reduzierten synthetischen Zementen, die weißen Portland Zement nachbilden, untersucht.

Schlecht kristalline Calcium-Silikat-Hydrate (C-S-H), die sich in zementären Pasten während der Hydratation bilden, können mithilfe eines erarbeiteten Modells mittels in-situ Röntgenbeugungsanalyse quantifiziert werden. Die kohärent streuenden Bereiche der röntgenographisch detektierbaren C-S-H Phasen („long-range-ordered" C-S-H, C-S-H_{lro}) sind (mindestens) innerhalb der ersten Tage der Hydratation nur wenige Nanometer groß. Das zeigt, dass die Fällung von C-S-H_{lro} in einem kontinuierlichen Keimbildungs- und Aggregationsprozess und nicht durch die Bildung von Keimen und einem darauf folgenden Kristallitwachstum von statten geht.

Die Hydratation von Alit kann sehr gut durch die gemessene Alitabnahme und die Annahme eines gleichzeitigen Lösungs- und Fällungsprozesses nachvollzogen werden. Jedoch findet die erste Bildung von röntgenographisch detektierbarem C-S-H_{lro} später statt als die beginnende Auflösung von Alit. Die durchgeführten Experimente weisen auf die Ausfällung von röntgenamorphen C-S-H Phasen vor der Bildung von C-S-H_{lro} hin. Die röntgenamorphen C-S-H Phasen wandeln sich im weiteren Verlauf der Hydratationsreaktion in C-S-H_{lro} um.

Die Ergebnisse dieser Studien zeigen, dass die Fällung von röntgenamorphem C-S-H, welches nur aus monomerischen Silikattetraedern besteht, die Hydratation nicht beschleunigen kann. Die Fällung von röntgenamorphem C-S-H, welches aus dimerischen Silikattetraedern besteht, ist dagegen in der Lage die Hydratationsgeschwindigkeit langsam zu erhöhen. Höhere Hydratationsgeschwindigkeiten und eine beschleunigte Alitauflösung sind eng mit der Bildung von C-S-H_{lro} verknüpft. Die Beschleunigung der Hauptperiode der Alithydratation wird durch die Vergrößerung der reaktiven Substratoberfläche von C-S-H_{lro} gesteuert. In synthetischen Zementen mit niedrigem Sulfatgehalt kann beobachtet werden, dass die Hydratation von Alit durch schnell ausfallende AFm Phasen gestört und in ihrer Geschwindigkeit deutlich reduziert werden kann. Dabei wird die reaktive Oberfläche von C-S-H_{lro} teilweise von den AFm Phasen blockiert und die Geschwindigkeit der Hydratation von Alit so verringert.

Die mechanische Aktivierung von Alit führt zu einer deutlich beschleunigten und intensivierten Hydratationskinetik. Der kristalline Anteil der aktivierten Proben besitzt kleine Kristallitgrößen und eine große Anzahl von Gitterstörungen. Dies führt zu einem kompletten Reaktionsumsatz innerhalb von 24 h. Der röntgenamorphe Anteil in den aktivierten Alitproben besitzt eine höhere Löslichkeit im Vergleich zu kristallinem Alit. Röntgenamorpher „Alit" kann in deutlicher Menge gelöst werden, ohne dass C-S-H_{lro} gebildet wird. Ein deutlich höherer Gehalt an röntgenamorphen C-S-H Phasen bildet sich stattdessen in Pasten aus aktivierten Aliten im Vergleich zu Pasten aus rein kristallinem Alit. Der röntgenamorphe „Alit" löst sich vor dem kristallinen Alit, und zwar entweder während der initialen Periode oder während der frühen Beschleunigungsperiode. Der Zeitpunkt der Auflösung hängt von der Konzentration und der Reaktivität des röntgenamorphen „Alits" ab.

Die komplette Auflösung der kleinen Alitpartikel und die daraus folgende Verkleinerung der reaktiven Alitoberfläche sind für den Übergang von der Beschleunigungsperiode zur Abklingperiode in Pasten aus mechanisch aktivierten Aliten verantwortlich. Die mittlere Größe der kohärent streuenden Bereiche von noch vorhandenem, kristallinem Alit vergrößert sich

während der Beschleunigungsperiode und verkleinert sich wieder während der Abklingperiode. Es ist plausibel, dass auch in Pasten aus nicht aktiviertem Alit die Verkleinerung der reaktiven Alitoberfläche der Verursacher der Abklingperiode ist.

Bei identischen Alitproben hängt der Reaktionsumsatz bis zur Abklingperiode stark von der Kinetik der Hydratation ab. Es ist wahrscheinlich, dass eine höhere Untersättigung der Lösung in Bezug auf Alit innerhalb der ersten Stunden der Hydratation zu einem vermehrten Öffnen von Ätzgruben und einer daraus resultierenden Vergrößerung der initialen, reaktiven Alitoberfläche führt. Diese Prozesse erhöhen den Reaktionsumsatz während der Beschleunigungsperiode. Ein höherer Reaktionsumsatz kann beobachtet werden, wenn der hochreaktive, röntgenamorphe „Alit“ in aktivierten Aliten passiviert wird. Außerdem verursachen höhere Temperaturen und die daraus folgende, schnellere C-S-H Bildung höhere Reaktionsumsätze. Die Untersuchung von synthetischen Zementen zeigt, dass die initiale Fällung von sehr feinem (Nano-)Ettringit die Ursache für eine vermehrte Bildung von C-S-H sein könnte. Außerdem ist sie wahrscheinlich für einen höheren Reaktionsumsatz von Alit in den synthetischen Zementpasten im Vergleich zu reinen Alitpasten verantwortlich. Die initiale Fällung von Ettringit in Portlandzementen scheint ein intrinsischer Beschleuniger für die Alithydratation zu sein.

Content

Danksagung i
Abstract ii
Zusammenfassung iv
Content vi
1. Introduction 1
2. Scope of the thesis 2
3. State of knowledge 4
3.1. The hydration process of alite 4
3.2. C-S-H in hydrating cementitious pastes 8
4. Main Results 9
4.1. Quantitative analysis of C-S-H in alite and other cementitious pastes 9
4.2. C-S-H_{lro} precipitation and crystalline alite dissolution 11
4.3. C-S-H_{lro} precipitation is a continuous nucleation and aggregation process 13
4.4. Analysis of portlandite by XRD is challenging 14
4.5. Implications from hydration of mechanically activated alite pastes 14
4.6. Interaction of silicate and aluminate reaction 18
5. Conclusions 22
6. References 23
7. Publications 30
7.1. The hydration of alite: a time-resolved quantitative X-ray diffraction approach using the G-factor method compared with heat release 30
7.2. In-situ XRD phase analysis of the early hydration of alite: time resolved quantification of the poorly crystalline C-S-H gel 38
7.3. Development of C-S-H during the early hydration of alite with water at different temperatures: direct quantification by in-situ XRD 46
7.4. Quantitative analysis of C-S-H in hydrating alite pastes by in-situ XRD 53
7.5. Mechanically activated alite: New insights into alite hydration 62
7.6. Influence of the reactivity of the amorphous part of mechanically activated alite on its hydration kinetics 73
7.7. Hydration at the edge: Changing the balance between silicate and aluminate reaction in a synthetic cement system 93
8. Appendix 129

1. Introduction

Concrete has developed to the most used building material worldwide, because the raw materials for Portland cement production are readily available, the production is of low cost, and the benefits of concrete construction for civil engineering are enormous. Between 2004 and 2014, the estimated world cement production nearly doubled from 2,130 [1] to 4,180 million metric tons [2]. The Chinese cement production increased by the factor 2.7 during this time period, while the German cement production remained constant (around 30 million metric tons) [1, 2].

With increasing specialization of the applications, concrete formulations have significantly become more complex. Nowadays, one or more organic admixtures are used in customized formulations combined with the inorganic cement phases, aggregates, and water [3]. In addition, the clinker content of the cements is reduced in order to decrease the CO_2 footprint of cements. Pulverized limestones and supplementary cementitious materials like ground granulated blast furnace slags, fly ashes, silica fumes, and in future likely steel mill slags and calcined clays as well are used for this purpose [4].

Modern Portland cements have been produced since the 19th century. In spite of their long-time use in construction and of decades of scientific research, the underlying kinetic mechanisms of the hydration are still not completely understood. In order to examine the principle hydration processes, it is essential to decrease the complexity of the hydrating mixture.

The hydration of pure Portland cement (without admixtures) basically consists of two different interacting reaction regimes: The silicate reaction and the aluminate reaction. C_3A, calcium sulfates, and water react to form ettringite or AFm phases in the aluminate reaction. This leads to the setting of the cement determining the open time and workability. The silicate reaction comprises of the dissolution of alite (monoclinic modification of Ca_3SiO_5, notation C_3S) and belite (β-Ca_2SiO_4, during later hydration stages) and the precipitation of crystalline portlandite ($Ca(OH)_2$) and nano-sized colloidal and poorly crystalline Calcium-Silicate-Hydrate phases (notation: C-S-H). The latter are mainly responsible for the strength development of the cementitious pastes. The balance between these two reactions is therefore of great importance for the application of a cement.

Especially the hydration process of the main clinker phase alite is still debated intensively. New experimental evidence and theoretical ideas have questioned existing theories about the alite hydration process, particularly in recent years (see section 3).

2. Scope of the thesis

The idea for this thesis originates from experiments with a reduced synthetic cement system, (comprising of a mixture of alite and C_3A in a ratio of 95:5) that followed on the thesis of Hesse [5]. The addition of a sufficiently low amount of calcium sulfate to the synthetic cement resulted in a significant interference of the sharp renewed aluminate reaction peak (Fig. 1, marked by arrow) with the silicate reaction. The silicate reaction considerably decelerated and reaccelerated from a lower hydration rate after the end of the aluminate reaction (Fig. 1). However, this interruption of the silicate reaction could not have been explained straightforwardly with the existing theories for alite hydration (section 3). Therefore, in this thesis, the process of alite hydration will be examined to test existing theories of the kinetic steps during the early alite reaction.

Heat flow calorimetry will be used to observe the sum of all chemical processes during hydration. Quantitative in-situ XRD proved to be the best method to determine the phase development of the crystalline phases in pastes over time [5-8]. During the early stage of this study, Jansen et al. showed that the use of the external standard method [9] is a promising method for the quantitative phase analysis of dry cements [10] as well as of cementitious pastes [11]. In a first step, the hydration of alite will be examined at different temperatures and water/alite ratios using this revised methodology.

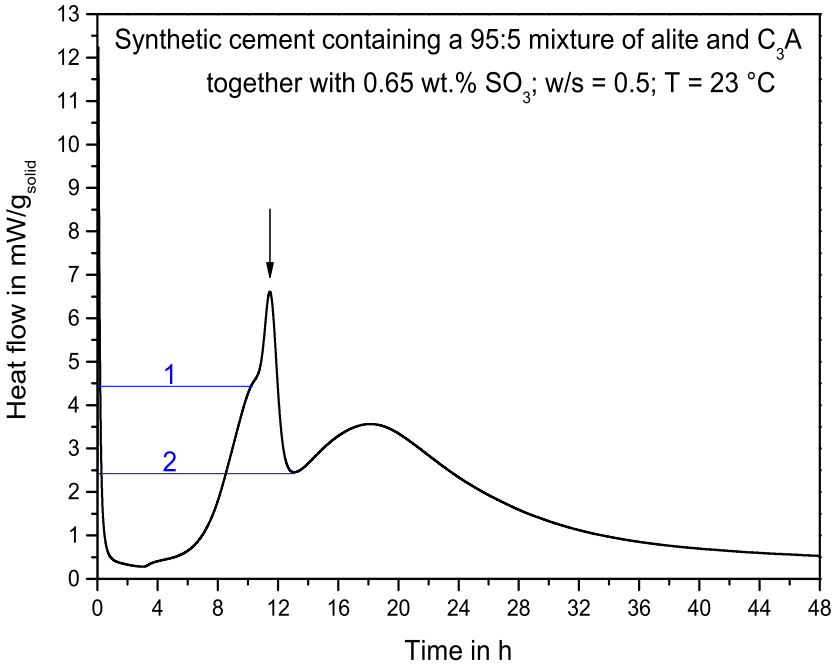

Fig.1: Released heat flow during hydration of an undersulfated synthetic cement. The silicate reaction is partially interrupted by a short intensive heat flow event of the aluminate reaction (marked by arrow) during the acceleration of the silicate reaction. Afterwards, the silicate reaction reaccelerates from a lower hydration rate (horizontal bar 2) than before the sharp heat flow event of the aluminate reaction (horizontal bar 1).

The quantitative analysis of alite pastes by XRD is challenging. The phase development of alite could be examined very well. On the other hand, the growth of portlandite impeded its quantitative analysis and XRD amorphous water and C-S-H could not be analyzed yet. C-S-H phases in hydrating pastes were described to be XRD amorphous or very poorly crystalline [12]. On the other hand, some structural proposals for C-S-H-like phases exist [13-18]. This leads to the question whether also the poorly crystalline C-S-H phases can be analyzed by quantitative in-situ XRD. If C-S-H phases can be analyzed by in-situ XRD, the phase development will be compared to alite dissolution. In this case, the alite hydration could be described as synchronous dissolution and precipitation process.

In a next step, the alite hydration will be enhanced by mechanically activation of alite powder. It has been shown before that mechanical activation of alite can lead to a decrease in alite crystallite size and to partial amorphous powders [19]. Odler & Schüppstuhl showed that the induction period was decreased for finer alite powders [20]. Bellmann et al. observed a high amount of an intermediate hydration product during hydration of a C_3S with very small particle sizes [21]. Therefore, the differences and similarities in the hydration kinetics of pastes of such activated alites and pure crystalline alite could enable a better insight into the processes occurring during the alite hydration.

After achieving a better understanding of the alite hydration with these steps, the interaction of the silicate and the aluminate reaction will be the subject of a detailed examination. The hydration of differently sulfated synthetic cement pastes - modelling white Portland cements - will be analyzed in order to explain the hydration behavior presented in Fig. 1.

3. State of knowledge

3.1. The hydration process of alite

In cement chemistry the term hydration includes all chemical processes taking place when an anhydrous cementitious material is mixed with water - forming a paste - and reacts with it to hydrate phases [22]. Alite is the monoclinic modification of tricalcium silicate (Ca_3SiO_5, in cement notation C_3S), which is stabilized at room temperature by incorporation of foreign ions into the crystal structure, mostly Al^{3+}, Mg^{2+} and Fe^{3+} [23]. In Ordinary Portland cements alite constitutes the main clinker phase (50-70 wt.% [24]), usually in form of the M3 and M1 modification [23].

Alite hydration does not proceed in one single reaction after the addition of water. It runs through a complex sequence of reactions. Alite hydration is usually separated by different stages (Fig. 2) appearing in the heat flow measured by calorimetry [25]. An initial period (Stage I) occurs after the contact of alite with water. After this short heat flow event, the heat flow declines followed by an induction period or period of slow reaction (Stage II). The main hydration period can be divided into the acceleration (III) and deceleration period (IV). After the main hydration, the alite reaction proceeds on low hydration rates for at least several weeks (Stage V).

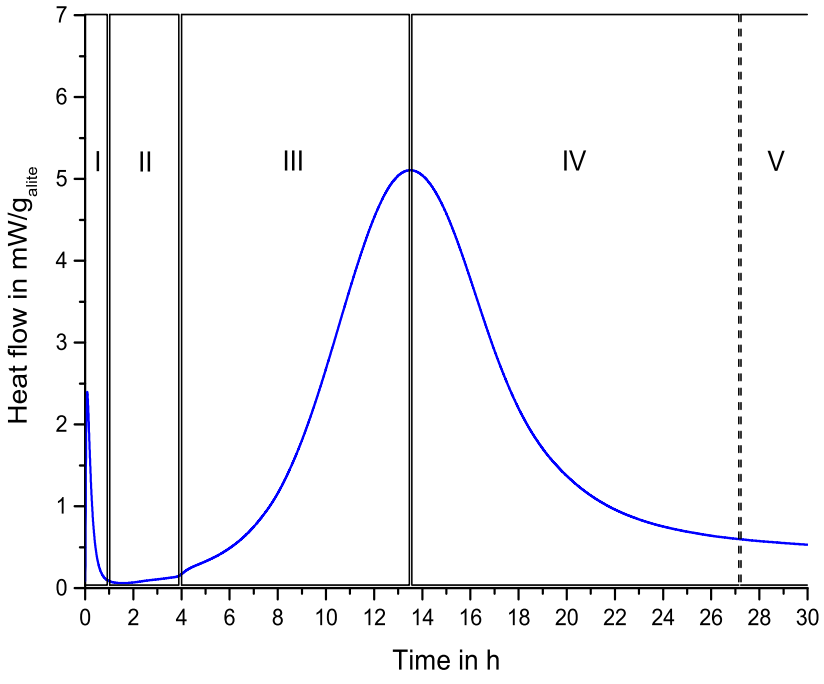

Fig. 2: Released heat flow during alite hydration at a water/solid ratio of 0.5 and 23 °C. The different stages of hydration are outlined. The transition from IV to V cannot be assigned to an exact point in time.

During the different hydration stages, alite reacts with water to produce C-S-H phases and portlandite by a dissolution and precipitation process following Equation 1:

$$Ca_3SiO_5 + (x+y)\ H_2O \rightarrow (CaO)_{(3-y)}(SiO_2)(H_2O)_x + y\ Ca(OH)_2;$$
$$\text{with } 1.5 < x < 4 \text{ and } 0.7 < y < 1.8 \text{ [26]} \quad (1)$$

3.1.1. The initial (I) and induction period (II)

For a long time, the most accepted theory for the appearance of an induction period during alite hydration has been the formation of a protective metastable barrier on alite surfaces after water contact [25, 27]. The protective layer was suggested to exist, because pore solution does by far not reach the theoretical solubility product of alite, as calculated from thermodynamic data [28], when the heat flow declines. According to the theory, the induction period complies the time necessary to destabilize the protective layer on alite surfaces. The protective character of the layer decreases as soon as a stable, less protective C-S-H precipitates [25, 27, 29, 30]. Other authors suggested that the protective layer would break due to osmotic pressure resulting from incongruent dissolution of alite and the differences between the silicate-rich grain surface and the calcium-rich solution [31].

A completely different theory implied that the induction period is not a separate hydration stage but represents a period of slow reaction, where nucleation and growth of C-S-H take place continuously [32, 33]. C-S-H nucleates during the first few minutes of hydration [32], as the silicon concentration in solution was found to decrease [34]. The growth of the initially nucleated C-S-H continuously increases the C-S-H reactive surface accelerating the hydration reaction [32, 33, 35].

Odler et al. suggested that a first hydrate forms directly after mixing, while simultaneously Ca^{2+} goes into solution [36]. This process could go on until the solution cannot take up more Ca^{2+} (for an unknown reason) followed by a slower hydration reaction [36]. The induction period would end when nuclei of the second hydrate reach a critical size [36].

In 2010, Juilland et al. suggested that the dissolution of alite proceeds at different mechanisms at different degrees of undersaturation [37], like it has been found for other minerals before [38]. They stated that etch pits form at the complete alite surface under highly undersaturated conditions and only on sites of crystallographic defects at moderately high undersaturations [37]. At lower undersaturations, step retreat on existing pits would be the only dissolution mechanism [37]. In 2013, Nicoleau et al. [39] experimentally proved that indeed the dissolution of alite strongly depends on the composition of the pore solution, showing a significantly lower dissolution rate in a less undersaturated solution. In addition, it was demonstrated that the dissolution of alite is congruent [39]. This was not unquestioned before due to the significant differences between Ca and Si in solution during hydration. Nicoleau & Nonat suggested that the difference between the theoretical solubility of alite and the experimentally observed one is related to protonation of the free oxygen in the alite structure, which is only bound to Ca and not to monomeric silicate tetrahedra [40].

However, the possible presence of a metastable protective layer was still not completely ruled out. Bellmann et al. [41] suggested that the hydration reaction in a paste still proceeds

more slowly than the alite could dissolve, based on dissolution experiments where C-S-H formation was excluded [41]. Indeed, there is experimental evidence suggesting the precipitation of an intermediate kind of C-S-H. Using ^{29}Si CP MAS NMR, Rodger et al. demonstrated that a hydrated monomeric silicate species precipitates during the induction period [42]. After the end of the induction period, dimeric silicate tetrahedra are formed. The amount of the dimeric silicate tetrahedra increased during further hydration, while the monomeric species related to hydrogen remained constant [42]. A high amount of a monomeric intermediate hydrate phase was described by Bellmann et al. [21] examining a C_3S with very small particle sizes. Bellmann et al. [43] reported the presence of a high amount of a hydrate phase different from C-S-H on alite surface using X-ray photoelectron spectroscopy. They suggested that this would support the theory of the formation of a protective layer on C_3S [43].

3.1.2. The acceleration period (III)

The start of the acceleration period (Stage III, Fig. 2) is usually considered to be the point in time when a hump in the heat flow can be detected (although the hump is not always observed). On the other hand, Fig. 2 shows that the hydration rate slowly increases also before that point in time.

Most of the existing theories suggest that the acceleration of the hydration reaction is caused by the nucleation and growth of C-S-H. In the case of a protective metastable barrier, the hydration accelerates due to the formation of a less protective C-S-H at the end of the induction period [25, 27]. In the case of the ongoing nucleation and growth mechanism, starting at the initial stage of hydration, nucleation and growth also govern the acceleration period [32, 33, 35].

Other authors suggested that the precipitation of portlandite leads to the acceleration of the alite hydration. Si in solution could poison portlandite nuclei and lead to the induction period due to the need of a high supersaturation degree with respect to portlandite for portlandite precipitation [44]. The high supersaturations in solution with respect to portlandite were observed in measurements of the solution composition up to the end of the induction period [34, 44, 45].

Nevertheless, Damidot et al. examined the hydration of C_3S in differently diluted CaO saturated suspensions, and found a dependency between the point in time when portlandite precipitated and the extent of dilution [46]. Depending on the time that was required to reach the maximum supersaturation with respect to portlandite due to the different dilutions, portlandite also precipitated in the middle of the main hydration period [46]. Therefore, portlandite precipitation was interpreted to be the consequence and not the cause of the acceleration period [46]. Furthermore, Odler & Dörr [36] showed that the addition of portlandite nuclei did not significantly shorten stage II.

However, Bullard & Flatt suggested that the rapid portlandite precipitation under already Ca saturated conditions affects the alite hydration and not the mere presence of portlandite in paste [47]. Kumar et al. assigned the bump between stage II and III (Fig. 2) to the precipitation of portlandite [48]. The portlandite precipitation would result in an exothermic reaction because it leads to a higher alite dissolution due to the increase of the undersaturation with respect to alite [48]. Portlandite precipitation itself was found to be endothermic [46].

Recently, Nicoleau & Bertolim mathematically showed that the acceleration of the alite hydration could also derive from a complex dissolution process of the alite surface [49]. The alite dissolution would accelerate due to an increasing reactive alite surface caused by the opening of etch pits [49].

3.1.3. The transition from acceleration (III) to deceleration period (IV)

There is also no consensus about the cause of the deceleration of the alite hydration. Garrault & Nonat suggested that C-S-H would grow at different rates perpendicular and parallel to the alite surface [32, 50]. The alite surfaces would be covered by a layer of C-S-H of sufficient thickness resulting in a diffusion-controlled hydration regime when the reaction approaches stage IV. This consequently decreases the hydration rate [32, 50]. It was argued that a diffusion controlled reaction regime governs the reaction after the transition from stage III to IV, as a change in the apparent activation energies was found in the literature from the acceleration period to the post acceleration periods [29]. However, Thomas [51] determined instantaneous apparent activation energies using a revised methodology. The determined values up to a reaction turnover of 65 % were found to be constant and assumed to be too high to represent diffusion-controlled reaction kinetics [51]. The simulations of Bullard et al. [52] indicated that the product layer on C_3S should remain permeable without the need of diffusion controlled kinetics.

Bishnoi & Scrivener simulated the main hydration period and found that for a proper fit of the deceleration period, a loosely-packed C-S-H needs to form first, which densifies afterwards [53]. After filling the available pore space, the impingement of the loosely packed C-S-H would lead to the deceleration of the alite hydration [53]. Kirby and Biernacki [54] stated that this two-step precipitation process needed revision. In the present set up, it could not explain why the alite hydration is not significantly affected by the water/cement ratio [54]. With more available space due to a higher water/cement ratio the reaction turnover in the simulation significantly increased [54]. Masoero et al. [55] suggested a reaction zone around C_3S particles to explain the effect of water/cement ratio and particle size distribution on C_3S hydration. The initial C-S-H would grow outwards until a specific distance to the grain is reached (extent of the reaction zone). This was found to coincidence with the tangential impingement of C-S-H on the alite grains [55]. Subsequently, the remaining space in the reaction zone would be filled and the outward growth stopped, which could be caused by a diffusion-controlled regime [55]. Bazzoni suggested that C-S-H grows in form of needles away from the alite surface [56]. More and more needles would grow away from the grain until the surface of alite is completely covered by needles at the maximum of the main hydration period [56]. Subsequently, the longitudinal growth of the needles would slow down and an inner product would begin to form [56].

Garrault et al. suggested that the deceleration would be caused by the decrease of the alite dissolution rate. The diminution of both, dissolution flows and dissolving surface area, could explain the deceleration of the hydration without the need to account for available space for C-S-H precipitation [57]. Nicoleau & Nonat [58, 59] compiled data sets of pore solution compositions from the literature and showed that the undersaturation with respect to alite increases after the maximum of the main hydration period. Therefore, not the C-S-H precipitation should be the rate-limiting factor in stage IV, as the ion concentration in solution decreases although the reaction rate decreases too [58, 59]. Bullard et al. [52] stated that the

solution is supersaturated with respect to C-S-H and undersaturated with respect to C_3S during the complete reaction. Therefore, they suggested that not a single process but the combination of both, alite dissolution and C-S-H precipitation influences the hydration process during the main hydration period [52]. The dissolvable alite surface would be reduced by the precipitated C-S-H which should lead to a decrease in available material for further acceleration and in consequence to the deceleration of the hydration reaction [52].

3.2. C-S-H in hydrating cementitious pastes

The notation C-S-H indicates, that the chemical composition as well as the structure of C-S-H are not fixed during hydration but evolve during the hydration progress. Until the end of the induction period, the Ca/Si ratio possibly follows a thermodynamic path, where the Ca/Si ratio continuously increases for higher Ca concentrations in solution [37]. Subsequently, at ambient temperatures and water/cement ratios around 0.5, a mean Ca/Si ratio of 1.7 was often reported during the early hydration of alite and of neat Portland cements [60-62].

The Ca/Si ratio of C-S-H generally depends on the composition of the pore solution [63, 64]. Furthermore, the Ca/Si ratio of C-S-H is affected by the temperature (lower with higher temperature) [65], the water/cement ratio (higher with lower amounts of water) [66], and the composition of the cement used [26]. The mean length of silicate chains in C-S-H was reported to shorten with a higher CaO concentration in solution [12, 63, 68]. The structure of C-S-H changes due to polymerization of silicate tetrahedra. The tetrahedra chain length is bound to the sequence m = 3n – 1 (with n = 1, 2, …) [12, 67]. This means that two dimeric silicate tetrahedra and a monomeric one can merge to a pentameric silicate tetrahedra chain and so on.

It was proposed that C-S-H shows structural similarities with the minerals tobermorite ($Ca_5Si_6O_{16}(OH)_2.4H_2O$) and jennite ($Ca_9Si_6O_{18}(OH)_6.8H_2O$) [69]. However, C-S-H was found to possess a significantly higher atomic packing density than tobermorite or jennite [76]. This was attributed to the highly defective atomic structure of C-S-H with relatively short silicate tetrahedra chains, and to a nano-solid densification effect (near the surface, bonds with lower coordination number contract) caused by the nano-particulate structure of C-S-H [76]. Taylor suggested that a mixture of imperfect 14 Å tobermorite layers and imperfect jennite layers with omission of many of the silicate tetrahedra could explain C-S-H from C_3S hydration [12]. Richardson & Groves suggested a model for C-S-H arriving from a mixture of tobermorite with jennite and tobermorite with calcium hydroxide [70, 71]. Richardson developed several structural models for different silicate tetrahedra chain lengths [72]. He stated that a crystal-chemical consisting model should be based on a 14 Å clinotobermorite (not found in nature) [72]. He also stated that synthetic preparations of C-S-H with Ca/Si ratios > 1.4 would contain an intermixed Ca-rich phase [72]. Modelling $C_{1.67}SH_x$ starting from a 11 Å tobermorite, Kovacevic et al. found that the model containing only dimeric and pentameric silicate tetrahedra (and no monomeric ones) was the energetically most stable model with the highest density and the closest one to experimental data [73].

C-S-H precipitating in cement hydration was described to be very poorly crystalline [12]. And C-S-H was found to remain poorly crystalline for decades after an almost complete reaction turnover [74, 75].

4. Main Results

The results of this thesis are presented in seven scientific publications. This section provides a short overview of the three peer reviewed, the two submitted, and the two conference papers. The following sections present the main results of this thesis.

In the first publication (section 7.1), the external standard method is used to analyze the phase development of alite and portlandite in hydrating alite pastes by in-situ XRD analysis. The phase development of alite is compared with the heat flow measured by calorimetry at different w/s ratios and temperatures.

The two conference papers and one of the peer reviewed papers deal with the quantitative analysis of the poorly crystalline C-S-H by in-situ XRD. In sections 7.2 and 7.3 the analysis of C-S-H is performed using the scale factor method. It is demonstrated how C-S-H contributes to XRD patterns of alite pastes (section 7.2) and how the phase development of C-S-H proceeds at different temperatures (section 7.3). The final development of the phase model for the quantitative analysis of C-S-H in cementitious pastes using XRD is presented in section 7.4. Here, the external standard method [9-11] is applied in combination with the PONKCS method [77] and an advanced modelling of the background of in-situ diffractograms. In addition, the phase development of the analyzed C-S-H during alite hydration is discussed.

In a next step, the developed C-S-H model is used to characterize the hydration mechanisms of mechanically activated alite pastes (section 7.5). Due to the significant enhancement of the hydration, a unique view on the kinetics of alite hydration is possible. Subsequently, one mechanically activated alite sample is analyzed, which underwent different drying procedures after the wet (ethanol) grinding process (section 7.6). The reactivity of the different samples is significantly altered by the drying method, giving additional information about alite hydration.

Finally, the hydration kinetics and phase developments in synthetic white Portland cement pastes containing low calcium sulfate contents are analyzed (section 7.7). It can be shown that the silicate and aluminate reaction strongly interact with each other during the entire hydration process. The impact of the aluminate reaction on alite hydration is discussed.

4.1. Quantitative analysis of C-S-H in alite and other cementitious pastes

The use of existing structural proposals of tobermorites (9 Å [17], 11 Å [13, 16, 18, and 15 (Clinotobermorite)], or 14 Å [14]) for the quantitative analysis of C-S-H in pastes did not result in satisfactory fits of in-situ diffractograms of alite pastes. Only a significant variation of the lattice parameters in combination with the application of a strong preferred orientation could account for the main C-S-H reflections. The refinement of those structures to examine the phase development of C-S-H in a paste is not promising.

Therefore, a Pawley fit or "hkl" phase model is developed for the poorly crystalline C-S-H phases, which precipitate during alite hydration. The space group (F2dd) and lattice parameters of a 14 Å tobermorite [15] were used as a basis. The alite hydration has been accelerated by mechanical activation (section 7.5). In pastes of activated alites only portlandite, C-S-H phases, and water contribute to the diffractogram after 24 h (Fig. 3). To allocate the contribution of C-S-H to the diffractogram, it is necessary to model the background of the diffracto-

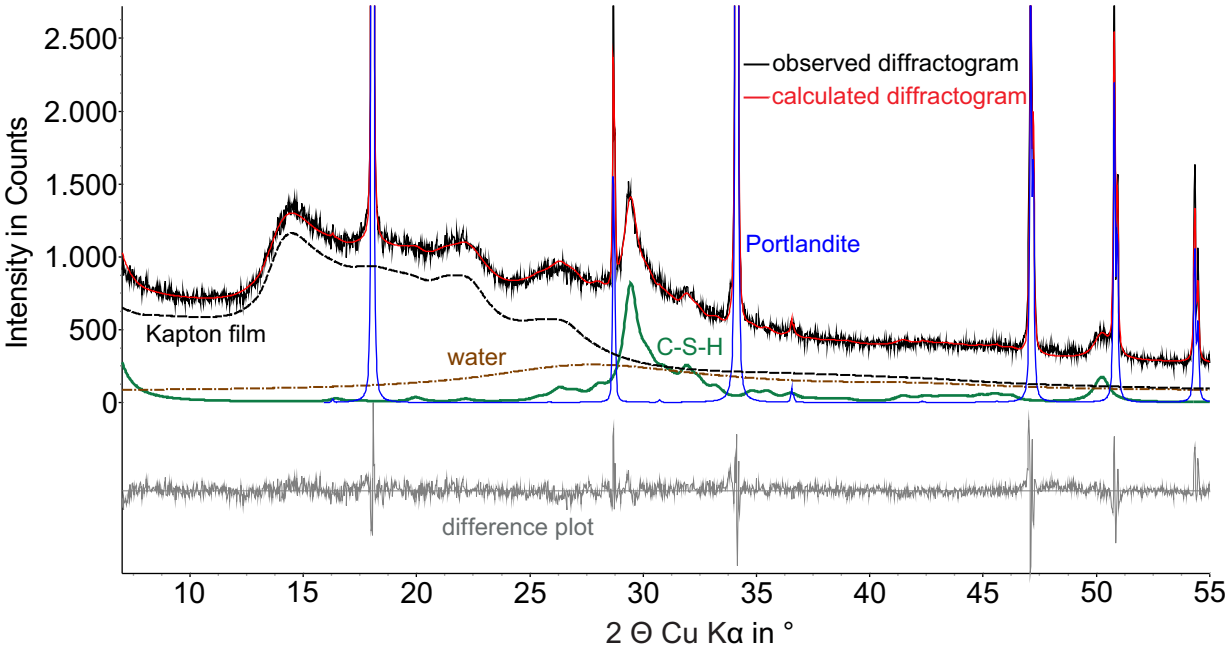

Fig. 3: Rietveld refinement of activated alite paste after 24 h of hydration at w/s = 1 and T = 23 °C. Alite is dissolved completely, while "long-range ordered" C–S–H, portlandite, and the remaining free water can be detected. The background is fitted with "hkl"-phases for free water and Kapton polyimide film, and with a Chebyshev polynomial of 1st order.

gram carefully (Kapton® polyimide film covering the sample and unbound water; section 7.5).

Scarlett & Madsen described a method to analyze phases with "partial or no known crystal structure" (PONKCS method) [77]. This PONKCS method is adapted for its use in combination with the external standard method [9-11] instead of the ZMV-algorithm [78]. The volume of the unit cell and the phase density of the C-S-H phase model are calibrated via calculation of the expected C-S-H phase content after 22 h of hydration (Equation 2) for more than 10 different alite pastes (section 7.4). The phase development of C-S-H can be monitored quantitatively over time with the resulting C-S-H phase model, although no crystallographic statement about the structure of C-S-H can be given.

$$Ca_3SiO_5 + 3.9\ H_2O \rightarrow (CaO)_{1.7}(SiO_2)(H_2O)_{2.6} + 1.3\ Ca(OH)_2 \qquad (2)$$

The fit of the Rietveld refinements were significantly improved with incorporation of the C-S-H phase model compared to the refinements without the model (section 7.2). Section 4.4 discusses in more detail that not the total C-S-H can be analyzed by this phase model. XRD amorphous C-S-H very likely precipitates before the precipitation of XRD detectable C-S-H. Therefore, the C-S-H analyzed by the phase model is termed "long-range ordered" C-S-H (C-S-H_{lro}) in the following sections.

The quantitative analysis of C-S-H_{lro} is independent from alite dissolution for further examined pastes when the external standard method is applied. This is the main advantage over

the scale factor method (sections 7.2 and 7.3), where the C-S-H_{lro} scale factor has to be scaled to wt.% for each single experiment. There might be a systematic shift to the true phase content of C-S-H_{lro}, if the assumption of Equation 2 would not be correct. Nevertheless, the course of the phase development of C-S-H_{lro} is not affected by a possible systematic shift to higher or lower true phase contents. The shift would be the same for all experiments.

The resulting C-S-H_{lro} phase (section 7.4) and the described calibration can be used to calculate the phase content of C-S-H in every cementitious paste. A minimum value of 7° 2Θ for the start of the refinement of the XRD data set has to be maintained. Additionally, it is decisive to account for effects on the background of the diffractogram (like amorphous phases, free water, or Kapton film) in order to obtain a significant quantitative result.

In addition to the experiments of this thesis (sections 7.2-7.7), the C-S-H_{lro} phase model has already been used successfully in cement pastes containing fly ash [79, 80]. The method works, although the Ca/Si ratio of such pastes was found to be lower than 1.7 - at least on longer time scales (e.g. after 28 d [62]).

4.2. C-S-H_{lro} precipitation and crystalline alite dissolution

The heat flow calculated from measured alite dissolution by in-situ XRD accords to a great extent with the measured heat flow in calorimetric experiments (section 7.1 and 7.4). This leads to the conclusion that the heat released during alite hydration can be described by considering the alite dissolution solely. This substantiates that the alite hydration indeed proceeds in a synchronous solution and precipitation process according to Equation 2. The heat release during hydration of alite (at 23 °C and w/s = 1, section 7.5) indicates a dissolution of 0.5 ± 0.2 wt.% alite during the first 1.5 h.

However, precipitation of C-S-H_{lro} starts significantly later than the dissolution of crystalline alite or the precipitation of portlandite can be observed (sections 7.2-7.7). This proves that the hydration process is far more complicated (section 7.4). Fig. 4 compares the heat flow measured by calorimetry with the dissolution rate of alite and the precipitation rate of C-S-H_{lro} calculated from the phase development measured by in-situ XRD. After the first precipitation of C-S-H_{lro} (marked by the blue star in Fig. 4), the precipitation rate of C-S-H_{lro} accelerates faster than the dissolution rate of alite. The precipitation rate of C-S-H_{lro} exceeds the dissolution rate of alite and shows a higher rate maximum. During the deceleration period, the rates of both precipitation of C-S-H_{lro} and dissolution of alite merge and proceed according to the measured heat flow (section 7.4).

C-S-H_{lro} precipitation is connected to the time when crystalline alite dissolution starts to accelerate in all analyzed pastes (sections 7.2-7.7). Measurements of the solution composition have shown that some kind of Calcium-Silicate-Hydrate precipitates during the first minutes of alite hydration, as the Si concentration in solution increases at first and decreases again within the first minutes [32, 34, 44, 81]. In addition, the Si concentration in solution is in the order of some µmol/l in comparison to some mmol/l for Ca [34, 44, 81]. This leads to the conclusion that XRD amorphous C-S-H phases precipitate before C-S-H_{lro} (shown in Fig. 4).

The precipitation of XRD amorphous C-S-H follows the dissolution of alite until C-S-H_{lro} precipitates. Thereafter, the precipitation rates of XRD amorphous C-S-H decrease. XRD amorphous C-S-H dissolves again, very likely by transformation to C-S-H_{lro}, as the latter shows an

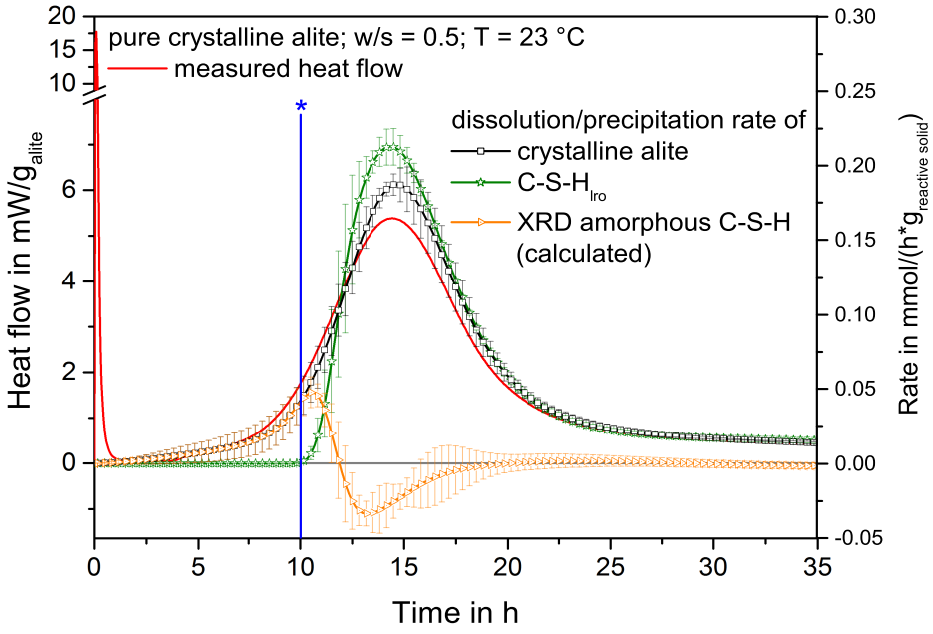

Fig. 4: The heat flow measured by calorimetry, compared with the alite dissolution rate, the precipitation rate of C-S-H$_{lro}$, and the expected rate of XRD amorphous C-S-H (calculated from Equation 2 and the alite dissolution) in hydrating alite paste at w/s =0.5 and T = 23° C. The blue star marks the point in time after which C-S-H$_{lro}$ precipitates.

enhanced accelerated precipitation rate in comparison to the dissolution rate of alite. The maximum phase content of XRD amorphous C-S-H phases in paste is reached very soon after the first precipitation of C-S-H$_{lro}$ (section 7.4). Within the error of analysis, the expected C-S-H$_{lro}$ phase content (according to Equation 2) can be found in crystalline alite (section 7.4) and synthetic cement pastes (section 7.7) after the end of the main hydration period. C-S-H$_{lro}$ is therefore the metastable product during the early alite hydration, which precipitates in the further hydration process together with portlandite (Equation 2).

By ^{29}Si CP MAS NMR the first dimeric silicate tetrahedra in paste could be found at the start of the acceleration period during C_3S hydration [42]. The lasting presence of a monomeric silicate species associated with hydrogen during the early hydration [42] was interpreted to show that a two-step precipitation would always be required for C-S-H formation [43]: the first step is the formation of an intermediate phase and the second step is the evolution into dimeric C-S-H. Recently, it has been shown that the amount of monomeric silicon tetrahedra associated with hydrogen is related to the alite surface [82]. Therefore, the results of Pustovgar et al. [82] support the view that C-S-H$_{lro}$ probably consists of an at least dimeric silicate species. Mohan & Taylor found C-S-H to consist of dimeric silicate species between 3-7 d of hydration, while later polymers occurred in addition to the dimers [74]. When alite was completely dissolved, the dimers decreased under formation of polymers [74].

The precipitation of a kind of C-S-H that is able to accelerate the hydration reaction obviously takes time. This might be explained with the need of a high Ca concentration in solution to enable the precipitation of a C-S-H with a high Ca/Si ratio [61]. Since the alite dissolution rate

was shown to be significantly decreased with higher Ca concentrations in solution [37, 39, 83], the reaction proceeds very slowly until the required kind of hydrate precipitates.

The proposed hydration mechanism is very close to the one proposed by Odler & Dörr [36]. The precipitation of a dimeric kind of C-S-H should be able to slowly accelerate the silicate reaction [42]. However, the significantly accelerated dissolution of alite is associated with the precipitation of C-S-H_{lro}. This questions existing numerical models for alite hydration that start with a specific number of C-S-H nuclei being present very soon after mixing, which subsequently grow [32, 33, 84]. First of all, C-S-H precipitation will also proceed as a function of supersaturation [52]. Additionally, the kind of C-S-H precipitating has to be considered.

It remains an open question how long C-S-H_{lro} is the metastable product during alite hydration. Apart from slightly varying coherently scattering domain sizes, the patterns of C-S-H_{lro} was the same for activated and not activated alite pastes (compare 7.5 and 7.4), although the hydration was completed within 24 h in activated alite pastes. It remains unsolved how significant the XRD pattern of C-S-H would change in a hydrating paste when the ordering of silicate tetrahedra changes from purely dimeric to a combination of dimeric and pentameric tetrahedra chains. Kovacevic et al. suggested that a model containing dimeric and pentameric silicate tetrahedra reproduced experimental results the best [73].

4.3. C-S-H_{lro} precipitation is a continuous nucleation and aggregation process

The mean coherently scattering domain (CSD) size of C-S-H_{lro} does not evolve but remains at very small dimensions throughout the hydration reaction. For alite and synthetic cement pastes, the CSD size of C-S-H_{lro} was slightly lower (5.5-6.5 nm (Vol-IB); section 7.4 and 5.6 ± 0.7 nm (Vol-IB); section 7.7, respectively) than for the activated alite pastes (8 ± 1 nm (Vol-IB); section 7.5). Intermediate CSD sizes were found in the differently dried activated alite pastes (5.6-7.7 nm (Vol-IB); section 7.6). The slightly larger CSD size for C-S-H_{lro} in activated alite pastes probably is related to a higher supersaturation in the activated alite pastes resulting from the dissolution of amorphous “alite”. This is indicated by the high amounts of XRD amorphous C-S-H phases that have been precipitated in the activated alite pastes (section 7.6).

The very small dimensions of C-S-H particles has been observed by various techniques before. It was shown with atomic force microscopy that C-S-H precipitation proceeds as aggregation of elements of 60 x 30 x 5 nm or 60 x 50 x 5 nm on flat alite surfaces [85]. Richardson stated from transmission electron microscopic images that the inner product C-S-H appeared to be composed of small globular particles of 4-8 nm at 20° C, whereas the outer product C-S-H exhibited fibrils with a smallest size of 3 nm and a length of a few up to many tens of nanometers [71]. Jennings proposed that non-spherical C-S-H “globules” with an internal sheet like structure would form and assemble in statistically well-defined patterns of two different packing densities (colloid model) [86]. Jennings et al. considered the size of those “globules” to be about 5 nm using small angle neutron scattering experiments [87]. Allen et al. [88] earlier confirmed that value using the same technique. The mechanical behavior of C-S-H as measured by nano-indentation tests showed that C-S-H could indeed be described as a nano-sized granular material with two limited packing densities [89].

Different measurement techniques result in comparable very small sizes for C-S-H crystallites and particles. Assuming a tobermorite-like structure for C-S-H_{lro}, 5 nm corresponds to

two unit cells [90]. This leads to the conclusion that C-S-H_{lro} precipitation proceeds as a continuous heterogeneous nucleation process of very small crystallites, rather than a nucleation and subsequent growth in crystallite size, like it appears for portlandite. The preferred substrate for heterogeneous nucleation of C-S-H_{lro} seems to be the surface of earlier precipitated C-S-H_{lro}.

4.4. Analysis of portlandite by XRD is challenging

The quantitative analysis of portlandite by in-situ XRD is challenging, as shown in section 7.3. A 2-dimensional XRD pattern reveals that portlandite precipitates in form of a few big crystallites. Portlandite clusters could also be observed in backscattered electron images [91]. The required statistical information for analysis of a crystalline phase by powder XRD technique is thus not provided for portlandite. Instead spottiness is observed due to the presence of few big crystallites. In the Rietveld analysis this spottiness can only be computed with a preferred orientation model in order to fit the diffractograms properly. Therefore, portlandite quantities are downscaled in addition to the missing statistical information. This leads to a significant under-determination of portlandite in crystalline alite pastes (sections 7.1, 7.2, 7.3, 7.4, 7.7). In the case of mechanically activated alites, the supersaturation in solution for portlandite is probably very high. Portlandite precipitates in significant amounts during the initial stage of the hydration (section 7.5). This might lead to a higher amount of portlandite nuclei, which subsequently grow during the further hydration process. This leads to an improved statistical information in the diffractograms and thereby to a more realistic portlandite content in paste. However, portlandite still exhibits considerable spottiness in the pastes of the differently dried activated alites (section 7.6).

4.5. Implications from hydration of mechanically activated alite pastes

4.5.1. Initial to acceleration period

The intensive mechanical activation of alite results in partially amorphous alite powders with a large BET surface area (sections 7.5 and 7.6). The remaining alite crystallites exhibit very small coherently scattering domain sizes and high lattice distortions. The activated alite powders show a significantly enhanced hydration behavior with a complete reaction turnover within 24 h.

Fig. 5 compares the heat flow measured by calorimetry and the dissolution/precipitation rates of crystalline alite, C-S-H_{lro}, and portlandite, and the theoretically calculated rates for total C-S-H and XRD amorphous C-S-H. The main hydration period matches with the crystalline alite dissolution. The gap between the theoretically calculated total C-S-H precipitation rates and the rates of crystalline alite dissolution can only be explained by dissolution of amorphous “alite” combined with precipitation of XRD amorphous C-S-H phases. The amorphous parts of the alite powders thus react before the crystalline alites, either during the initial period or during the early acceleration period, depending on the activation intensity (section 7.5) and the reactivity of the amorphous “alite” (Fig. 5 and section 7.6). The initial and main hydration period merged with a high amount of highly reactive amorphous “alite”.

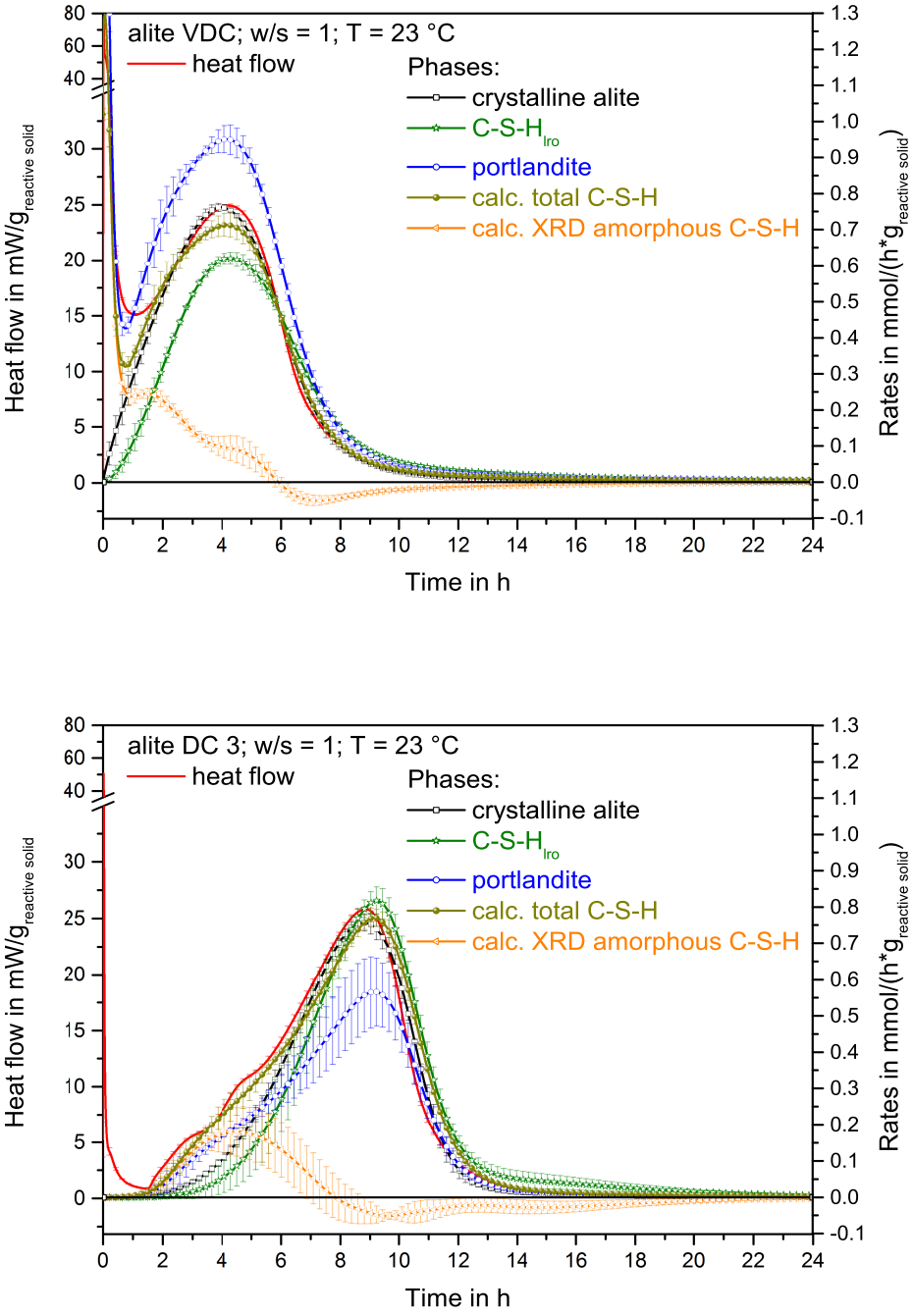

Fig. 5: Comparison of heat flow measured by calorimetry and dissolution/precipitation rates calculated from quantitative in-situ XRD analysis during hydration of alite pastes VDC (top) and DC 3 (bottom). The total C-S-H rates are calculated by scaling the portlandite content to the theoretically expected amount (Equation 2). For the content of XRD amorphous C-S-H phases, the measured C-S-H$_{lro}$ content is subtracted from the total C-S-H content (section 7.6).

The amount of XRD amorphous C-S-H phases is significantly higher in activated alite pastes than in pure crystalline alite pastes. Alike in the pure crystalline alite pastes (sections 7.2-7.4 and 7.7), the XRD detectable C-S-H_{lro} can always be detected when the crystalline alite dissolution accelerates during hydration of the activated alite powders (sections 7.5 and 7.6). Even during hydration of the highest activated alite (section 7.5), where initial and main hydration period merged, a considerable amount of XRD amorphous C-S-H is indicated. The amount of XRD amorphous C-S-H decreases for slower hydration kinetics in the case of passivation of the amorphous "alite" (section 7.6). Summarizing this, a protective effect of this XRD amorphous C-S-H is not indicated. The widespread theory of a metastable protective layer on the alite surface [25, 27-29, 31] as explanation for the presence of the induction period thus becomes implausible.

It has been shown that alite dissolution proceeds more slowly at lower undersaturations with respect to alite [37, 39, 83]. Nicoleau & Nonat [58, 59] suggested that the dissolution of alite would also be the rate-limiting factor during the acceleration period due to a complex dissolution mechanism [49]. On the one hand, this seems to be plausible as the reaction takes place faster, the more intensive the mechanically activation of alites had been and the less crystalline alite dissolution could limit the hydration process (section 7.5). On the other hand, Fig. 6 shows that the maximum dissolution rates of crystalline alite are comparable for all activated alites, although the mean CSD size and the lattice distortion of those crystalline alites are extremely different (section 7.5). It is more likely that another factor is rate-limiting during the acceleration stage than the crystalline alite dissolution.

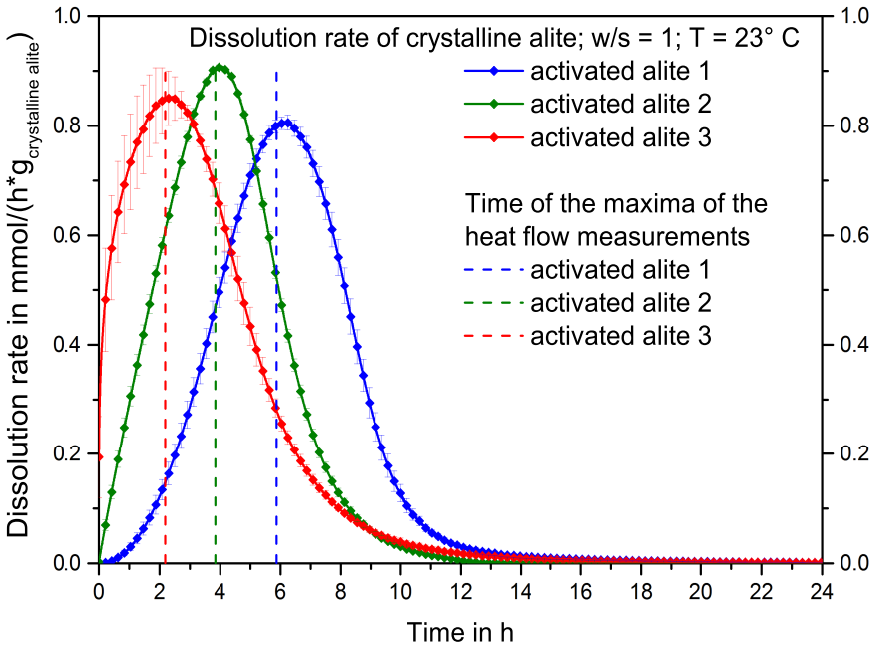

Fig. 6: Dissolution rate of crystalline alite during hydration of differently intensive activated alite powders (activation intensity 1 < 2 < 3), as determined by quantitative in-situ XRD (section 7.5). The dashed lines show the time of the heat flow maximum during the main hydration period measured by calorimetry.

The first precipitation of C-S-H_{lro} can always be detected at the same point in time: during the accelerating dissolution of crystalline alite (sections 7.2-7.7). Therefore, the evolution of C-S-H with the intermediately final transformation to C-S-H_{lro} probably enables the acceleration of the hydration reaction.

4.5.2. Transition to the deceleration period

In the activated alite pastes, the cause of the transition from acceleration to deceleration period is clearly indicated. The mean coherently scattering domain (CSD) size of crystalline alite increases during the acceleration period and decreases during the deceleration period with a maximum value close to the rate maximum of the main hydration reaction (Fig. 7, sections 7.5 and 7.6). Therefore, the small alite crystallites dissolve during the acceleration period. The small alite crystallites are probably closely related to the small alite particles in the case of the activated alites. At the rate maximum, only the large crystallites remain and in consequence the available alite surface is significantly reduced. The dissolution of alite is thus the rate-limiting factor during the deceleration period.

The crystalline alite parts of the activated alites (shown in Fig. 7) have CSD sizes between 40 and 100 nm, while the one of non-activated pure crystalline alite is 2600 nm (section 7.5). The significance of the CSD size decreases considerably for larger crystallite sizes. Therefore, the information of the development of the CSD size during the hydration of pure crystalline alite cannot be resolved. However, it is not implausible that the alite dissolution is rate-limiting during the deceleration period also for pure crystalline alite. It was spotted by Nicoleau & Nonat [58, 59] and also by Bullard et al. [52] that the supersaturation in solution with respect to C-S-H decreases and the undersaturation with respect to alite increases after the rate maximum, although the hydration rate decreases. Based on the results from the activated alites, it seems plausible that this is related to the diminution of small alite particles and the consecutive decrease in available alite surface for dissolution.

The reaction turnover up to the transition from acceleration to deceleration period is not the same at different reaction kinetics in spite of the use of a comparable crystalline alite material. The activated alites show a slower reaction process when the amorphous “alite” is passivated. The slower reaction process leads to a higher reaction turnover during the acceleration period (section 7.6). For non-activated alites, changes in the reaction kinetics due to temperature variations (sections 7.1 and 7.3), the addition of seeding materials [81, 92-94] or the presence of an aluminate reaction (section 7.7, [95, 96]) lead to a higher reaction turnover of the same alite during the acceleration period.

Sobolkina et al. suggested a mechanism to explain the higher reaction turnover [81]. The opening of etch pits is related to high degrees of undersaturation with respect to alite [37, 39]. The presence of a material that is able to lower the Ca content in solution during the initial period would increase the extent of opened etch pits during this initial stage [81]. The reactive surface area of alite and the reaction turnover during the main hydration period would consequently increase [81].

In the case of the activated alites, the dissolution of amorphous “alite” probably leads to a very high supersaturation with respect to C-S-H. Due to the resulting high nucleation pressure, a high amount of XRD amorphous C-S-H precipitates before C-S-H_{lro} evolves. Opening of etch pits on the surface of crystalline alite cannot take place, or at least the extent of etch pit

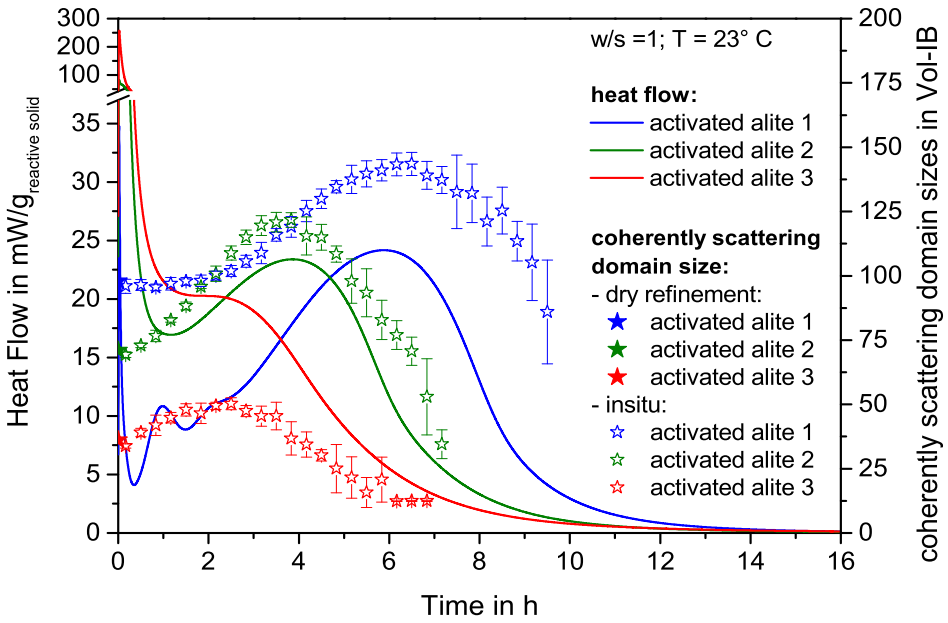

Fig. 7: Comparison between the measured heat flow and the development of CSD sizes of crystalline alite during hydration given as Vol-IB in nm. Filled stars at time zero represent the CSD sizes determined in the dry refinement.

opening will be much lower than for the case of a passivation of the amorphous "alite" (section 7.6). When the amorphous "alite" is not able to dissolve that fast, opening of etch pits on crystalline alite could lead to a higher reactive surface area of the crystalline alites. This could lead to the complete dissolution of also medium sized particles before the hydration enters the transition to the deceleration period. In section 7.6 it is shown that the reaction turnover and the mean CSD size of remaining crystalline alite slightly increases for slower hydration kinetics.

In the case of an increasing reaction turnover for higher hydration temperatures (sections 7.1 and 7.3 and [97, 98]), the enhanced precipitation of C-S-H_{lro} could lead to a higher undersaturation with respect to alite. This could lead to an enlarged surface area of alite due to an enhanced etch pit opening and thus to a higher reaction turnover in the early hydration.

4.6. Interaction of silicate and aluminate reaction

Understanding the interaction of the aluminate reaction with the silicate reaction has been the main motivation for this study. The results from pure alite hydration and the hydration of the mechanically activated alites allow a closer examination of the Portland cement hydration. For this purpose, a reduced synthetic cement (SynCem) mixture is used. In section 7.7, mixtures of alite and C_3A (ratio 95:5) are mixed with different amounts of calcium sulfates (bassanite and anhydrite of 20:80 ratio) to simulate white Portland cement pastes from typical undersulfated to properly sulfated conditions.

In all examined SynCem pastes the aluminate reaction proceeds as follows: Directly after mixing, about 1/3 of the C_3A content and total bassanite dissolve. This results in a continuous precipitation of ettringite during the initial, induction and a part of the acceleration period of the alite reaction. Initially the slow and steady dissolution of anhydrite takes place simultaneous. The ettringite precipitation also continuous after the complete dissolution of anhydrite. The C_3A content remains constant during this time period. The Al source for the precipitation of ettringite is probably an XRD amorphous Al-containing phase that forms during the initial rapid C_3A dissolution as suggested by Hesse et al. [6]. Minard et al. suggested that Ca and/or sulfate on C_3A reactive surface sites prevents a further hydration of C_3A [99]. The results of this study agree with this finding as the renewed aluminate reaction starts the later, the higher the SO_3 content in paste is (section 7.7). When the C_3A surface is not prevented from further dissolution by adsorbed sulfate, the aluminate reaction is renewed. C_3A dissolves and ettringite and AFm phases are subsequently precipitated together. After a short period, a part of the initially precipitated ettringite dissolves and supplies the further AFm precipitation with SO_3. After the decline of this sharp reaction peak, AFm phase precipitation and C_3A dissolution proceed on low levels until the end of the experiments. This demonstrates a continuous presence of an aluminate reaction throughout the entire hydration reaction of the SynCem pastes.

Three main interactions between the silicate reaction and aluminate reaction are identified. The most significant is the interference of the renewed aluminate reaction (marked by arrow in Fig. 8) with the silicate reaction. The alite hydration decelerates and reaccelerates after the deceleration of the renewed aluminate reaction (Fig. 9). The often suggested Al inhibition on C-S-H precipitation [95, 96, 100, 101] or on alite dissolution [102, 103] seems unlikely to be resonsible for the interference, as discussed in detail in section 7.7. Instead, the precipitation of AFm phases on the surface of C-S-H_{lro} due to the opposite zeta potential of both phases [104, 105] can explain the reaction kinetics. The partial blockage of the C-S-H_{lro} surface caused by coagulation can explain why the silicate reaction decelerates after the onset of the rapid AFm phase precipitation (Fig. 10). The reactive surface area of C-S-H_{lro} decreases due to the coagulation with AFm phases. After the rapid AFm precipitation declines, the reactive C-S-H_{lro} substrate surface increases again and the reaction reaccelerates (Fig. 10). This reacceleration starts at lower hydration rates, because the C-S-H_{lro} surface remains blocked by AFm phases also after the deceleration of the renewed aluminate reaction.

This mechanism also provides an explanation for the second main interaction of the aluminate and silicate reaction that occurs after the renewed aluminate reaction has decelerated and proceeds on low levels. Continuously precipitating AFm phases could be the explanation for the slower reacceleration of the alite hydration in comparison to the acceleration of the main hydration reaction in the SynCem paste (Fig. 9) or in the pure alite paste (Fig.8). A part of the acceleration driving C-S-H_{lro} substrate surface is continuously covered by AFm phases. Therefore, the acceleration is slower than it would be without the C-S-H_{lro} surface blockage.

The most significant interaction between both reaction regimes is present in all SynCem pastes irrespective of a lower or higher SO_3 content. The acceleration of the alite hydration and the reaction degree of alite suring the main hydration period in the SynCem pastes are significantly higher than in pure alite pastes (Fig. 7, section 7.7). In the literature, this was

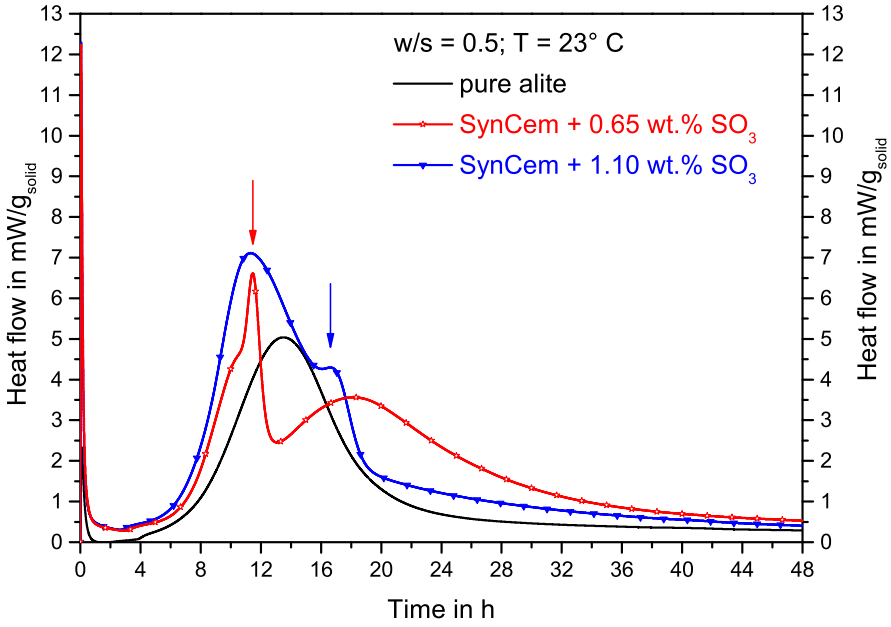

Fig. 8: Heat flow calorimetry of pure alite and of SynCem with different SO_3 content. The arrows mark the main rate peak of the respective renewed aluminate reaction.

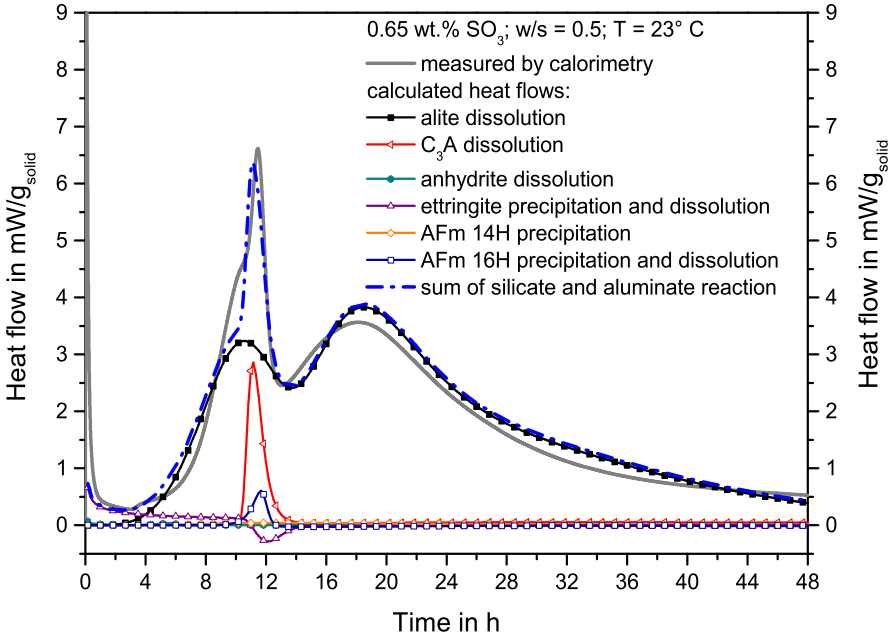

Fig. 9: Comparison of the heat flow measured by calorimetry and calculated from the phase development measured by in-situ XRD analysis for SynCem with 0.65 wt.% SO_3.

assigned to the eleminition of the Al inhibition on alite hydration due to the presence of sulfate [95] or to a different mode of C-S-H growth when sulfate is adsorbed on C-S-H surfaces [106]. Instead, the results of section 7.7 suggest that Al should be available during the complete SynCem hydration in spite of sulfate beeing in the paste. The process, which causes the higher reaction turnover, has to take place during the first few hours of hydration and not later than the start of the acceleration period. This statement is founded on the similar reaction paths of all SynCem pastes during this time interval and the fact that the hydration of all SynCem pastes results in similar released heats up to 48 h. The explanation is in accordance with the higher reaction turnover in the same activated alite that underwent different drying proceedures (sections 4.5 and 7.6). Comparable to the coagulation of AFm phases and C-S-H, it is suggested that the initially precipitated very fine grained (nano-)ettringite acts as a seeding material for C-S-H. This could result in a higher extent of C-S-H surfaces in the early acceleration period. In this case, a faster acceleration of the hydration is possible. The higher extent of C-S-H surfaces could explain why a higher undersaturation with respect to alite could exist in the first hours of hydration causing a higher extent of opened etch pits. This would lead to an increase of the alite surface responsible for the higher reaction turnover in the SynCem pastes compared to the pure alite paste. The initial precipitation of very fine (nano-)ettringite might represent an intrinsic accelerator for the silicate hydration reaction in Portland cements.

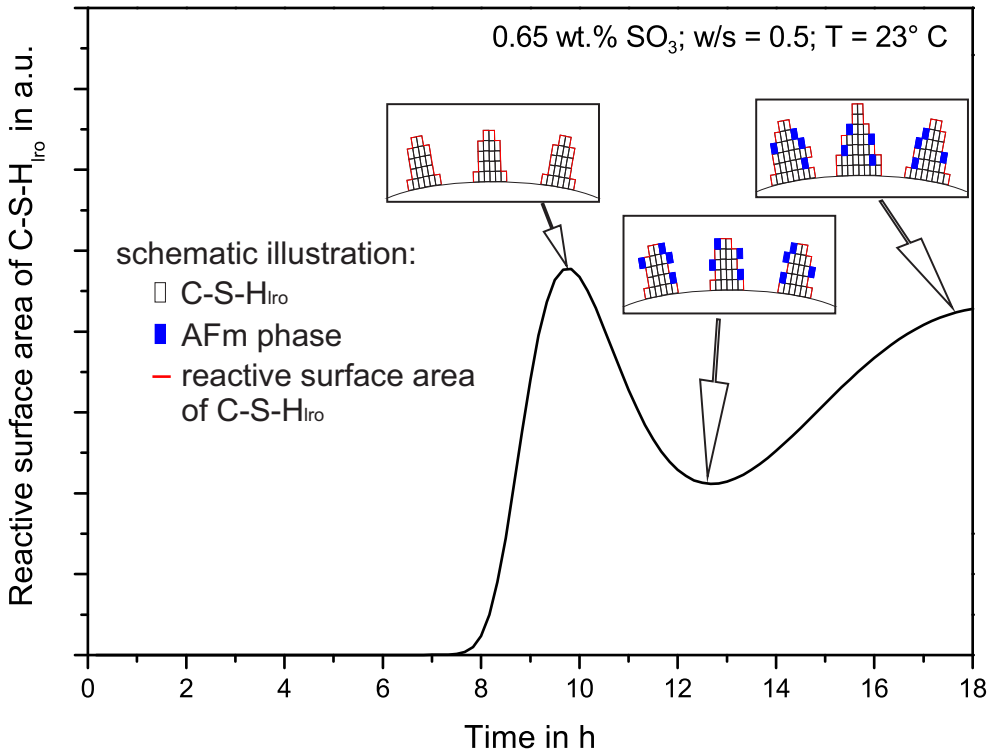

Fig. 10: Development of the reactive surface area of C-S-H$_{lro}$ in arbitrary units, on the simplifying assumption of a constant surface precipitation rate of C-S-H$_{lro}$, together with a schematic illustration. The precipitation of AFm phases decreases the reactive surface area of C-S-H$_{lro}$ between about 9.5 and 12.5 h. The reactive surface area subsequently increases again and consequentially accelerates the hydration rate.

5. Conclusions

The development and application of a C-S-H_{lro} phase model combined with experiments with mechanically activated alites and a synthetic white Portland cement offer an improved understanding of the alite hydration process.

Directly after contact with water, a small amount of alite dissolves. In the first minutes of hydration, XRD amorphous C-S-H phases precipitate, as expected from measurements of the solution composition [32, 34, 44, 81]. The hydration enters the period of slow reaction as the degree of undersaturation with respect to alite in solution decreases [37, 39].

The start of the acceleration period is connected to the evolution of monomeric XRD amorphous C-S-H to dimeric XRD amorphous C-S-H [42] and finally to XRD detectable C-S-H_{lro}. C-S-H_{lro} can be detected in pastes when the crystalline alite dissolution accelerates. C-S-H_{lro} is the further metastable product of the early alite hydration. XRD amorphous C-S-H phases initially precipitate and subsequently transform into C-S-H_{lro} in the further hydration process. As soon as the maximum supersaturation with respect to portlandite is reached, it precipitates. Portlandite precipitation seems rather to be a consequence of the acceleration period than the trigger for it. The acceleration is probably driven by the increase of the C-S-H_{lro} reactive substrate surface area.

The transition from acceleration to deceleration period probably proceeds when the ion supply resulting from alite dissolution is too low to maintain the possible precipitation rate of C-S-H_{lro}. This is a reasonable assumption, as Nicoleau & Nonat [58, 59] and Bullard et al. [52] noticed decreasing amounts of ions in solution in spite of the deceleration of C-S-H precipitation. In addition, the diminution of small crystalline alite crystallites is experimentally confirmed in the activated alite pastes. The reaction turnover up to the transition into the deceleration period depends on the particle size distribution of the alite powder and the reaction kinetics during the first hours of hydration. If the hydration kinetics enable a larger extent of opened etch pits on crystalline alite surfaces, the hydration will result in a higher reaction turnover until the end of the main reaction period.

The better understanding of the alite hydration process has practical use for cement applications. The period of slow reaction for cements admixed with amorphous “alite” could be significantly shortened. The required high Ca concentrations for the formation of the kind of C-S-H necessary to accelerate the hydration can be reached significantly faster. However, the total reaction turnover during the main hydration period would probably be reduced at the same time. This is caused by the decrease of the extent of opened etch pits under less undersaturated conditions with respect to alite. Therefore, the reactive crystalline alite surface would be lower than possible without the addition of amorphous “alite”. The negative effect on the total reaction turnover could even be higher, if the cement-intrinsic seeding effect by the initial ettringite formation would be decreased in the presence of amorphous “alite”.

The experimental results lead to the conclusion that the well-known use of seeding materials provides the best method to reduce the period of slow reaction, and to enhance the reaction turnover of alite during the main hydration period simultaneously. Of course, the addition of a reactive C-S-H_{lro} would be the best seeding material for C-S-H_{lro}. However, all kinds of seeding materials can be used for this purpose. It is important that they supply a surface that is able to serve as preferred substrate for the initial heterogeneous nucleation of C-S-H_{lro}. Thereby, the Ca demand in the initial hydration stage and consequently the extent of opened

etch pits increases. This shortens the period of slow reaction und increases both, the acceleration rate and the total reaction turnover.

6. References

[1] H.G. v. Oss in U.S. Geological Survey, Mineral commodity summaries 2015, U.S. Geological Survey (2006) p. 45.

[2] H.G. v. Oss in U.S. Geological Survey, Mineral commodity summaries 2015, U.S. Geological Survey (2015) p. 39, http://dx.doi.org/10.3133/70140094.

[3] J. Plank, Concrete Admixtures – Where are we now and what can we expect in the future?, Conference proceedings ibausil 2015, Weimar, F.A. Finger-Institut für Baustoffkunde, 1-27 – 1-42.

[4] H.-M. Ludwig, CO_2 arme Zemente für nachhaltige Betone, Conference proceedings ibausil 2015, Weimar, F.A. Finger-Institut für Baustoffkunde, 1-1 – 1-26.

[5] C. Hesse, Der Reaktionsverlauf der frühen Hydratation von Portlandzementen in Relation zur Temperatur, doctoral thesis, Friedrich-Alexander-Universität Erlangen-Nürnberg, 2009.

[6] C. Hesse, F. Goetz-Neunhoeffer, J. Neubauer, A new approach in quantitative in-situ XRD of cement pastes. Correlation of heat flow curves with early hydration reactions, Cement Concr. Res. 41 (2011) 123–128.

[7] S. Seufert, Einfluss des Sulfatträgers auf ein Portlandzement/Calciumaluminatzement – Schnellzementsystem, doctoral thesis, Friedrich-Alexander-Universität Erlangen-Nürnberg, 2011.

[8] D. Jansen, The hydration of an Ordinary Portland Cement (OPC) and the influence of selected polymers: A mineralogical study using an external standard method for quantitative X-ray diffraction, doctoral thesis, Friedrich-Alexander-Universität Erlangen-Nürnberg, 2011.

[9] B.H. O'Connor, M.D. Raven, Application of the Rietveld refinement procedure in assaying powdered mixtures, Powder Diffr. 3 (1) (1988) 2–6.

[10] D. Jansen, C. Stabler, F. Goetz-Neunhoeffer, S. Dittrich, J. Neubauer, Does ordinary Portland cement contain amorphous phase? A quantitative study using an external standard method, Powder Diffr. 26 (1) (2011) 31–38.

[11] D. Jansen, F. Goetz-Neunhoeffer, C. Stabler, J. Neubauer, A remastered external standard method applied to the quantification of early OPC hydration, Cem. Concr. Res. 41 (2011) 602–608.

[12] H.F.W. Taylor, Proposed structure for calcium silicate hydrate gel, J. Am. Ceram. Soc. 69 (1986) 464-467.

[13] S.A. Hamid, The crystal structure of the 11Å natural tobermorite $Ca_{2.25}[Si_3O_{7.5}(OH)_{1.5}] \cdot 1\ H_2O$, Z. Kristallogr. – Crystalline Materials 154 (1981) 189-198.

[14] E. Bonaccorsi, S. Merlino, A.R. Kampf, The crystal structure of tobermorite 14 Å (Plombierite), a C-S-H Phase, J. Am. Ceram. Soc. 88 (2005) 505-512.

[15] C. Hoffmann, T. Armbruster, Clinotobermorite, $Ca_5[Si_3O_8(OH)_2] \cdot 4\ H_2O$ – $Ca_5[Si_6O_{17}] \cdot 5\ H_2O$, a natural C-S-H(I) type cement mineral: determination of the substructure, Z. Kristallogr. – Crystalline Materials 212 (1997) 864-873.

[16] S. Merlino, E. Bonaccorsi, T. Armbruster, Tobermorites: Their real structure and order-disorder character, Am. Mineral. 84 (1999) 1612-1621.

[17] S. Merlino, E. Bonaccorsi, T. Armbruster, The real structures of clinotobermorite and tobermorite 9 Å, OD character, polytypes, and structural relationships, Eur. J. Mineral. 12 (2000) 411-429.

[18] S. Merlino, E. Bonaccorsi, T. Armbruster, The real structure of tobermorite 11 Å: normal and anomalous forms, OD, character and polytypic modifications, Eur. J. Mineral. 13 (2001) 577-590.

[19] R. Schrader, H. Schuhmann, Zur mechanischen Aktivierung von Silikaten, Z. Chem. 7 (1967) 322.

[20] I. Odler, J. Schüppstuhl, Early hydration of tricalcium silicate, III. Control of the induction period, Cem. Concr. Res. 11 (1981) 765–774.

[21] F. Bellmann, D. Damidot, B. Möser, J. Skibsted, Improved evidence for the existence of an intermediate phase during hydration of tricalcium silicate, Cem. Concr. Res. 40 (2010) 875–884.

[22] H.F.W. Taylor, Cement Chemistry, 2nd ed., Thomas Telford Publishing, London, 1997, p. 113.

[23] H.F.W. Taylor, Cement Chemistry, 2nd ed., Thomas Telford Publishing, London, 1997, p. 7-9.

[24] H.F.W. Taylor, Cement Chemistry, 2nd ed., Thomas Telford Publishing, London, 1997, p. 1.

[25] E.M. Gartner, J.M. Gaidis, W.R. Grace & Co., Hydration Mechanisms, I, In: J.P: Skalny, Materials Science of Concrete I, The American Ceramic Society, 1989, p. 95-126.

[26] I.G. Richardson, The nature of C-S-H in hardened cements, Cement Concr. Res. 29 (1999) 1131-1147.

[27] H.N. Stein, J.M. Stevels, Influence of silica on the hydration of $3CaO,SiO_2$, J. appl. Chem. 14 (1964) 338-346.

[28] H.N. Stein, Thermodynamic considerations on the hydrate on mechanisms of Ca_3SiO_5 and $Ca_3Al_2O_6$, Cement Concr. Res. 2 (1972) 167-177.

[29] P.W. Brown, J. Pommersheim, G. Frohnsdorff, A kinetic model for the hydration of tricalcium silicate, Cement Concr. Res. 15 (1985) 34-41.

[30] E.M. Gartner, H.M. Jennings, Thermodynamics of calcium silicate hydrates and their solutions, J. Am. Ceram. Soc. 70 (1987) 743-749.

[31] R.A. Livingston, J.S. Schweitzer, C. Rolfs, H.-W. Becker, S. Kubsky, T. Spillane, J. Zickefoose, M. Castellote, P.G. de Viedma, J. Cheung, Heavy ion beam measurements of the hydration of cementitious materials, Appl. Radiat. Isot. 68 (2010) 683–687.

[32] S. Garrault, A. Nonat, Hydrated layer formation on tricalcium and dicalcium silicate surfaces: experimental study and numerical simulations, Langmuir 17 (2001) 8131–8139.

[33] J.J. Thomas, A new approach to modeling the nucleation and growth kinetics of tricalcium silicate hydration, J. Am. Ceram. Soc. 90 (2007) 3282–3288.

[34] P.W. Brown, E. Franz, G. Frohnsdorff, H.F.W. Taylor, Analyses of the aqueous phase during early C_3S hydration, Cement Concr. Res. 14 (1984) 257-262.

[35] V.K. Peterson, A.E. Whitten, Hydration processes in tricalcium silicate: Application of the boundary nucleation model to quasielastic neutron scattering data, J. Phys. Chem. C. 113 (2009) 2347-2351.

[36] I. Odler, H. Dörr, Early hydration of tricalcium silicate, II. The induction period, Cement Concr. Res. 9 (1979) 277-284.

[37] P. Juilland, E. Gallucci, R. Flatt, K. Scrivener, Dissolution theory applied to the induction period in alite hydration, Cem. Concr. Res. 40 (2010) 831–844.

[38] A.C. Lasaga, A. Lüttge, Variation of crystal dissolution rate based on a dissolution stepwave model, Science 291 (2001) 2400–2404.

[39] L. Nicoleau, A. Nonat, D. Perry, The di- and tricalcium silicate dissolutions, Cem. Concr. Res. 47 (2013) 14–30.

[40] L. Nicoleau, A. Nonat, The solubility of C_3S and its related factors, Proceedings of ICCC, Beijing 2015.

[41] F. Bellmann, T. Sowoidnich, H.-M. Ludwig, D. Damidot, Dissolution rates during the early hydration of tricalcium silicate, Cement Concr. Res. 72 (2015) 108-116.

[42] S.A. Rodger, G.W. Groves, N.J. Clayden, C.M. Dobson, Hydration of tricalcium silicate followed by ^{29}Si NMR with cross-polarization, J. Am. Ceram. Soc. 71 (1988) 91–96.

[43] F. Bellmann, T. Sowoidnich, H.-M. Ludwig, D. Damidot, Analysis of the surface of tricalcium silicate during the induction period by X-ray photoelectron spectroscopy, Cement Concr. Res. 42 (2012) 1189-1198.

[44] Z.-Q. Wu, J.F. Young, Formation of calcium hydroxide from aqueous suspensions of tricalcium silicate, J. Am. Ceram. Soc. 67 (1984) 48-51.

[45] J.F. Young, H.S. Tong, R.L. Berger, Compositions of solutions in contact with hydrating tricalcium silicate pastes, J. Am. Ceram. Soc. 60 (1977) 193-198.

[46] D. Damidot, A. Nonat, P. Barret, Kinetics of tricalcium silicate hydration in diluted suspensions by microcalorimetric measurements, J. Am. Ceram. Soc. 73 (1990) 3319-3322.

[47] J.W. Bullard, R.J. Flatt, New insights into the effect of calcium hydroxide precipitation on the kinetics of tricalcium silicate hydration, J. Am. Ceram. Soc. 93 (2010) 1894-1903.

[48] A. Kumar, S. Bishnoi, K.L. Scrivener, Modelling early age hydration kinetics of alite, Cement Concr. Res. 42 (2012) 903-918.

[49] L. Nicoleau, M.A. Bertolim, Analytical model for the alite (C_3S) dissolution topography, J. Am. Ceram. Soc. doi:10.1111/jace.13647.

[50] S. Garrault, T. Behr, A. Nonat, Formation of the C-S-H layer during early hydration of tricalcium silicate grains with different sizes, J. Phys. Chem. B 110 (2006) 270-275.

[51] J.J. Thomas, The instantaneous apparent activation energy of cement hydration measured using a novel calorimetry-based method, J. Am. Ceram. Soc. 95 (2012) 3291-3296.

[52] J.W. Bullard, G.W. Scherer, J.J. Thomas, Time dependent driving forces and the kinetics of tricalcium silicate hydration, Cement Concr. Res. 74 (2015) 26-34.

[53] S. Bishnoi, K.L. Scrivener, Studying the nucleation and growth kinetics of alite hydration using μic, Cement Concr. Res. 39 (2009) 849-860.

[54] D.M. Kirby, J.J. Biernacki, The effect of water-to-cement ratio on the hydration kinetics of tricalcium silicate cements: Testing the two-step hydration hypothesis, Cement Concr. Res. 42 (2012) 1147-1156.

[55] E. Masoero, J.J. Thomas, H.M. Jennings, A reaction zone hypothesis for the effects of particle size and water-to-cement ratio on the hydration kinetics of C_3S, J. Am. Ceram. Soc. 97 (2014) 967-975.

[56] A. Bazzoni, Study of early hydration mechanisms of cement by means of electron microscopy, doctoral thesis, École Polytechnique Fédérale De Lausanne, 2014.

[57] S. Garrault, L. Nicoleau, A. Nonat, Tricalcium silicate hydration modeling and numerical simulations, Proceedings of CONMOD 10 (2010) 91-94.

[58] L. Nicoleau, The C_3S dissolution, a determining kinetic factor during hydration?, Proceedings of ICCC, Beijing 2015.

[59] L. Nicoleau, A. Nonat, A new view on the kinetics of tricalcium silicate hydration, submitted to Cement Concr. Res.

[60] A.J. Allen, J.J. Thomas, H.M. Jennings, Composition and density of nanoscale calcium–silicate–hydrate in cement, Nat. Mater. 6 (2007) 311–316.

[61] B. Lothenbach, A. Nonat, Calcium silicate hydrates: Solid and liquid phase composition, Cement Concr. Res. 78 Part A (2015) 57-70.

[62] F. Deschner, F. Winnefeld, B. Lothenbach, S. Seufert, P. Schwesig, S. Dittrich, F. Goetz-Neunhoeffer, J. Neubauer, Hydration of Portland cement with high replacement by siliceous fly ash, Cement Concr. Res. 42 (2012) 1389-1400.

[63] A. Nonat, Interactions between chemical evolution (hydration) and physical evolution (setting) in the case of tricalcium silicate, Mater. Struct. 27 (1994) 187-195.

[64] J.J. Chen, J.J. Thomas, H.F.W. Taylor, H.M. Jennings, Solubility and structure of calcium silicate hydrate, Cement Concr. Res. 34 (2004) 1499-1519.

[65] J.I. Escalante-Garcia, J.H. Sharp, Variation in composition of C-S-H gel in Portland cement pastes cured at various temperatures, J. Am. Ceram. Soc. 82 (1999) 3237-3241.

[66] F.W. Locher, Stöchiometrie der Hydratation von Tricalciumsilicat, Zem.-Kalk-Gips 20 (1967) 402–407.

[67] A. Ayuela, J.S. Dolado, I. Campillo, Y.R. de Miguel, E. Erkizia, D. Sanchez-Portal, A. Rubio, A. Porro, P.M. Echenique, Silicate chain formation in the nanostructure of cement-based materials, J. Chem. Phys. 127 (2007) 164710-(1-8).

[68] P. Yu, R.J. Kirkpatrick, B. Poe, P. McMillan, X. Cong, Structure of calcium silicate hydrate (C-S-H): Near-, mid-, far-infrared spectroscopy, J. Am. Ceram. Soc. 82 (1999) 742-748.

[69] H.M. Jennings, Aqueous solubility relationships for two types of calcium silicate hydrate, J. Am. Ceram. Soc. 69 (1986) 614–618.

[70] I.G. Richardson, G.W. Groves, Model for the composition and structure of calcium silicate hydrate (C-S-H) gel in hardened tricalcium silicate pastes, Cement Concr. Res. 22 (1992) 1001-1010.

[71] I.G. Richardson, Tobermorite/jennite- and tobermorite/calcium hydroxide-based models for the structure of C-S-H: applicability to hardened pastes of tricalcium silicate, β-dicalcium silicate, Portland cement, and blends of Portland cement with blast-furnace slag, metakaolin, or silica fume, Cement Concr. Res. 34 (2004) 1733-1777.

[72] I.G. Richardson, Model structures for C-(A)-S-H(I), Acta Cryst. B 70 (2014) 903-923.

[73] G. Kovacevic, B. Persson, L. Nicoleau, A. Nonat, V. Veryazov, Atomistic modelling of crystal structure $Ca_{1.67}SiH_x$, Cement Concr. Res. 67 (2015) 197-203.

[74] K. Mohan, H.F.W. Taylor, Analytical electron microscopy of cement pastes: IV, β-dicalcium silicate pastes, J. Am. Ceram. Soc. 64 (1981) 717-719.

[75] G. Geng, R. Taylor, S. Bae, D. Hernandez-Cruz, D.A. Kilcoyne, A.-H. Emwas, P.J.M: Monteiro, Atomic and nano-scale characterization of a 50-year-old hydrated C_3S paste, Cement Concr. Res. 77 (2015) 36-46.

[76] J.J. Thomas, H.M. Jennings, A.J. Allen, Relationships between composition and density of tobermorite, jennite, and nanoscale $CaO\text{-}SiO_2\text{-}H_2O$, J. Phys. Chem. C 114 (2010) 7594-7601.

[77] N.V.Y. Scarlett, I.C. Madsen, Quantification of phases with partial or no known crystal structures, Powder Diffr. 21 (4) (2006) 278–284.

[78] R.J. Hill, C.J. Howard, Quantitative phase analysis from neutron powder diffraction data using the Rietveld method, J. Appl. Cryst. 20 (1987) 467–474.

[79] S. Dittrich, Quantitative phase development of crystalline, nanocrystalline and amorphous phase during hydration of OPC blended siliceous fly ash, doctoral thesis, Friedrich-Alexander-Universität Erlangen-Nürnberg, 2015.

[80] S. Dittrich, J. Neubauer, F. Goetz-Neunhoeffer, The influence of fly ash on the hydration of OPC within the first 44 h – A quantitative in situ XRD and heat flow calorimetry study, Cement Concr. Res. 56 (2014) 129-138.

[81]A. Sobolkina, V. Mechtcherine, S. T. Bergold, J. Neubauer, C. Bellmann, V. Khavrusa, S. Oswald, A. Leonhardt, W. Reschetilowski, Effect of carbon-based materials on the early hydration of tricalcium silicate, J. Am. Ceram. Soc., accepted for publication, doi: 10.1111/jace.14187.

[82] E. Pustovgar, J.-B. d'Espinose, M. Palacios, A. Andreev, R. Sangodkar, R., B. Chmelka, R. J. Flatt, Revealing the steps of tricalcium silicate hydration, Proceedings of the ICCC, 1130-FP-SN450, Beijing 2015.

[83] P. Juilland, E. Gallucci, Morpho-topological investigation of the mechanisms and kinetic regimes of alite dissolution, Cement Concr. Res. 76 (2015) 180-191.

[84] L. Nicoleau, Accelerated growth of calcium silicate hydrates: experiments and simulations, Cem. Concr. Res. 41 (2011) 1339–1348.

[85] S. Gauffinet, E. Finot, E. Lesniewska, A. Nonat, Observation directe de la croissance d'ydrosilicate de calcium sur de surfaces d'alite et de silice par microscopie à force atomique, C. R. Acad. Sci. Paris, Sciences de la terre et des planets 327 (1998) 231-236.

[86] H.M. Jennings, Refinements to colloid model of C-S-H in cement: CM-II, Cement Concr. Res. 38 (2008) 275-289.

[87] H.M. Jennings, J.J. Thomas, J.S. Gevrenov, G. Constantinides, F.-J. Ulm, A multi-technique investigation of the nanoporosity of cement paste, Cement Concr. Res. 37 (2007) 329–336.

[88] A.J. Allen, R.C. Oberthur, D. Pearson, P. Schofield, C.R. Wilding, Development of the fine porosity and gel structure of hydrating cement systems, Philos. Mag. B 56 (1987) 263–288.

[89] G. Constantinides, F.-J. Ulm, The nanogranular nature of C–S–H, J. Mech. Phys. Solids 55 (2007) 64–90.

[90] J. Haas, A. Nonat, From C-S-H to C-A-S-H: Experimental study and thermodynamic modelling, Cement Concr. Res. 68 (2015) 124-138.

[91] A. Bazzoni, M. Cantoni, K.L. Scrivener, Impact of annealing on the early hydration of tricalcium silicate, J. Am. Ceram. Soc. 97 (2014) 584-591.

[92] J. J. Thomas, H. M. Jennings, J. J. Chen, Influence of nucleation seeding on the hydration mechanisms of tricalcium silicate and cement, J. Phys. Chem. C 113 (2009) 4327-4334.

[93] T. Sato, F. Diallo, Seeding effect of nano-$CaCO_3$ on the hydration of tricalcium silicate, Transport. Res. Rec. 2141 (2010) 61-67.

[94] B. Yeon Lee, K. E. Kurtis, Influence of TiO_2 nanoparticles on early C_3S hydration, J. Am. Ceram. Soc. 93 (2010) 3399-3405.

[95] A. Quennoz, K. L. Scrivener, Interactions between alite and C_3A-gypsum hydrations in model cements, Cement Concr. Res. 44 (2013) 46-54.

[96] T. Matschei, M. Costoya, A contribution to an improved understanding of the hydration kinetics of OPC, Conference proceedings ibausil 2012, Weimar, 1-0276 – 1-0285.

[97] I. Odler, J. Skalny, Hydration of tricalcium silicate at elevated temperatures, J. Appl. Chem. Biotechnol. 23 (1973) 661-667.

[98] I.F. Sáez del Bosque, M. Martín-Pastor, S. Martínez-Ramírez, M.T. Blanco-Varela, Effect of temperature on C_3S and C_3S + nanosilica hydration and C-S-H structure, J. Am. Ceram. Soc. 96 (2013) 957-965.

[99] H. Minard, S. Garrault, L. Renaud, A. Nonat, Mechanisms and parameters controlling the tricalcium aluminate reactivity in the presence of gypsum, Cement Concr. Res. 37 (2007) 1418-1426.

[100] F. Begarin, S. Garrault, A. Nonat, L. Nicoleau, Hydration of alite containing aluminum, Adv. Appl. Ceram. 110 (2011) 127-130.

[101] S. Garrault, A. Nonat, Y. Sallier, L. Nicoleau, On the origin of the dormant period of cement hydration, ICCC, Madrid 2011.

[102] L. Nicoleau, E. Schreiner, A. Nonat, Ion-specific effects influencing the dissolution of tricalcium silicate, Cement Concr. Res. 59 (2014) 118-138.

[103] P. Suraneni, R. J. Flatt, Use of micro-reactors to obtain new insights into the factors influencing tricalcium silicate dissolution, Cement Concr. Res. 78 Part B (2015) 208-215.

[104] A. Zingg, F. Winnefeld, L. Holzer, J. Pakusch, S. Becker, L. Gauckler, Adsorption of polyelectrolytes and its influence on the rheology, zeta potential, and microstructure of various cement and hydrate phases, J. Colloid Interface Sci. 323 (2008) 301-302.

[105] J. Plank, C. Hirsch, Impact of zeta potential of early cement hydration phases on superplasticizer adsorption, Cement Concr. Res. 37 (2007) 537-542.

[106] B. Mota, T. Matschei, K. Scrivener, The influence of sodium salts and gypsum on alite hydration, Cement Concr. Res. 75 (2015) 53-65.

7. Publications

7.1. The hydration of alite: a time-resolved quantitative X-ray diffraction approach using the G-factor method compared with heat release

Reprint

Published in the Journal "Journal of Applied Crystallography"
Vol. 44 (2011) 895-901, doi: 10.1107/S0021889811025933

Authors: D. Jansen, S. T. Bergold, F. Götz-Neunhoeffer, and J. Neubauer

research papers

Journal of
Applied Crystallography
ISSN 0021-8898

Received 21 March 2011
Accepted 30 June 2011

The hydration of alite: a time-resolved quantitative X-ray diffraction approach using the *G*-factor method compared with heat release

Daniel Jansen,* Sebastian T. Bergold, Friedlinde Goetz-Neunhoeffer and Jürgen Neubauer*

GeoZentrum Nordbayern, Chair for Mineralogy, University of Erlangen–Nuremberg, Schlossgarten 5a, Erlangen, Bavaria, 91054, Germany. Correspondence e-mail: danherjansen@googlemail.com, neubauer.gzn@me.com

The classical external-standard method derived from the work of O'Connor & Raven [*Powder Diffr.* (1988), **3**, 2–6] was used to examine the hydration of the major phase, alite, of ordinary Portland cements at different temperatures and different water/alite ratios. In order to estimate the accuracy of the method, heat-flow curves were calculated from the alite dissolution curves obtained from X-ray diffraction *in situ* experiments. The heat-flow curves calculated in this way were compared with heat-flow curves recorded using a calorimeter. It is shown that the calculated curves agree well with the curves obtained from heat-flow experiments.

1. Introduction

Even though ordinary Portland cements (OPCs) have been used and studied for decades, the hydration kinetics of their major phase, alite (doped tricalcium silicate, C_3S), are still not completely understood. Several theories have persisted alongside each other. The major concern of these theories has been to explain the reaction kinetics of alite hydration which are commonly determined from heat-flow calorimetric measurements (Fig. 1). An initial heat flow can be detected directly after mixing (I). This is followed by a period of slow reaction which is known as the induction period (II). This induction period is followed by the main hydration reaction (III), which is separated into the acceleration (III*a*) and the deceleration period (III*b*). The main hydration reaction is normally completed after the elapse of 24 h, but the hydration continues at low heat-flow levels for months. The hydration results in the formation of an amorphous calcium–silicate–hydrate (C–S–H) gel and crystalline portlandite. The Ca/Si ratio of C–S–H depends on the temperature (Escalante-Garcia & Sharp, 1999), on the water-to-cement ratio (Locher, 1967) and, in the case of an OPC, on the composition of the OPC used (Richardson, 1999). After 28 d, the Ca/Si ratio of a C–S–H gel formed in a hydrated OPC at 293 K with a water-to-cement ratio of 0.4 stands at 1.7, according to Allen *et al.* (2007). We thus arrive at equation (1) for the hydration of C_3S after this point in time:

$$C_3S + 3.9H \rightarrow C_{1.7}SH_{2.6} + 1.3CH, \quad \Delta H = -561\,J\,g^{-1}. \quad (1)$$

The enthalpy of reaction ΔH is the difference between the sum of the formation enthalpies of the products ($\Delta HF_{products}$) and the sum of the formation enthalpies of the reactants ($\Delta HF_{reactants}$).

The enthalpy for equation (1) was calculated using data acquired by means of the thermodynamic software *GEMS* (Kulik, 2010) using the *GEMS* version of the Nagra/PSI thermodynamic database (Hummel *et al.*, 2002; Thoenen & Kulik, 2003), the cemdata07 database (Lothenbach *et al.*, 2008) and the enthalpy of formation for $C_{1.7}SH_{2.6}$ derived following Fuji & Kondo (1983).

The most widely used theory for the hydration of alite predicts the formation of a metastable protective C–S–H layer on the C_3S grain surface directly after wetting. This protective layer suppresses further hydration of the C_3S and ends the initial period (Stein & Stevels, 1964; Gartner & Gaidis, 1989). At the end of the induction period, this protective layer is destabilized, giving rise either to a more permeable layer or to the dissolution of the layer, which allows the hydration reaction to start again. Livingston *et al.* (2010) assume, from the results of their nuclear resonance reaction analysis of C_3S

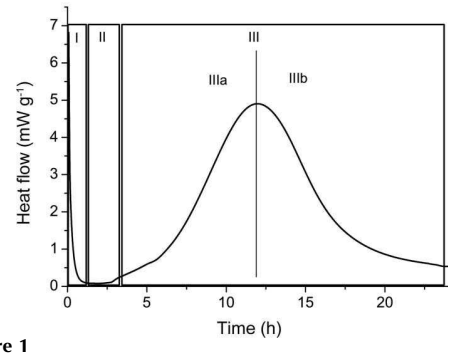

Figure 1
Heat-flow curve of alite; water/alite ratio = 0.5; T = 296 K.

hydration, that an existing protective layer breaks because of the osmotic pressure attained between the silicate-rich grain surface and the calcium-rich solution.

Another theory does not require this assumption of the emergence of a protective layer in order to explain the progress of alite hydration. For example, Garrault & Nonat (2001) and Peterson & Whitten (2009) assume that a single process is responsible for both the nucleation and the growth of C–S–H, which begins, according to Rodgers *et al.* (1988), directly after mixing. Thomas (2007) concludes, from mathematical calculation of a boundary nucleation and growth model, that the hydration continues at low levels during the period of slow reaction. This, he suggests, is because there are only a small number of C–S–H nucleons present, so that this period does not form a separate chemical process in itself. Assuming a constant rate for the C–S–H nucleation process (Thomas, 2007), the acceleration period would begin once a sufficient number of C–S–H nucleons have been precipitated. Juilland *et al.* (2010) suggest that there are different solution mechanisms working at different degrees of undersaturated solution, as described by Lasaga & Luttge (2001) for several minerals.

At a certain point, the hydration of alite becomes diffusion controlled, because the unreacted alite grains come to be covered by a continuous product layer. Some authors (*e.g.* Garrault & Nonat, 2001) claim that the diffusion regime has already begun with the onset of the deceleration period, while others consider it to begin only with the end of the deceleration period, when the hydration has reached very low levels, or at even later points in time (Thomas *et al.*, 2009).

X-ray diffraction (XRD) *in situ* analysis is a suitable method for examining the phase development of hydrating alite/water mixtures during the process of hydration. This is the case even though the C–S–H phase that is formed during this process is not detectable by X-ray diffraction in the first 24 h because of its low degree of crystallinity. Besides this, the water added to the alite cannot be quantified directly with X-rays.

Software for Rietveld (1969) refinement usually gives the total of the crystalline phases determined, normalized to 100 wt% (*ZMV* algorithm; Hill & Howard, 1987). In cases where amorphous phases are present (in the case of alite/water mixtures, there is likely to be at least C–S–H phase and water) the amounts of the crystalline phases calculated from Rietveld analysis will differ from the actual amounts. Moreover, any computing error of any phase of the mixture will have an influence on the calculated amounts of all phases in the mixture.

There exists the possibility of plotting peak areas or peak intensities in order to show phase developments in pastes in quantitative terms (Pöllmann *et al.*, 2009; Pelletier *et al.*, 2009) and without normalization to 100 wt%. Unfortunately it is not possible to calculate actual quantities, given in wt% of the alite/water mixture, by this method.

An internal-standard method can be applied in order to establish the phase composition of the crystalline phases as well as the amount of the amorphous content of an alite/water mixture (Scrivener *et al.*, 2004). If an internal standard is added to the cement, there exists the possibility of the standard material exerting an influence on the hydration of the cement.

Westphal *et al.* (2009) have examined the mathematical consequences of the internal-standard method and have concluded that there is such a thing as an optimal amount of internal standard that can be added to the sample. Assuming an amorphous content of 35 wt% on average in the first 22 h of hydration (depending on the C–S–H phase and water/alite ratio), the most advisable option, they propose, is to work with an amount of internal standard of at least 40 wt%. Where this is not done, the user will have to accept a considerable analysis error. Such a high amount of internal standard might possibly have an influence on the hydration inasmuch as it might bring about alterations in nucleation and growth kinetics or the water/alite ratio.

In order to avoid complications that might be caused by mixing an internal standard with the alite phase, we decided to make use of an external-standard method, which was first described by O'Connor & Raven (1988) but has not subsequently been used for the quantification of hydration reactions.

The scope set for this paper is to provide an answer to the question of whether or not XRD *in situ* analysis is a suitable method for characterizing the hydration process of the alite phase. It is also the intention of the authors to focus attention on the comparison between heat-flow curves as calculated from XRD data and heat-flow curves as measured from heat-flow experiments. The main focus is on the main hydration period of the cement, which sets in after several hours and is concluded within 24 h at room and higher temperatures.

However, a question that can be answered using XRD experiments is how the reaction from alite to portlandite and the C–S–H phase emerges. Assuming that there exist at least two processes here that release heat, namely the dissolution of the alite phase and the precipitation of portlandite and the C–S–H phase, it necessarily follows that dissolution and precipitation have to run synchronously in order to make it possible to calculate the heat flow using only the dissolution curve of the alite phase obtained from Rietveld analysis.

2. Materials and methods

Alite was synthesized using $CaCO_3$, Al_2O_3 and SiO_2 from Alfa Aesar and MgO from Merck. Al_2O_3 and MgO were added to stabilize a monoclinic (*M*3) alite structure (De La Torre *et al.*, 2002). The chemicals were homogenized in a vibration disc mill and placed in platinum crucibles. The thermal treatment was carried out three times at a temperature of 1673 K for 4 h in a chamber furnace. The synthesized alite was checked for phase purity using XRD. The specific surface of the synthesized alite was measured to be 0.29 $m^2 g^{-1}$, using the Blaine method.

For the *in situ* XRD analysis a custom-made sample holder with a heater/cooler unit was used (Hesse *et al.*, 2008). Cement and water were mixed by external stirring for 1 min. The paste was then put into the sample holder and covered by a 7.5 µm-

Table 1
Structure models used for Rietveld refinements.

Phase	ICSD code	Author
Alite	94742	De La Torre *et al.* (2002)
Silicon	51688	Többens *et al.* (2001)
Portlandite	34241	Greaves & Thomas (1986)

Table 2
Chemical composition of the samples (wt%).

CaO	71.8
Al_2O_3	0.6
SiO_2	25.9
MgO	1.8

thick Kapton polyimide film. The diffraction patterns were recorded using a D8 diffractometer (Bruker) equipped with a LynxEye position-sensitive detector. We made use of Cu $K\alpha$ radiation at 40 kV and 40 mA, and recorded from 7° 2θ to 40° 2θ with a step width of 0.0236 and 0.58 s counting time per step. Under these conditions, it is possible to record 88 ranges within the first 22 h of hydration. For the Rietveld refinements, the program *Topas* version 4.2 from Bruker AXS Inc. (Madison, Wisconsin, USA) (fundamental parameters approach) was used. There was no evidence for any difference in the results when working with a longer range from 7° 2θ to 70° 2θ.

The quantitative phase composition of the alite paste was determined using the *G*-factor method, which was first described by O'Connor & Raven (1988) and which has already been used successfully for the examination of cements and cement pastes (Jansen, Goetz-Neunhoeffer *et al.*, 2011; Jansen, Stabler *et al.*, 2011). In addition, the method was recommended by Schreyer *et al.* (2011) for the examination of organic mixtures. For this purpose, a well known standard (in our case silicon; Jansen, Stabler *et al.*, 2011) is used in order to calculate the *G* factor [equation (2)]:

$$G = s_{\mathrm{Si}} \frac{\rho_{\mathrm{Si}} V_{\mathrm{Si}}^2 \mu_{\mathrm{Si}}^*}{c_{\mathrm{Si}}}, \qquad (2)$$

where s_{Si} is the Rietveld scale factor of silicon from Rietveld analysis, ρ_{Si} the density of silicon, V_{Si} the unit-cell volume of silicon, c_{Si} the weight fraction of silicon (100 wt%) and μ_{Si}^* the mass attenuation coefficient of silicon.

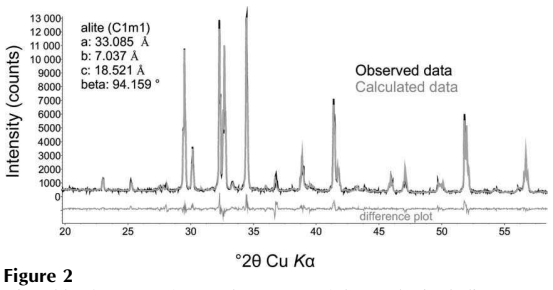

Figure 2
Rietveld refinement of a powder pattern of the synthesized alite.

Table 3
Mass attenuation coefficients (MAC) ($cm^2\ g^{-1}$) of the samples.

$MAC_{\mathrm{dry\ alite}}$	99
MAC_{H2O}	10.2
MAC(alite/water paste; water/alite ratio = 0.5)	69.4
MAC(alite/water paste; water/alite ratio = 1)	54.6

Table 4
Computed *G* factor and structural details regarding the silicon standard employed.

Scale factor from Rietveld refinement	0.007695
Cell volume	1.6×10^{-22} cm^3
Density	2.33 g cm^{-3}
Mass attenuation coefficient	63.7 cm^2 g^{-1}
G factor	2.92×10^{-44} cm^5 per wt%

The *G* factor was then used to determine the mass concentration of each crystalline phase *j* in the hydrating alite paste [equation (3)]:

$$c_j = s_j \frac{\rho_j V_j^2 \mu_{\mathrm{sample}}^*}{G}. \qquad (3)$$

This made it imperative that the sample be measured under the same conditions as the standard. Since the alite paste was covered during the measurement process with a Kapton film, which can cause absorption of X-rays and thereby intensity loss, it was necessary that the standard material be likewise covered with a Kapton film during its measurement process. The structure models and the respective ICSD codes are shown in Table 1. The chemical composition of the alite samples is shown in Table 2. The mass attenuation coefficients of the dry alite powder and the pastes are shown in Table 3. Mass attenuation coefficients for the various elements were drawn from *International Tables for Crystallography* (Prince, 2004). The mass attenuation coefficient of the alite powder was calculated from the chemical composition. More details about the standard used are shown in Table 4. The *G* factor was evaluated from six powder samples with individual preparations. The mean value of all measurements was used for the quantification of the water/alite pastes. The standard deviation of the mean value for the scale factor of the silicon powder was 0.8 wt%.

The *G*-factor method of O'Connor & Raven (1988) displays enormous advantages where it is applied to the quantification of alite hydration. Where this method is adopted, the crys-

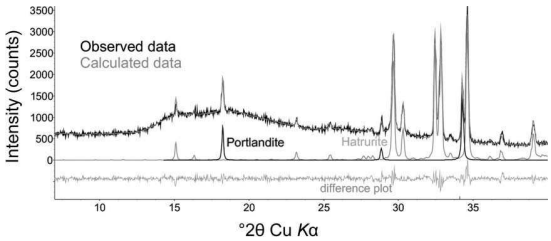

Figure 3
Rietveld refinement of a paste after 11 h hydration; water/alite ratio = 0.5; T = 310 K.

research papers

talline phases can be quantified directly from the scale factors. No error in the determination of any individual phase has any influence on the determined amounts of the other phases. In addition, the amorphous phases, namely water and the C–S–H phase, cannot be quantified using the standard Rietveld *ZMV* algorithm, which only considers the crystalline phases.

Heat-flow experiments were carried out using a commercial TAM Air calorimeter. Alite and water were equilibrated before the measurements in a calibrated heat chamber. Mixing of the alite with the water was carried out externally by means of a special mixer which allows reproducible stirring for 1 min. The samples were then put in the calorimeter. The first half-hour of the heat-flow experiments cannot be evaluated because of the disturbance of the signal caused by opening the calorimeter.

Heat-flow curves were calculated from the *in situ* XRD results (alite dissolution curves) using equation (4) (modified from Hesse *et al.*, 2011):

$$\mathrm{HF} = \frac{\partial \mathrm{wt\%\ alite}/\partial t}{100}\frac{\Delta H\mathrm{R}}{3.6}(-1), \qquad (4)$$

where $\partial \mathrm{wt\%\ alite}/\partial \mathrm{t}$ is the derivation of the alite curve from XRD *in situ* experiments, and ΔHR is the enthalpy of reaction of equation (1).

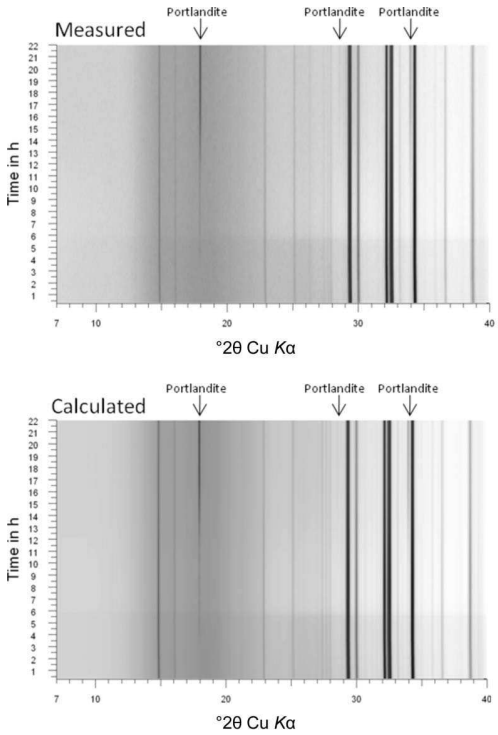

Figure 4
Level plots of all patterns measured and calculated for the system at 296 K and a water/alite ratio of 0.5. (Portlandite peaks are marked, the remaining peaks are alite peaks.)

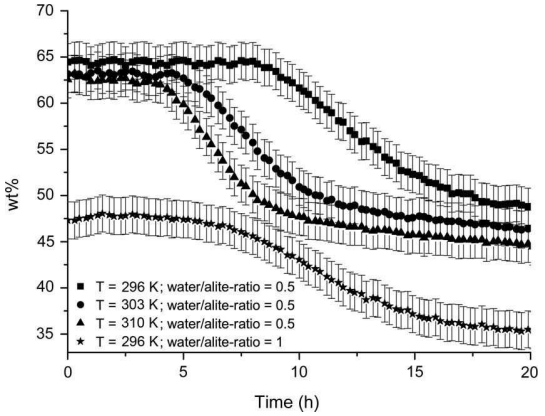

Figure 5
Content of alite in different alite/water pastes during the process of hydration.

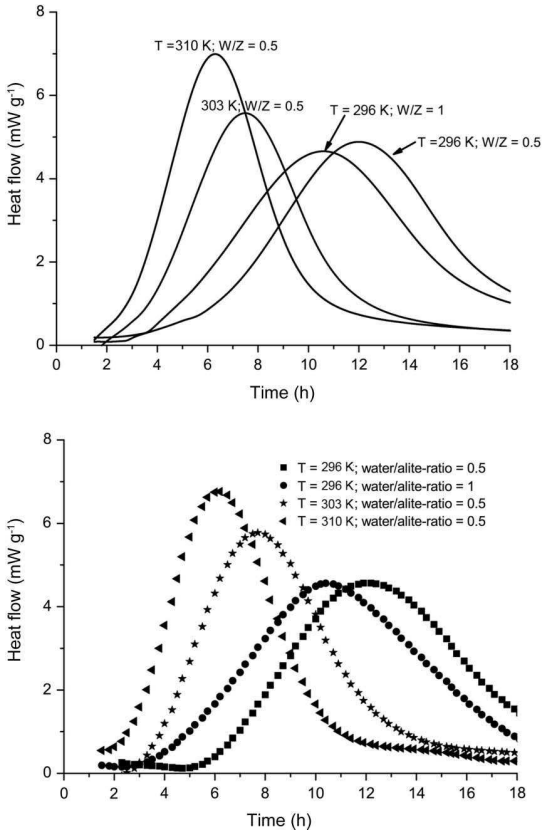

Figure 6
Measured heat flows (top) and calculated heat flows (bottom) of the alite/water pastes at different temperatures and water/alite ratios (from 1.5 h).

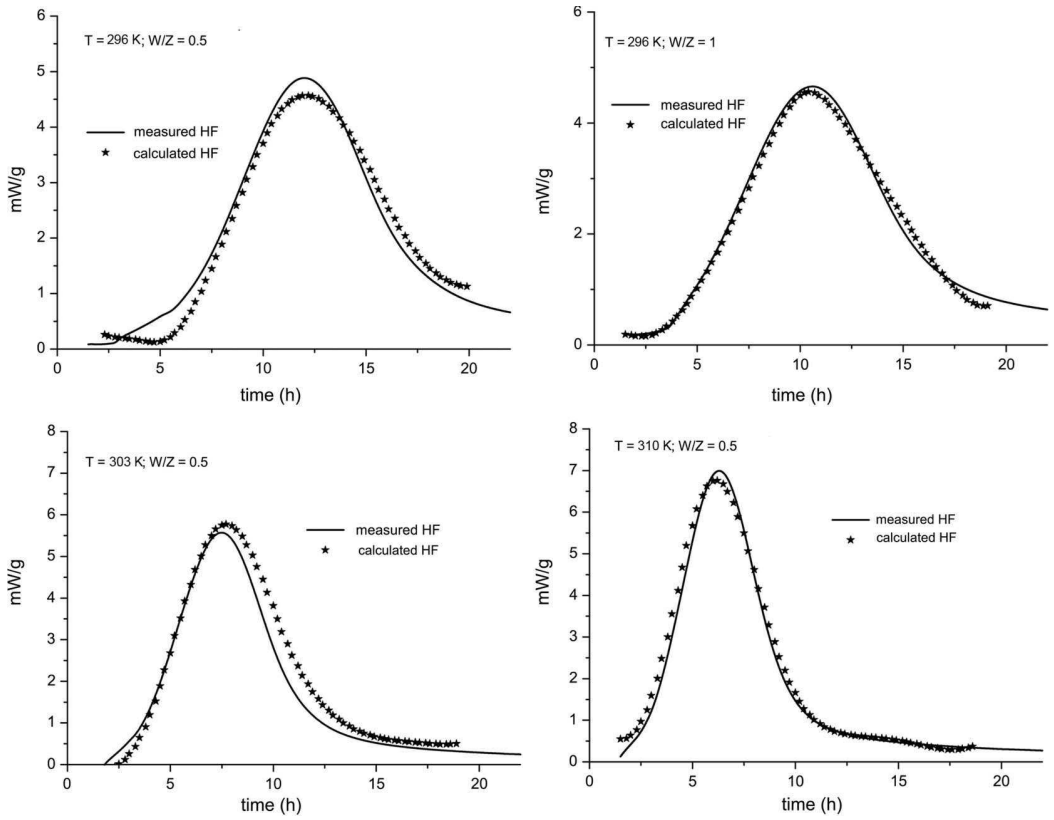

Figure 7
Comparison between measured and calculated heat flows of synthetic alite at different temperatures and water/alite ratios (from 1.5 h).

3. Results

The Rietveld refinement of the synthesized alite is shown in Fig. 2.[1] There was no sign of any phase except the alite phase. The calculation of the amount of alite using the *G* factor, which was derived from the standard material silicon, resulted in 96 (2) wt% of alite in our sample and 4 (2) wt% of amorphous or non-fitted phase. We assume that the structures used, as well as inaccurate dislocation parameters, might possibly be the reasons for the underquantification of the alite phase (Jansen, Stabler *et al.*, 2011). An amorphous, glassy phase is not verified.

The Rietveld refinement of the hydrating alite/water paste is shown in Fig. 3. There is close agreement between the intensity as observed and the intensity as calculated. The hump between 15° 2θ and 25° 2θ is created by the Kapton foil which covered the sample in order to avoid interaction with atmospheric CO_2 or water loss. The background of the Kapton foil and the water was considered using a special peaks phase model (Hesse *et al.*, 2009).

[1] Supplementary data for this paper are available from the IUCr electronic archives (Reference: CG5188). Services for accessing these data are described at the back of the journal.

Fig. 4 shows level plots of all patterns calculated and measured for the system at 296 K and a water/alite ratio of 0.5 as a function of time, representative of all measurements performed and refined. All Rietveld refinements were as good as the refinement shown in Fig. 4.

The results from the XRD *in situ* experiments are shown in Fig. 5. It can be seen that the reaction of the alite phase strongly depends on both the temperature and water/alite ratio. Since about 96 wt% of crystalline alite could be detected in the dry sample, we can expect an absolute alite content of around 64 wt% in the cement paste, when working with a water/alite ratio of 0.5. A water/alite ratio of 1 would result in an amount of 48 wt% of alite in the paste, assuming that no alite reacts immediately after mixing the alite with water. Fig. 5 shows that no dissolution of the alite phase directly after mixing could be proven by means of the *G*-factor method. This leads us to the conclusion that either no alite reacts immediately with water or only very low amounts of alite are dissolved immediately, the amounts being lower than the standard deviations of the results of our experiments (±2 wt%).

The heat-flow curves as measured and the heat-flow curves as calculated from XRD data using equation (4) are shown in

research papers

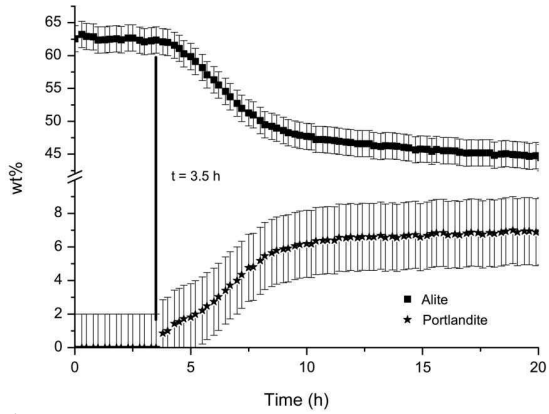

Figure 8
Quantitative phase development of alite and portlandite during the hydration of alite and water (water/alite = 0.5, T = 310 K).

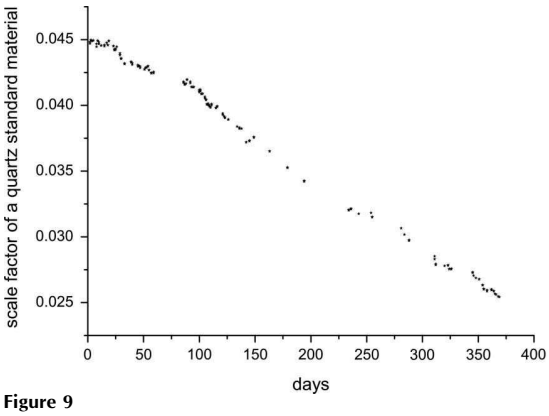

Figure 9
Development of the scale factor of a quartz standard material over time.

Fig. 6. It can be seen that the calculated heat-flow curves accord to a great extent with the measured heat-flow curves. It is a fact that slow reactions are much harder to track by X-ray experiments than fast reactions. Therefore it is not surprising that the main period of the hydration is much easier to reproduce by means of X-ray diffraction than is the induction period.

The direct comparison of the curves is shown in Fig. 7. There is close agreement between the heat-flow curves as measured and the calculated heat-flow curves evaluated using the determined alite content measured by X-ray diffraction. It can be proven that the heat-flow curve obtained from the heat-flow experiments can be explained by the hydration reaction of the alite phase. This leads us to the conclusion that the quantification method chosen for the experiments can be recommended for the quantification of hydration reactions, such as the reaction of alite with water.

The fact that the complete hydration reaction [equation (1)] can be described by the alite dissolution curve can be interpreted in two ways. The first is that all heat is released during the dissolution of the alite phase. The precipitation of portlandite and the C–S–H phase does not contribute to the heat flow that can be detected from heat-flow experiments.

Another, more likely, explanation is that the dissolution of alite and the precipitation of portlandite and the C–S–H phase take place synchronously. This makes it conceivable that the heat-flow curve of alite with water is correctly described by the dissolution of alite.

A plot of the alite curve and the portlandite curve in the same diagram also shows that the dissolution of the alite phase and the precipitation of the portlandite phase emerge synchronously. Fig. 8 shows both curves at a water/alite ratio of 0.5 and at a temperature of 310 K, representative of all experiments performed. Under these conditions, the dissolution of alite and the precipitation of portlandite begin at a point in time some 3.5 h after mixing of the reactants.

4. Conclusion

The method presented by O'Connor & Raven (1988) was a crucial step in developing a method for quantifying materials with amorphous portions. The implementation of this method for the characterization of hydration processes turned out to be very promising. It transpires that the calculation of a calibration factor G is of great practical use in the day-to-day work of a laboratory where hydration processes of materials containing crystalline phases are under examination.

It could be shown that the dissolution of alite, which was quantified by means of X-ray diffraction using the G-factor method, is suitable for characterizing the kinetics of the reaction of alite and water. The heat-flow curves obtained from heat-flow experiments could be simulated by using the quantitative XRD data for the calculation of heat-flow diagrams.

It is, however, imperative in every case that the user of the G-factor method always takes care to ensure that the right G factor is used. This is because the factor depends on the performance of the X-ray tube and the detector, and therefore strongly depends on time. As shown in Fig. 9, it is not advisable to calculate the G factor a long time before or after the point in time at which the experiment is actually performed.

The authors would like to thank Natalia Illenseer, Sebastian Klaus and Sebastian Scherb for their support during the experiments.

References

Allen, A. J., Thomas, J. J. & Jennings, H. M. (2007). *Nat. Mater.* **6**, 311–316.
De La Torre, A. G., Bruque, S., Campo, S. & Aranda, M. (2002). *Cem. Concr. Res.* **32**, 1347–1356.
Escalante-Garcia, J. I. & Sharp, J. H. (1999). *J. Am. Ceram. Soc.* **82**, 3237–3241.
Fuji, K. & Kondo, W. (1983). *J. Am. Ceram. Soc.* pp. C220–C221.
Garrault, S. & Nonat, A. (2001). *Langmuir*, **17**, 8131–8138.

Gartner, E. M. & Gaidis, J. M. (1989). *Materials Science of Concrete I*, pp. 95–125. Westerville: The American Ceramic Society.
Greaves, C. & Thomas, M. A. (1986). *Acta Cryst.* B**42**, 51–55.
Hesse, C., Degenkolb, M., Gäberlein, M., Goetz-Neunhoeffer, F., Neubauer, J. & Schwarz, V. (2008). *Cem. Int.* **6**, 68–78.
Hesse, C., Goetz-Neunhoeffer, F. & Neubauer, J. (2011). *Cem. Concr. Res.* **41**, 123–128.
Hesse, C., Goetz-Neunhoeffer, F., Neubauer, J., Braeu, M. & Gaeberlein, P. (2009). *Powder Diffr.* **24**, 112–115.
Hill, R. J. & Howard, C. J. (1987). *J. Appl. Cryst.* **20**, 467–474.
Hummel, W., Berner, U., Curti, E., Pearson, F. J. & Thoenen, T. (2002). *Nagra/PSI Chemical Thermodynamic Data Base 01/01*. Parkland: Universal Publishers/uPUBLISH.com.
Jansen, D., Goetz-Neunhoeffer, F., Stabler, C. & Neubauer, J. (2011). *Cem. Concr. Res.* **41**, 602–608.
Jansen, D., Stabler, C., Goetz-Neunhoeffer, F., Dittrich, S. & Neubauer, J. (2011). *Powder Diffr.* **26**, 31–38.
Juilland, P., Gallucci, E., Flatt, R. & Scrivener, K. (2010). *Cem. Concr. Res.* **40**, 831–844.
Kulik, D. (2010). *GEMS-PSI* 3.0 2010, PSI-Villingen, Switzerland, http://gems.web.psi.ch.
Lasaga, A. C. & Luttge, A. (2001). *Science*, **291**, 2400–2404.
Livingston, R. A., Schweitzer, J. S., Rolfs, C., Becker, H. W., Kubsky, S., Spillane, T., Zickefoose, J., Castellote, M., de Viedma, P. G. & Cheung, J. (2010). *Appl. Radiat. Isot.* **68**, 683–687.
Locher, F. W. (1967). *Zement-Kalk-Gips*, **20**, 402–407.
Lothenbach, B., Matschei, T., Möschner, G. & Glasser, F. P. (2008). *Cem. Concr. Res.* **38**, 1–18.
O'Connor, B. H. & Raven, M. D. (1988). *Powder Diffr.* **3**, 2–6.
Pelletier, L., Winnefeld, F. & Lothenbach, B. (2009). *Tagungsbericht 17. Internationale Baustofftagung, Weimar*, 1-0277-1-0282. Weimar: F. A. Finger-Institut für Baustoffkunde.
Peterson, V. K. & Whitten, A. E. (2009). *J. Phys. Chem. C*, **113**, 2347–2351.
Pöllmann, H., Fylak, M. & Wenda, R. (2009). *Tagungsbericht 17. Internationale Baustofftagung, Weimar*, 1-0161-1-0176. Weimar: F. A. Finger-Institut für Baustoffkunde.
Prince, E. (2004). Editor. *International Tables for Crystallography*, Vol. C. Dordrecht: Kluwer.
Richardson, I. G. (1999). *Cem. Concr. Res.* **29**, 1134–1147.
Rietveld, H. M. (1969). *J. Appl. Cryst.* **2**, 65–71.
Rodgers, S. A., Groves, G. W., Clayden, N. J. & Dobson, C. M. (1988). *J. Am. Ceram. Soc.* **71**, 91–96.
Schreyer, M., Guo, L., Tjahjono, M. & Garland, M. (2011). *J. Appl. Cryst.* **44**, 17–24.
Scrivener, K. L., Füllmann, T., Gallucci, E., Walenta, G. & Bermejo, E. (2004). *Cem. Concr. Res.* **34**, 1541–1547.
Stein, H. N. & Stevels, J. M. (1964). *J. Appl. Chem.* **14**, 338–346.
Thoenen, T. & Kulik, D. (2003). Nagra/PSI Chemical Thermodynamic Database 01/01 for the *GEM-Selektor* (V.2-PSI) Geochemical Modelling Code. Villingen, Switzerland.
Thomas, J. J. (2007). *J. Am. Ceram. Soc.* **90**, 3282–3288.
Thomas, J. J., Allen, A. J. & Jennings, H. M. (2009). *J. Phys. Chem. C*, **113**, 19836–19844.
Többens, D. M., Stuesser, N., Knorr, K., Mayer, H. M. & Lampert, G. (2001). *Mater. Sci. Forum*, pp. 378–381.
Westphal, T., Füllmann, T. & Pöllmann, H. (2009). *Powder Diffr.* **21**, 239–243.

7.2. In-situ XRD phase analysis of the early hydration of alite: time resolved quantification of the poorly crystalline C-S-H gel

Reprint

Published in Tagungsbericht 18. Internationale Baustofftagung, Weimar,
F.A. Finger-Institut für Baustoffkunde (2012) 1-0261 – 1-0267,
ISBN 978-3-00-034075-8.

Authors: S. T. Bergold, F. Goetz-Neunhoeffer, and J. Neubauer

Bergold, S.T., Goetz-Neunhoeffer, F., Neubauer, J.

In-situ XRD phase analysis of the early hydration of alite: time resolved quantification of the poorly crystalline C-S-H gel

Abstract

The results of a study of the early hydration of monoclinic (MgO- and Al_2O_3- doped) alite will be presented. It is shown, that the development of the phases alite, portlandite and also of the poorly crystalline C-S-H gel can be followed quantitatively over time. A C-S-H gel model was refined and the resulting scale factor was scaled up to the expected C-S-H gel content according to an assumed silicate reaction described by [1].

Introduction

[1] showed, that the kinetic of the silicate reaction as measured can be followed by quantitative in-situ X-ray diffraction by the assumption, that the silicate reaction can be described by Equation 1 [1] and the use of the external standard method from [2]. As it can be seen in Figure 1, it was possible to calculate the heat from the dissolution of alite determined by XRD [1].

$$1\ C_3S + 3.9\ H \rightarrow 1\ C_{1.7}SH_{2.6} + 1.3\ CH;\quad \Delta H = -561\ J/g \qquad \text{Equation 1}$$

This study is intending to show, that the evolution of the poorly crystalline C-S-H gel can be followed quantitatively over time by in-situ XRD and scale factor method.

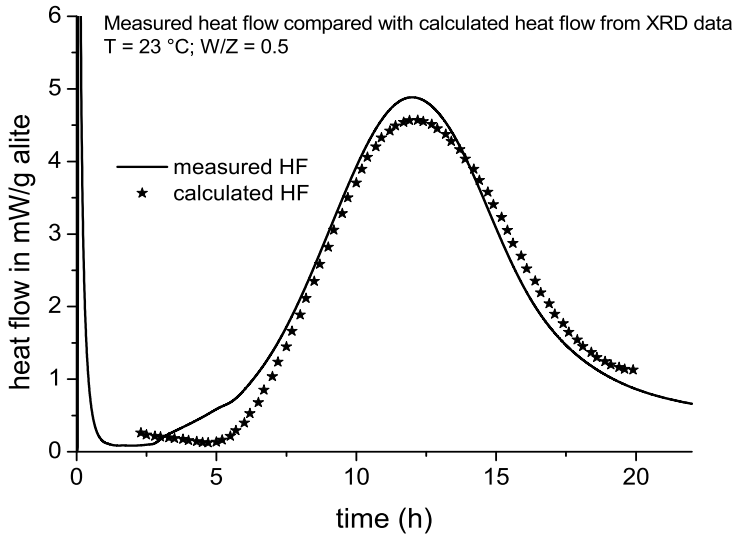

Figure 1: Comparison between measured heat flow by calorimetry and calculated one determined from the dissolution of alite detected by XRD [1].

Materials and Methods

The monoclinic M3 form of alite was synthesized according to [1]. The specific surface area was determined to be 0.29 m^2/g by Blaine method. The hydration of alite was investigated by in-situ paste X-ray diffraction which was performed on a D8 Advance from BRUKER-AXS equipped with a LynxEye detector. Copper Kα radiation was used at 40 kV and 40 mA. A diffractogram was taken every 15 minutes for 22 h from 7 to 40 ° 2 Θ with a counting time of 0.58 s per 0.0236 ° 2 Θ. The samples were covered with Kapton polyimide film to avoid interaction of the sample with the atmosphere. The alite was mixed with water using a water to alite ratio of 0.5 at the beginning of the measurements. The sample holder was equipped with a special heating and cooling device [3] to ensure a constant temperature of the sample of 23 °C. The quantitative analysis was performed with the Rietveld software TOPAS 4.2 from BRUKER-AXS and the G-factor method as recently revised for the use for in-situ paste experiments by [4].

For C-S-H gel, a Pawley fit was modelled on an alite-water mix which was fully hydrated with only the phases portlandite and C-S-H gel present. For the quantitative analysis of the in-situ patterns, a peaks phase model for the covering Kapton film and the free water together with a Chebychev polynomial of 1st order was used to describe the background of the diffractograms. The structure data of [5] and [6] were used for

alite and portlandite, respectively. For the calibration of C-S-H content, the scale factor of the C-S-H gel after 22 h was scaled up to the expected weight content of C-S-H gel determined from Equation 1 according to the differences of alite content at the beginning of the measurements and the alite content after 22 h.

Results and Discussion

As presented in Figure 2, the evolution with time of all phases present in the alite paste can be followed. The quantification of portlandite is most problematic, because it developed very strong spottiness, which led to a too low determination of portlandite in comparison to the expected portlandite content after 22 h calculated from the alite dissolution according to Equation 1. The spottiness could not be refined correctly with preferred orientation, which finally makes the quantification very uncertain. Because of the use of the G-factor method, this has no influence on the alite or C-S-H gel quantification. Interesting is, that the first portlandite is precipitating before any C-S-H gel can be detected by XRD. The precipitation of the C-S-H gel and the dissolution of alite are matching very well to each other. When the first dissolution of alite is detected, the precipitation of C-S-H gel is starting.

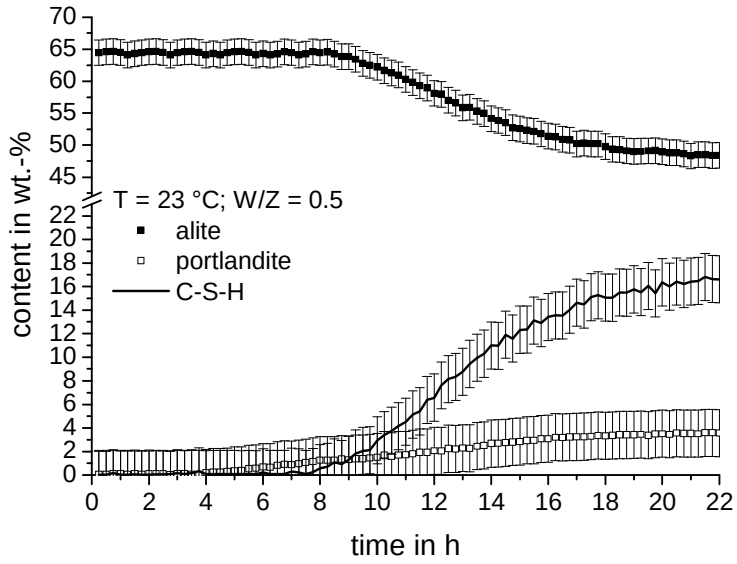

Figure 2: Quantitative phase analysis of the hydration of alite with water at 23 °C and w/a = 0.5.

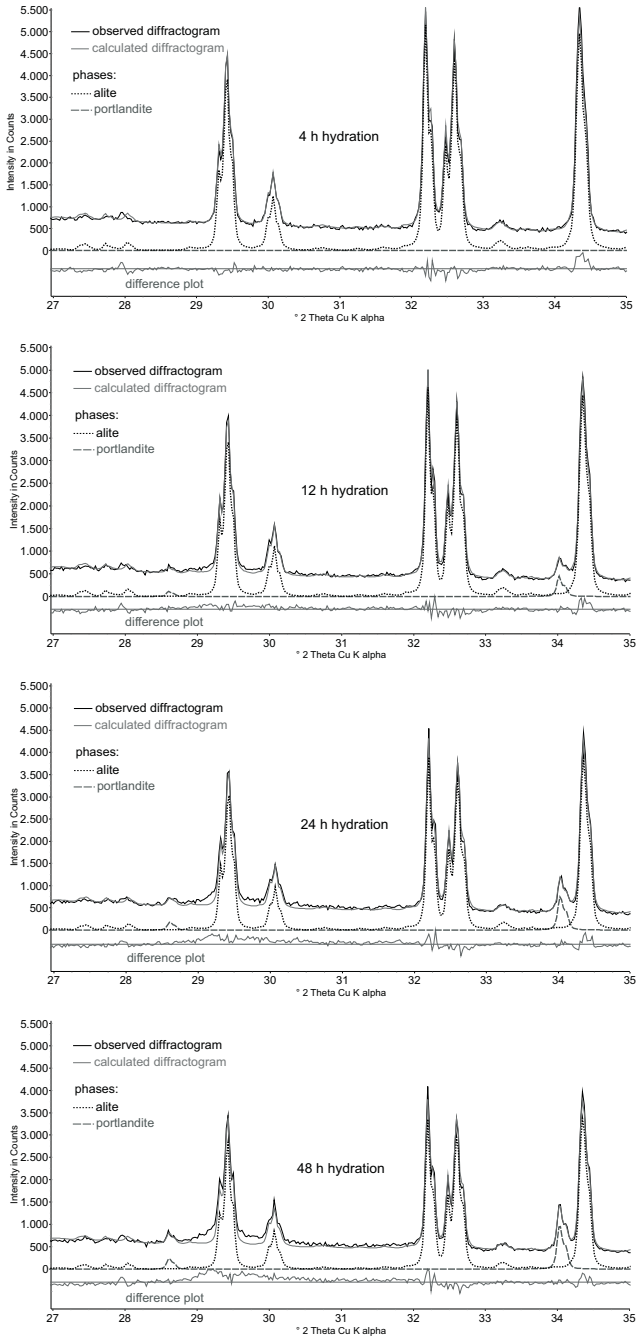

Figure 3: Section of XRD patterns of a hydrating alite paste at w/a = 0.5 and 23 °C measured to 48 h hydration analyzed without the C-S-H gel model.

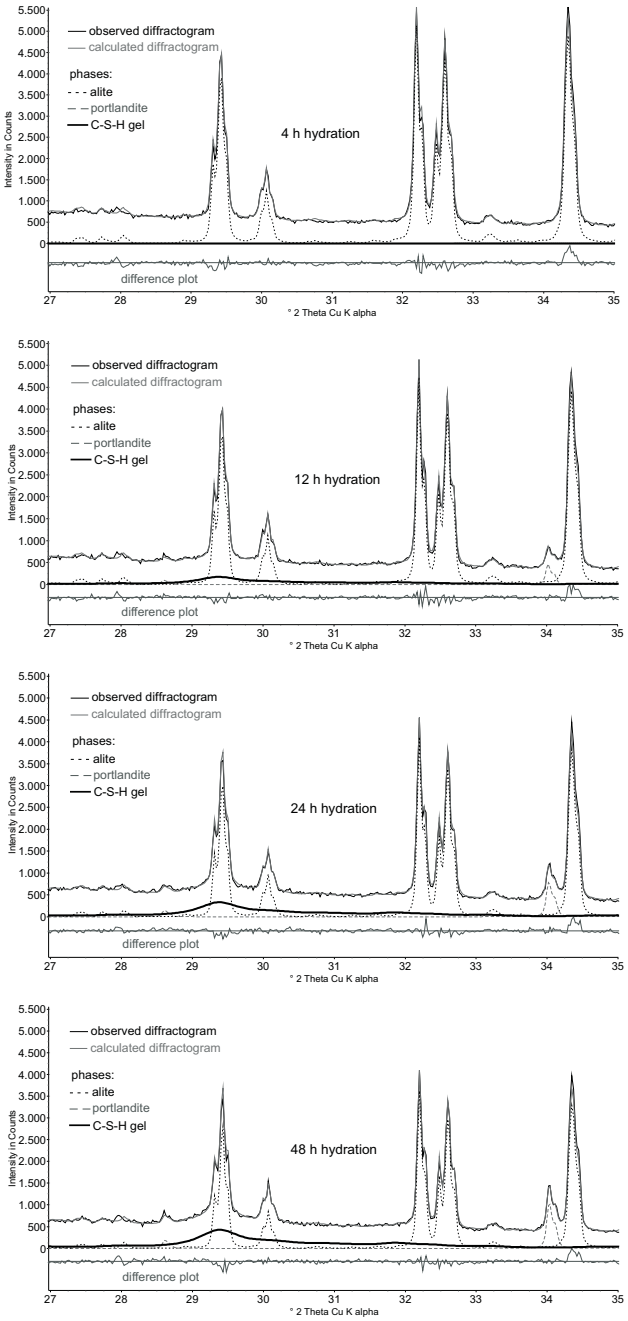

Figure 4: Section of XRD patterns of a hydrating alite paste at w/a = 0.5 and 23 °C measured to 48 h hydration analyzed with C-S-H gel model.

In Figures 3 and 4 the analysis of in-situ XRD patterns from an investigation of alite hydration of up to 48 h is shown in the range of 27 to 35 ° 2 Θ. The same diffractograms are shown in both figures, in Figure 2, when the C-S-H gel model was not refined, to highlight that the C-S-H gel is detected by XRD in the early hydration of alite pastes. As it can be seen, from 12 h of hydration on, a misfit between the measured and the calculated diffractograms becomes obvious especially around the alite reflections between 29 and 30 ° 2 Θ. This miscalculated part of the diffractogram can be assigned to C-S-H gel as is shown in Figure 4, where the same diffractograms are presented with the C-S-H gel model refined. In this case, the evolution of the C-S-H gel can be followed very well.

Since the up-scaling of the C-S-H gel underlies the assumption of Equation 1 to describe the silicate reaction correctly, the real quantification of C-S-H gel as shown here could represent a too high or too low determination. Also the accurate quantification of alite was important since the up-scaling factor was calculated for every experiment according to the alite decrease during the experiment. The evolution of the C-S-H gel itself is not affected by this.

Conclusion

The quantitative phase in-situ XRD of the early hydration of alite presented at [1] was extended to the quantitative analysis of the development of C-S-H gel. It can be seen, that the alite dissolution starts at about 7.5 h. The precipitation of portlandite could be detected from 4 h on. The formation of C-S-H gel proceeds contemporaneously and synchronously with the dissolution of alite.

Literature

[1] Jansen, D., Bergold, S.T., Goetz-Neunhoeffer, F., Neubauer, J., The hydration of alite: a time resolved quantitative X-ray diffraction approach using G-factor method compared with heat release, J. Appl. Crystallogr. 44 (5) (2011) 895–901.

[2] O'Connor, B.H., Raven, M.D., Application of the Rietveld refinement procedure in assaying powdered mixtures, Powder Diffr. 3 (1) (1988) 2-6.

[3] Hesse, C., Degenkolb, M., Gäberlein, P., Goetz-Neunhoeffer, F., Neubauer, J., Schwarz, V., Investigation into the influence of temperature and w/c-ratio on the early hydration of white cement, Cement International (2008) 68-78.

[4] Jansen, D., Goetz-Neunhoeffer, F., Stabler, C., Neubauer, J., A remastered external standard method applied to the quantification of early OPC hydration, Cement Concrete Res. 41 (2011) 602–608.

[5] De La Torre, A.G., Bruque S., Campo, J., Aranda, M.A.G., The superstructure of C_3S from synchrotron and neutron powder diffraction and its role in quantitative phase analyses, Cement Concrete Res. 32 (2002) 1347–1356.

[6] Busing, W.R., Levy, H.A., Neutron Diffraction Study of Calcium Hydroxide, J. Chem. Phys. 26 (3) (1957) 563–568.

Contact:

Dipl.-Min. Sebastian T. Bergold bergold@geol.uni-erlangen.de
Prof. Dr. Jürgen Neubauer juergen.neubauer.gzn@me.com
Friedrich-Alexander Universität Erlangen-Nürnberg
GeoZentrum Nordbayern, Mineralogie Erlangen
Schlossgarten 5a
91054 Erlangen

7.3. Development of C-S-H during the early hydration of alite with water at different temperatures: direct quantification by in-situ XRD

Reprint

Published in Monographie zur Tagung Bauchemie 2012, Dübendorf/Schweiz,
Vol. 45, 91-96, Gesellschaft Deutscher Chemiker e. V., Frankfurt am Main,
ISBN 978-3-936028-72-0.

Authors: S. T. Bergold, D. Jansen, S. Dittrich, S., F. Goetz-Neunhoeffer, and J. Neubauer

Development of C-S-H during the early hydration of alite with water at different temperatures: direct quantification by in-situ XRD

Bergold, S.T., Jansen, D., Dittrich, S., Goetz-Neunhoeffer, F., Neubauer, J.

Mineralogy, GeoZentrum Nordbayern, University Erlangen-Nuernberg, Schlossgarten 5a, 91054 Erlangen, Germany

Abstract

The early hydration of monoclinic alite at different curing temperatures was investigated by in-situ X-ray diffractometry. It could be shown from /1/ and /2/ that by the use of the G-factor method as external standard method /3/, the quantification of the crystalline alite in pastes can be performed very well. This was possible even though amorphous and poorly crystalline phases - e.g. water and C-S-H - are present. In this study, it is shown that in-situ XRD is not limited to the quantitative analysis of crystalline phases like alite and portlandite. It is also possible to analyse the poorly crystalline C-S-H phase forming within the paste quantitatively. A phase model was developed, which makes it possible to quantify C-S-H directly via scale factor method without the need to know the exact structure of the colloidal C-S-H. The possibility to directly analyse C-S-H elevates the informative value of in-situ XRD for paste experiments. Portlandite seems to form few big crystals, which makes it hard to analyse it quantitatively.

Introduction

The early hydration of alite is still an issue in spite of the long lasting scientific discussion of this task. In last years' monograph /1/ and Jansen et al. /2/ it was shown, that the use of the G-factor method from O'Connor & Raven /3/ enables the quantification of the phase development of alite within alite pastes without the need to take into

account portlandite and C-S-H gel, nor the XRD amorphous water. The heat flow detected by calorimetry could also be calculated from the decrease of alite very well. Nevertheless, it is very interesting, that especially the poorly crystalline C-S-H can be directly followed by in-situ XRD as well.

Materials and methods

The alite for the investigation was synthesized as described in /1/. X-ray diffractometry was performed at a D8 Advance equipped with LynxEye detector. A diffractogram was taken every 15 min from 7 to 40° 2Θ with a time of 0.58 s per 0.0236° 2Θ step at 40 kV and 40 mA over 22 h of hydration. The diffractometer was equipped with a temperature device, allowing in-situ measurements at defined temperatures (23, 30 and 37 °C in that case). The alite samples were stirred manually by spatula for 1 minute at the beginning of the measurement, transferred into the sample carrier and covered by a KAPTON film. A water to alite ratio of 0.5 was used for all measurements.

The quantitative analysis of the diffractograms was performed with the Rietveld-software TOPAS 4.2 from BRUKER-AXS followed by the calculation of absolute phase contents using the G-factor method of O'Connor & Raven /3/ as it is shown in Jansen et al. /4/. Besides the structure proposals for alite /5/ and portlandite /6/, a Pawley fit for the C-S-H phase - based on a 1.4 nm tobermorite with the space group F2dd from Richardson /7/ - was used for refinement. The background of the diffractograms was refined with a Chebychev polynomial of 1st order and with models for the increased background due to water and KAPTON film. From the scale factors obtained from Rietveld analysis, the content of C-S-H was calculated by fitting C-S-H after 22 h hydration to the C-S-H content in the paste which could be expected with respect to the decrease of alite. With the thus received factor, all scale factors of C-S-H within one measurement were multiplied. The expected amount of C-S-H precipitation was calculated according to the silicate reaction (equation 1 in /2/).

Results and Discussion

The quantitative phase development of the hydrating alite pastes at 23, 30 and 37 °C analysed by in-situ XRD are shown in Figure 1, representing average values of at least three independent measurements with error bars of the standard deviation. In the dry alite sample, a content of about 96 wt.-% crystalline alite could be detected. Since a water to alite ratio of 0.5 was used in this study, an alite content of 64 wt.-% can be expected in the paste, assuming that alite did not start to dissolve during first contact with water. The alite content at the start of hydration ranges between 62-63 wt.-% alite (Figures 1 and 2a). Within the analytical error, only few or no alite is dissolved within the first few hours. Then, following the phase development as shown in Figure 1, alite starts to dissolve depending on the temperature adjusted. After dissolution of small amounts of alite the precipitation of C-S-H can be detected. As soon as C-S-H can be detected, the dissolution of alite

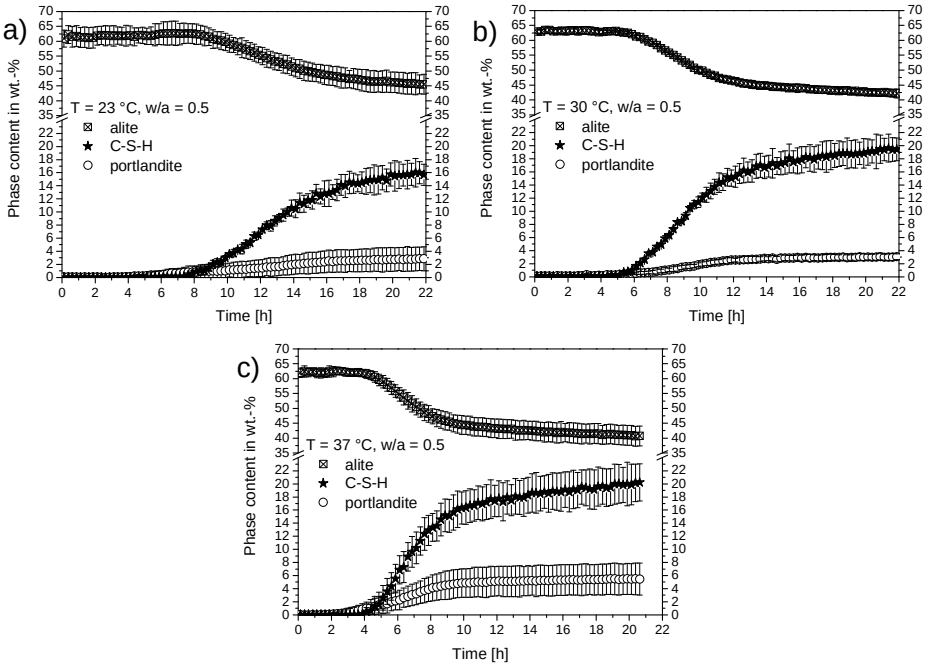

Figure 1: Phase development within hydration alite pastes at a water/alite ratio of 0.5 and 23 °C (a), 30 °C (b) and 37 °C (c) detected by in-situ XRD.

is accelerated. The period of accelerated alite dissolution and C-S-H precipitation is followed by a slowing down of both, whereafter alite dissolution and C-S-H precipitation are running continuously on low levels.

As can be seen in Figure 1, the described course of reaction is similar for all investigated temperatures. Only the start of the precipitation of C-S-H and the dissolution of alite is shifted to earlier times for higher temperatures (Figure 2). The comparison of the phase development of the single phases at different temperatures (Figure 2) shows that the amount of alite dissolved increases with higher temperatures. The phase development of C-S-H is not corresponding directly with alite dissolution, so the direct quantification of C-S-H provides new information.

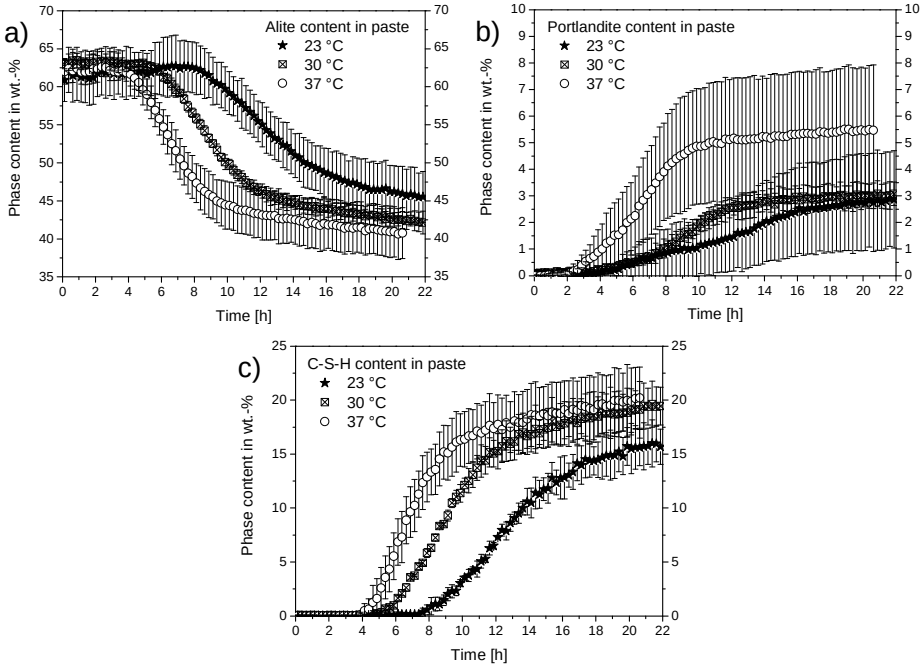

Figure 2: Comparison of the phase development of alite (a), C-S-H (b) and portlandite (c) during hydration of alite paste at 23, 30 and 37 °C and a water/alite of 0.5.

The phase development of portlandite is not perfectly described by in-situ XRD analysis. At all temperatures portlandite can be detected before precipitation of C-S-H and the visible dissolution of alite. But the quantitative amount of portlandite in the developing paste is less than expected when assuming Equation 1 in /2/. Its misfit is huge with respect to the determined amount (Figure 2b). The problem of analysing portlandite in the pastes can be explained by 2-dimensional XRD. In Figure 3 a 2-dimensional diffractogram of an alite paste after 24 h of hydration at 23 °C and water/alite of 0.5 is shown. The continuous diffraction rings representing the phase alite can be observed. For portlandite only few individual dots appear. So Figure 3 suggests the growth of few big portlandite individuals. The white lines mark the in-formation, a 1-dimensional detector as it was used in this study is able to detect.

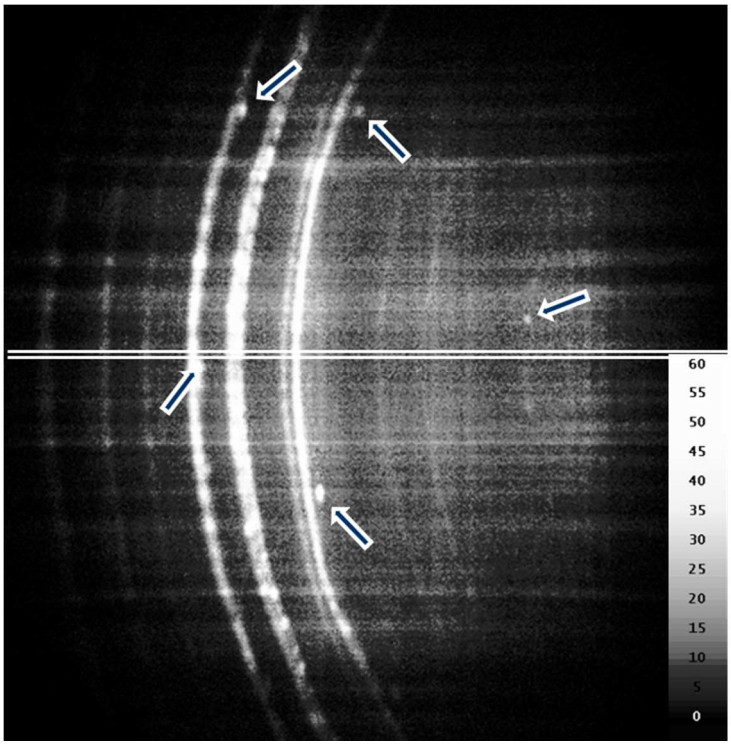

Figure 3: 2-dimensional XRD image of hydrated alite paste after 24 h of hydration. The continuous diffraction rings are caused by alite, Portlandite can be seen as individual dots marked with white arrows. The white lines show the information, a 1-dimensional detector is able to detect.

It is obvious, that the information within the white line will not be sufficient to describe the quantitative phase content of portlandite correctly.

Literature

/1/ Bergold, S. T., Jansen, D., Goetz-Neunhoeffer, F., Neubauer, J.:
„Vergleich von Wärmeflusskalorimetrie und quantitativer in-situ XRD nach der G-Faktor Methode am Beispiel der Hydratation von Alit“
GDCh-Monographie (2011) 44 (Tagung Bauchemie 2011), 165-170.

/2/ Jansen, D., Bergold, S. T., Goetz-Neunhoeffer, F., Neubauer, J.:
„The hydration of alite: a time resolved quantitative X-ray diffraction approach using G-factor method compared with heat release”
J. Appl. Crystallogr. (2011) 44 (5), 895-901.

/3/ O’Connor, B. H., Raven, M. D.:
“Application of the Rietveld refinement procedure in assaying powdered mixtures“
Powder Diffr. (1988) 3 (1), 2-6.

/4/ Jansen, D., Goetz-Neunhoeffer, F., Stabler, C., Neubauer, J.:
“A remastered external standard method applied to the quantification of early OPC hydration”

Cement Concrete Res. (2011) 41, 602–608.

/5/ De La Torre, A. G., Bruque, S., Campo, S., Aranda, M.:
“The superstructure of C_3S from synchrotron and neutron powder diffraction and its role in quantitative phase analyses”
Cement Concrete Res. (2002) 32, 1347–1356.

/6/ Busing, W. R., Levy, H. A.:
“Neutron Diffraction Study of Calcium Hydroxide”
J. Chem. Phys. (1957) 26 (3), 563–568.

/7/ Richardson, I.G.: “The calcium silicate hydrates”
Cement Concrete Res. (2008) 38, 137–158.

7.4. Quantitative analysis of C-S-H in hydrating alite pastes by in-situ XRD

Reprint

Published in the Journal “Cement and Concrete Research”
Vol. 53 (2013) 119-126, doi: 10.1016/j.cemconres.2013.06.001

Authors: S. T. Bergold, F. Götz-Neunhoeffer, and J. Neubauer

Cement and Concrete Research 53 (2013) 119–126

Contents lists available at SciVerse ScienceDirect

Cement and Concrete Research

journal homepage: http://ees.elsevier.com/CEMCON/default.asp

Quantitative analysis of C–S–H in hydrating alite pastes by in-situ XRD

S.T. Bergold *, F. Goetz-Neunhoeffer, J. Neubauer *

Mineralogy, GeoZentrum Nordbayern, University Erlangen-Nuernberg, Schlossgarten 5a, 91054 Erlangen, Germany

ARTICLE INFO

Article history:
Received 20 September 2012
Accepted 3 June 2013
Available online xxxx

Keywords:
Calcium–silicate–hydrates (C–S–H)
X-ray diffraction (B)
Ca_3SiO_5 (D)
Calorimetry (A)
Hydration (A)

ABSTRACT

In this study about the early hydration of monoclinic alite, a method is presented that allows to follow the formation of the Calcium–Silicate–Hydrates directly and quantitatively over time. The combination of the PONKCS method [20] and the G-factor method [6] allowed the refinement and calibration of a C–S–H phase model which can be used for direct quantification of C–S–H in cementitious pastes.
The comparison between the heat flow measured by calorimetry and the heat flow calculated from the phase development of C–S–H revealed that C–S–H formation starts later than is indicated by the measured heat flow. It is therefore assumed that the silicate reaction proceeds the following way: A not XRD-detectable C–S–H phase is precipitated which then evolves into a long-range ordered, XRD-detectable C–S–H. This C–S–H acts as a nucleation site for further long-range ordered C–S–H and leads to the acceleration of alite dissolution and direct formation of C–S–H.

1. Introduction

The quantitative phase analysis of hydrating cement pastes by in-situ XRD proved to be an ideal way of linking the phase development of the cement paste to the hydration kinetics detected by heat flow calorimetry, as previously shown [1–4]. Hesse et al. [1] used Rietveld refinements where the quantitative results were calculated by the ZMV algorithm of Hill and Howard [5]. This ZMV algorithm normalizes all refined phases to 100 wt.%. Phases present in the sample which are undetectable, or only barely detectable by in-situ XRD, such as unbound water and the Calcium–Silicate–Hydrates (C–S–H), had to be calculated with respect to several assumptions to arrive at the true phase content of the crystalline phases in the paste [1]. Jansen et al. [2–4] have proven that the external standard method of O'Connor and Raven [6] is of enormous potential for in-situ paste experiments, since they demonstrated that the phase content of the crystalline phases can be calculated by the G-factor method directly, once the chemical composition of the sample is known. It is therefore not necessary, when using this method, to account for XRD amorphous phases present in the sample, since these latter do not affect the quantification of the other phases. It was shown [2] that the heat flow measured in calorimetric experiments bearing on the early hydration of alite can be calculated from the decrease of alite within the paste, assuming the hydration of alite to proceed according to the following equation (Eq. (1)) [2]:

$$C_3S + 3.9\ H \rightarrow C_{1.7}SH_{2.6} + 1.3\ CH. \quad (1)$$

The exact reaction kinetics of the silicate reaction is still a matter of discussion. The formation of C–S–H, especially, is still the topic of much debate. There seems to be a consensus that C–S–H displays a preference for nucleating on alite surfaces. The nuclei thus emerging then grow, in a next step, to cover the alite surface and the pore space between the particles (e.g. [7–9]). Jennings [10,11] has proposed that C–S–H "globules", which are non-spherical C–S–H basic units, would form two different packing densities of C–S–H as hydration progressed. This colloidal model for C–S–H seems to be confirmed by the results of the nanoindentation measurements of Constantinides and Ulm [12] and the results of Bishnoi and Scrivener, who showed that they could simulate the deceleration period by assuming a loosely packed C–S–H at the beginning of hydration the density of which would then increase as hydration progressed [8]. Thomas et al. [13] showed that the presence of C–S–H stimulates its own formation. They argued that the autocatalytic process of C–S–H formation would technically represent a nucleation process. But with respect to the macroscopic kinetics, this process could be described as a process of the growth of C–S–H [13].

The investigation of C–S–H via X-ray diffraction is, generally speaking, difficult because C–S–H forming in cementitious pastes typically displays no long-range ordering of its atoms [14] and therefore does not offer any defined Bragg reflections like crystalline materials. Nevertheless, C–S–H does possess a nanostructure, as the summarizing article of Richardson shows [15]. This nanostructure will be different, however, depending on the time of hydration, since the mean chain length of silicate tetrahedrons is two in young pastes and five in mature pastes [15]. Because of this nanostructure, C–S–H shows very broad peaks in X-ray diffractograms, as can be seen, for example, in a study published by Mohan and Taylor [16]. The aim of this study is to show that, in spite of these problems, the phase development of poorly-crystalline C–S–H can be followed quantitatively via XRD.

* Corresponding authors. Tel.: +49 9131 85 23986; fax: +49 9131 85 23734.
E-mail addresses: sebastian.bergold@fau.de (S.T. Bergold), juergen.neubauer@fau.de (J. Neubauer).

0008-8846/$ – see front matter © 2013 Elsevier Ltd. All rights reserved.
http://dx.doi.org/10.1016/j.cemconres.2013.06.001

2. Materials and methods

2.1. Materials

For the investigations, the monoclinic M3 form of tricalcium silicate was synthesized. $CaCO_3$, SiO_2 and Al_2O_3 from ALPHA AESAR and MgO from MERCK were weighted in to achieve an alite composition of 75.1 wt.% CaO, 25.9 wt.% SiO_2, 0.6 wt.% Al_2O_3 and 1.8 wt.% MgO according to Regourd [17]. The mixture was homogenized and milled in a vibratory disk mill (agate tool), decalcinated at 1000 °C and sintered three times at 1400 °C in Pt crucibles for 4 h in a chamber furnace in air. The furnace was calibrated with a Pt/Rh30 − Pt/Rh70 thermocouple which had itself been calibrated by the melting point of gold (1064.4 °C) according to IPTS-68. The powder was checked for phase purity by XRD and milled to a specific surface of 0.3 $m^2\ g^{-1}$ determined by the BLAINE method. The particle size distribution measured by laser granulometry using a Mastersizer 3000 from MALVERN is given in Fig. 1.

2.2. Methods

The heat flow calorimetry was performed with a TAM Air calorimeter from TA INSTRUMENTS at 23 °C ± 0.2 °C and a water-to-solid ratio (w/s) of 0.5. The samples were mixed with water in the air-conditioned calorimeter room at 23 °C, stirred for 1 min with a spatula at the beginning of the measurement, and placed in the calorimeter.

In-situ X-ray diffraction was performed using a D8 Advance diffractometer equipped with a LynxEye detector. The power generator operated at 40 kV and 40 mA. Cu Kα radiation was used. Alite was mixed with water, stirred for 1 min, prepared into a PVC sample-holder, and covered with a KAPTON polyimide film so as to minimize water loss and CO_2 contamination of the specimen. The sample-holder was equipped with a custom-made heating and cooling device [18] which ensured a constant temperature of 23 °C ± 0.2 °C. During the in-situ experiments, one diffractogram was recorded every 10 min, up to 46 h, with a range from 7° to 55° 2Θ and a step-width of 0.0236° 2Θ. The Rietveld refinement was performed using the software TOPAS 4.2 from BRUKER-AXS using the fundamental parameter approach. For quantitative analysis of the phases the G-factor method was applied (Eq. (2), [6,19]). Silicon (standard reference material 640d from NIST) was used to calibrate the factor G. In the case of in-situ experiments, where the samples were covered with Kapton film, the standard material for the determination of the factor G was covered with Kapton film as well.

2.3. Application of PONKCS to the external standard method

The PONKCS method of Scarlett and Madsen [20] provides the possibility of analyzing materials with "partial or no known crystal structure" quantitatively by XRD without having to perform a crystal structure analysis beforehand. As Madsen et al. [21] explicitly show, the PONKCS method can be used for the direct quantification of materials which are almost XRD-amorphous due to their nanocrystallinity. So called "peaks phases" or Pawley fits can be built and calibrated with samples of the particular phase of interest, with a known amount of internal standard added [20].

The application of the PONKCS method in the form in which it is presented by Scarlett and Madsen [20] to in-situ paste experiments is a difficult matter, since the latter use their method in combination with the ZMV algorithm of Hill and Howard [5], which is not the method of choice for paste experiments, as was shown previously [2–4]. The adaption, however, of the PONKCS method to the G-factor method is very easy, since only the parameters that are necessary to calibrate the phase model change. Scarlett and Madsen [20] showed that it is possible to calibrate the factors that are normally determined by the crystal structure, thus achieving a kind of phase constant. The external standard method of O'Connor and Raven [6], that was recently revised as G-factor method by Jansen et al. [19] is based on Eq. (2):

$$c_p = \frac{s_p \cdot \rho_p \cdot V_p^2 \cdot \mu^*_{sample}}{G} \tag{2}$$

where:

c_p	phase content of phase p in wt.%,
s_p	scale factor of phase p,
ρ_p	density of phase p,
V_p	Volume of the unit cell of phase p,
μ^*_{sample}	mass attenuation coefficient of the bulk sample
G	device parameter, that has to be calibrated on a standard material.

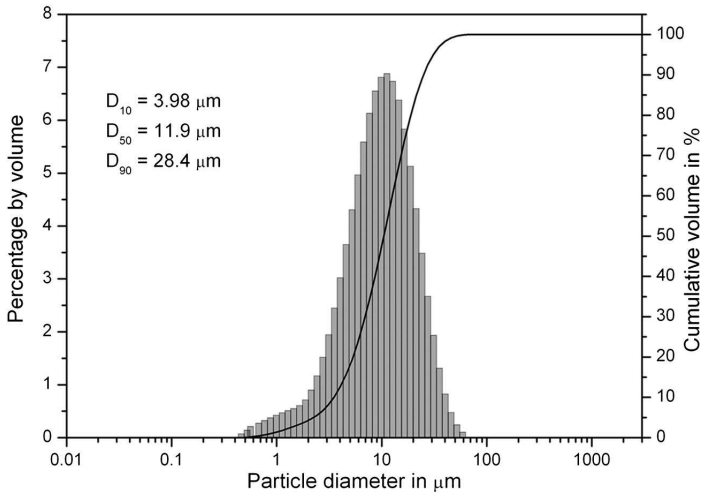

Fig. 1. Particle size distribution of the synthesized alite measured in 2-propanol by laser granulometry using a Mastersizer 3000 from MALVERN.

It follows that, for the use of a phase model in combination with the G-factor method, the phase density ρ_p and the volume of the unit cell V_p have to be calibrated by determining the calibration factor F (Eq. (3)).

$$F = \left(\rho_p \cdot V_p^2\right). \quad (3)$$

2.4. Modeling of the non-phase-specific background of experimental in-situ XRD data

It proved to be vitally necessary, in order to achieve optimized quantification of C–S–H, to meticulously control the background fit of the diffractograms used, since C–S–H forms only poorly crystalline aggregates. This means that a misfit in the background can have a huge impact on the quantification. Fig. 2 shows a diffractogram of an alite paste after 1 h hydration at 23 °C and a w/s of 0.5. The Kapton film covering the sample and the unbound water inside the sample cause an increased background between 12–25° 2Θ and 20–35° 2Θ, respectively. For the computation of the in-situ experiments three models for an optimized background fit were needed:

2.4.1. Kapton film model

A Pawley fit was used to simulate the increased background caused by the Kapton film. For the modeling of the Kapton film several CaF_2 samples were measured using XRD covered with Kapton film. The cubic CaF_2 shows only 8 reflections in the 2Θ range from 7 to 80° 2Θ and makes it possible to reproduce the shape of the background induced by the Kapton film in a refined model without being influenced by the reflections of CaF_2. The advantage of the use of CaF_2 is that it results in a more comparable background to alite pastes than is the case with the silicon single crystal which was used before [22]. Additionally, knowing the position of the CaF_2 reflections makes it possible to refine correctly the position of the Kapton film within the diffractogram. The diffractograms were refined coupled using the structure proposal for CaF_2 from Strel'tsov et al. [23] and a Chebychev polynomial of 0^{th} order. The residual intensity was computed with a peaks phase model. For this reason, the model contains contributions for Kapton film and the instrumental background. In this way, a low Chebychev polynomial can be used for the quantification of the in-situ XRD patterns, which reduces the risk of miscalculation of the background leading in turn to the ascription of a false intensity to the C–S–H. So as to make this Kapton film model easier to apply, the peaks phase was computed using a Pawley fit.

2.4.2. Water model

The hump induced by the water present in the sample was computed in a very similar way. Several diffractograms of a mixture of CaF_2 and water, in a water/CaF_2-ratio of 0.3 covered with Kapton film, were recorded and refined coupled using the structure proposal for CaF_2 [23], the Kapton film model described in Section 2.4.1 and a Chebychev polynomial of 0^{th} order. The residual intensities were computed with a peaks phase and, finally, this peaks phase was converted into a Pawley fit.

2.4.3. Background with Chebychev polynomial

To account for differences between the instrumental background within the diffractograms of CaF_2 and alite, a Chebychev polynomial of 1^{st} order was, in a final stage, used for the refinement of the in-situ XRD patterns. A 1^{st} order polynomial produced the most reliable results, since a higher background tended to produce an extreme effect on the other background models and thus involved the risk of destabilizing the refinement routine. A polynomial of 0^{th} order led in some cases to a visible misfit of the diffractograms taken in the first hours of hydration.

2.5. Phase model for C–S–H

The non-stoichiometric composition and the structure of C–S–H can change during long-term hydration time. The present study focuses on the C–S–H which is likely to develop during the first few hours and days of the hydration of ordinary Portland cement. To simulate the C–S–H forming within the early period of hydration, an hkl model for C–S–H was developed based on a paste of hydrating alite.

The model for C–S–H phase was developed on the basis of several diffractograms of a completed alite hydration, where only portlandite, C–S–H and some water were present. This way the peak overlap of the C–S–H with alite (Fig. 3) represented no problem for the development of the C–S–H phase model. The C–S–H model was built by refining the lattice parameters and peak intensities of a Pawley fit coupled within over ten diffractograms. Lorentz functions for strain were kept fixed at 0.1 and were refined for crystallite size. The scale factor was refined uncoupled to account for differences in the C–S–H content within the different samples. The starting lattice parameters of the Pawley fit were derived from a 14 Å tobermorite with the space

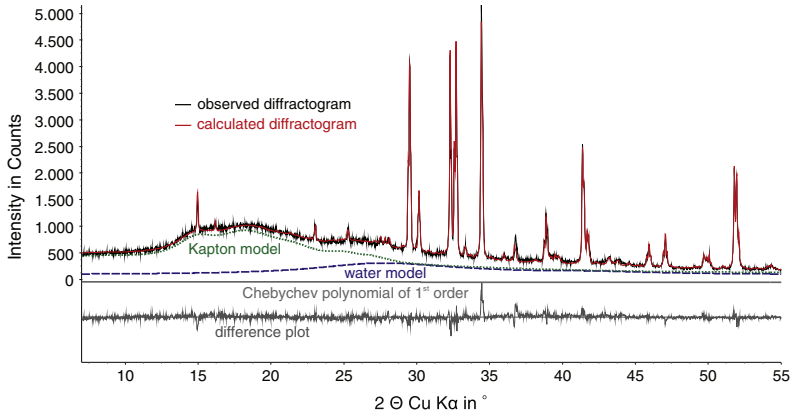

Fig. 2. In-situ XRD pattern of hydrating alite paste at 23 °C and w/s of 0.5 after 1 h of hydration. The background models used for the Rietveld refinements of alite paste experiments are shown here.

group F2dd [15]. The structure proposal of Busing and Levy [24] was used to fit the portlandite reflections.

The calibration factor F (see Section 2.3) for the phase model was determined by reference to data bearing on the early hydration of alite with a w/s of 0.5. According to the silicate reaction (Eq. (1); [2]), the expected amount of $C_{1.7}SH_{2.6}$ after 22 h hydration was calculated on the basis of that decrease in alite which had already occurred by that same point in time (22 h). The calibration factor F was then determined by minimization of the squared differences of the expected content of $C_{1.7}SH_{2.6}$ and the calculated content of C–S–H resulting from the quantification (Eq. (4)). For this procedure, it was assumed that the hydration of alite would be a synchronous dissolution and precipitation process. More than ten independent in-situ experiments of alite hydration at 23 °C with a w/s of 0.5 were used for the calibration.

$$\sum_{i=1}^{n}\left(c_{C-S-H_{\text{expafter 22 h},i}}-c_{C-S-H_{calc\text{ after 22 h},i}}\right)^2=0. \tag{4}$$

2.6. Refinement of in-situ XRD experimental data

All the diffractograms of one individual experiment of alite hydration were refined at once. The scale factor of the Kapton film model (Section 2.4.1) was refined coupled for all diffractograms of each individual experiment since the instrumental background and the background caused by the Kapton film should remain constant during an experiment. The scale factor of the water model (Section 2.4.2) was refined uncoupled, so as to allow the decrease of unbound water. The other parameters of the Kapton film and water model were kept fixed to the values derived from the CaF_2 samples. The crystalline phases alite and portlandite were calculated using the structure proposals of De la Torre et al. [25] and Busing and Levy [24], respectively. Their lattice parameters were refined coupled for each individual experiment. The crystallite sizes and the strain were refined as Lorentz functions and for portlandite a preferred orientation model was refined (spherical harmonics 4th order). For the C–S–H phase model, the scale factor and the crystallite size (by Lorentz function) were refined uncoupled. The lattice parameters of the C–S–H model were kept fixed so as to reduce the number of refined parameters, since the refinement of the C–S–H lattice parameters led to only minimal changes between different experiments, and no effect on the quantification of C–S–H could be observed. The sample displacement and a Chebychev polynomial of 1st order were also refined.

2.7. Calculation of the heat flow from in-situ XRD experimental data

Jansen et al. demonstrated that it is possible to calculate the heat flow from alite dissolution recorded using in-situ XRD, assuming a synchronous silicate reaction in accordance with Eq. (1) [2]. The heat flow can be calculated according to a general equation for a precipitating phase (Eq. (5)):

$$\mathrm{HF}=\frac{\partial \mathrm{wt.\%phase}_i/\partial t}{100}\frac{\Delta H_{\mathrm{phase}_i}}{3.6}\cdot(1+w/s) \tag{5}$$

where

HF the heat flow,
$\partial wt.\%\ phase\ /\ \partial t$ derivative of the development of phase i recorded by in-situ XRD
$\Delta H_{phase\ i}$ enthalpy of reaction of Eq. (1) (referring to 1 g of phase i)
w/s water-to-solid ratio in the paste.

For the dissolution of a phase, the factor (−1) has to be multiplied in order to yield an increasing heat from the decreasing of the phase content, approaching to the following equation (Eq. (6)):

$$\mathrm{HF}=\frac{\partial \mathrm{wt.\%phase_i}/\partial \mathrm{t}}{100}\frac{\Delta \mathrm{H_{phase_i}}}{3.6}\cdot(1+\mathrm{w/s})\cdot(-1). \tag{6}$$

The enthalpy of reaction of the silicate reaction (Eq. (1)) is −561 J/g alite or −633 J/g $C_{1.7}SH_{2.6}$ calculated from standard enthalpies of formation [2].

3. Results and discussion

3.1. Results of the in-situ XRD

Fig. 3 shows the Rietveld refinement of an in-situ XRD pattern after 65 h of hydration at 23 °C and a w/s of 0.5. The phases determined here are alite, portlandite and C–S–H. For the refinement of the background, models were used for Kapton film and water, along with a Chebychev polynomial of 1st order as described under Section 2.4 and in Fig. 2. The C–S–H phase peaks are situated below several alite reflections. The increased background induced by unbound water is also situated

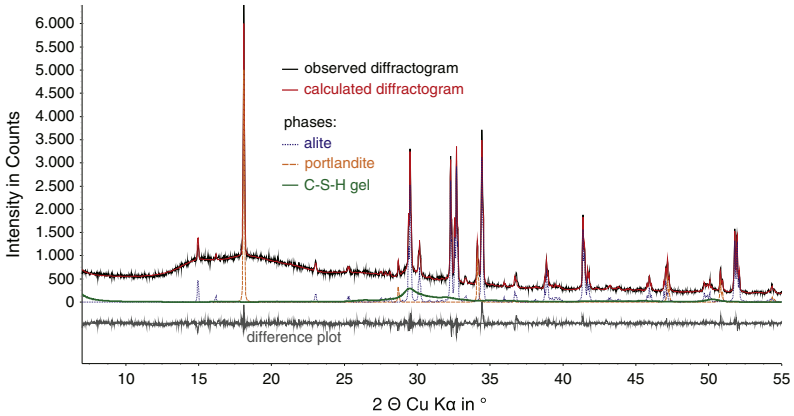

Fig. 3. In-situ XRD pattern of alite paste at 23 °C with w/s = 0.5 after 65 h of hydration. Shown here are the crystalline phases alite and portlandite and the C–S–H. The background models used can be seen in Fig. 1.

Table 1
Synopsis of the phase model for dimeric C–S–H. All "hkl" are shown in Table 2.

```
hkl_Is
    hkl_m_d_th2   0  0  4  2  14.7305  5.9950   I  20.9832
    hkl_m_d_th2   1  1  5  8  5.3948   16.4182  I  1.2114
    hkl_m_d_th2   2  0  6  4  5.0634   17.5007  I  0.4709
    .
    .
    .
    phase_name "C–S–H gel"
    space_group F2dd
    scale @ 0.1
    a !CSH_a 11.81906
    b !CSH_b 7.07097
    c !CSH_c 58.92196
    CS_L(@, 14 min = 6; max = 30;)
    Strain_L(!C–S–H_str, 0.1)
```

near the main peaks of C–S–H, as is shown by a comparison between Figs. 2 and 3. By controlling the evolution of alite and the different background models it is possible to achieve a stable quantification of C–S–H. The data of the Pawley fit used for the refinement of C–S–H is shown in Tables 1 and 2. The calibration factor F for the C–S–H phase model (see Section 2.5) resulted in $8.86 \cdot 10^{-46}$ g cm^3, thus giving a standard deviation of ± 2 wt.% from more than ten independent samples. It has to be pointed out, that an incorrect determination of the calibration factor F for the phase model of C–S–H would only affect the quantified wt.% of C–S–H by a constant factor. It would not affect the evolution of this quantified wt.% of C–S–H.

The calculation of the crystallite size of C–S–H as carried out during refinement resulted in values lying between 7.7 and 9.1 nm (FWHM). After these latter values have been reached, the crystallite sizes tend to remain unchanged up to 46 h of hydration. From this observation we can conclude, that the size of the coherently scattering areas does not increase within the early stages of hydration. Due to these very low crystallite-size dimensions, small differences of the calculated crystallite size can have a strong influence on the resulting scale factors. This in turn can cause a lesser degree of precision of the calculated phase content. The estimated error of the C–S–H quantification, using the G-factor method, is thus assumed to be ± 4 wt.%. The limit of detection (4σ) and the limit of determination (12σ) were calculated to be 0.1 wt.% and 0.2 wt.% for C–S–H. The first diffractogram of each measurement of alite hydration was used for the determination of these limits assuming that no detectable C–S–H has been formed up to 10 min of hydration.

The phase development of alite, C–S–H and portlandite during the hydration of pure alite with water at 23 °C and w/s of 0.5 is presented in Fig. 4 as an average of 5 independent measurements, with error bars of the standard deviation. The alite content within the first few hours ranges between 63 and 64 wt.%. Since the pure alite sample contained a not determined amount of 5.7 ± 1.0 wt.%, and since the water/alite-ratio was 0.5, about 63 wt.% alite should have been detected at the start of the experiment, assuming that no alite would have dissolved during the first range (10 min). Within the following 4 h no dissolution of alite could be detected. After about 4 h of hydration, alite started to dissolve very slowly. C–S–H could be detected for the first time after 11 h of hydration. The alite dissolution was accelerated as soon as C–S–H was formed. At about 12 h of hydration, the speed of C–S–H formation had already reached its maximum, since the content of C–S–H was increasing linearly until about 17 h of hydration. In the same time period, the alite dissolution was also proceeding linearly. Afterwards both alite dissolution and C–S–H precipitation decelerated synchronously, proceeding at low levels until the end of the experiment.

The quantification of portlandite in alite pastes using XRD is a challenging procedure to attempt, because portlandite seems to form few large crystals [26]. The random orientation of these few large crystals leads to random reflection intensities for different reflections which are incidentally different from experiment to experiment. This spottiness of portlandite cannot be sufficiently compensated by preferred orientation or by any other method. The refinement of preferred orientation using spherical harmonics, as in the present study, leads to a proper fit of the portlandite reflections, but the resulting scale factor does not correspond with correct quantities. Also, the point in time from which portlandite begins to be detectable varied slightly from experiment to experiment. Nevertheless, portlandite could generally be detected after about 5 h of hydration, suggesting that it forms during a period of time which is approximately synchronous with that of the dissolution of alite. The calculated portlandite content after a hydration

Table 2
Summary of all the "hkl" of which the C–S–H phase model consists. The quotation marks on "hkl" are intended to make it clear that the C–S–H phase model is not an indexed crystallographic structure.

"hkl"	m	d	° 2 Θ	Intensity	"hkl"	m	d	° 2 Θ	Intensity
(0 0 4)	2	14.730	5.9950	21.0	(2 2 12)	8	2.5810	34.729	15.5
(1 1 5)	8	5.3948	16.418	1.21	(4 0 12)	4	2.5317	35.427	16.5
(2 0 6)	4	5.0634	17.501	0.47	(2 2 14)	8	2.4611	36.478	15.8
(1 1 9)	8	4.4504	19.935	2.61	(0 2 18)	4	2.4020	37.410	4.93
(1 1 11)	8	4.0157	22.118	2.01	(1 1 23)	8	2.3601	38.099	3.02
(0 2 2)	4	3.5103	25.352	2.73	(2 2 16)	8	2.3416	38.411	2.66
(0 2 4)	4	3.4379	25.896	1.87	(1 3 1)	8	2.3097	38.963	5.71
(3 1 3)	8	3.3899	26.268	10.3	(1 3 9)	8	2.1796	41.392	14.8
(0 2 6)	4	3.3265	26.778	3.38	(3 1 12)	8	2.1747	41.490	1.09
(1 1 15)	8	3.2975	27.018	4.82	(4 2 8)	8	2.1669	41.646	1.35
(0 2 8)	4	3.1873	27.971	4.92	(0 2 22)	4	2.1349	42.301	10.0
(3 1 7)	8	3.1856	27.986	7.31	(1 3 11)	8	2.1223	42.563	5.40
(3 1 9)	8	3.0463	29.294	34.2	(0 0 28)	2	2.1044	42.944	5.38
(2 2 0)	4	3.0340	29.416	76.2	(4 0 20)	4	2.0863	43.335	11.4
(0 2 10)	4	3.0316	29.439	43.0	(5 1 11)	8	2.0680	43.737	3.17
(1 1 17)	8	3.0096	29.659	3.66	(3 1 23)	8	2.0550	44.029	4.24
(2 2 4)	8	2.9716	30.048	25.6	(1 1 27)	8	2.0535	44.062	8.59
(0 0 20)	2	2.9461	30.314	21.1	(3 3 1)	8	2.0215	44.799	16.5
(2 2 6)	8	2.8988	30.821	12.9	(4 2 14)	8	1.9960	45.401	4.84
(4 0 4)	4	2.8971	30.840	9.24	(3 3 5)	8	1.9935	45.462	8.11
(2 0 18)	4	2.8635	31.210	15.7	(1 3 15)	8	1.9922	45.494	10.4
(2 2 8)	8	2.8053	31.875	40.9	(6 0 2)	4	1.9655	46.148	20.9
(1 1 19)	8	2.7614	32.395	21.5	(1 1 29)	8	1.9267	47.133	0.92
(0 2 14)	4	2.7071	33.064	2.82	(5 1 19)	8	1.8168	50.172	127.5
(2 2 10)	8	2.6974	33.186	16.1					

time of 35 h is lower than expected in respect to Eq. (1), according to which about 10.5 wt.% of portlandite should have been formed by the said point in time. The under determination of the phase content of portlandite is caused by the use of a preferred orientation model to account for the spottiness of portlandite in order to get a proper fit of the diffractogram.

3.2. Comparison of calculated and measured heat flow

In Fig. 5, a comparison is made between the heat flow measured by calorimetric experiments and the heat flow calculated from the quantification of the in-situ XRD experiments. The heat flow of the silicate reaction (Eq. (1)) was calculated according to Eqs. (5) and (6) from both the decrease of alite and the increase of C–S–H, as described in Section 2.7. Both heat flow curves represent the mean values and one standard deviation calculated from the phase content development in paste. As already shown by Jansen et al. [2] and shown again in Fig. 5, the silicate reaction can be described very well by the dissolution of alite with a silicate reaction, according to Eq. (1).

When the formation of C–S–H is used to calculate the heat flow following the same silicate reaction path a different heat flow curve results. The data of C–S–H formation do not suffice to explain the heat flow occurring within the 5 h to 15 h period as detected by calorimetry and calculated following the alite dissolution. The main period, as calculated from the C–S–H precipitation, results in a considerably faster acceleration and a higher heat flow at the maximum of the main period of hydration than the measured heat flow and the heat flow calculated from the decrease of alite. The time of the maximum of hydration remains unchanged. The deceleration period is very similar for all three heat flow curves shown in Fig. 5.

The heat of hydration, as measured and calculated from the two reaction paths, is presented in Fig. 6. Neither alite dissolution nor C–S–H formation can account for the initial heat release detected by calorimetry. The heat of hydration as calculated from the alite dissolution corresponds pretty closely, throughout, to the measured one. The differences in the heat release between the calculated heat of hydration from the C–S–H formation and the measured one are plotted in Fig. 6. Up until the point of the formation of C–S–H, and also between the point of the first detection of C–S–H and about 11.7 h, the differences in the heat release tend to increase. After 11.7 h, the calculated heat flow exceeds the measured one, reducing the disparity between calculated and measured heat of hydration until about 22 h of hydration (Fig. 6). After 22 h the difference in the slope between calculated and measured heat flow tends towards zero.

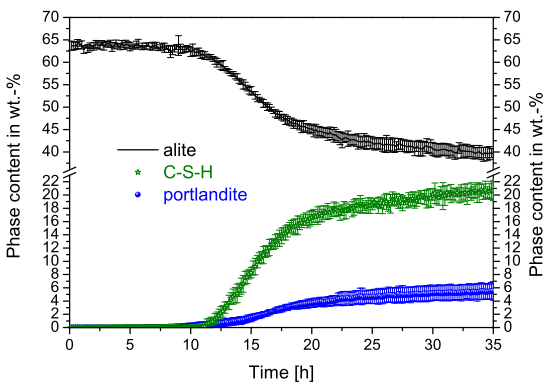

Fig. 4. Phase development of alite, C–S–H and portlandite during hydration of alite with water at 23 °C and w/s = 0.5.

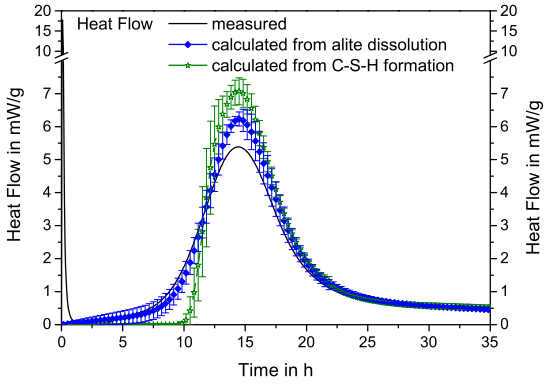

Fig. 5. Comparison of the heat flow of the alite hydration at 23 °C and w/s = 0.5, as detected by heat flow calorimetry, and calculated heat flow from the alite dissolution and from C–S–H formation, as detected by XRD.

4. Discussion and conclusions

The refined crystallite size (FWHM) of the C–S–H remained unchanged between 7.7 and 9.1 nm from the first formation of C–S–H to the end of the experiments. Even though a constant value for strain was applied to the C–S–H phase model, X-ray diffraction is very sensible in these small dimensions of coherently scattering areas and gives due to the use of the fundamental parameters approach significant information. The constant size of coherently scattering domains supports the idea that the "growth" of C–S–H does not lead to the formation of an amorphous gel bulk, but proceeds by the aggregation of C–S–H particles, as shown by Jennings in the colloid model for C–S–H [10,11]. For crystal growth an increasing of the sizes of coherently scattering areas should be expected. Jennings et al. [27] calculated from SANS analysis that the size of C–S–H "globules", which are non-spherical basic building blocks that aggregate to different packing densities [11], is about 5 nm. This is about the same size as the refined sizes of coherently scattering areas are in this study, as a constant value for the strain was applied.

The results presented in Section 3 show that during curing of alite paste, the formation of the detected C–S–H does not proceed completely synchronously with alite dissolution. After 11 h, about 3.4 wt.% of alite had already been dissolved according to the measured heat release following the silicate reaction (Eq. (1)). Assuming

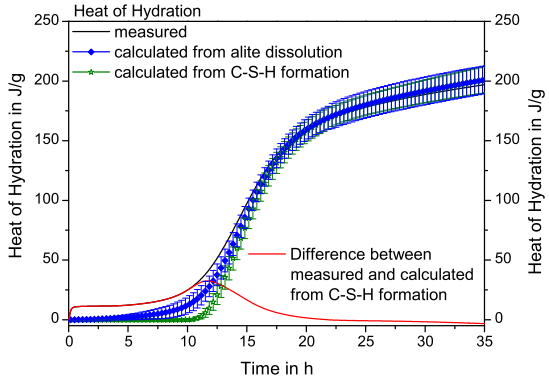

Fig. 6. Comparison of the heat of hydration of alite hydration at 23 °C and w/s = 0.5, as detected by heat flow calorimetry, and the calculated heat flow from the alite dissolution and from C–S–H formation, as detected by XRD.

a synchronously proceeding reaction (as in Eq. (1)) the C–S–H tends to form later than the measured heat flow indicates. With the beginning of C–S–H formation, the heat flow calculated from its formation significantly exceeds the measured heat flow. As shown in Fig. 4, the phase development of both the decrease of alite and the formation of C–S–H proceeds linearly between 12 and 17 h of hydration. In Fig. 5 it can be seen, that the slope of the C–S–H formation during the acceleration period is steeper than the one for the alite dissolution.

The misfit, after the start of the main hydration period, between the heat flow as calculated from the C–S–H precipitation and the measured heat flow indicates the existence of an early calcium–silicate–hydrate phase, as it was described e.g. by Bellmann et al. [28]. This hydrate phase is XRD-amorphous and probably possesses a short-range ordered nanostructure only. Since the Ca/Si-ratio and the water content of C–S–H are very variable, depending on the chemical composition of the pore solution, it might be possible, that different chemical compositions of short range ordered C–S–H exist simultaneously.

The presence of an intermediate phase would explain the differences found in the present study between the measured heat flow and the heat flow calculated from C–S–H formation. We suggest that an intermediate, short-range ordered C–S–H phase is formed either directly after mixing with water — according to Brown et al. [29] who described a decrease of silicon in the pore solution in the first minutes of hydration which indicates the formation of C–S–H phase or when alite starts slowly to dissolve (after 4–10 h). This short-range ordered C–S–H then evolves into a long-range ordered C–S–H nanostructure, which could consist in mean of dimeric silicate tetrahedrons as described by Richardson [15].

Since we cannot detect the intermediate phase, we cannot derive information about this phase. It remains therefore unclear, if the not detected C–S–H phase is close to the monomeric C–S–H phase described by NMR spectrometry within the induction period e. g. by Rodger et al. [30]. Rodger et al. [30] detected the first dimeric silicate tetrahedrons at the beginning of the acceleration period. This seems to be significantly earlier than the XRD detectable C–S–H in the present study which is forming from the monoclinic alite used in the present study. Therefore, it is possible, that the first C–S–H with condensed silicate tetrahedrons possesses also only a short-range ordered structure and is therefore also not detectable for XRD.

As soon as C–S–H can be detected by XRD the domain size of C–S–H does not grow any further nor undergo any further evolution during the early hydration of alite, since the size of coherently scattering areas does not increase. After the first formation of long-range ordered C–S–H out of the intermediate, short-range ordered C–S–H, long-range ordered C–S–H is probably the most effective nucleation site for new long-range ordered C–S–H, since C–S–H tends to auto-catalyze its own formation [13]. This leads to a strong acceleration of alite dissolution and direct long-range ordered C–S–H precipitation at that point in time.

Taking into account the results of this study, the silicate reaction cannot be described as a synchronous reaction in the sense of Eq. (1). Assuming an intermediate, short-range ordered C–S–H to form as soon as an alite dissolution can be detected, the evolution from intermediate, short-range ordered C–S–H to the first detectable, long-range ordered C–S–H takes about 6 h in our study with monoclinic alite. The proposed assumption here is that the intermediate C–S–H continues to be formed until the first formation of long-range ordered C–S–H is detected (Eq. (7)). From 10 to 22 h, intermediate, short-range ordered C–S–H is transformed into long-range ordered C–S–H (Eq. (8)). After 22 h, no differences can be detected between measured heat flow and heat flow calculated from the detected C–S–H formation (Fig. 6). As soon as long-range ordered C–S–H is formed, it should be thermodynamically more favorable to directly nucleate long-range ordered C–S–H on existing long-range ordered C–S–H (Eq. (9)). The size of the coherently scattering areas of C–S–H does not evolve with time. The subsequent expansion of long-range ordered C–S–H regions should be caused by a nucleation, rather than a growth process as it was argued by Thomas et al. [13] and by the aggregation of these C–S–H individuals as described by Jennings colloid model [10,11] and by Constantinides and Ulms [12] nanoindentation measurements.

Proposed schematic silicate reaction:

$$C_3S + H \rightarrow C\text{–}S\text{–}H_{short-rangeordered} + CH(\text{from4to10h}) \quad (7)$$

$$C\text{–}S\text{–}H_{short-rangeordered} \rightarrow C\text{–}S\text{–}H_{long-rangeordered}(\text{from10to22h}) \quad (8)$$

$$C_3S + H \rightarrow C\text{–}S\text{–}H_{long-rangeordered} + CH(\text{from10to35h}). \quad (9)$$

The difference in calculated heat flow from the alite dissolution shows only a minor deviation from the measured heat flow at the start of the accelerating period as previously reported [2]. This indicates that there is no significant difference between the respective enthalpies of formation of short-range ordered and long-range ordered C–S–H. Therefore, the evolution from intermediate, short-range ordered C–S–H to long-range ordered C–S–H does not contribute to the released heat notably. Nevertheless, it seems to be the key process, since the formation of long-range ordered C–S–H appears to give rise to a strong acceleration of the main hydration period.

References

[1] Ch. Hesse, F. Goetz-Neunhoeffer, J. Neubauer, A new approach in quantitative in-situ XRD of cement pastes. Correlation of heat flow curves with early hydration reactions, Cement Concr. Res. 41 (2011) 123–128.
[2] D. Jansen, S.T. Bergold, F. Goetz-Neunhoeffer, J. Neubauer, The hydration of alite: a time resolved quantitative X-ray diffraction approach using G-factor method compared with heat release, J. Appl. Crystallogr. 44 (5) (2011) 895–901.
[3] D. Jansen, F. Goetz-Neunhoeffer, C. Stabler, J. Neubauer, A remastered external standard method applied to the quantification of early OPC hydration, Cement Concr. Res. 41 (2011) 602–608.
[4] D. Jansen, F. Goetz-Neunhoeffer, B. Lothenbach, J. Neubauer, The early hydration of Ordinary Portland Cement (OPC): An approach comparing measured heat flow with calculated heat flow from QXRD, Cement Concr. Res. 42 (2012) 134–138.
[5] R.J. Hill, C.J. Howard, Quantitative phase analysis from neutron powder diffraction data using the Rietveld method, J. Appl. Cryst. 20 (1987) 467–474.
[6] B.H. O'Connor, M.D. Raven, Application of the Rietveld refinement procedure in assaying powdered mixtures, Powder Diffr. 3 (1) (1988) 2–6.
[7] J.J. Thomas, A new approach to modelling the nucleation and growth kinetics of tricalcium silicate hydration, J. Am. Ceram. Soc. 90 (2007) 3282–3288.
[8] S. Bishnoi, K.L. Scrivener, Studying nucleation and growth kinetics of alite hydration using μic, Cement Concr. Res. 39 (2009) 849–860.
[9] L. Nicoleau, Accelerated growth of calcium silicate hydrates: experiments and simulations, Cement Concr. Res. 41 (2011) 1339–1348.
[10] H.M. Jennings, A model for the microstructure of calcium silicate hydrate in cement paste, Cement Concr. Res. 30 (2000) 101–116.
[11] H.M. Jennings, Refinements to colloid model of C–S–H in cement: CM-II, Cement Concr. Res. 38 (2008) 275–289.
[12] G. Constantinides, F.-J. Ulm, The nanogranular nature of C–S–H, J. Mech. Phys. Solids 55 (2007) 64–90.
[13] J.J. Thomas, H.M. Jennings, J.J. Chen, Influence of nucleation seeding on the hydration mechanisms of tricalcium silicate and cement, J. Phys. Chem. C 113 (2009) 4327–4334.
[14] H.F.W. Taylor, Cement Chemistry, second ed. Thomas Telford Services Ltd., 1997. , (128 pp.).
[15] I.G. Richardson, The calcium silicate hydrates, Cement Concr. Res. 38 (2008) 137–158.
[16] K. Mohan, H.F.W. Taylor, Analytical electron microscopy of cement pastes: IV, β-dicalcium silicate pastes, J. Am. Ceram. Soc. 64 (1981) 717–719.
[17] M. Regourd, Centre Technique Industriel, Paris, France, Private communication about the results of a microprobe analysis to The International Centre for Diffraction Data, Powder Diffraction File 42-0551, 1979.
[18] C. Hesse, M. Degenkolb, M. Gäberlein, F. Goetz-Neunhoeffer, J. Neubauer, V. Schwarz, Investigation into the influence of temperature and w/c-ratio on the early hydration of white cement, Cement Int. 6 (2008) 68–78.
[19] D. Jansen, C. Stabler, F. Goetz-Neunhoeffer, S. Dittrich, J. Neubauer, Does ordinary Portland cement contain amorphous phase? A quantitative study using an external standard method, Powder Diffr. 26 (1) (2011) 31–38.

[20] N.V.Y. Scarlett, I.C. Madsen, Quantification of phases with partial or no known crystal structures, Powder Diffr. 21 (4) (2006) 278–284.
[21] I.C. Madsen, N.V.Y. Scarlett, A. Kern, Description and survey of methodologies for the determination of amorphous content via X-ray powder diffraction, Z. Kristallogr. 226 (2011) 944–955.
[22] Ch. Hesse, F. Goetz-Neunhoeffer, J. Neubauer, M. Braeu, P. Gaeberlein, Quantitative in-situ X-ray diffraction analysis of early hydration of Portland cement at defined temperatures, Powder Diffr. 24 (2009) 112–115.
[23] V.A. Strel'tsov, V.G. Tsirel'son, R.P. Ozerov, O.A. Golovanov, Electronic and thermal parameters of ions in CaF_2: regularized least squares treatment, Kristallografiya 33 (1988) 90–97.
[24] W.R. Busing, H.A. Levy, Neutron diffraction study of calcium hydroxide, J. Chem. Phys. 26 (3) (1957) 563–568.
[25] A.G. De La Torre, S. Bruque, J. Campo, M.A.G. Aranda, The superstructure of C_3S from synchrotron and neutron powder diffraction and its role in quantitative phase analyses, Cement Concr. Res. 32 (2002) 1347–1356.
[26] Bergold, S.T., Jansen, D., Dittrich, S., Goetz-Neunhoeffer, F., Neubauer, J., Development of C-S-H during the early hydration of alite with water at different temperatures: direct quantification by in-situ XRD, GDCh-Monographie (2012), 45 (Tagung Bauchemie, 2012), 91–96.
[27] H.M. Jennings, J.J. Thomas, J.S. Gevrenov, G. Constantinides, F.-J. Ulm, A multi-technique investigation of the nanoporosity of cement paste, Cement Concr. Res. 37 (2007) 329–336.
[28] F. Bellman, D. Damidot, B. Möser, J. Skibsted, Improved evidence for the existence of an intermediate phase during hydration of tricalcium silicate, Cement Concr. Res. 40 (2010) 875–884.
[29] P.W. Brown, E. Franz, G. Frohnsdorff, H.F.W. Taylor, Analyses of the aqueous phase during early C_3S hydration, Cement Concr. Res. 14 (1984) 257–262.
[30] A.A. Rodger, G.W. Groves, N.J. Clayden, C.M. Dobsen, Hydration of tricalcium silicate followed by ^{29}Si NMR with cross-polarization, J. Am. Ceram. Soc. 71 (1988) 91–96.

Erratum

In section 2.1, there is a typo at the weighted alite composition for the wt.% of CaO. It has to be 71.7 wt.% instead of 75.1 wt.%. The correct alite composition is therefore 71.7 wt.% CaO, 25.9 wt.% SiO_2, 0.6 wt.% Al_2O_3 and 1.8 wt.% MgO.

7.5. Mechanically activated alite: New insights into alite hydration

Reprint

Published in the Journal “Cement and Concrete Research”
Vol. 76 (2015) 202-211, doi: 10.1016/j.cemconres.2015.06.005

Authors: S. T. Bergold, F. Goetz-Neunhoeffer, and J. Neubauer

Cement and Concrete Research 76 (2015) 202–211

Contents lists available at ScienceDirect

Cement and Concrete Research

journal homepage: http://ees.elsevier.com/CEMCON/default.asp

Mechanically activated alite: New insights into alite hydration

S.T. Bergold *, F. Goetz-Neunhoeffer, J. Neubauer *

Friedrich-Alexander-Universität Erlangen-Nürnberg, GeoZentrum Nordbayern, Mineralogy, Schlossgarten 5a, 91054 Erlangen, Germany

ARTICLE INFO

Article history:
Received 11 March 2015
Accepted 5 June 2015
Available online xxxx

Keywords:
Ca_3SiO_5 (D)
Amorphous material (B)
Acceleration (A)
Hydration (A)
Calcium–Silicate–Hydrate (C–S–H) (B)

ABSTRACT

For superior understanding of alite hydration an investigation of mechanically activated alite (M3 modification) was performed by XRD and heat flow calorimetry. Activation resulted in reduced particle size, a decreased mean crystallite size and partial amorphization. For the samples of activated alite a significantly accelerated and intensified hydration was observed and complete conversion of alite was found after 24 h. The enthalpy of reaction for crystalline alite was determined to be −548 J/g from measured heat of hydration after 24 h. The enthalpy of reaction of amorphous "alite" was found to be less exothermic (−386 J/g). The main hydration period is controlled by nucleation of C–S–H, while the transition from acceleration to deceleration period takes place after consumption of the small alite particles. XRD amorphous C–S–H phase is indicated to precipitate in considerable amount even in the highest activated alite before "long-range ordered", XRD detectable C–S–H was observed.

1. Introduction

The mechanisms behind the reaction of tricalcium silicate (Ca_3SiO_5, notation C_3S, called alite if foreign atoms are incorporated stabilizing a monoclinic modification) with water are not completely understood yet. It is well established, that the reaction products of this reaction are portlandite ($Ca(OH)_2$) and calcium–silicate–hydrates (notation C–S–H). While chemical composition and crystallographic structure of portlandite are constant, C–S–H shows variable chemical composition and different ordering. The notation C–S–H indicates, that the Ca/Si-ratio and the H/Si-ratio of C–S–H are evolving with the pore solution composition during the hydration process, following from one metastable equilibrium to a new metastable equilibrium [1]. The mean Ca/Si-ratio within the early hydration of C–S–H is often reported to be around 1.7 [2].

One of the most discussed issues within the cement community is the occurrence and cause of the induction period or period of slow reaction. There is still no consensus about the reaction path from the first reaction of C_3S with water up to the start of the main hydration period. An open question is, why the reaction does not start right away after mixing. Juilland et al. [3] proposed that alite is dissolving differently depending on the pore solution composition as described for other crystalline materials before [4]. Nicoleau [5] showed by an experimental approach that the alite dissolution rate is strongly depending on the composition of the liquid phase. The dissolution rates were decreased by two orders of magnitude when C_3S was dissolved in $Ca(OH)_2$–saturated water instead of pure water. From that point of view, the induction period is the time that is necessary to dissolve enough alite for a sufficient supersaturation of the pore solution and for the formation of stable C–S–H nuclei.

The other commonly proposed explanation for the presence of an induction period is, that an intermediate C–S–H phase precipitates terminating the initial hydration period [e.g. [6–10]]. This acts as a barrier which hinders the further progress of alite dissolution. This metastable barrier becomes unstable at the end of the induction period and therefore the reaction is finally starting to accelerate. There are a lot of indications that suggest the precipitation of an intermediate C–S–H phase [e.g. [7,8,11]]. But there is no final proof of a continuous layer on the surface of alite grains.

When looking at pore solution compositions, the silica concentration in solution is increasing at first, giving evidence of a congruent dissolution of alite. But then after a very short period of time the silica concentration decreases, which must be interpreted as precipitation of C–S–H [12,13]. NMR spectroscopic analysis demonstrated that the first silicon tetrahedra dimers can be found at the beginning of the acceleration period [14,15]. Prior to that – until the end of the induction period – C–S–H is formed, which contains only monomeric species [7]. Recently we have shown by in-situ XRD measurements, that during hydration of alite (M3 modification) XRD detectable, "long-range ordered" C–S–H (C–S–H_{lro}) was detected within the acceleration period [11]. Furthermore in this study it was discovered that an XRD amorphous C–S–H precursor must have formed before C–S–H_{lro} precipitates.

The effects of mechanical activation of C_3S were described about 50 years ago by Schrader & Schumann [16]. They investigated dry alite samples and concluded that the crystallite size of alite was reduced and that lattice distortions were detected — suggesting an

* Corresponding authors. Tel.: +49 9131 85 23987; fax: +49 9131 85 23734.
E-mail addresses: sebastian.bergold@fau.de (S.T. Bergold), juergen.neubauer@fau.de (J. Neubauer).

http://dx.doi.org/10.1016/j.cemconres.2015.06.005

amorphization of the mechanically treated C_3S. Odler & Schüppstuhl [17] found, that grinding of C_3S (up to 7000 cm^2/g Blaine surface) leads to an acceleration of the main hydration period and the omission of the commonly occurring induction period. Costoya investigated alite mixtures with different particle size distributions, and found that the induction period was decreased for finer sized alite powders [18]. Alite material with the presumably highest reactivity was described by Bellmann et al. [7]. Approximately 50 nm sized C_3S particles were analyzed by NMR-spectroscopy and it was supposed that a very high amount of intermediate C–S–H phase containing only monomeric silicon tetrahedra has formed after 5 min of hydration from this highly reactive C_3S.

Some other techniques to increase the reactivity of alite were reported before. Odler & Schüppstuhl [17] introduced defects into C_3S lattice by cooling in N_2. They showed, that this treatment caused the minimum heat flow during the induction period to increase and the induction period was shortened. In contrast, Juilland et al. [3] chose thermal treatment of alite to decrease the defect density and found that the initial dissolution rate of such alite is actually reduced and that the induction period is prolonged.

The principal aim of this study was to achieve more analytical data on the influence of mechanical treatment on the reactivity of alite. For the investigation alite powder was synthesized and mechanically activated for different times and then characterized by a combination of heat flow calorimetry and quantitative XRD phase analysis. At first we wanted to confirm experimentally that a different intensive mechanical treatment is leading to a differently high increase of alite reactivity. But principally the study was aimed at allowing a better understanding of the underlying hydration mechanisms of alite hydration.

2. Materials and methods

The monoclinic M3 form of alite was synthesized (Mg^{2+} and Al^{3+} doped Ca_3SiO_5) with a composition of 71.7 wt.% CaO, 25.9 wt.% SiO_2, 1.8 wt.% MgO, and 0.6 wt.% Al_2O_3. The powders ($CaCO_3$, SiO_2, MgO and Al_2O_3) were homogenized in a vibratory disk mill (agate tool), calcinated at 1000 °C and sintered four times in a chamber furnace at 1400 °C ± 30 °C in Pt crucibles in air. The alite was quenched by removing the sample from the furnace and cooling it down to room temperature within few minutes. After the final sinter step the mixture was ground in a vibratory disk mill (agate tool) to the desired specific surface area. For its mechanical activation this alite (further called not activated alite) was ground from 1 h up to 30 h long in agate jars with 1.25 mm Y:ZrO_2 balls in 40 ml ethanol by use of a planetary ball mill from RETSCH. The load of 175 g milling balls in contrast to 10 g alite ensured a high energy transfer on the alite powders. After the milling process the alite–ethanol suspension was centrifuged, detached and finally dried for 2 days in a vacuum drying chamber at 50 °C operated with 20 mbar of N_2 atmosphere. The drying chamber was flushed 6 times with N_2 within 2 days. After this drying procedure, the powders were ground carefully in an agate mortar and sieved in order to ensure better deagglomeration of the particles. The BET surface areas of all produced samples were determined with the measuring gas N_2 with a GEMINI Model 236 from MICROMERITICS in liquid N_2. The surfaces of the samples were cleaned by heating the samples to 350 °C under He flow for at least 4 h.

The samples then were investigated by heat flow calorimetry (TAM Air, TA INSTRUMENTS) in combination with the InMixEr (injection & mixing device for internal preparation) which allows equilibration, injection of water and mixing within the calorimeter cell. This experimental setup enables an accurate detection of the initial heat flow at the beginning of the hydration reaction. All heat flow measurements were performed at 23 °C ± 0.2 °C and because of the high water demand of the activated alite powders at a water to solid ratio (w/s) of 1. Prior to the measurements the powders and liquids were equilibrated within the calorimeter in the InMixEr device (minimum 2 h). The measurement was started with the injection of water and mixing of the sample for 1 min at 860 rpm in polystyrene ampoules.

The calibration of the InMixEr device was performed with a 10 kΩ resistor at several voltages that covered the whole range of different heat outputs of the alite hydration. This calibration was necessary to account for loss of heat during the measurements, which is caused by the mixing unit of the InMixEr device. The stirring tool is made of steel to be able to get an efficient and homogeneous mixing result. The calibration showed that the loss of heat versus induced heat flow follows a linear trend over the complete range of heat values detected for alite hydration (R^2 of 0.9999997). Additionally the heat flow curves were corrected for the determined calorimeter time constant of 198 s and for the baseline shift.

XRD experiments were performed with a D8 Advance from BRUKER-AXS equipped with a LynxEye detector using generator settings at 40 kV and 40 mA. For determination of the phase contents of alite and of amorphous material in the dry powder the measurements were recorded from 7° to 80° 2Θ with step size of 0.0223° 2Θ and 0.5 s counting time. Rietveld refinements using the fundamental parameter approach were performed with TOPAS 4.2 from BRUKER-AXS with subsequent calculation of the absolute phase quantity by use of the external standard method [19,20]. The calibration of the factor G was performed with NIST Silicon SRM 640d. For analysis of the dry alite samples, two different alite phase models (data of De la Torre et al. [21]) with different refined crystallite sizes and strains (both as Lorentzian functions) were used simultaneously to stabilize the refinement.

Loss of ignition (LOI) of the dried powders due to retained ethanol in the sample was determined at 1000 °C ± 30 °C in a chamber furnace in Pt-crucibles in air. The above described drying method reduced the retained ethanol to a minimum. Although the retained ethanol is not supposed to support the alite hydration in a positive way its presence could be avoided largely. All presented results were normalized to the mass of reactive solid, which is the sum of crystalline and amorphous alite. This way only the reactive part of the samples is accounted for in the presented results. The amount of amorphous "alite" was determined as difference to 100 wt.% after subtracting the amount of crystalline alite and LOI.

The in-situ paste XRD measurements were performed with a custom-made heating and cooling device at a constant temperature of 23 °C ± 0.2 °C. The housing of the diffractometer was air conditioned to 23 °C ± 2 °C. The diffractograms were recorded every 10 min from 7° to 55° 2Θ and a step width of 0.0236° 2Θ. A Kapton® polyimide film was used for the in-situ experiments to minimize water loss and CO_2 intake of the paste. The standard for determination of factor G was also covered with Kapton® polyimide film.

For the refinement lattice parameter, crystallite size and strain of alite were kept fixed to the refined parameters from the dry powders. The structure model of Busing and Levy [22] was employed for portlandite. The development and use of the PONKCS phase model for C–S–H in combination with the G-factor method were described in detail recently [11]. The PONKCS phase model for C–S–H_{Iro} that was introduced for quantification in a not activated alite paste could also be used unchanged for analysis of the activated alite samples. The crystallite size (as Lorentzian function) of C–S–H was refined for a fixed strain of 0.1. The background was calculated using a Chebyshev polynomial of 1st order and "hkl" models for Kapton® polyimide film and free water [11]. For further data handling the resulting time-dependent phase contents were fitted with one or two 5 parameter logistic functions [23] by use of the program Fityk [24].

3. Results

3.1. Analysis of dry activated alite powders

The results of the Rietveld refinements of not activated and activated alite samples with subsequent use of the G-factor method are shown in Table 1. Due to mechanical activation the mean crystallite size of alite is

Table 1
Quantitative data of the not activated and activated alite samples from XRD, BET, and LOI.

Activation time in h	Activated alite	Crystalline alite in wt.%	Amorphous alite in wt.%	BET surface in m^2/g	LOI in wt.%	Crystallite size (Vol-IB) in nm	Strain in %
0	Not activated			0.6 ± 0.03	0.2 ± 0.1	2562	0.02
1		99.0 ± 0.1	1.0 ± 0.2	7.8 ± 0.1	1.39 ± 0.06	328	0.13
2 × 0.5		99.1 ± 0.3	0.9 ± 0.3	8.5 ± 0.1	1.43 ± 0.04	168	0.15
2	1	94.4 ± 0.0	5.6 ± 0.2	12.5 ± 0.2	2.21 ± 0.18	98	0.18
4 × 1		90.5 ± 0.4	9.5 ± 0.6	17.6 ± 0.1	2.97 ± 0.16	85	0.20
5	2	86.8 ± 2.1	13.2 ± 2.2	19.8 ± 0.2	3.27 ± 0.07	71	0.20
10		83.3 ± 2.6	16.7 ± 2.8	26.1 ± 0.01	4.88 ± 0.20	50	0.21
20		78.8 ± 0.1	21.2 ± 0.4	31.9 ± 0.4	5.76 ± 0.30	42	0.21
30	3	75.9 ± 0.2	24.1 ± 0.3	35.2 ± 0.6	5.58 ± 0.11	36	0.21

reduced and a higher lattice distortion is introduced into alite crystals. The significantly lower crystallite sizes of activated alites might be taken as an indication, that also the particle sizes of the alites are significantly decreased by mechanical activation. The determined crystallite size generally is lower than the particle size. Only for the special case that the particle is a single crystal then the particle and the crystallite size are concordant.

Additionally a partial amorphization and a considerably increased specific BET surface area of the samples are found after longer mechanical activation. With increasing specific surface area we observe an increased LOI, indicating that more ethanol from the grinding process was retained. But the retained ethanol is not expected to promote the hydration reaction.

3.2. Heat flow calorimetry

The heat flow curves and the heat of hydration of not activated and three of the mechanically activated alites are plotted in Fig. 1 as mean values with σ from at least three independent experiments. Not activated alite exhibits the typical four periods of hydration as described for the alite hydration reaction [25–27]: initial period, period of slow reaction or induction period, acceleration period and deceleration period could be observed within 24 h of hydration. During the initial period of not activated alite (0–1.5 h) only 2.7 ± 1.0 $J/g_{reactive\ solid}$ could be detected. This indicates, that only a very small amount of alite has dissolved up to 1.5 h (~0.5 ± 0.2 wt.% alite).

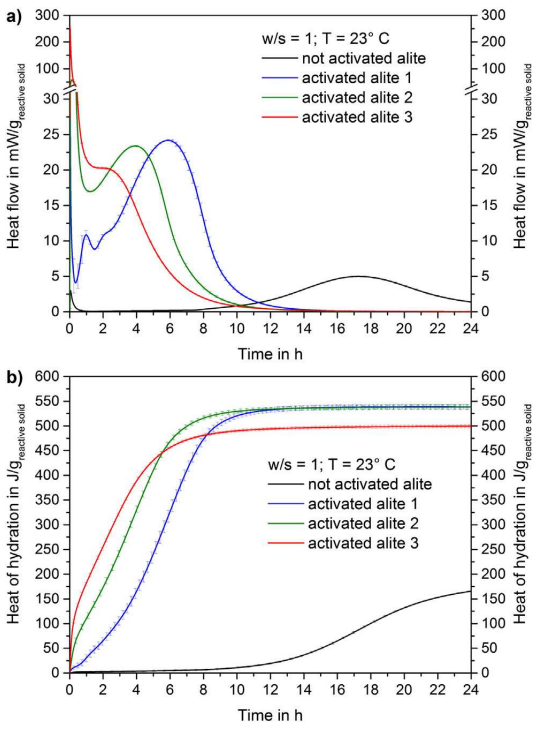

Fig. 1. Heat flow (a) and heat of hydration (b) of not activated and mechanically activated alites 1–3 at a w/s of 1 and 23 °C.

Mechanical activation of alite leads to a strong acceleration and intensification of alite hydration. Stronger mechanical activation leads to a more intense initial heat flow and an earlier start of the main hydration reaction. The main hydration period and the initial period are completely overlapping in the case of the most activated sample (alite 3). The period of slow reaction is dramatically shortened or disappears completely with increasing alite activation. The initial heat flow maximum increases with higher activation. The heat flow maxima of the main hydration of all activated alites are strongly enhanced in comparison to not activated alite. The hydration reaction for all activated alite samples is completed after about 16 h.

The values for heat of hydration of all activated samples and of not activated alite detected within 24 h and 48 h, respectively, are shown in Table 2. The values of all activated alites after 24 h are significantly higher than for not activated alite after the end of the main hydration period. The activated alites with activation times up to 5 h arrive at about the same total heat of hydration after 24 h, while a clear decrease in total heat of hydration could be observed for samples with activation times above 10 h.

3.3. In-situ XRD of the alite pastes

3.3.1. Phase development

The quantitative phase developments of activated alite 1–3 pastes as measured by in-situ XRD are shown in Fig. 2a–c. The decrease of crystalline alite and the increase of portlandite and C–S–H_{lro} as mean values of at least three separate experiments with 1 σ are compared with the corresponding heat flow. Solid lines represent the fitted graph of the mean values for each curve that were used for further analysis (fitted with one or two 5 parameter logistic functions).

Table 2
Heat of hydration of not activated and all mechanically activated alites after 24 h of hydration at a w/s of 1 and 23 °C.

Activation time in h	Activated alite	$\Delta H_{24\ h}$ in $J/g_{reactive\ solid}$
0	Not activated	219.0 ± 2.1 ($\Delta H_{48\ h}$)
1		539.9 ± 2.0
2 × 0.5		540.2 ± 2.6
2	1	538.4 ± 4.7
4		543.9 ± 1.7
5	2	537.9 ± 4.8
10		521.5 ± 1.6
20		511.6 ± 11.1
30	3	499.4 ± 3.1

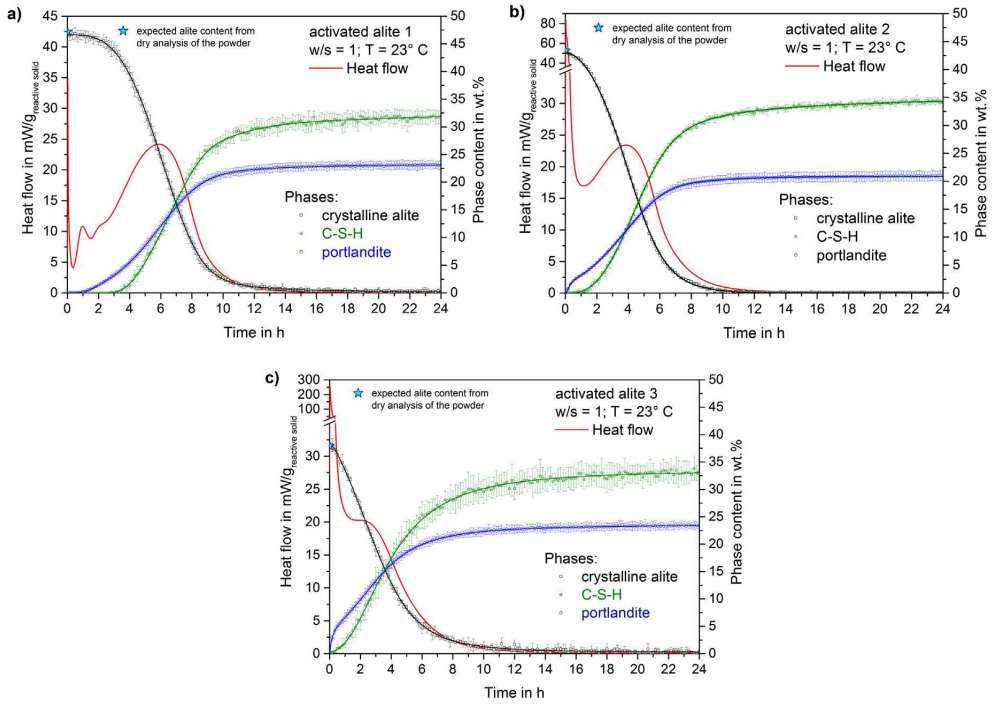

Fig. 2. Hydration of mechanically activated alite samples 1–3 at w/s = 1 and T = 23 °C (a–c, respectively). Comparison of heat flow measured by calorimetry and phase development detected by in-situ paste XRD. The mean values ± σ of at least three measurements are shown together with the fitted curve.

The theoretically expected crystalline alite content (according to XRD analysis of the dry powder) can be found as first value of the in-situ XRD experiments (time scale of ca. 2–12 min after mixing) within the errors of analysis in all samples. Due to the presence of more amorphous "alite" in higher activated alites the crystalline alite content is reduced. Since crystalline alite has not been dissolved directly after mixing and the amorphous "alite" content is increased by activation, the intensification of the initial period with longer activation of alite (Fig. 1) can be accounted to the hydration of the amorphous "alite" content of the samples.

In the activated alite 1 sample (Fig. 2a) the alite content is constant for the first hour and then starts to decrease slowly. The dissolution increases and arrives at apparently linear alite dissolution per unit of time. After 8 h of hydration, the dissolution of alite is decelerating. The complete crystalline alite has been dissolved between 14 and 16 h.

The dissolution of crystalline alite directly after mixing in the activated alite 2 sample proceeds alike in sample 1 after ~2 h of hydration (Fig. 2b). Crystalline alite content decreases continuously and is dissolved completely after 12–14 h of hydration. For hydration of activated alite 3 (Fig. 2c), the apparently linear alite dissolution per unit of time can already be observed within the first hour of hydration. The dissolution kinetics for crystalline alite in sample 3 directly after mixing is alike in sample 1 (after 3.5 h) or 2 (after 2.5 h). The deceleration of the dissolution of alite in sample 3 takes a little longer compared to the other samples.

The phase development of portlandite in the higher activated alite pastes proceeds in two main precipitation steps separated from each other, indicating different regimes of precipitation. This can be observed most markedly in activated alite 2 (Fig. 2b). The precipitation of portlandite is very fast within the first hour, then slows down and finally is accelerated again after 2 h of hydration. The latter acceleration corresponds very well in time to the dissolution of crystalline alite, whereas the first portlandite precipitation does not correspond to dissolution of crystalline alite. For the highest activated alite sample 3 (Fig. 2c), 2.7 ± 0.5 wt.% portlandite can be detected within the first diffractogram (after 2–12 min of hydration), while no crystalline alite has been dissolved (36.0 ± 1.1 wt.% in the paste, while 35.8 ± 0.2 wt.% would be expected from dry powder analysis). For sample 3, the precipitation rate of portlandite is much higher within the first 0.5 h of hydration than in the following time period. Later in time, the alite dissolution is proceeding faster. So we can summarize that the early precipitation of portlandite provides further evidence, that amorphous "alite" already reacts before crystalline alite is starting to dissolve.

Precipitation of C–S–H_{Iro} can always be detected significantly later than dissolution of crystalline alite and precipitation of portlandite. In the activated alite 3 sample, precipitation of C–S–H_{Iro} can be detected within the first 0.5 h of hydration. In all samples, C–S–H_{Iro} can be detected at the point in time, when crystalline alite is starting to show a linear dissolution per unit of time as already reported before for not activated alite at a w/s of 0.5 [11]. A direct comparison of the activated alite with not activated alite by in-situ XRD at a w/s of 1 was not possible because of sedimentation of alite particles to the bottom of the sample.

3.3.2. Precipitation of "long-range ordered" C–S–H (C–S–H_{Iro})

The in-situ XRD shows that high mechanical activation can lead to complete alite dissolution in the activated alite samples within 24 h. In Fig. 3 an in-situ XRD pattern of a hydrated activated alite 2 paste after 24 h of hydration is presented. Alite is dissolved completely and only portlandite and C–S–H_{Iro} reflections and an increased background from the remaining free water can be detected.

For Rietveld refinement of the in-situ diffractograms the coherently scattering domain (CSD) size of C–S–H_{Iro} is used to fit the line broadening of C–S–H reflections. No differentiation between crystallite size and strain is possible due to the low time resolution from the in-situ

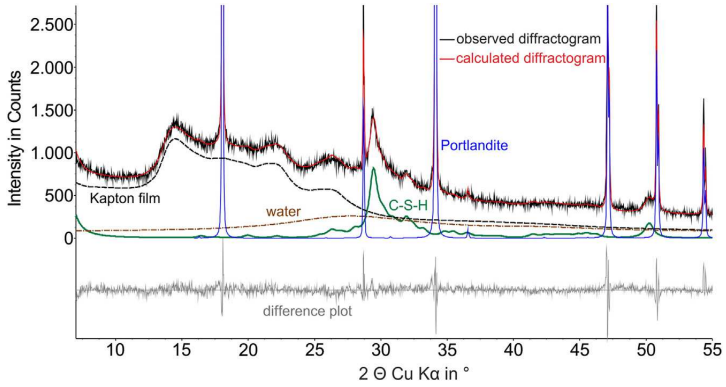

Fig. 3. Rietveld refinement of activated alite 2 after 24 h of hydration at w/s = 1 and T = 23 °C. Alite is dissolved completely, while "long-range ordered" C–S–H, portlandite, and the remaining free water can be detected. The background is fitted with "hkl"-phases for free water and Kapton® polyimide film and with a Chebyshev polynomial of 1st order.

quantification. Another handicap for differentiation between both parameters is the low ° 2Θ range, where significant C–S–H peaks are found. The determined mean CSD sizes of C–S–H_{lro} of 8 ± 1 nm (as Vol-IB) are very similar for all activated alites. A sufficient amount of C–S–H must have formed to ensure a meaningful refinement outcome. In respect of the limits of analysis, the CSD sizes do not change significantly during 24 h of hydration. The CSD sizes of C–S–H_{lro} remain at very low levels, indicating that no explicit crystallite growth occurs.

3.3.3. Dissolution and precipitation rates calculated from in-situ XRD

Dissolution rates of crystalline alite together with precipitation rates of portlandite and C–S–H_{lro} in hydrating activated alite pastes were calculated from the fitted curves of quantitative phase analysis (Fig. 2) recorded by in-situ XRD.

The maximum dissolution rates of crystalline alite (Fig. 4) are determined between 0.65 and 0.79 mmol/(h•$g_{reactive\ solid}$) for the different alite samples. The maximum dissolution rates of alite are always observed at the same point in time as the maxima of the heat flow measurements are occurring. The maximum dissolution rates of crystalline alite for samples 1 and 2 are very comparable and slightly lower for sample 3 (activated alite 3: highest amorphous content and specific surface area). The maximum dissolution rates of crystalline alite are in a comparable magnitude as the dissolution rates for alite reported by Nicoleau et al. [5] at w/s ratio 10,000: 0.97 mmol/(h•g) for the dissolution of C_3S-m in 20 mM $Ca(OH)_2$ solution and 0.32 or 0.45 mmol/(h•g) for the dissolution of C_3S-t2 in different prior filtrated C_3S solutions with relatively low Si concentrations.

The precipitation rates of portlandite in samples 2 and 3 are higher in the initial period than in the main hydration period (Fig. 5). The maximum precipitation rates of portlandite for the main hydration period in activated alites 1–3 are very close to each other at 0.91 to 0.96 mmol/(h•$g_{reactive\ solid}$). Portlandite precipitation also occurs at times when there is no or very low crystalline alite dissolution rate. This is the case during the initial period for samples 2 and 3 and between 1 and 2 h of hydration in activated alite 1.

The precipitation rates of C–S–H_{lro} (Fig. 5) increase significantly later than the precipitation rates of portlandite and accordingly the dissolution rates of crystalline alite. The maximum precipitation rate of C–S–H_{lro} is comparable for all activated alite samples between 0.56 and 0.64 mmol/(h•$g_{reactive\ solid}$). The precipitation rates of C–S–H_{lro} start to increase at the same time as the dissolution rates of crystalline alite have reached values between 0.1 and 0.15 mmol/(h•$g_{reactive\ solid}$) in the acceleration period of hydration.

For better comparison the dissolution rate of crystalline alite together with the precipitation rates of portlandite and C–S–H_{lro} is shown in Fig. 6 exemplarily for the activated alite 1 sample. The dissolution rate of crystalline alite increases significantly later in time than the precipitation rate of portlandite. The precipitation rate of portlandite in the activated alite 1 sample increases between 1 and 2 h of hydration, which represents the same time period when two additional maxima of heat flow are detected (Fig. 1). The precipitation rate of portlandite plotted

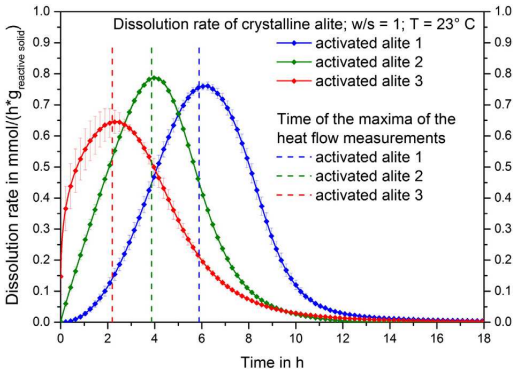

Fig. 4. Dissolution rates of crystalline alite during hydration of activated alites 1–3 at w/s = 1 and T = 23 °C as calculated from the results of in-situ XRD.

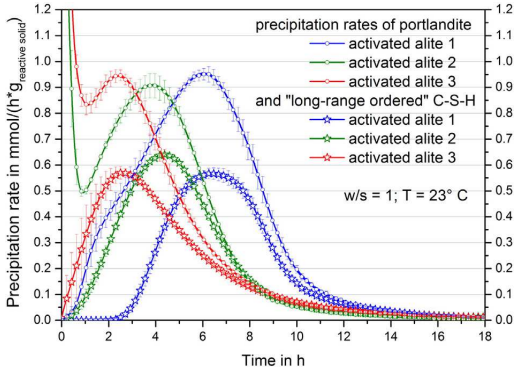

Fig. 5. Precipitation rates of portlandite and "long-range ordered" C–S–H during hydration of activated alites 1–3 at w/s = 1 and T = 23 °C as calculated from the results of in-situ XRD.

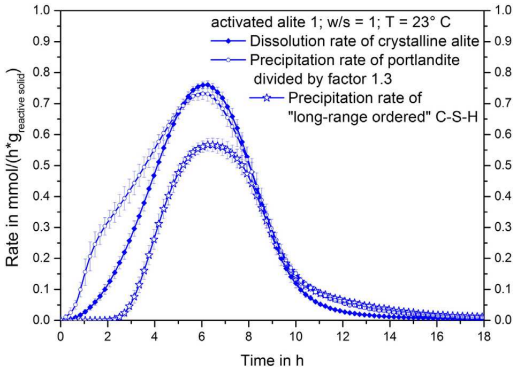

Fig. 6. Dissolution rate of crystalline alite, precipitation rates of portlandite (divided by factor 1.3) and "long-range ordered" C–S–H during hydration of activated alite 1 at w/s = 1 and T = 23 °C as calculated from the results of in-situ paste XRD.

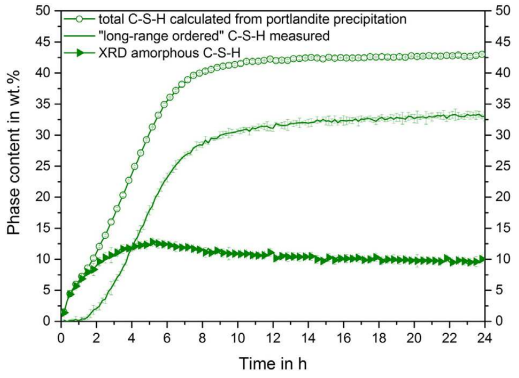

Fig. 7. Calculated expected total C–S–H phase content from portlandite precipitation, measured "long-range ordered" C–S–H content and resulting XRD amorphous C–S–H content in activated alite 2 paste.

in Fig. 6 is divided by the factor 1.3 for comparison. Provided, that the pore solution composition, which was not measured in this study, is not changed significantly during the main hydration period the ratio of dissolving alite and precipitating portlandite indicates, that about 1.3 mol portlandite precipitates from 1 mol of dissolved alite. This indicates, that the mean Ca/Si of C–S–H is around 1.7 and that portlandite and C–S–H precipitate rather synchronously within the main hydration period. The precipitation rate of C–S–H_{lro} increases significantly later in time than dissolution rate of alite and the precipitation rate of portlandite. The maximum precipitation rate of C–S–H_{lro} was found to be lower than the maximum dissolution rate of crystalline alite. There are two possible explanations for this. First of all, the assigned stoichiometry of C–S–H with $C_{1.7}SH_{2.6}$ (M = 202.2556 g/mol) might not be correct. As the Ca/Si ratio around 1.7 is a common value in literature for the early hydration of alite only the amount of water could be erroneous. But this would only have a small effect on the above described calculations. The more probable explanation is, that not all C–S–H is precipitating in the "long-range ordered" structure, which can be detected by XRD.

3.3.4. Estimation of XRD amorphous C–S–H phase content

Precipitation of C–S–H_{lro} could be detected significantly longer than dissolution of alite. From the phase development of portlandite we observed two separate precipitation events, indicating that the dissolution of amorphous "alite" is leading to the precipitation of portlandite in advance of the dissolution of crystalline alite. Hence an XRD amorphous form of C–S–H is very likely to exist in advance to C–S–H_{lro}.

From the course of precipitation of portlandite and C–S–H_{lro} as measured by in-situ XRD we could calculate an estimated amount of XRD amorphous C–S–H present in paste. For practical reasons both XRD amorphous C–S–H and C–S–H_{lro} were assigned the same average stoichiometry of $C_{1.7}SH_{2.6}$. Additionally we assumed that the complete reactive solid is converted into C–S–H and portlandite after 24 h of hydration. In Fig. 7 the overall calculated C–S–H content correlated to portlandite precipitation, the measured C–S–H_{lro} content and difference of both, which represents the content of XRD amorphous C–S–H in hydrating activated alite 2 paste are shown. The graph shows quite clearly that about two third of the XRD amorphous C–S–H precipitated before C–S–H_{lro} was detected. As soon as C–S–H_{lro} could be detected, the precipitation rate of XRD amorphous C–S–H decreased and finally came to an end as C–S–H_{lro} increased. Eventually, some of the XRD amorphous C–S–H was consumed again within the 24 h of hydration. In Fig. 8, the estimated development of XRD amorphous C–S–H for activated alites 1–3 is presented. All activated alite samples show comparable amounts of XRD amorphous C–S–H, so there is no correlation between amount of amorphous C–S–H and the amount of amorphous "alite". A small part of the XRD amorphous C–S–H decreased again within the 24 h hydration process, probably by conversion into C–S–H_{lro}. About 1/4 of the calculated expected C–S–H in the activated alite samples have to be present in an XRD amorphous form. But this was not the case for not activated alite. Such high amount of XRD amorphous C–S–H was definitely not indicated by the in-situ XRD analysis [11]. Instead, the heat flow calculation indicated, that the XRD amorphous C–S–H content has been converted to C–S–H_{lro} at the end of the main hydration period. The above presented results suggest that the high XRD amorphous C–S–H content in the samples must be due to the highly accelerated hydration reaction in the activated alites.

3.3.5. Development of the mean coherently scattering domain size of the remaining crystalline alite during hydration

In Fig. 9 the development of the mean sizes of coherently scattering domains (CSDs) of crystalline alite is shown with time as average ± σ. Only values for more than 3 wt.% of alite in the paste are taken into account. For activated alite 1, the mean CSD size is unchanged up to 2 h. Then the mean CSD sizes conduct the same way for all activated alites: The mean CSD size increases during the acceleration period. After the maximum of the main hydration period, the trend is reversed and the mean CSD size decreases.

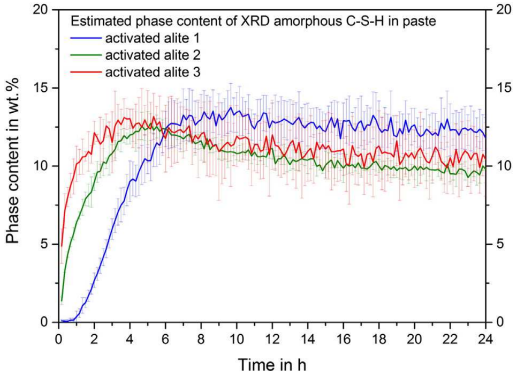

Fig. 8. Calculated XRD amorphous C–S–H content in activated alite 1–3 paste.

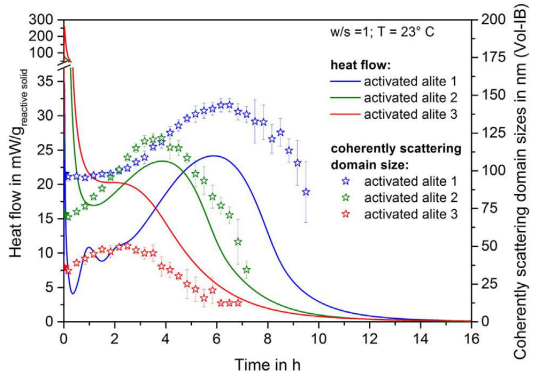

Fig. 9. Comparison between the measured heat flow and the development of the sizes of CSD of crystalline alite during hydration given as Vol-IB in nm. Filled stars at time zero represent the CSD sizes determined in the dry refinement.

3.4. Calculation of heat of hydration from powder XRD

The results of the in-situ XRD analysis as well as of the heat flow calorimetry indicated that the hydration reactions of all activated alite samples are completed within 24 h. Alite was dissolved completely but the contents of portlandite and C–S–H_{Iro} (Fig. 2) and also the calculated XRD amorphous C–S–H (Fig. 8) stayed unchanged in the paste between 18 and 24 h of hydration. The measured heat flow was close to 0 mW/g after 18 h of hydration in all activated samples.

Therefore we can assume that the heats of hydration measured after 24 h of hydration (ΔH_{24h}) of activated alite paste represent the total enthalpy of reaction. The ΔH_{24h} values (Table 2) are lower for the higher activated alite samples. This suggests that the hydration reactions of crystalline and amorphous "alite" exhibit different enthalpies of reaction.

The heat contributions of both crystalline and amorphous "alite" sum up to the measured total enthalpy of reaction ΔH_{24h} in every alite sample, but in different proportions for each sample. The enthalpies for the hydration reaction of crystalline alite ($\Delta H_{crystalline.alite}$) and of amorphous "alite" ($\Delta H_{amorphous.alite}$) were determined by regression from the total heat of hydration (ΔH 24 h) over the range of amorphous "alite" contents which were found in the activated alite samples. The so derived enthalpies of reaction for the hydration of crystalline alite and for amorphous "alite" are presented in Fig. 10. The best solution by regression gives $\Delta H_{crystalline.alite} = 548$ J/g ± 5.2 J/g, and $\Delta H_{amorphous.alite} =$ 386 J/g ± 32 J/g.

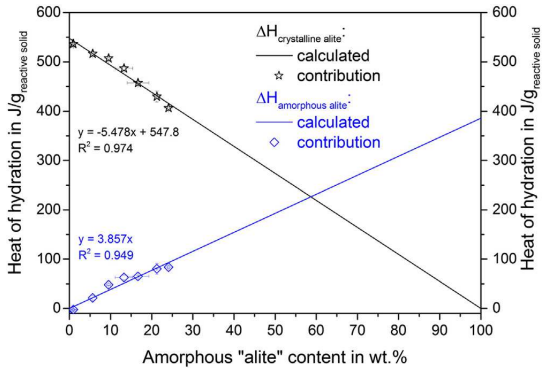

Fig. 10. Calculated heat contribution for the hydration reaction of reactive solid from amorphous "alite" (blue) and from crystalline alite (black) in dependence of the amorphous "alite" content. (For interpretation of the references to color in this figure legend, the reader is referred to the web version of this article.)

3.5. Calculation of heat of hydration from crystalline alite dissolution

It was shown before, that from dissolution of crystalline alite during hydration by in-situ XRD a "calculated" heat flow curve can be derived [11,28,29]. On the one hand it could be proven, that the main period of alite hydration is described very well by this approach. This approach is reasonable when assuming that the alite hydration is a process of synchronous alite dissolution and precipitation of portlandite plus C–S–H. It has been shown nevertheless, that the approach works although the precipitation of XRD detectable C–S–H_{Iro} was found not to proceed synchronously with the alite dissolution [11].

The heat of hydration was calculated from the dissolution of crystalline alite measured by in-situ XRD using $\Delta H_{crystalline.alite}$ of −548 J/g as determined in Section 3.4.

The comparison of calculated with the heat flow measured by isothermal calorimetry is shown in Fig. 11. The calculated heat flow describes well the period of main hydration and the point in time of the heat flow maximum. The highest deviation is found for activated alite 1 where the maximum is shifted by 19 min to later times. But the calculated heat flow is systematically higher than the measured one. This might be explained by slightly different reaction conditions for calorimetric and in-situ XRD experiments and was also observed for not activated alite before when using a calculated ΔH of 561 J/g [11]. The most obvious conclusion from Fig. 11 is that the initial heat flow, which is increasing with higher mechanical activation of alite, cannot be assigned to the hydration of crystalline alite. Furthermore, the two local maxima within the acceleration period of activated alite 1 cannot be explained with the hydration of crystalline alite. This suggests that this heat flow was caused by the dissolution and reaction of the amorphous "alite" content of the samples.

4. Discussion

4.1. Complete reaction degree in activated alites

We suggest, that the complete dissolution of crystalline alite during the first 24 h can be explained by the very small particle size of the crystalline alites. Costoya [18] showed that for alites with fractionated particle size distributions, the main hydration reaction was intensified with lower mean particle size, giving a higher degree of hydration for

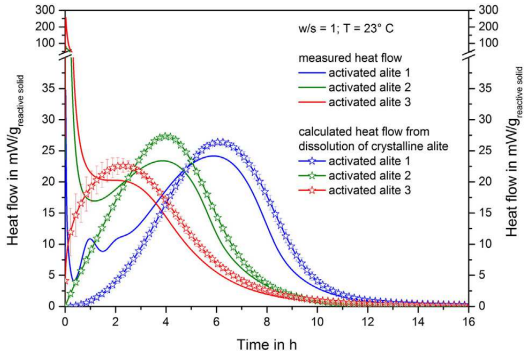

Fig. 11. Comparison of the measured heat flow and the heat flow calculated from the dissolution–precipitation reaction of crystalline alite as measured by in-situ XRD.

smaller particles. Since the mildest mechanical activation of alite introduced in this study arrived at a significantly higher specific surface area than the alites studied by Costoya, it is plausible that alite conversion in our experiments is complete for activated alites. The particle size distribution of the activated alites was not measurable by laser granulometry due to their very small sizes. It is also not helpful to calculate a medium particle size from the BET specific surface, because it cannot be distinguished between the surfaces of amorphous and crystalline alite.

4.2. Standard enthalpy of alite hydration reaction

Alites that showed a complete hydration reaction within 24 h (samples after 1 h of activation) were analyzed. For not activated alite samples, the hydration reaction would continue for months to arrive at a complete alite conversion. The instability of the baseline of a calorimeter makes it impossible to obtain a meaningful heat of hydration value for such long measurements. Therefore, standard enthalpies of formation are commonly used for the calculation of the enthalpy of reaction of alite hydration. The observed value of -548 J/g $\pm$ 5.2 J/g for $\Delta H_{crystalline,alite}$ is quite close to the values calculated for the silicate reaction following Eq. (1) of -561 J/g [11,28,29] and to the calculated value of -544 J/g by Bellmann et al. [8] from slightly different thermodynamic data.

$$C_3S + 3.9H_2O \rightarrow C_{1.7}SH_{2.6} + 1.3CH \quad (1)$$

The reaction of the amorphous parts of alite in the samples was found to be significantly less exothermic than the reaction of the crystalline alite. Assuming that the reaction of the amorphous "alite" resulted in the same hydration products as the reaction of the crystalline alite (portlandite and $C_{1.7}SH_{2.6}$), the difference in ΔH of 162 J/g would represent the decrease in standard enthalpy of formation of alite due to the amorphization process.

4.3. The main hydration period

The highest activated alite sample 3 did not exhibit higher maximum dissolution rates of crystalline alite than the other activated alites. In this sample we could determine the highest amount of amorphous "alite", the highest specific surface area and the crystalline alite crystallites with the highest lattice distortion and the smallest crystallite size of all samples. All this was not leading to higher dissolution rates for the crystalline alite during the main hydration period of sample 3. From this findings we conclude, that the main hydration period is not only dominated by the alite dissolution rate, but also by nucleation and growth processes of one of the hydration products. As portlandite exhibits even higher precipitation rates in the initial period than in the main hydration period for activated alites 2 and 3, it is not likely that precipitation obstacles of portlandite are dominating the main hydration period. Even though different reasons for beginning and ending of the induction period have been discussed, it is indeed well established that the main hydration period is controlled by the precipitation of C–S–H [27].

4.3.1. Initial, induction and acceleration period

Pore solution analysis of not activated alite showed that silicate species in solution achieved their maximum during the initial period [12,13]. Shortly afterwards, the silicate concentration significantly decreased. This can only be explained by precipitation of a silicate phase. This kind of initially precipitated C–S–H is obviously not leading to an acceleration of the hydration reaction. On the contrary, the reaction slowed down, resulting in the induction period. From this initially precipitated C–S–H it is known, that it contains monomeric silicate species [7,14,15] and that it exhibits an XRD amorphous ordering. But it is unknown, if a continuous layer around alite is formed which then causes the beginning of the induction period.

The hydration mechanism in all activated alite samples seems to be concordant. Even the calculated XRD amorphous C–S–H content is obviously proceeding comparably within all samples (Fig. 8). It is therefore unlikely that the precipitated XRD amorphous C–S–H present in the samples is hindering the further dissolution of alite by formation of a metastable barrier covering the alite.

Considering that the alite dissolution rate is influenced by the pore solution concentration [3,5], the precipitation of hydration products would actually be the trigger for a faster dissolution of alite in the period after initial heat flow. In case that the hydrate phases, present at this point in time, are not providing ideal surfaces for additional hydrate phases to precipitate, an induction period is resulting. Then at the end of the induction period, a different kind of C–S–H has to nucleate, respectively the initial C–S–H has to evolve. Both effects are leading to the start of the acceleration period.

Precipitation of C–S–H_{lro} could be detected within the first 0.5 h of hydration for activated alite sample 3. The very soluble amorphous "alite" with very high specific surface area in combination with a crystalline but highly distorted alite of very small mean crystallite size results in a very strong shift of the reaction kinetics to earlier times (Fig. 2). Pore solution composition must be highly supersaturated directly after mixing and a high probability is given, that within this short period of time the type of C–S–H evolves that is offering the ideal surface for more C–S–H to precipitate.

With the start of the acceleration period, the first silicate dimers were observed by ^{29}Si NMR investigations. Intermediate C–S–H formed before that point in time consists of monomeric silicate tetrahedra only [7,14,15]. The formation of dimeric silicate species seems therefore to be the crucial step for precipitation or evolution of a C–S–H-type that is providing proper surfaces for further hydrate precipitation.

A second crucial step to such type of C–S–H seems to be the development of a nanoparticular C–S–H with a "long-range ordered" crystal structure. It was previously reported for not activated alite paste, that the first C–S–H_{lro} was observed during the acceleration period, i.e. before the dissolution of alite is proceeding linearly with time [11]. The hydration experiments of activated alite showed, that the point in time of the first detection of C–S–H_{lro} is well defined. The C–S–H_{lro} precipitation could always be observed at the same stage of hydration, namely when the crystalline alite dissolution rate increased above 0.1–0.15 mmol/(h•$g_{reactive\ solid}$). The occurrence of C–S–H_{lro} seems to control the main hydration period as the precipitation of XRD amorphous C–S–H comes to an end after the development of C–S–H_{lro}. We conclude that the development of dimeric silicate species must be the initial step for the development of C–S–H_{lro}. Amorphous dimeric precursors of C–S–H finally lead to the end of the induction period. But the development of a "long-range ordered" structure is an essential step for the acceleration of the hydration reaction.

4.3.2. Transition between acceleration and deceleration period

With the introduction of the Boundary Nucleation and Growth Model, Thomas [30] showed that the shift between acceleration and deceleration period can be described by a nucleation and growth mechanism solely. Bishnoi & Scrivener [31] stated that the hindrance of growing C–S–H clusters on the same particle and impingement with nuclei from other particles can lead to deceleration of the main hydration period. According to Nicoleau [32,33] the deceleration can only result from the decrease of the dissolution rate of alite due to the coverage of the alite surfaces with C–S–H. Bullard et al. [27] stated, that in addition to diffusion processes the factors consumption of small particles, lack of water or lack of space might be responsible for the deceleration.

We mainly agree with the idea of Bullard et al. that the depletion of small particles plays an important role. The results in Section 3.3.5 show an increase of the mean CSD size of alite in the acceleration period and a decrease in the deceleration period (Fig. 9). At the beginning of the acceleration period alite is dissolving at all available alite surfaces. The dissolution of alite strongly depends on the necessary precipitation of

C–S–H and portlandite, so it is not responsible for the acceleration itself. Alites with small mean CSD size are dissolving relatively faster and the mean CSD size of the remaining alite increases therefore. At the maximum of the main hydration period, the alites with small CSD sizes are depleted. The acceleration of the hydration process has to come to an end. The remaining alite surfaces available for the hydration process are then around the larger crystallites of the residual particles. The dissolution of the remaining larger alite particles left in paste is then obviously leading to the deceleration of the hydration process of the activated alite pastes.

Unfortunately, it is not possible to analyze not activated alite pastes in the same way. This is because the CSD sizes of not activated alites are significantly larger, and the significance of the CSD size values decreases sharply for sizes far above 100 nm. The effect of higher CSD sizes on the peak profiles can be disregarded compared to the effect from the instrumental line broadening. The finding for activated alite that hydration decelerates after the consumption of the available small particles should nevertheless also be valid for not activated alites. With respect to not activated alite, all particles are smaller in the activated alites. This leads to a more intense hydration reaction and a complete reaction turnover. We recalculated surface and volume of the investigated not activated alite particles from laser granulometry results by assuming spherical particles. Only 10 vol.% of the alite particles resulted in a surface/volume-ratio above 1.9. After dissolution of this 10 vol.% the cumulated volume of the residual alite particles becomes higher than their cumulated surface. This in consequence leads to a significantly decreased available alite surface. We assume that less available surface area of alite generally is the dominating factor causing the deceleration of hydration reaction.

4.4. The "growth" of "long-range ordered" C–S–H (C–S–H_{lro})

A mean CSD size for C–S–H_{lro} of 8 ± 1 nm (as Vol-IB) was calculated by Rietveld analysis (Section 3.3.2). This value might be defective as the crystallite size was refined for a fixed strain. But as stated before by Nonat [34] C–S–H nanoparticles are not necessarily defective, so disregarding strain is not necessarily incorrect.

The mean CSD size of C–S–H_{lro} is larger for the activated alites than for not activated alite (5.5 to 6.5 nm Vol-IB in [11]). The formation of "larger" crystallites of C–S–H_{lro} in the activated alites is not leading to a higher number of reflections in XRD pattern than for not activated alite (Fig. 3). C–S–Hs with large CSD sizes from supersaturated solutions are obviously exhibiting more reflections than can be observed for C–S–H_{lro}. This difference is shown e.g. in Fig. 2 of Nonat [34] who is referring to Courault [35]. The C–S–H reflections from hydration of a mix of C_3S and SiO_2 presented by Nonat are matching the C–S–H_{lro} detected for the hydration of not activated or activated alites from this study (Fig. 3).

The mean CSD size found for C–S–H_{lro} is in good agreement with other experimental data. Atomic force microscopy imaging studies described C–S–H to consist of identical, aggregated nanoscale C–S–H particles with lamellae of 60 × 30 × 5 nm in size [34,36]. The smallest nanoparticles of 5 nm could be identified also in small-angle neutron scattering experiments [37]. Nano-indentation tests showed, that the mechanical behavior of C–S–H can be described with a nano-sized granular material with two limited packing densities [38]. The colloid model for C–S–H from Jennings [39] enables to describe the microstructure of cement paste, assuming C–S–H to be an assembly of non-spherical globules with a cross section of 5 nm. In the light of the different methodologies that arrive at very similar dimensions, the results from in-situ XRD support the idea of C–S–H being a colloidal material that is not undergoing a crystal growth in the same sense as portlandite is growing. The growth of C–S–H is therefore rather a continuous nucleation and aggregation process, while the existing C–S–H particles provide certainly the best substrate for nucleation of precipitating C–S–H nanoparticles.

5. Conclusions

The mechanical activation of alite is leading to several effects: partial amorphization of the alite powder, increase in specific surface area, reduction of the mean crystallite sizes and enhancement of lattice distortion in the remaining alite crystallites.

The observed hydration of such activated alite with water was strongly accelerated and intensified. The initial heat flow was intensified due to the hydration reaction of the amorphous "alite" content. The initial and the main period of higher activated alites were superposing. The crystalline alite was found firstly to dissolve during the main hydration period solely and secondly to dissolve completely within 24 h.

XRD amorphous C–S–H phase is indicated to precipitate in considerable amounts, before "long-range ordered" (XRD detectable) C–S–H is observed in each activated alite sample. This is also the case, when the "long-rage ordered" C–S–H is formed within the first 0.5 h of hydration as in the highest activated alite sample. This makes it unlikely, that the XRD amorphous C–S–H is forming a metastable barrier around the alite grains.

We conclude that the induction period is due to the time necessary for the formation of dimeric "long-range ordered" C–S–H from monomeric (XRD amorphous) C–S–H. The main hydration period therefore is controlled by the nucleation of C–S–H_{lro}, while the transition from acceleration to deceleration period can be attributed to the completed dissolution of smaller alite particles. The available alite surfaces are reduced to the surfaces of the remaining larger alite particles and consequently the dissolution rate of alite is slowed down in concordance with the decrease of heat flow.

The refinement of the coherently scattering domain (CSD) size of XRD detectable, "long-range ordered" C–S–H showed, that C–S–H forms nanoparticles. But CSD mean size was not increasing during the investigation time. The formation of C–S–H is therefore assumed to result from successive nucleation and aggregation processes.

The enthalpy of reaction for the crystalline alite hydration and the hydration reaction of the amorphous "alite" was calculated from the measured heat of hydration after completed hydration. The determined value for amorphous "alite" ($\Delta H_{amorphous.alite} = -386\ J/g \pm 32\ J/g$) was found to be distinctly less exothermic than for crystalline alite ($\Delta H_{crystalline.alite} = -548\ J/g \pm 5.2\ J/g$).

Appendix A. Supplementary data

Supplementary data to this article can be found online at http://dx.doi.org/10.1016/j.cemconres.2015.06.005.

References

[1] H.M. Jennings, Aqueous solubility relationships for two types of calcium silicate hydrate, J. Am. Ceram. Soc. 69 (1986) 614–618.
[2] A.J. Allen, J.J. Thomas, H.M. Jennings, Composition and density of nanoscale calcium–silicate–hydrate in cement, Nat. Mater. 6 (2007) 311–316.
[3] P. Juilland, E. Gallucci, R. Flatt, K. Scrivener, Dissolution theory applied to the induction period in alite hydration, Cem. Concr. Res. 40 (2010) 831–844.
[4] A.C. Lasaga, A. Lüttge, Variation of crystal dissolution rate based on a dissolution stepwave model, Science 291 (2001) 2400–2404.
[5] L. Nicoleau, A. Nonat, D. Perry, The di- and tricalcium silicate dissolutions, Cem. Concr. Res. 47 (2013) 14–30.
[6] H.F.W. Taylor, P. Barret, P.W. Brown, D.D. Double, G. Frohnsdorff, V. Johansen, D. Menetrier-Sorrentino, I. Odler, L.J. Parrott, J.M. Pommersheim, M. Regourd, J.F. Young, The hydration of tricalcium silicate; RILEM Committee 68-MMH, Task Group 3, Mater. Constr. 17 (1984) 457–468.
[7] F. Bellmann, D. Damidot, B. Möser, J. Skibsted, Improved evidence for the existence of an intermediate phase during hydration of tricalcium silicate, Cem. Concr. Res. 40 (2010) 875–884.
[8] F. Bellmann, T. Sowoidnich, B. Möser, Formation of an intermediate phase and influence of crystallographic defects on dissolution of C_3S, Proceedings of 13th ICCC, Instituto de Ciencias de la Construccion "eduardo Torroja", Madrid, Spain, 2011.
[9] R.A. Livingston, J.S. Schweitzer, C. Rolfs, H.-W. Becker, S. Kubsky, Characterization of the induction period in tricalcium silicate hydration by nuclear resonance reaction analysis, J. Mater. Res. 16 (2001) 687–693.

[10] R.A. Livingston, J.S. Schweitzer, C. Rolfs, H.-W. Becker, S. Kubsky, T. Spillane, J. Zickefoose, M. Castellote, P.G. de Viedma, J. Cheung, Heavy ion beam measurements of the hydration of cementitious materials, Appl. Radiat. Isot. 68 (2010) 683–687.
[11] S.T. Bergold, F. Goetz-Neunhoeffer, J. Neubauer, Quantitative analysis of C–S–H in hydrating alite pastes by in-situ XRD, Cem. Concr. Res. 53 (2013) 119–126.
[12] P.W. Brown, E. Franz, G. Frohnsdorff, H.F.W. Taylor, Analyses of the aqueous phase during early C3S hydration, Cem. Concr. Res. 14 (1984) 257–262.
[13] S. Garrault, A. Nonat, Hydrated layer formation on tricalcium and dicalcium silicate surfaces: experimental study and numerical simulations, Langmuir 17 (2001) 8131–8139.
[14] N.J. Clayden, C.M. Dobson, C.J. Hayes, S.A. Rodger, Hydration of tricalcium silicate followed by solid-state 29Si N.M.R. spectroscopy, J. Chem. Soc. Chem. Commun. (1984) 1396–1397.
[15] S.A. Rodger, G.W. Groves, N.J. Clayden, C.M. Dobson, Hydration of tricalcium silicate followed by 29Si NMR with cross-polarization, J. Am. Ceram. Soc. 71 (1988) 91–96.
[16] R. Schrader, H. Schuhmann, Zur mechanischen Aktivierung von Silikaten, Z. Chem. 7 (1967) 322.
[17] I. Odler, J. Schüppstuhl, Early hydration of tricalcium silicate III. Control of the induction period, Cem. Concr. Res. 11 (1981) 765–774.
[18] M. Costoya, Kinetics and Microstructural Investigation on the Hydration of Tricalcium Silicate(Doctoral Thesis) École Polytechnique Fédérale de Lausanne, Switzerland, 2008.
[19] B.H. O'Connor, M.D. Raven, Application of the Rietveld refinement procedure in assaying powdered mixtures, Powder Diffr. 3 (1) (1988) 2–6.
[20] D. Jansen, F. Goetz-Neunhoeffer, C. Stabler, J. Neubauer, A remastered external standard method applied to the quantification of early OPC hydration, Cem. Concr. Res. 41 (2011) 602–608.
[21] A.G. De La Torre, S. Bruque, J. Campo, M.A.G. Aranda, The superstructure of C3S from synchrotron and neutron powder diffraction and its role in quantitative phase analyses, Cem. Concr. Res. 32 (2002) 1347–1356.
[22] W.R. Busing, H.A. Levy, Neutron diffraction study of calcium hydroxide, J. Chem. Phys. 26 (3) (1957) 563–568.
[23] D. Ectors, J. Neubauer, F. Goetz-Neunhoeffer, The hydration of synthetic brownmillerite in presence of low Ca-sulfate content and calcite monitored by quantitative in-situ-XRD and heat flow calorimetry, Cem. Concr. Res. 54 (2013) 61–68.
[24] M. Wojdyr, Fityk: a general-purpose peak fitting program, J. Appl. Crystallogr. 43 (2010) 1126–1128.
[25] H.F.W. Taylor, Cement Chemistry, 2nd ed. Thomas Telford, London, 1997.
[26] E.M. Gartner, J.F. Young, D.A. Damidot, I. Jawed, Hydration of portland cement, in: J. Bensted, P. Barnes (Eds.), Structure and Performance of Cements, 2nd ed.Spon Press, New York 2002, pp. 57–113.
[27] J.W. Bullard, H.M. Jennings, R.A. Livingston, A. Nonat, G.W. Scherer, J.S. Schweitzer, K.L. Scrivener, J.J. Thomas, The mechanisms of cement hydration, Cem. Concr. Res. 41 (2011) 1208–1223.
[28] D. Jansen, S.T. Bergold, F. Goetz-Neunhoeffer, J. Neubauer, The hydration of alite: a time resolved quantitative X-ray diffraction approach using G-factor method compared with heat release, J. Appl. Crystallogr. 44 (5) (2011) 895–901.
[29] D. Jansen, F. Goetz-Neunhoeffer, B. Lothenbach, J. Neubauer, The early hydration of Ordinary Portland Cement (OPC): an approach comparing measured heat flow with calculated heat flow from QXRD, Cem. Concr. Res. 42 (2012) 134–138.
[30] J.J. Thomas, A new approach to modeling the nucleation and growth kinetics of tricalcium silicate hydration, J. Am. Ceram. Soc. 90 (2007) 3282–3288.
[31] S. Bishnoi, K.L. Scriverner, Studying nucleation and growth kinetics of alite hydration using μic, Cem. Concr. Res. 39 (2009) 849–860.
[32] L. Nicoleau, Accelerated growth of calcium silicate hydrates: experiments and simulations, Cem. Concr. Res. 41 (2011) 1339–1348.
[33] L. Nicoleau, A. Nonat, A reply to the discussion "Accelerated growth of calcium silicate hydrates: experiments and simulations" by S. Bishnoi and K. Scrivener, Cem. Concr. Res. 42 (2012) 881–887.
[34] A. Nonat, The structure and stoichiometry of C–S–H, Cem. Concr. Res. 34 (2004) 1521–1528.
[35] A.-C. Courault, Simulation Experimentale Des C–S–H Dans Les Betons Modernes: Etude De La Composition Et Des Proprietes A L'equilire Dans Des Milieux Complexes, Universite de Bourgogne, Dijon, 2000.
[36] S. Garrault, E. Finot, E. Lesniewska, A. Nonat, Study of C–S–H growth on C_3S surface during its early hydration, Mater. Struct. 38 (2005) 435–442.
[37] A.J. Allen, R.C. Oberthur, D. Pearson, P. Schofield, C.R. Wilding, Development of the fine porosity and gel structure of hydrating cement systems, Philos. Mag. B 56 (1987) 263–288.
[38] G. Constantinides, F.-J. Ulm, The nanogranular nature of C–S–H, J. Mech. Phys. Solids 55 (2007) 64–90.
[39] H.M. Jennings, Refinement to colloid model of C–S–H in cement: CM-II, Cem. Concr. Res. 38 (2008) 275–289.

7.6. Influence of the reactivity of the amorphous part of mechanically activated alite on its hydration kinetics

Submitted to the Journal "Cement and Concrete Research" on 17th of February 2016.

Authors: S. T. Bergold, F. Goetz-Neunhoeffer, and J. Neubauer

Friedrich-Alexander-Universität Erlangen-Nürnberg (FAU), GeoZentrum Nordbayern, Mineralogy, Schlossgarten 5a, 91054 Erlangen, Germany

7.6.1. Abstract

The hydration of one mechanically activated alite passing through different drying procedures is examined by heat flow calorimetry and quantitative in-situ XRD analysis. The reactivity of the alite powders is strongly affected by the drying technique. It is shown that the reactivity of the amorphous part of the activated alite sample is particularly affected. Due to the fast initial dissolution of the amorphous "alite" part, the hydration progression is speeded up significantly. However, if the hydration is not speeded up by the amorphous "alite" dissolution, as in the case of surface passivation, the heat released until the transition to the deceleration period will increase. It is discussed that a crystalline alite dissolution by etch pit opening could increase the reactive alite surface and therefore increase the reaction degree at the transition to the deceleration period.

Keywords: Hydration (A), Acceleration (A), Calcium-Silicate-Hydrate (B), Amorphous material (B), Ageing (C)

7.6.2. Introduction

The intensive mechanical activation of alite has been shown to result in partial amorphous alite powders and a significant enhancement of their hydration process [1]. The remaining crystalline alites exhibited very small coherently scattering domain (CSD) sizes and high strains. The powders exhibited a large BET surface area and showed a complete reaction turnover within 24 h [1]. It was found that the amorphous part of the alite powder reacted before the crystalline alite and that the initial and main hydration period merged with a high amount of amorphous "alite". The main hydration period could be attributed to the decrease of crystalline alite content as analyzed by in-situ XRD. A considerable amount of XRD amorphous C-S-H was indicated as being formed during hydration of the mechanically activated alites. The XRD detectable "long-range ordered" C-S-H (C-S-H_{lro}) was always detected when the dissolution of crystalline alite accelerated [1].The deceleration of the main hydration period was found to be caused by the diminution of small alite particles as the mean CSD size of crystalline alite increased during acceleration and decreased during deceleration of the hydration reaction [1].

Sprung examined the ageing of cements during storage in silos and found that the cements were showing retardation during hydration [2]. Effects on the aluminate reaction due to the precipitation of aluminate hydrates were found but no influence on silicate phases was described [2]. Winnefeld also described the delaying of hydration and reduction of the hydration rate and turnover of aged cement due to prehydration of aluminate phases [3]. Seifert et al. [4] showed for storage of cement at 70 % RH that the reactivity of the cement and the turnover during the main period was lower with longer storage. The start of the main hydration period was found to be comparably delayed for cement that was stored for different lengths of time in comparison to fresh cement [4]. Stoian et al. [5] found it unlikely that the reduced heat of hydration found in calorimetric experiments could derive from the already released heat of hydration during the prehydration process, as the required degree of reaction would be very high (21 % during prehydration of the sample that was stored for the longest time) [5].

Dubina et al. [6] stated that the adsorption of water vapor on C_3S surface would only start at 75 % RH and only a minor amount of water would be adsorbed. Nevertheless, Dubina et al. showed earlier that water was adsorbed on C_3S surfaces during storage with a higher amount of adsorbed water for higher relative humidities (up to 0.29 and 0.54 wt.% for 60 and 85 % RH) and non-linearly more for a longer storage [7,8]. The prehydration would cause the formation of C-S-H and portlandite on the surface of C_3S. Due to the thin product layer, water took longer to reach the bulk C_3S than in fresh pastes [7, 8]. They showed in calorimetric experiments that the main hydration reaction for C_3S shifted to later times with a prolonged induction period for a longer storage or a higher relative humidity [7, 8].

Black et al. showed the formation of $CaCO_3$ and a silicon-rich outer surface layer on stored C-S-H samples with Ca/Si ratios > 0.75 [9]. This could explain a passivation process of previously formed small amounts of C-S-H on the alite surface during storage. Stoian et al. assumed that C-S-H that precipitates during prehydration would differ from C-S-H formed in a normal hydration process [5]. This C-S-H would not be able to accelerate the hydration reaction but would form a layer of hydrated/carbonated solids on cement particles [5]. This layer would act as a mass transport barrier and therefore complicate the hydration reaction. They stated that surface relaxation/reconstruction could take place too [5]. Fierens and Verhaegen noted a significant loss in reactivity due to storage of C_3S in “careful anhydrous conditions” which was accompanied by the decrease or disappearance of previously intensive thermoluminescence peaks [10]. It was suggested that the energy of trapped electrons could accelerate the hydration reaction [11]. The chemisorption of water on the excited surface centres of C_3S grains with consecutive formation of C-S-H nuclei on those sites would be enhanced due to this energy [11].

In our previous study on alite hydration [1], differently intensive mechanically activated alites were examined. In this study we present results for one alite powder, mechanically activated by a wet grinding process, which afterwards underwent different drying proceedures. The reactivity of the variably-dried alites is significantly altered. The impact of this alteration on the hydration process of the activated alite will be shown and discussed.

7.6.3. Materials and Methods

7.6.3.1. Materials

Monoclinic alite (M3 modification) was synthesized with a composition of 71.7 wt.% CaO, 25.9 wt.% SiO_2, 1.8 wt.% MgO and 0.6 wt.% Al_2O_3 as described elsewhere [1]. This alite was mechanically activated by intense grinding for 3 x 1 h (with an intermission of 0.5 h) in agate jars in a planetary ball mill from RETSCH at 250 rpm. 10 g of alite were milled in 40 ml ethanol with 175 g of 1.25 mm Y:ZrO_2 grinding balls. After the milling process, the alite-ethanol suspension was centrifuged at 3500 rpm and detached.

The residuum was treated in two different ways: one activated alite was dried as described before [1]. The centrifuge tubes were put in a vacuum drying chamber at 50° C, operating at 20 mbar of N_2 atmosphere. The vacuum drying chamber was flushed with N_2 in 6 flushing and evacuation cycles during the 2 days of drying. This sample will be referred to as alite VDC. In the second case, the centrifuge tubes were put in a drying chamber at 50° C in air. In the drying chamber, the humidity was reduced by silica gel to 44 % RH during drying times of 21, 63 and 112 h (samples DC 1-3). After drying, all the samples were ground carefully in an agate mortar and sieved for better deagglomeration.

7.6.3.2. Methods

The BET surface areas of the resulting samples was measured with a GEMINI Model 236 from MICROMERITICS in liquid N_2 by adsorption of N_2 gas. The surfaces of the samples were conditioned by heating the samples to 150° C and 350° C under He flow for 3 h. The loss of ignition (LOI) of the dried powders was determined at 1000° C ± 30° C in Pt-crucibles in air.

The dried samples were analysed by powder XRD using a D8 Advance from BRUKER-AXS equipped with a Lynx-Eye detector at 40 kV and 40 mA. Measurements were recorded from 7° to 80° 2Θ with a step size of 0.0223° 2Θ and a counting time of 0.5 s. The samples were measured with and without Kapton® polyimide film. The diffractograms were refined with the help of the program TOPAS 4.2 from BRUKER-AXS with consecutive calculation of the absolute phase contents in the samples by the external standard method [12-14]. NIST Silicon SRM 640d was used for calibration of the factor G. Two alite structures (both based on the same structural proposal [15]) were refined with different crystallite sizes and strains, both with Lorentzian functions. The lattice parameters were refined in very narrow constraints. The recordings with and without Kapton film were refined by coupling parameters over all samples under the assumption that the powders should consist of the same relative amounts of crystalline alite and amorphous inorganic material. In addition, factors for the determined LOI, the respective mass attenuation coefficients and for the presence of the Kapton film were introduced in the refinement. As all samples were measured on the same day, one constant G-factor was used for all samples with Kapton film and for all samples without Kapton film. This way, lattice parameters, crystallite size, strain and scale factors were refined coupled over all 4 samples in a threefold analysis.

The results presented in section 7.6.4 were normalized to the mass of reactive solid, which is the sum of crystalline and amorphous alite. The amount of amorphous “alite” was determined to be the difference to 100 wt.% after subtracting the amount of crystalline alite and LOI. However, for the results of the in-situ XRD analysis, the phase content in paste will be given.

The hydration kinetic of the variously-dried activated alite samples was examined by heat flow calorimetry (TAM AIR, TA Instruments) in combination with the InMixEr that allows the equilibration, injection of water to the powder, and mixing of both to a paste within the calorimeter cell. The kinetics can thus be determined directly from the start of the hydration process. The measurements were performed at 23° C ± 0.2° C at a water/solid (w/s) ratio of 1 due to the high water demand of the activated alite powders. The InMixEr holding the samples was previously equilibrated for at least 2 h within the calorimeter cell. At the start of the measurements, the water was injected and the sample was mixed at 860 rpm for 1 min. The heat flow curves were corrected for the calorimeter time constant, the baseline shift, and the calibration constant of the InMixEr [1].

The phase development within the hydrating activated alite pastes was determined by in-situ XRD measurements at the above-described D8 advance. A custom-made heating and cooling device ensured the constant temperature of 23° C ± 0.2° C of the samples. Additionally, the housing of the diffractometer was air-conditioned to 23° C ± 2° C. The measurements were recorded from 7° to 55° 2Θ with a step size of 0.0236° 2Θ with a counting time of 0.27 s (one diffractogram every 10 min). The samples were equilibrated before the measurements at 23° C ± 0.2° C. After injection of water (w/s =1), the samples were mixed manually with a spatula to a paste for 1 min and prepared in the PVC sample carrier. The samples were covered by a Kapton polyimide film to minimize water loss or CO_2 uptake during the experiment.

For the refinement of the in-situ experiments, the lattice parameters, crystallite sizes and strains of the two alite structures were fixed to the values determined in the dry refinement. All diffractograms of one experiment were refined together. This allowed the refinement of, e.g., the scale factor of the Kapton film model or the lattice parameters of portlandite coupled over all diffractograms of one measurement. The structure proposal of Busing & Levy was used for portlandite [16]. The C-S-H_{lro} phase model of [17] was used in combination with "hkl" models for Kapton film and free water and a Chebychev polynomial of 1st order to model the background of the diffractogram [17]. The resulting phase contents were fitted with one to three 5 parameter logistic functions [18] with the progam Fityk [19].

The phase content of XRD amorphous C-S-H in the paste was calculated. For this, the phase development of portlandite was scaled to the expected content of total C-S-H in paste following Equation 1. For practical reasons it was assumed that also the amorphous part of the samples would react in the same manner as the crystalline alite and a stoichiometry of $C_{1.7}SH_{2.6}$ for both XRD amorphous C-S-H and C-S-H_{lro}. To get to the phase development of XRD amorphous C-S-H, the measured C-S-H_{lro} content was subtracted from the derived expected total C-S-H content.

$$C_3S + 3.9\ H_2O \rightarrow C_{1.7}SH_{2.6} + 1.3\ CH; \quad \Delta H = 548\ J/g_{crystalline\ alite}\ \text{or}\ 386\ J/g_{amorphous\ alite}\ [1] \qquad (1)$$

7.6.4. Results

7.6.4.1. Analysis of the dry alite powders

Table 1 shows the results of the determination of LOI and BET measurements for the two different temperatures of prior heating. A larger surface area was determined when samples were heated at 150° C than when they were heated at 350° C. At a heating temperature of 150° C, the specific surface for alites DC 2 and 3 is slightly larger than for alite VDC. The BET surface areas of all samples are comparable after heating to 350° C. The LOI of the alites CD 1-3 is higher than for alite VDC and the LOI increases with longer residence time in the drying chamber. These results indicate that the alites DC 1-3 probably adsorbe some water or CO_2 from the atmosphere in the drying chamber.

Nevertheless, in all samples only alite and no hydrate or carbonate phases could be detected by XRD. The quantitative Rietveld refinement resulted in 90.4 wt.% of crystalline alite in the reactive solid. About 3 wt.% is assumed to represent the insecurity in the determined value due to the chosen refinement routine. Therefore, the milling process (identical for all samples) resulted in a partial amorphization of 9.6 ± 3 wt.% of the reactive solid. The mean coherently scattering domain (CSD) size of alite was determined to be 98 nm (Vol-IB) and the mean strain was 0.2 % (e0).

Table 1: LOI and BET surface area of the samples.

sample	drying regime	LOI in wt.%	BET specific surface area in m^2/g	
			after heating at 150 °C	after heating at 350 °C
alite VDC	vacuum drying for 2 d at 50° C and 20 mbar of N_2	2.52 ± 0.05	17.3 ± 0.2	15.6 ± 0.6
alite DC 1	drying chamber at 50° C for 21 h	3.07 ± 0.04	n.d.	n.d.
alite DC 2	drying chamber at 50° C for 63 h	3.29 ± 0.07	18.8 ± 0.6	15.0 ± 1.1
alite DC 3	drying chamber at 50° C for 112 h	3.80 ± 0.05	18.5 ± 1.2	14.8 ± 1.0

7.6.4.2. Hydration behaviour of the alite powders with water

7.6.4.2.1. Heat flow calorimetry

Fig. 1 presents the hydration kinetics of the variably-dried activated alite samples with water as mean value of 4 independent measurements with 1 σ. It is worth restating that the samples differ in the drying procedure only. These differences in the drying lead to a significant shift of the main heat flow events of the different alite samples to later times. For alites DC 1-3, the shift increases for longer drying times. This could not be found for longer drying times in the vacuum drying chamber under 20 mbar of N_2.

Alite sample VDC exhibits fastest hydration kinetics (Fig 1). The initial period is enhanced and the main hydration maximum appears earlier compared to the other samples. The initial

heat flow of alite DC 1 is a little less intense than the one of alite VDC and exhibits a shoulder. The initial heat flow of alites DC 2 and 3 is significantly lower and for both samples a period

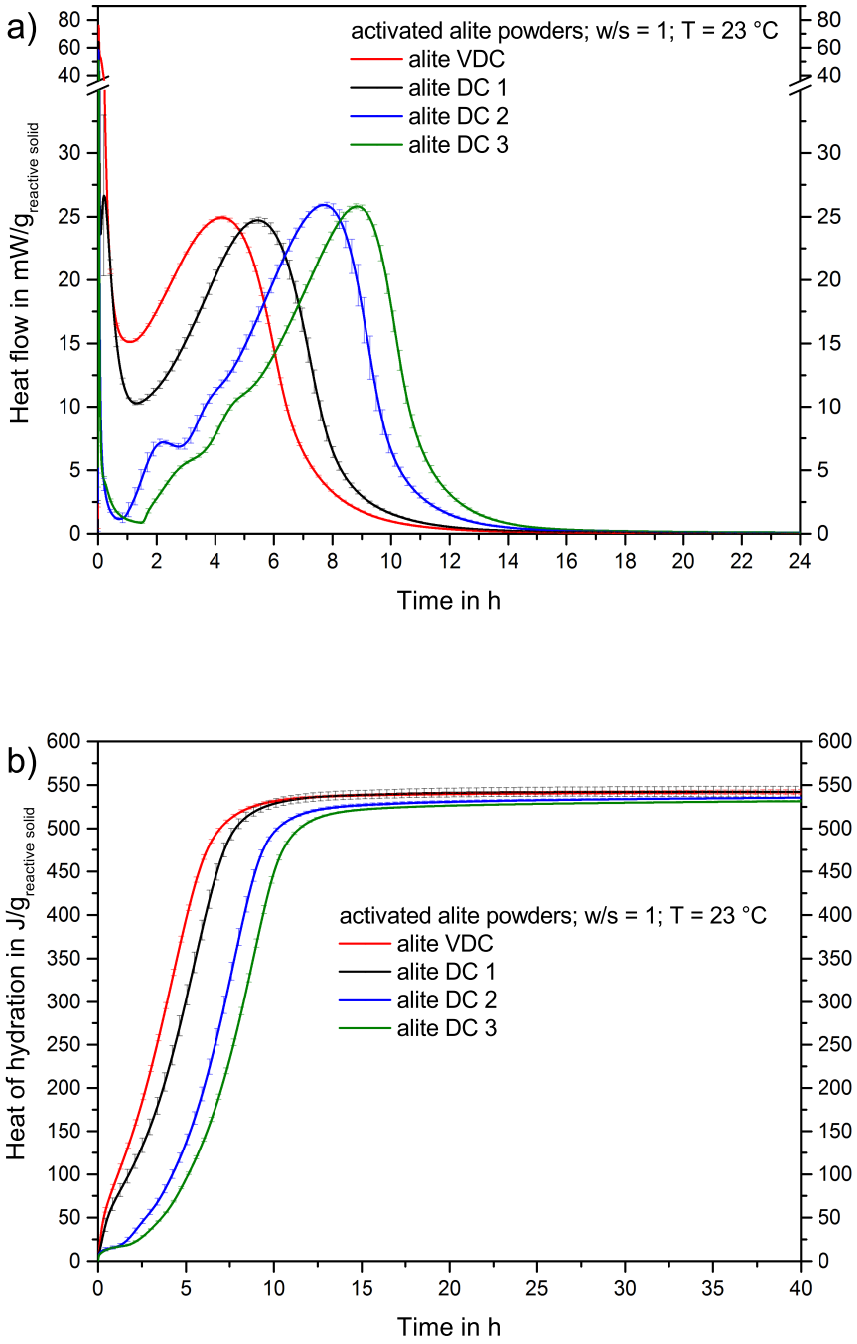

Fig. 1: Heat flow (a) and heat of hydration (b) released during the hydration of the activated alite samples at a w/s ratio of 1 and T = 23° C.

of slow reaction follows after the initial heat flow, which is not the case for alites VDC or DC 1. In the main hydration reaction, alites VDC and DC 1 exhibit one continuous acceleration. However, alites DC 2 and 3 show two humps in the acceleration of the main hydration reaction. The maximum of the main hydration reaction is around 1 $mW/g_{reactive\ solid}$ higher for alites DC 2 and 3 than for VDC and DC 1 (Table 2). The heat flow of all samples is around 0 $mW/g_{reactive\ solid}$ after 24 h of hydration. The heat of hydration after 24 h ($\Delta H_{24\ h}$ in Table 2) is similar for alites VDC and DC 1 as can be seen in Figure 1 and Table 2. The heats of hydration after 24 h for alites DC 2 and 3 are around 10 $J/g_{reactive\ solid}$ lower. Assuming that this heat has already been set free during sample drying, and therefore before the alite samples are mixed with water, this amount of heat would equal a dissolution of 2.6 wt.% of amorphous "alite" or 1.8 wt.% crystalline alite (with standard enthalpies of reaction of 386 J/g and 548 J/g respectively [1]).

Table 2: Comparison of the heat release of the activated alite samples: The time of the heat flow maximum of the main hydration period (t_{HFmax}) is given together with the heat flow ($HF_{t.max}$) and the heat of hydration ($\Delta H_{t.max}$) to that point in time. In addition, the heat of hydration after 24 h ($\Delta H_{24\ h}$) is presented.

Sample	t_{HFmax} in h	$HF_{t.max}$ in $mW/g_{reactive\ solid}$	$\Delta H_{t.max}$ in $J/g_{reactive\ solid}$	$\Delta H_{24\ h}$ in $J/g_{reactive\ solid}$
alite VDC	4.22 ± 0.02	24.9 ± 0.1	326.7 ± 1.8	540.3 ± 1.6
alite DC 1	5.45 ± 0.10	24.7 ± 0.2	341.8 ± 3.4	541.8 ± 5.2
alite DC 2	7.72 ± 0.13	26.0 ± 0.1	345.3 ± 2.8	532.2 ± 1.1
alite DC 3	8.85 ± 0.07	25.8 ± 0.2	351.2 ± 2.1	528.0 ± 0.4

In Fig. 2, in order to aid comparison the heat flows presented in Fig. 1 were mathematically time shifted by subtracting the time of the rate maximum of the main hydration period (Table 2). After the initial heat flow and a period of slow reaction, the acceleration period starts for the hydration reaction of the alite DC 3 paste at about 1.5 h of hydration. The acceleration proceeds slowly and displays two humps in the first 3.5 h of acceleration. After the time -3.5 h (time scale of Fig. 2), the hydration reactions of alites DC 2 and 3 proceed very similarly, regardless of the 1.1 h less time for the alite DC 2 paste to reach the same reaction behaviour. The paste of alite DC 1 showes a shoulder on the declining initial heat flow. After the decline of this shoulder, the hydration reaction is running in about the same manner as those of alites DC 2 and 3, regardless of the 3.4 h (in comparison to DC 3) less time to get to the same reaction behaviour. The paste of alite VDC shows an enhanced initial heat flow. After this initial heat flow declined, the hydration reaction proceeds in about the same manner as the other ones, regardless of the 4.6 h (in comparison to DC 3) less time to arrive at the same hydration behaviour.

Fig 2 also shows that the heat flow for the alites DC 2 and 3 decreases faster initially in the deceleration period than for the alites DC 1 or VDC. The slowest deceleration can be observed for alite VDC.

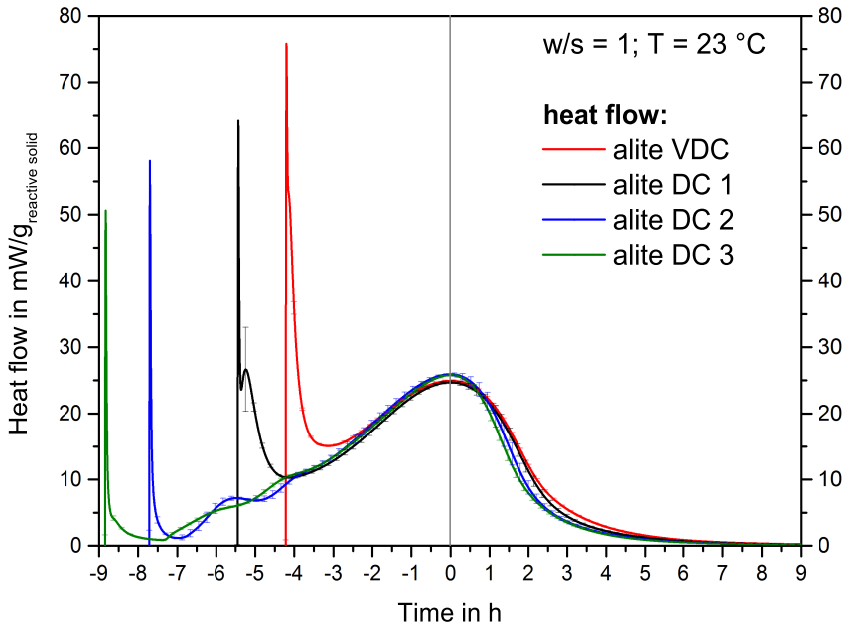

Fig. 2: Heat flow released during the hydration of the activated alite samples at a w/s ratio of 1 and T = 23° C. The measurements were shifted to the time of the maximum of the main hydration period to 0 h (Table 2) to allow a better comparison of the heat flow curves.

7.6.4.2.2. In-situ XRD analysis

Fig. 3 presents the results of the quantitative in-situ XRD measurements of the hydrating alite pastes in comparison with the respective heat flow as mean value of three independent measurements with 1 σ. The phase content of XRD amorphous C-S-H was calculated as stated in section 7.6.3.2.

The determined crystalline alite content in paste in the first diffractogram measured (2-12 min) was found to be 0.9 ± 0.2 wt.% (alite VDC) to 2.2 ± 0.9 wt.% (alite DC 1) lower than expected from the analysis of the dry samples (symbolized by the star in Fig. 3).

The phase content of crystalline alite in the VDC paste (Fig. 3a) decreases slowly at first and faster after around 1 h. After 13 h, the crystalline alite has been dissolved completely. Portlandite shows a fast precipitation during the initial period of the heat flow and precipitates further during the main hydration period. After 24 h, 21 ± 0.4 wt.% portlandite can be found in paste (20.5 wt.% are expected from Equation 1). After 1.3 h, C-S-H_{lro} precipitation can be determined. The main precipitation of C-S-H_{lro} takes place until 10 h of hydration, whereafter the phase content of C-S-H_{lro} increases very slowly. 33.6 ± 1.2 wt.% C-S-H_{lro} can be detected after 24 h. According to Equation 1, 43 wt.% C-S-H are expected to precipitate. Therefore, about ¼ of the C-S-H should be present in an XRD amorphous state. The calculated phase development of this XRD amorphous C-S-H shows that XRD amorphous C-S-H precipitates very quickly in the first 1.3 h when no C-S-H_{lro} is present in paste. After this time, some XRD amorphous C-S-H precipitates until 5 h of hydration. Thereafter the

.

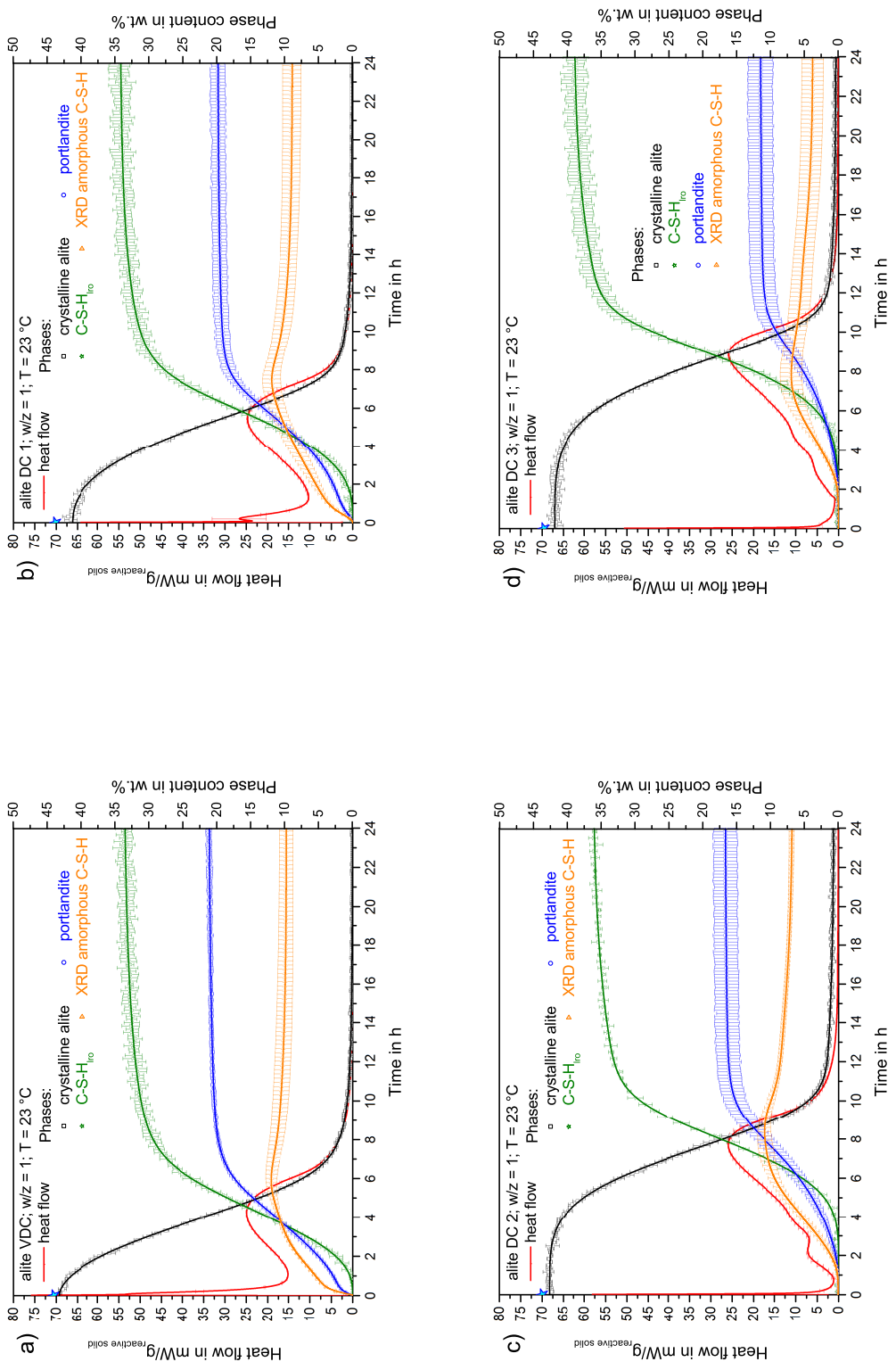

Fig. 3: Comparison of the phase development of alite VDC (a) and DC 1-3 (b-d) pastes as determined by XRD with the heat flow measured by calorimetry during hydration at w/s = 1 and T = 23° C. The mean values of three independent measurements with 1 σ are shown together with the fitted curve (section 7.6.3.2). The content of XRD amorphous C-S-H was calculated from the phase development of portlandite and C-S-H$_{Iro}$ (as described in section 7.6.3.2). The star at time 0 h represents the alite phase content expected from the dry refinement

phase content of XRD amorphous C-S-H decreases again slowly. It can be assumed that the amorphous part of the alite powder reacts before the crystalline alite [1] as portlandite precipitates in the alites VDC and DC 1 pastes (Fig. 3a and b) during the initial period of the hydration. The phase development within the alite DC 1 paste (Fig. 3b) is very similar to that of alite VDC except that the initial period of slow dissolution of crystalline alite is longer and C-S-H_{lro} starts to precipitate later in time.

The phase content of crystalline alite in the alite DC 2 paste remains constant for around 2 h whereafter the phase content decreases, slowly at first and then accelerated (Fig. 3c). After 24 h, 0.8 ± 0.1 wt.% crystalline alite is calculated to be in paste. We suggest that this is below the determination limit of crystalline alite in the hydrated pastes of a mechanically activated alite. C-S-H_{lro} precipitation starts after 4 h of hydration. Portlandite precipitates starting at 1.3 h of hydration and its phase content increases continuously, until around 5 h of hydration when the phase content increases more quickly with time. The phase development of the alite DC 3 paste is proceeding very similar to DC 2 with a shift to later times for the start of the changes in phase contents (Fig. 3d).

It is obvious that the portlandite content is significantly lower in alite DC 2 and 3 pastes than in alite DC 1 and VDC pastes. It was previously discovered that portlandite precipitates as few big crystallites in pure crystalline alite pastes [17, 20] as could be shown by 2-dimensional XRD with a GADDS system [20]. The precipitation of portlandite clusters has also been observed on backscattered electron images [21]. This leads to a significant underdetermination of portlandite in crystalline alite pastes [17, 20]. However, an underdetermination with respect to the expected phase content following eqation 1 did not occur notably for mechanically activated alite pastes before [1]. As can be seen, the standard deviation for portlandite increases from alite VDC to DC 1-3. It could be assumed that portlandite precipitates as smaller crystallites the faster the reaction proceeds. On the other hand, the examination of a 24 h hydrated alite VDC and a 24 h hydrated DC 3 paste by 2-dimensional XRD revealed that both samples showed spottiness (due to large crystallites) for portlandite.

The phase content of C-S-H_{lro} in paste after 24 h increases from alite VDC and DC 1 to DC 2 and DC 3. The calculated XRD amorphous content thus decreases in the same order. As can be seen, only 3.8 ± 1.6 wt.% XRD amorphous C-S-H is calculated for the alite DC 3 paste (Fig. 3d). Therefore, the slower reaction regime leads to a higher amount of C-S-H_{lro} in paste. The size of C-S-H_{lro} also seems to be influenced by the differing reaction kinetics. Fig. 4 shows that the mean coherently scattering domain (CSD) size calculated for C-S-H_{lro} during the Rietveld refinement is larger in alite VDC paste and lower in alite DC 3 paste than in DC 1 and 2 pastes. It also demonstrates the slight differences in the characteristic peaks of C-S-H_{lro} (between 29° and 33° 2Θ) between the XRD diagrams of the alite VDC and DC 3 pastes at 24 h of hydration.

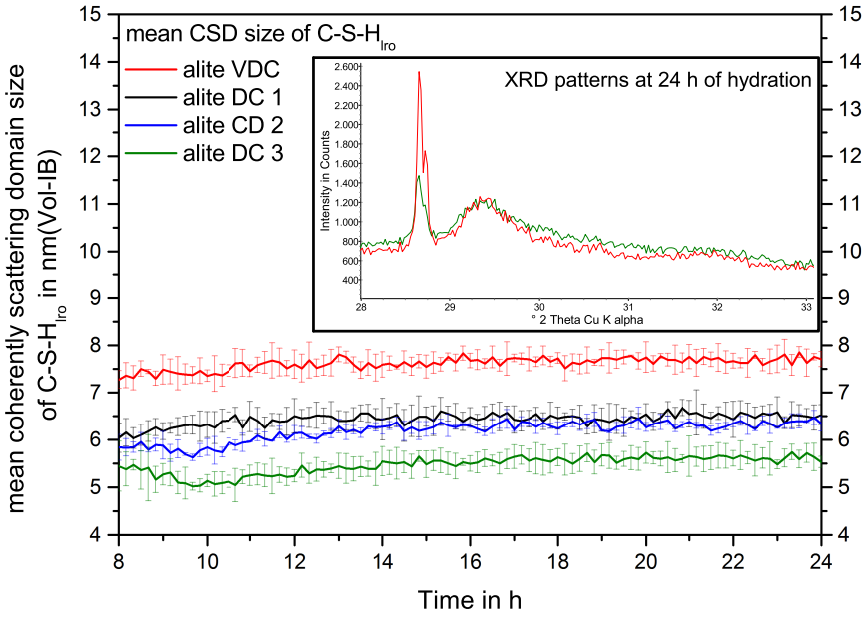

Fig. 4: Mean CSD sizes of C-S-H$_{lro}$ during hydration of the activated alite pastes. The window shows the XRD diagrams of alite paste VDC (red) and DC 3 (green) after 24 h of hydration. In addition to one portlandite reflection at 28.65° 2Θ, the characteristic peaks of C-S-H$_{lro}$ (between 29° and 33° 2Θ) are shown.

7.6.4.3. Dissolution and precipitation rates calculated from in-situ XRD

Fig. 5 compares the dissolution rate of crystalline alite together with the precipitation rates of portlandite and C-S-H$_{lro}$ as detected by in-situ XRD with the heat flow measured by calorimetry. In addition, the calculated precipitation rates of total C-S-H and XRD amorphous C-S-H (section 7.6.3.2) are shown for all analysed samples.

It can be seen that the precipitation rates of portlandite follow the main hydration periods for alite DC 2 and 3 pastes (Fig. 5c,d) with differences in the absolute values during the main period. For alite VDC and DC 1 pastes, portlandite precipitation follows both the initial and main hydration periods (Fig. 5a,b). The time of the maximum of the main hydration period corresponds well to that of the maximum of the portlandite precipitation (after the initial fast precipitation in the cases of VDC and DC 1). The maximum precipitation rates of portlandite of 0.95 and 0.94 mmol/(h•g$_{reactive\ solid}$) for alite VDC and alite DC 1 are congruent with previously reported ones for mechanically activated alites (0.91 to 0.96 mmol/(h•g$_{reactive\ solid}$) [1]). The precipitation rates in the pastes DC 2 and 3 are significantly lower as are the phase contents of portlandite (section 7.6.4.2).

The maximum dissolution rates of crystalline alite are found to be close in time to the maxima of the main hydration period (Fig. 5). The maximum dissolution rates are similar for all pastes (0.73 and 0.76 mmol/(h•g$_{reactive\ solid}$)). This is is also comparable to the values determined elsewhere as they were found to lie between 0.76 and 0.79 mmol/(h•g$_{reactive\ solid}$) for analogously mechanically treated alites [1]. The crystalline alite dissolution rate accelerates directly after mixing in the alite pastes VDC and DC 1. While the acceleration proceeds

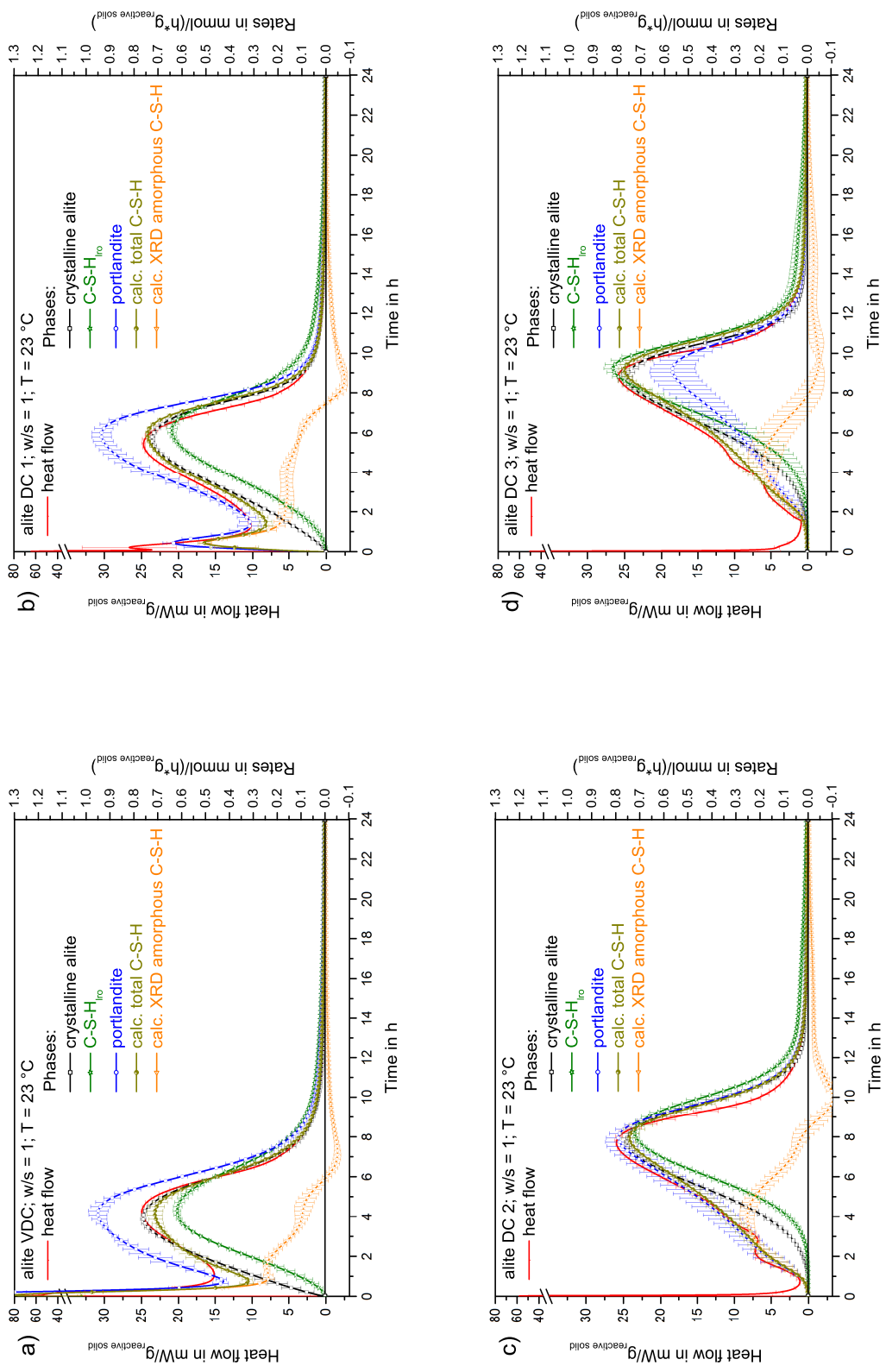

Fig. 5: Dissolution and precipitation rates during hydration of alite pastes VDC (a) and DC 1-3 (b-c) as calculated from quantitative in-situ XRD analyses. In addition, the total and the XRD amorphous C-S-H contents are shown (as calculated as stated in section 7.6.3.2).

roughly linearly in both cases, it is significantly steeper in the case of alite VDC. The dissolution rate of crystalline alite increases more slowly and with non-constant slope in alite pastes DC 2 and 3.

The maximum precipitation rates of C-S-H_{lro} are found to be slightly shifted to later times in comparison to the maximum dissolution rates of alite (0.3 h for alite VDC and 0.44 to 0.47 h in alites DC 1-3). The maximum precipitation rates for C-S-H_{lro} in alite pastes VDC and DC 1 (0.62 and 0.64 mmol/(h•$g_{reactive\ solid}$)) are concordant with the maximum rates determined elsewhere (0.56 – 64 mmol/(h•$g_{reactive\ solid}$) [1]). The maximum precipitation rates of 0.72 and 0.82 mmol/(h•$g_{reactive\ solid}$) for C-S-H_{lro} in alite pastes DC 2 and 3 are therefore higher than previously determined maximum precipitation rates. It can be observed that the C-S-H_{lro} precipitation rates are always lower and increase later in time than crystalline alite dissolution rates. During deceleration, the C-S-H_{lro} precipitation rates slightly exceed the dissolution rates of crystalline alite.

The precipitation rates of the calculated total C-S-H content can reproduce the initial period of the alite pastes of alite VDC and DC 1 and the main hydration period of all alite samples under investigation (Fig. 5). A comparison with the alite dissolution rates show a close match for the main hydration period between both rates in all pastes. However, it can be seen that differences in the initial period (alites VDC and DC 1) and at the start of the acceleration period (alites DC 2 and 3) exist between both rates. This clearly indicates that the amorphous part of the alite powder should dissolve during these time periods.

The calculated XRD amorphous C-S-H precipitation rates increase with the reaction kinetics but decrease as C-S-H_{lro} precipitates. During the deceleration period, XRD amorphous C-S-H dissolves, probably by evolution to C-S-H_{lro}.

The two humps in the acceleration period of alites DC 2 and 3 could not be explained by the phase development of crystalline alite or C-S-H_{lro}. The standard deviation of portlandite is too high to make a statement. The reason for the appearance of the two humps can only be the dissolution of amorphous “alite” or the precipitation process of XRD amorphous C-S-H.

7.6.4.4. Development of the mean CSD sizes of crystalline alite during hydration

Fig. 6 compares the development of the mean CSD sizes of remaining crystalline alite during hydration in the investigated samples with the heat flow measured by calorimetry. It can be seen that the mean CSD sizes increase in the acceleration period and decrease in the deceleration period. Moreover, it can be seen that the absolute value of the mean CSD size slightly increases in the pastes of the less reactive alite samples.

As stated before [1], the significance of CSD sizes lower than 100 nm is very good. Nevertheless, the crystalline alites possess low CSD sizes and high strains and the absolute relation between both cannot be decided in this study. We therefore conclude that the relatively higher mean CSD size for crystalline alite in the alites VDC and DC 3 could still be significant.

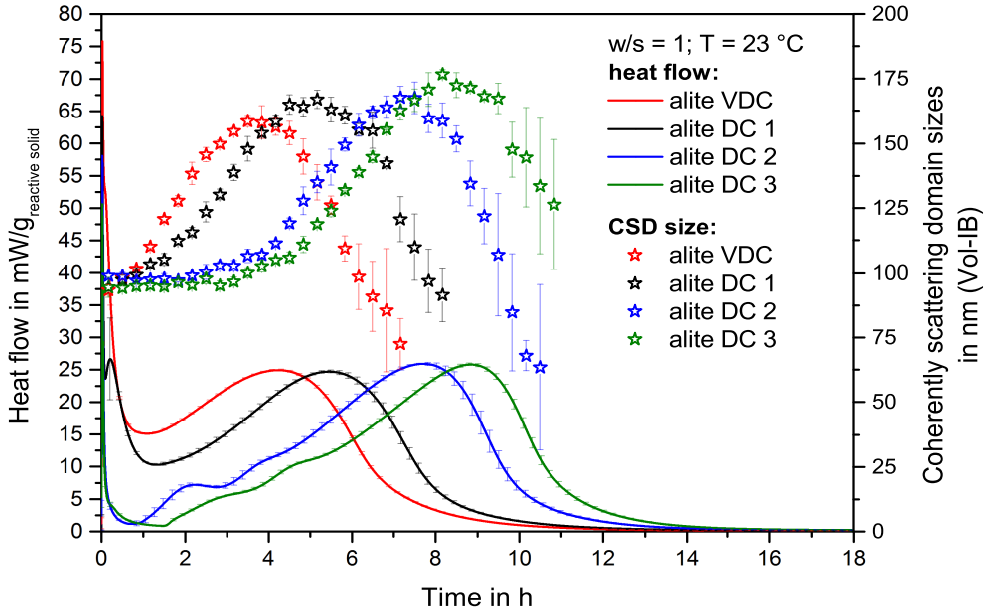

Fig. 6: Mean CSD size of alite during hydration of activated alite samples, as calculated from Rietveld refinement. The CSD size is presented for times with a higher alite content in paste than 3 wt.%.

7.6.5. Discussion

7.6.5.1. Consequences of the drying procedure

The drying procedure used in [1] and in this study for alite VDC (drying at 20 mbar N_2 atmosphere and with silica gel present at 50° C) leads to a very reactive alite powder. Although ethanol is probably retained in the sample (Table 1), this does not seem to decrease the reactivity significantly. The reactivity of the same activated alite (alite DC 1-3) decreased markedly by drying in a drying chamber under ambient atmosphere with silica gel present at 50° C (Fig. 1).

It is clear that the LOI is higher with longer drying times for the alites DC 1-3, which obviously correlates with the lower reactivity. The main difference between the alites VDC and DC 1-3 is that in samples VDC and DC 1 the reaction of the amorphous part of the powders takes place mainly during the initial period (Fig. 5a,b), while it takes place in the acceleration period for alites DC 2 and 3 (Fig. 5c,d). So the drying procedure for alites DC and the longer residence times result in a significant decrease in the amorphous "alite" reactivity. The higher LOI indicates indeed the adsorption of water and/or CO_2 on alite surfaces. It is, however, not clear whether this is accompanied by the precipitation of hydrate phases as suggested by [5, 7, 8]. The alite powders never touched liquid water but only vapour at a low RH. Condensation is therefore very unlikely. Neither portlandite nor C-S-H_{lro} could be found by XRD in the dry powders. Therefore the most probable explanation seems to be surface relaxation or surface reconstruction [5, 10, 11] due to the surface reaction with the water vapour, which removes the advantage of the amorphous part of the powder, which is the readily dissolvable alite.

7.6.5.2. Acceleration of the hydration reaction

Amorphous “alite” was found to be able to dissolve much easier than crystalline alite [1]. Dissolution of crystalline alite is always correlated with the precipitation of C-S-H_{lro} during the early acceleration of the crystalline alite dissolution (Fig. 3 and 5, and in [1, 17]). The amorphous part of the alite obviously does not need a “long-range ordered” C-S-H to precipitate in order to dissolve significantly. This in turn seems to lead to the markedly higher amount of XRD amorphous C-S-H in mechanically activated alites than in pure crystalline alite pastes, where only a small amount of XRD amorphous C-S-H precipitates, which evolves in the further progress of the hydration to C-S-H_{lro} [17].

In the pastes of alites DC 2 and 3, the precipitation of C-S-H_{lro} starts later and at lower levels with a less steep acceleration rate (Fig. 5c,d). However, three other effects can also be detected: the maximum C-S-H_{lro} precipitation rate and its phase content after 24 h are higher in alite DC 2 and 3 pastes than for alite VDC and DC 1 pastes (Fig. 5). In addition, the mean CSD size for C-S-H_{lro} is smaller in the paste of alite DC 3 and larger in alite VDC (Fig. 4) paste than in alite DC 1 and 2 pastes.

It seems that the nucleation and aggregation mechanism of C-S-H_{lro} has been changed due to the different kinetics of the samples. The dissolution of the XRD amorphous ”alite” content should lead to a highly supersaturated pore solution in a very short time. Crystalline alite seems not to be able to provide a comparable fast dissolution because the dissolution of crystalline alite decelerates significantly with lower undersaturation due to the dependence on the dissolution mechanism and the saturation degree of the solution [22, 23]. Therefore, high supersaturation degrees could be reached in a short time, which seem to be necessary to precipitate C-S-H_{lro}. Lothenbach and Nonat stated that the high Ca concentrations in solution are probably required to precipitate a C-S-H with such a high Ca/Si ratio, as is found in alite pastes (in mean 1.7) [24]. The faster evolution to the kind of C-S-H necessary to accelerate the alite dissolution leads to the enhanced reaction of the alite VDC pastes. In addition, for higher supersaturation degrees the pressure on C-S-H increases to precipitate, which explains the higher XRD amorphous C-S-H content. This could also lead to a significantly higher amount of C-S-H_{lro} phases, which are probably evolving from XRD amorphous C-S-H. When the increase in C-S-H surface is responsible for the acceleration of the main hydration period [e.g. 25-27] than the higher available surface of C-S-H_{lro} at very early times in hydration could lead to a faster acceleration of the hydration reaction (as observed in calorimetry and in-situ XRD, Fig. 1 and 3).

When the amorphous “alite” is altered by drying, as for samples DC 1-3, it cannot lead to a comparable effect. Therefore, a higher oversaturation for C-S-H results only if the surface of the amorphous “alite” is not aged. Crystalline alite dissolution probably cannot lead to a similar supersaturation with respect to C-S-H. Therefore, a smaller amount of C-S-H_{lro} is precipitated in a first step. During the further hydration the reactive surface of this C-S-H_{lro} supplied nucleation sites for further C-S-H_{lro} to precipitate. Therefore, in the case of a minor reactive amorphous “alite” part, the C-S-H_{lro} surface increases significantly more slowly and therefore the acceleration period is less steep. Fig. 2 shows impressively that with the presence of a fast initial reaction, the same hydration rate is reached in shorter times.

7.6.5.3. Transition from acceleration to deceleration period

As highlighted in the dissolution step theory [22], etch pits open at crystallographic defects if the undersaturation of the solution is high enough. Otherwise, the dissolution mainly proceeds with step retreat at previously opened etch pits [22]. The dependence of a change in dissolution mechanism and the staturation degree has been experimentally proved [23].

The fast reaction of amorphous "alite" seems to be blocked for the alite DC 1-3 powders due to the unfavourable drying technique used. The hydration reaction should thus start at a higher undersaturated solution and favour the opening of etch pits. This increased the surface of the alite powder as etch pits will form. As suggested by Sobolkina et al. [28] previously, the consecutive step retreat of those opened etch pits could increase the reaction turnover of the alite powder until the time of the rate maximum.

This has been observed precisely to happen (Table 2, Fig. 7). For alite DC 3 paste, the heat of hydration is already 24.5 J/$g_{reactive\ solid}$ higher than for the alite VDC paste at the heat flow maximum. This is true although the total heat of hydration after 24 h is 10 J/$g_{reactive\ solid}$ less for the alite DC 3 than for alite VDC. For the heat of hydration of 24.5 J/$g_{reactive\ solid}$, nominally 4.5 wt.% crystalline alite could react according to Equation 1.

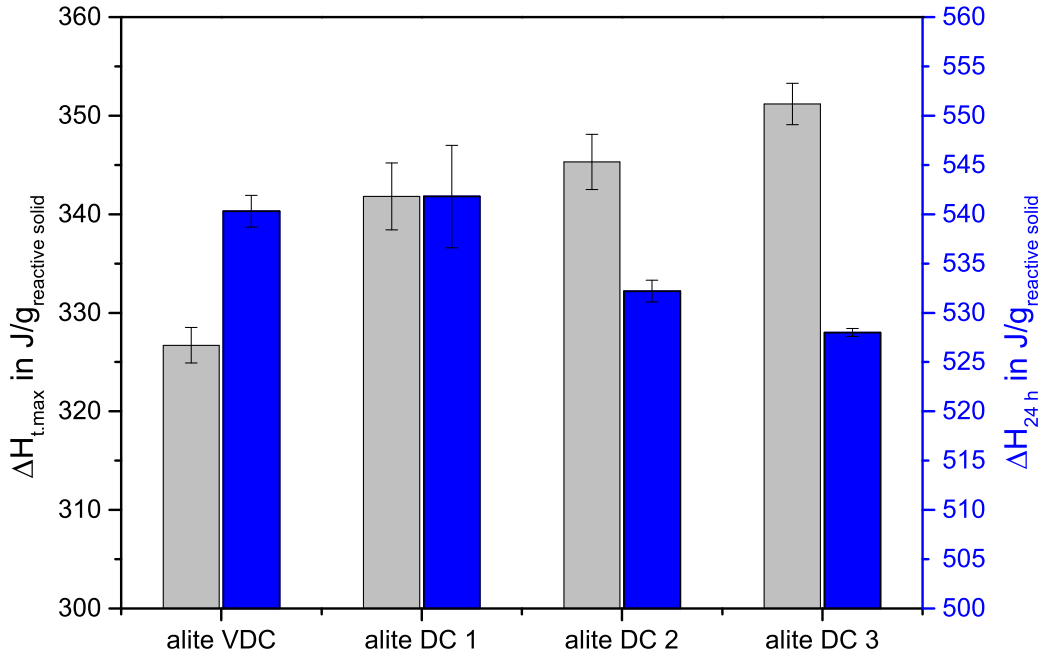

Fig. 7: Comparison of the heat released until the maximum of the main hydration period ($\Delta H_{t.max}$, the respective first bar, grey) and the heat released during 24 h of hydration ($\Delta H_{t.max}$, the second bar, blue) for the variably-activated alite samples.

It was previously reported that the mean CSD size of crystalline alite in mechanically activated alite powders increased during the acceleration period and decreased again during the deceleration period [1], as is also found in this study. This was interpreted to show that the consumption of small particles (which are consistent with small crystallite sizes for the given activated samples) would lead to larger mean CSD sizes during acceleration. Around

the rate maximum, the mean CSD sizes of crystalline alite are at maximum. Only residues of large particles with large crystallites are present in paste [1]. As the reaction turnover increased until the transition to the deceleration period, the extended opening of etch pits probably led to an even higher amount of dissolved smaller alite particles until the transition from acceleration to deceleration period. Therefore, in average even larger alite particles would remain at the transition to the deceleration period when only the large particles remain to be dissolved. This strengthens the conclusion that the mean CSD sizes calculated from the in-situ XRD analyses could show a significant result (Fig. 6).

In addition to the effect of the addition of seeding material to alite [28], the same kind of reaction mechanism could also explain the dependence of the hydration turnover on temperature. It was found that in the first day of hydration (after the main hydration period was completed), the reaction turnover of alite in the early hydration was higher for higher temperatures although the same alite was used [20, 29-31]. As the hydration process is accelerated at higher temperatures, a faster precipitation of C-S-H could lead to a higher undersaturation for alite and a consecutive higher amount of opened etch pits. Therefore a higher reactive alite surface would result during hydration at higher temperatures. The increase in alite surface area at the beginning of the hydration reaction could lead to a higher reaction degree at the transition from acceleration to deceleration period.

7.6.6. Conclusions

The drying technique after a wet (ethanol) grinding process is essentially determinating the reactivity of the milled material. Although the mechanical activation is the same for all the examined alite powders, the drying technique and the duration of the drying influence the reactivity of the powder. It could be shown that the reactivity of particularly the amorphous "alite" is significantly reduced by the unfavourable drying technique.

The adsorption of water vapour and/or CO_2 probably lead to relaxation or reconstruction of the alite surfaces. It appears that the amorphous part of the alite powder is particularly affected by these surface processes due to the high and very reactive surface of the amorphous material, leading to significantly lower reactivity of the total alite powder.

The fast dissolution of amorphous "alite" is obviously not influenced by the same contraints as the dissolution of crystalline alite. In the early acceleration of the crystalline alite dissolution, C-S-H_{lro} always starts to precipitate. The dissolution of crystalline alite slows down during the initial period of alite hydration because the undersaturation of the pore solution decreases and a different dissolution mechanism results from this slowing down of the rate [22, 23]. So the precipitation of a C-S-H that increases the undersaturation for alite - at least locally – seems to be essential for the dissolution of crystalline alite. The solubility of amorphous "alite" seems to be higher than that of crystalline alite and it can therefore dissolve in the very initial period without the constraints of the crystalline alite. A high amount of XRD amorphous C-S-H precipitates as C-S-H_{lro} has not evolved yet but the pressure to precipitate C-S-H is high.

At the transition to the deceleration period, the reaction turnover is higher for the alite samples in which the reaction of amorphous "alite" could not take place directly after mixing due to the passivation of its surface. It is suggested that the longer time for the opening of etch pits during the very initial hydration has increased the available alite surface. It is

suggested that the transition to the deceleration period proceeds when the available crystalline alite surface cannot supply enough ions for the hydration process. Therefore an increased surface area at the start of hydration should lead to the higher reaction turnover until the end of the acceleration period.

With respect to the application of amorphous "alite" as additive for crystalline alite or for cements, this means that a reactive amorphous "alite" is able to shorten the induction period by providing a high supersaturation for C-S-H. On the other hand, due to the consequential decreased undersaturation for alite, less opening of etch pits will appear and a smaller reaction turnover will follow in consequence during the main hydration period. Therefore an acceleration and simultaneous intensification of the alite hydration with amorphous "alite" addition seems not to be possible.

The ageing of mechanically activated alite also has implications for normal, not activated cements as the fines content, exhibiting the highest and most reactive surface of the cement material, experiences the highest influence of an ageing process. The surface of the fines of a cement is more receptive for the relaxation or reconstruction of its surface. This probably leads to less etch pit opening in spite of a probable higher undersaturation for alite and in turn to a lower reaction turnover of a cement during the main hydration period as was detected by [4].

7.6.7. References

[1] S. T. Bergold, F. Goetz-Neunhoeffer, J. Neubauer, Mechanically activated alite: New insights into alite hydration, Cement Concr. Res. 76 (2015) 202-201.

[2] S. Sprung, Effect of storage conditions on the properties of cement, Zem.-Kalk-Gips 31 (1978) 305-309.

[3] F. Winnefeld, Influence of cement aging and addition time on performance of superplasticizers, ZGK Int. 61 (2008) 68-77.

[4] S. Seifert, F. Goetz-Neunhoeffer, J. Neubauer, Lagerungsverhalten von Portlandzement in feuchter Atmosphäre, GDCh-Monographie 41 (Tagung Bauchemie, 2009), 223-226.

[5] J. Stoian, T. Oey, J.W. Bullard, J. Huang, A. Kumar, M. Balonis, J. Terill, N. Neithalath, G. Sant, New insights into the prehydration of cement and its mitigation, Cement Concr. Res. 70 (2015) 94-103.

[6] E. Dubina, L. Wadsö, J. Plank, A sorption balance study of water vapour sorption on anhydrous cement minerals and cement constituents, Cement Concr. Res. 41 (2011) 1196-1204.

[7] E. Dubina, R. Sieber, J. Plank, L. Black, Untersuchungen zu Vorhydratation von Zement, GDCh-Monographie 39 (Tagung Bauchemie, 2008), 329-337.

[8] E. Dubina, L. Black, R. Sieber, J. Plank, Interaction of water vapour with anhydrous cement minerals, Adv. Appl. Ceram. 109 (2010) 260-268.

[9] L. Black, K. Garbev, I. Gee, Surface carbonation of synthetic C-S-H samples: A comparison between fresh and aged C-S-H using X-ray photoelectron spectroscopy, Cement Concr. Res. 38 (2008) 745-750.

[10] P. Fierens, J.P. Verhaegen, Energy storage and tricalcium silicate reactivity, Cement Concr. Res. 5 (1975) 89.

[11] P. Fierens, J.P. Verhaegen, Induction period of hydration of tricalcium silicate, Cement Concr. Res. 6 (1976) 287-292.

[12] B.H. O'Connor, M.D. Raven, Application of the Rietveld refinement procedure in assaying powdered mixtures, Powder Diffr. 3 (1) (1988) 2–6.

[13] D. Jansen, C. Stabler, F. Goetz-Neunhoeffer, S. Dittrich, J. Neubauer, Does ordinary Portland cement contain amorphous phase? A quantitative study using an external standard method, Powder Diffr. 26 (1) (2011) 31–38.

[14] D. Jansen, F. Goetz-Neunhoeffer, C. Stabler, J. Neubauer, A remastered external standard method applied to the quantification of early OPC hydration, Cement Concr. Res. 41 (2011) 602–608.

[15] A.G. De La Torre, S. Bruque, J. Campo, M.A.G. Aranda, The superstructure of C_3S from synchrotron and neutron powder diffraction and its role in quantitative phase analyses, Cement Concr. Res. 32 (2002) 1347–1356.

[16] W.R. Busing, H.A. Levy, Neutron diffraction study of calcium hydroxide, J. Chem. Phys. 26 (3) (1957) 563–568.

[17] S.T. Bergold, F. Goetz-Neunhoeffer, J. Neubauer, Quantitative analysis of C–S–H in hydrating alite pastes by in-situ XRD, Cement Concr. Res. 53 (2013) 119–126.

[18] D. Ectors, J. Neubauer, F. Goetz-Neunhoeffer, The hydration of synthetic brownmillerite in presence of low Ca-sulfate content and calcite monitored by quantitative in-situ-XRD and heat flow calorimetry, Cement Concr. Res. 54 (2013) 61–68.

[19] M. Wojdyr, Fityk: a general-purpose peak fitting program, J. Appl. Crystallogr. 43 (2010) 1126–1128.

[20] S.T. Bergold, D. Jansen, S. Dittrich, F. Goetz-Neunhoeffer, J. Neubauer, Development of C-S-H during the early hydration of alite with water at different temperatures: direct quantification by in-situ XRD, GDCh-Monographie 45 (Tagung Bauchemie, 2012), 91–96.

[21] A. Bazzoni, M. Cantoni, K.L. Scrivener, Impact of annealing on the early hydration of tricalcium silicate, J. Am. Ceram. Soc. 97 (2014) 584-591.

[22] P. Juilland, E. Gallucci, R. Flatt, K. Scrivener, Dissolution theory applied to the induction period in alite hydration, Cement Concr. Res. 40 (2010) 831–844.

[23] L.Nicoleau, A.Nonat, D. Perry, The di- and tricalcium silicate dissolutions, Cement Concr. Res. 47 (2013) 14–30.

[24] B. Lothenbach, A. Nonat, Calcium silicate hydrates: Solid and liquid phase composition, Cement Concr. Res. 78 Part A (2015) 57-70.

[25] S. Garrault, A. Nonat, Hydrated layer formation on tricalcium and dicalicum silicate surfaces: Experimental study and numerical simulations, Langmuir 17 (2001) 8131-8138.

[26] J.J. Thomas, A new approach to modelling the nucleation and growth kinetics of tricalcium silicate hydration, J. Am. Ceram. Soc. 90 (2007) 3282–3288.

[27] S. Bishnoi, K.L. Scrivener, Studying nucleation and growth kinetics of alite hydration using μic, Cement Concr. Res. 39 (2009) 849–860.

[28] A. Sobolkina, V. Mechtcherine, S. T. Bergold, J. Neubauer, C. Bellmann, V. Khavrusa, S. Oswald, A. Leonhardt, W. Reschetilowski, Effect of carbon-based materials on the early hydration of tricalcium silicate, J. Am. Ceram. Soc., accepted for publication, doi: 10.1111/jace.14187.

[29] D. Jansen, S.T. Bergold, F. Goetz-Neunhoeffer, J. Neubauer, The hydration of alite: a time resolved quantitative X-ray diffraction approach using G-factor method compared with heat release, J. Appl. Crystallogr. 44 (5) (2011) 895–901.

[30] I.F. Saez del Bolsque, M. Martin-Pastor, S. Martinez-Ramirez, M. T. Blanco-Varela, Effect of temperature on C_3S and C_3S + nanosilica hydration and C-S-H Structure, J. Am. Ceram. Soc. 96 (2013) 957-965.

[31] I. Odler, J. Skalny, Hydration of tricalcium silicate at elevated temperatures, J. Appl. Chem. Biotechnol. 23 (1973) 661-667.

7.7. Hydration at the edge: Changing the balance between silicate and aluminate reaction in a synthetic cement system

Submitted to the Journal "Cement and Concrete Research" on 26th of January 2016.

Authors: S. T. Bergold, F. Goetz-Neunhoeffer, and J. Neubauer

Friedrich-Alexander-Universität Erlangen-Nürnberg (FAU), GeoZentrum Nordbayern, Mineralogy, Schlossgarten 5a, 91054 Erlangen, Germany

7.7.1. Abstract

Synthetic cement with different sulfate additions is investigated by means of heat flow calorimetry and quantitative in-situ XRD. This study especially analyses different sulfate additions between a typical undersulfated and a properly sulfated white Portland cement. A series of sulfate additions were monitored, and the interference of aluminate and silicate reactions was observed. This interference has never received closer examination before. It is shown that while interference occurs at different times during hydration, the reaction turnover of all synthetic cements is the same after 48 h. The results indicate that negative effects on silicate hydration are likely due to the precipitation of AFm phases and not an Al-inhibition process. The accelerating effect of sulfate on alite hydration is most likely caused by a seeding effect of the very fine ettringite that has just precipitated, resulting in more substrate surface for C-S-H precipitation in comparison to pure alite paste.

Keywords: X-Ray Diffraction (B), Calorimetry (A), Hydration (A), Kinetics (A), Ca_3SiO_5 (D)

7.7.2. Introduction

The hydration of Portland cements basically consists of two different reaction regimes that interact with each other. These are the silicate reaction and the aluminate reaction. The silicate reaction consists of alite dissolution (monoclinic form of C_3S, doped with foreign ions) and the precipitation of C-S-H phases and portlandite. The nano-sized, colloidal C-S-H phases are mainly responsible for developing the strength of the cement paste. The aluminate reaction is responsible for the setting of the cement, thereby regulating the workability and the rheological properties of the cement. The dissolution of the clinker phase C_3A is controlled by sulfate present in the cement [1]. If a cement system is not properly retarded, flash setting of the cement occurs, which just means that the C_3A reacts very fast to form ettringite or AFm phases, spoiling the workability and delaying the silicate reaction [1]. In the review of Bullard et al. [2], the results of Lerch [1] were classified for more modern cements.

The hydration of a properly sulfated OPC can be divided into different stages following the released heat flow by calorimetry as it is shown exemplarily in Fig. 1 for one of the synthetic cements analyzed in this study. In the initial period (stage I) directly after contact with water,

C_3A and very soluble sulfate carriers dissolve significantly (arcanite and bassanite dissolve completely [3]). Ettringite precipitates very rapidly as a hydration product of the aluminate reaction. It was shown by Minard et al. [4] in a pure C_3A - gypsum system that mainly OH^--containing AFm precipitated before ettringite formation, when the dissolution of the sulfate carriers is slower than the dissolution of C_3A. A small portion of alite will also dissolve during the initial period [5] (around 0.5 wt.% alite in pure alite pastes [6]).

In stage II, the heat flow declines significantly because alite and C_3A dissolution have been stopped or at least are extremely slow. From pore solution experiments of pure C_3S, it is known that a calcium silicate hydrate precipitates within a few minutes after mixing [5]. This form of C-S-H is obviously not capable of accelerating the hydration, as the silicate reaction is moved into the induction period (a period of slow chemical reaction). A lot of insight has been given into the dissolution of alite in the past years [7-11]. It was found that the dissolution of alite proceeds at near-equilibrium conditions [7-9] during cement hydration, with the exception of the very first dissolution of alite when the surface of alite comes into contact with water. In the OPC, the aluminate reaction proceeds during the induction period of the silicate reaction by continuous precipitation of ettringite and dissolution of sulfate carriers, but without further dissolution of C_3A [3, 12]. Because of that and because not all of the initially dissolved C_3A is converted into ettringite, Hesse et al. [12] proposed the formation of an XRD amorphous aluminate phase, which would be the reservoir from which the further ettringite would be formed. If different kinds of sulfate carriers are used, the sulfates dissolve successively according to their solubility [3]. The most accepted theory about the blockage of C_3A by sulfate [2, 13] was given by Minard et al. [4], who attributed this effect to the adsorp-

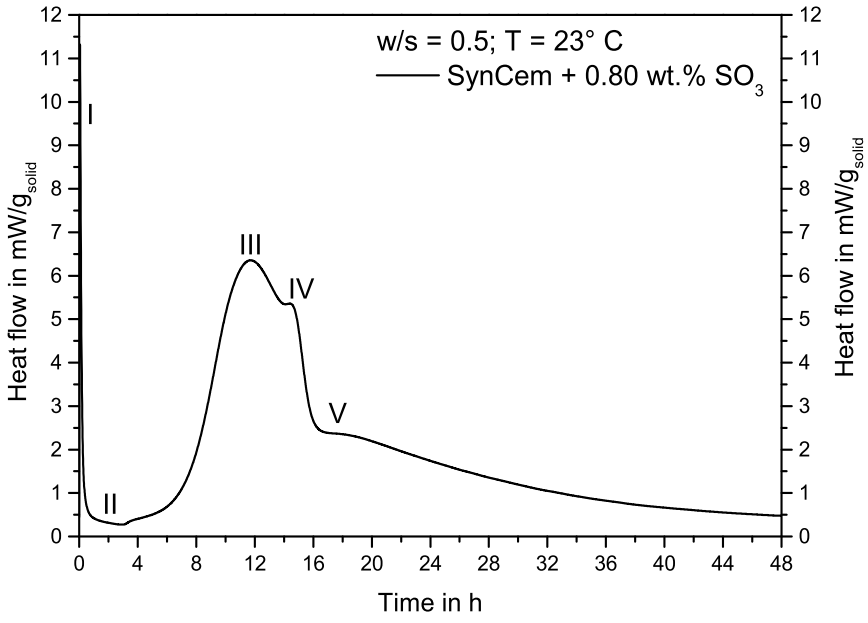

Fig. 1: Schematic hydration process of a properly sulfated OPC system.

tion of Ca and/or sulfate ions on the C_3A surface, which blocked the reactive dissolution sites of C_3A.

At the beginning of stage III, alite dissolution and the precipitation of C-S-H and portlandite starts to accelerate (after about 3 h in Fig. 1). There is still no consensus about the rate-controlling mechanisms during the hydration of alite. The acceleration of the main silicate hydration is attributed to the precipitation of C-S-H most of the time [2]. Recently, however, Nicoleau & Bertolim showed that it is mathematically possible to simulate an acceleration period by the complex dissolution of alite surfaces [14]. Therefore, the alite dissolution alone could be responsible for the course of the reaction. Bullard et al. concluded from the comparison of simulations that neither C-S-H precipitation nor alite dissolution would be the single rate-determining step during the early hydration of alite [15].

A phenomenon that accompanies the process of acceleration is a change in the kind of C-S-H that precipitates. After the end of the induction period, silicate tetrahedra incorporated in C-S-H are linked as dimers, while there had only been monomeric silicate species earlier [16, 17]. At the time during acceleration when the heat flow accelerates linearly with time, a "long-range ordered" form of C-S-H (C-S-H_{lro}) starts to precipitate and replaces the previously precipitated XRD amorphous form of C-S-H during the hydration process [18].

While it is clear that the dissolution rate of alite and the precipitation rates of C-S-H and portlandite decline at the transition from acceleration to deceleration in stage III, the reason for the transition is also still under debate. Provided that the acceleration is driven by the nucleation and growth of C-S-H, the transition to the deceleration period can be explained by the impingement of C-S-H growing on the same grain [19], leading to a situation where the diffusion of ions through the C-S-H layer is believed to decelerate the reaction. Bischnoi & Scrivener [20] explained the transition to the deceleration period suggesting that C-S-H would be formed with two different densities. The one with the lower density would fill the space and be densified afterwards. C-S-H clusters growing on different grains would impinge and thus reduce the C-S-H surface to grow new C-S-H [20]. This model was refined by a reaction zone to account for experimental evidence that the water-to-solid ratio (w/s ratio) does not affect the hydration of alite a lot [21].

Recently the idea was brought forward by Garrault et al. [22] that the dissolution of alite could become rate-limiting in the decelerating period. Nicoleau & Nonat presented convincing evidence that the dissolution of alite becomes rate-limiting during the deceleration of the silicate reaction as they gathered solution data and showed that as the reaction decelerates, the solution composition departs from alite solubility [23, 24]. Therefore, although the reaction decelerates, the ion concentration decreases in the ions produced by alite dissolution [23, 24].

Stage IV represents a renewed C_3A dissolution accompanied by faster precipitation of ettringite [3, 13] or AFm phases. The time of occurrence of the renewed aluminate reaction is determined by the disappearance of an available sulfate carrier – usually anhydrite - in the hydrating cement system due to the continuously ongoing ettringite formation [3, 4, 12, 25, 26]. The C_3A dissolution is renewed as soon as sulfate is not available, but the product formed in ordinary Portland cement was still found to be ettringite [3]. This was explained with adsorption of sulfate on C-S-H surfaces during the period of time when the sulfate carriers dissolve and sulfate is available in solution, while it is released back into the solution when the sulfate carriers are used up or stopped to dissolve [13, 26, 27]. In Stage IV, the deceleration of the

silicate reaction and the renewed aluminate reaction take place simultaneously [3, 12]. In model cement hydration, Quennoz & Scrivener found a second sharp aluminate peak after the peak of accelerated ettringite formation, which was due to a strong dissolution of C_3A associated with the formation of AFm phases [26].

In stage V, the silicate reaction proceeds on low levels, and an additional peak can often be seen in this stage, which most of the time is accompanied by the formation of AFm phases [2, 12]. However, in the characterization of cementitious pastes, an additional peak sometimes occurred although no AFm phase could be detected at all. In the model cement (alite - C_3A - gypsum) of Quennoz & Scrivener [26], an additional peak was detected after the sulfate depletion peak that resulted in the formation of AFm phases from C_3A and ettringite dissolution. This peak was attributed to an aluminate reaction, but its reason remained unexplained [26].

In the present contribution, similar to Hesse et al. [12, 28] and Quennoz & Scrivener [26], a reduced synthetic cement system is set up and analyzed to gain deeper insight into the hydration processes taking place and into the silicate - aluminate reaction balance. The main point of interest will be calcium sulfate additions to the synthetic cement, which lead to an interference between the aluminate and silicate reaction. The interference of silicate reaction by aluminate reaction has been observed several times in the literature, e.g., in some calcium sulfate additions by Lerch [1] and for the 3.3 wt.% gypsum containing model cement by Quennoz & Scrivener [26], but the interference has never really been addressed.

7.7.3. Materials and Methods

7.7.3.1. Materials

The monoclinic M3 form of alite was synthesized with the composition of 71.7 wt.% CaO, 25.9 wt.% SiO_2, 0.6 wt.% Al_2O_3 and 1.8 wt.% MgO from $CaCO_3$ and the metal oxides. The cubic modification of C_3A was synthesized from $CaCO_3$ and α-Al_2O_3 in stoichiometric composition. Both alite and C_3A powders were homogenized in a vibratory disc mill (agate tool), calcinated at 1000° C for 16 h and sintered 4 (alite) and 3 times (C_3A) for 4 h at 1400° C ± 30° C in Pt-crucibles in a chamber furnace in air. The specimens were air-quenched by removing them from the furnace and cooling them down to room temperature within minutes. Between and after the sintering steps, the samples were milled in a vibratory disc mill (agate tool). As sulfate carriers, α-bassanite ($CaSO_4 \cdot 0.5H_2O$, Raddichem) and anhydrite ($CaSO_4$) were used. Anhydrite was produced by dehydration of gypsum (Fluka, 99.9 % purity) at 380° C ± 30° C for 20 h in corundum crucibles in a chamber furnace in air. The cement phases were characterized by laser granulometry (Fig. 2) and quantitative XRD using the external standard method (Table 1).

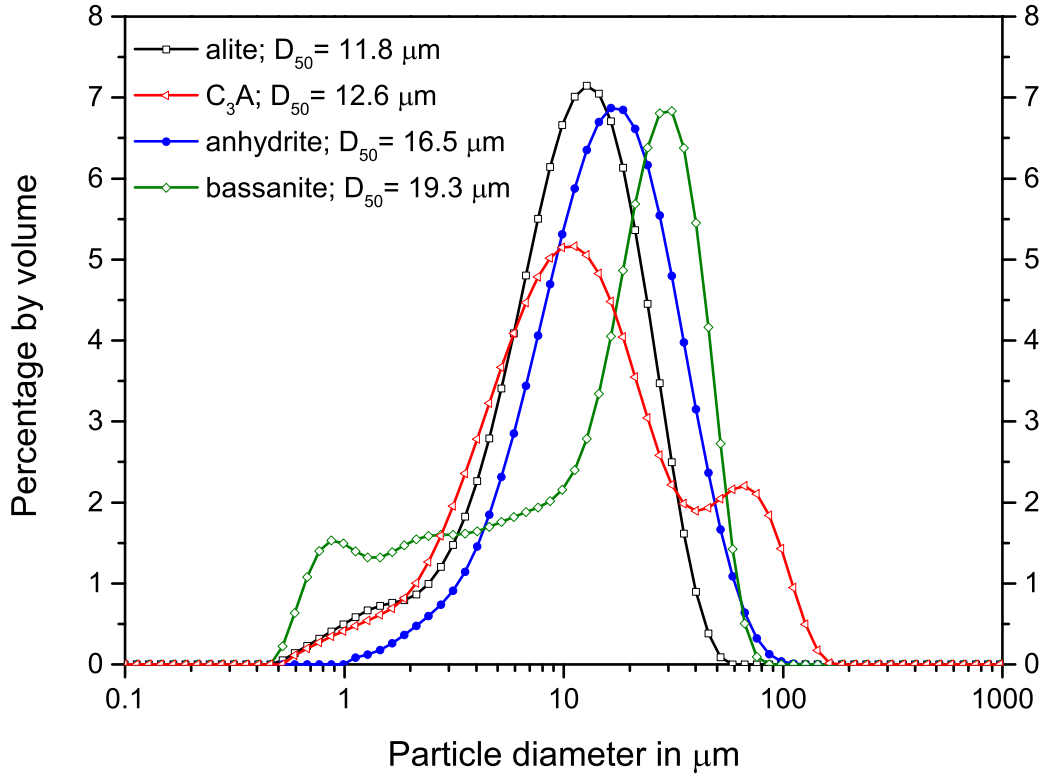

Fig. 2: Particle size distribution of the materials used, as measured by laser granulometry.

Table 1: Result of the quantitative XRD phase analysis of the synthetic cement components.

Sample	Phase content in wt.%						
	alite	C_3A_{cubic}	bassanite	anhydrite	$C_{12}A_7$	CaO	amorphous/ undetermined
alite	96.5 ± 0.9	-	-	-	-	< 0.2	3.5 ± 0.9
C3Acubic	-	98.2 ± 0.6	-	-	0.9 ± 0.1	< 0.2	1.1 ± 0.7
α-bassanite	-	-	101.2 ± 4.5	-	-	-	0 ± 4.5
anhydrite	-	-	2.3 ± 0.2	94.0 ± 3.0	-	-	3.7 ± 2.8

7.7.3.2. Set up of a synthetic cement

A synthetic cement (SynCem) was investigated to adapt the hydration characteristics of a white Portland cement adjusted to the system investigated by Hesse [12, 28]. Therefore, an alite:C_3A ratio of 95:5 in weight was used to model the reactive clinker part. Two sulfate carriers were used with a fixed ratio of 20 wt.% bassanite and 80 wt.% anhydrite during all experiments. Since bassanite dissolves immediately after powder and water are mixed [3, 28], sulfate is directly provided to the pore solution while anhydrite dissolves more slowly.

The above described phases were weighted to a total of 1.6 g powder and homogenized within the InMixEr at a mixing speed of 570 rpm for 5 min (a tool designed in Erlangen that

allows injection and intensive mixing inside a TAM Air calorimeter). Dry powder and mixing water (0.8 g, w/s ratio of 0.5) were then equilibriated in the InMixEr within a TAM Air (TA Instruments) calorimeter channel at 23° C ± 0.2° C before the start of an experiment.

7.7.3.3. Heat flow calorimetry

Heat flow calorimetry was performed with a TAM Air calorimeter at 23° C ± 0.2° C. At the start of the experiments, water (w/s = 0.5) was injected and powder and water were mixed to a paste at 860 rpm for 1 min in the calorimeter with the help of the InMixEr. This way, the initial heat can also be determined correctly.

The sulfate additions to the SynCem differed only a little in the weight of the single components (between 0.6-1.1 wt.% SO_3), while it will be shown that the effect on hydration was significant. This can explain why very small devaitions in weighing, homogenization, and preparation can lead to a small change in the position of specific heat flow events (up to 1 h), while the hydration kinetics themselves are very similar. Because the presentation of mean values would lead to the conclusion of broader reactions than actually measured, except for the pure alite, and SynCem with 0.65 and 1.1 wt.% SO_3, single measurement curves are presented in Fig. 3 and 4. In Fig. 5, where the heat of hydration is presented, all curves represent mean values of at least 2 and mostly 3 independent experiments.

7.7.3.4. In-situ XRD

In-situ XRD was performed with a D8 Advance from Bruker-AXS equipped with a LynxEye detector at Bragg-Brentano geometry. The samples were mixed in the InMixEr exactly as for the heat flow calorimetry. Afterwards, the paste was prepared in a PVC sample carrier and placed in a custom-made sample holder equipped with a heating and cooling device that ensured that the temperature of the sample was 23° C ± 0.2° C. The aluminate reaction is very sensitive to temperature deviations [25]. With this experimental setup, the phase content is detected within the top of the sample. To ensure that the temperature (and thus the kinetics of the hydration reaction) between the top and the bulk of the sample that is conditioned by the sample holder is the same, the housing of the diffractometer was air-conditioned to a temperature of 23° C ± 2° C, measured at the sample position. The sample was covered with a Kapton® polyimide film to limit water loss and to avoid CO_2 uptake of the sample. After the preparation, which lasted about 2.5 to 3 min, the sample is continuously measured every 10 min from 7 to 55° 2Θ with a step width of 0.0236° 2Θ at 0.27 s counting time per step.

The quantitative analysis was performed with the software TOPAS 4.2 from Bruker-AXS using the fundamental parameter approach with a consecutive calculation of the absolute phase contents in the paste with the external standard method [3, 29]. Table 2 presents the structure proposals used in the Rietveld refinements. Because of the lack of proper structural data, the structure proposal of kuzelite from Allmann [36] was used for the refinement of both sulfate-AFm phases. The starting lattice parameter c was adapted from the ICDD qualitative patterns #42-0062 for AFm-14H and #44-0602 for AFm-16H. This procedure includes a systematic error within the quantification of those phases, because of a variation of the phase density and because the c lattice parameter is extended without the refinement of the interlayer atomic positions (which was not necessary in the context of this study). The

phase development is not affected by this error but the absolute quantitative value could be erroneous. For analysis of the contribution of "long-range ordered" C-S-H (C-S-H_{lro}) to the diffractograms, the PONKCS phase described in [18] was used. All diffractograms of one experiment were refined coupled, which allowed the coupled refinement of parameters over the complete reaction (for example, the scale factor of the Kapton film model and lattice parameters of individual phases).

Table 2: Structures used for Rietveld refinement.

Phase	ICSD #	Authors
alite	94742	[30]
C_3A_{cubic}	1841	[31]
bassanite	79529	[32]
anhydrite	16382	[33]
ettringite	155395	[34]
portlandite	34241	[35]
AFm-14H	100138	[36]
AFm-16H	100138	[36]

7.7.3.5. Calculation of heat flow from in-situ XRD analysis

The resulting heat flow from the change in phase development as analyzed by in-situ XRD was calculated as described by Jansen et al. [37]. For this, the data set was fitted with one to three 5-parameter logistic functions [38] in the program Fityk [39]. As with Jansen et al. [37], the heat flow was calculated assuming that species in solution fit a pH of 13.3 (aqueous species: roughly 50 % Ca^{2+} and 50 % $CaOH^+$, $Al(OH)_4^-$, SO_4^{2-}, OH^-). The hydration reactions were therefore assumed to proceed as presented in Equations 1-7. The thermodynamic data from Matschei et al. [40] and for the $C_{1.7}SH_{2.6}$ the value from Fuji & Kondo [41] were used to calculate the resulting heat from the reactions (presented in Table 3). For calculation of the silicate reaction, the value for the standard enthalpy of formation of C_3S was reduced from -2931 kJ/mol [40] to -2934 kJ/mol. This way, the resulting heat of reaction for the silicate hydration as presented in Equation 1 is 548 J/g_{alite}, which meets the value determined to represent the heat of hydration released during the hydration of pure crystalline alite before [6]. The silicate reaction was calculated according to Equation 1 for simultaneous alite dissolution and precipitation of C-S-H_{lro} plus portlandite.

$$Ca_3SiO_5 + 3.9\ H_2O \rightarrow (CaO)_{1.7}.SiO_2.(H_2O)_{2.6} + 1.3\ Ca(OH)_2 \quad (1)$$

$$Ca_3Al_2O_6 + 6\ H_2O \rightarrow 2\ Al(OH)_4^- + 2.5\ OH^- + 1.5\ Ca^{2+} + 1.5\ CaOH^+ \quad (2)$$

$$3\ CaSO_4 + 1.5\ OH^- \rightarrow 1.5\ Ca^{2+} + 1.5\ Ca(OH)^+ + 3\ SO_4^{2-} \quad (3)$$

$$3\ CaSO_4.0.5H_2O \rightarrow 1.5\ Ca^{2+} + 1.5\ Ca(OH)^+ + 3\ SO_4^{2-} \quad (4)$$

$$3\ Ca^{2+} + 3\ CaOH^+ + 2\ Al(OH)_4^- + 3\ SO_4^{2-} + OH^- + 26\ H_2O \rightarrow Ca_3Al_2O_6.3CaSO_4.32H_2O \quad (5)$$

$$2\ Ca^{2+} + 2\ CaOH^{+} + 2\ Al(OH)_4^{-} + SO_4^{2-} + 2\ OH^{-} + 8\ H_2O \rightarrow Ca_3Al_2O_6.CaSO_4.14H_2O \quad (6)$$

$$2\ Ca^{2+} + 2\ CaOH^{+} + 2\ Al(OH)_4^{-} + SO_4^{2-} + 2\ OH^{-} + 10\ H_2O \rightarrow Ca_3Al_2O_6.CaSO_4.16H_2O \quad (7)$$

Table 3: Enthalpies of reaction used for the calculation of the heat flow.

Reaction	Enthalpy of reaction
silicate reaction (Equation 1)	- 548 J/g_{alite} - 619 J/$g_{C\text{-}S\text{-}H}$ - 1299 J/$g_{portlandite}$
C_3A dissolution (Equation 2)	- 871 J/g_{C3A}
anhydrite dissolution (Equation 3)	- 52 J/$g_{anhydrite}$
bassanite dissolution (Equation 4)	not considered
ettringite precipitation (Equation 5)	- 208 J/$g_{ettringite}$
AFm-14H precipitation (Equation 6)	- 115 J/$g_{AFm\text{-}14H}$
AFm-16H precipitation (Equation 7)	- 121 J/$g_{AFm\text{-}16H}$

7.7.4. Results

7.7.4.1. Heat flow calorimetry

Fig. 3 compares the reaction of a hydrating alite paste to synthetic cement (SynCem) consisting of intermixed C_3S and C_3A in a ratio of 95:5 with different sulfate additions with a bassanite-to-anhydrite ratio of 20:80. The SynCem with the lower SO_3 content represents an undersulfated system, where aluminate reaction takes place before silicate reaction [1, 26]. With the higher SO_3 content, the SynCem hydration behaves like a properly sulfated white Portland cement paste as the renewed aluminate reaction occurrs after the main hydration peak [26]. The heat flow during the initial and induction period are higher for SynCem pastes than for the pure alite paste. It can be clearly seen that the acceleration of the reaction is faster for the properly sulfated SynCem paste than for pure alite paste. On the contrary, in the undersulfated system, the acceleration of the silicate reaction is delayed, less intensitve and broader. These effects were reported before by Quennoz & Scrivener [26], who showed about the same reaction behaviour resulting from a model cement with an alite-to-C_3A ratio of 92:8 with different additions of gypsum, while the C_3A/SO_3 ratio was comparable for similar effects.

It is especially interesting to have a closer look at the balance between aluminate and silicate reaction between both sulfatation cases shown in Fig. 3. In Fig. 4, it can be seen that as the SO_3 content increases from 0.6 wt.% (Fig. 3 in the undersulfated mix) to 0.65 wt.%, the

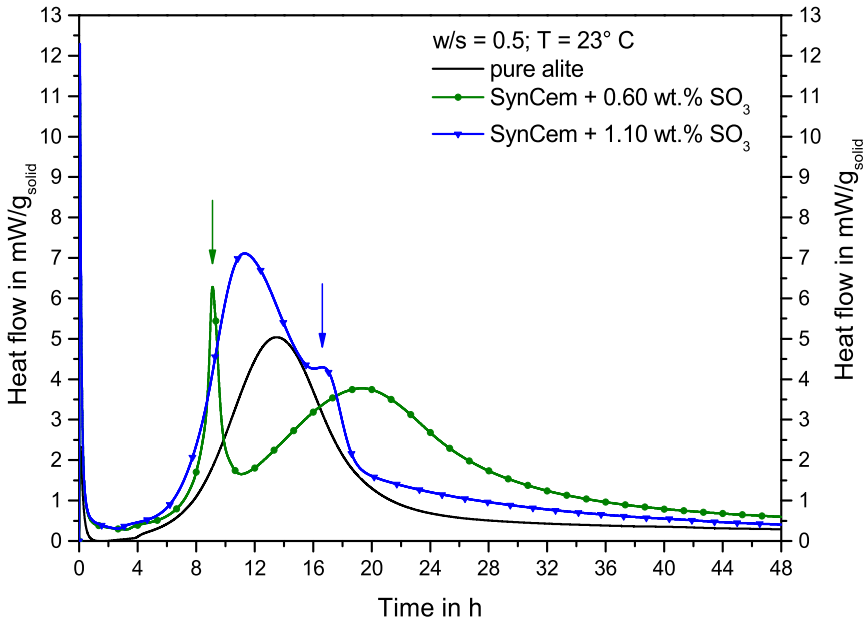

Fig. 3: Heat flow calorimetry of pure alite and of SynCem in an undersulfated and a properly sulfated case. The arrows mark the main rate peak of the respective renewed aluminate reaction.

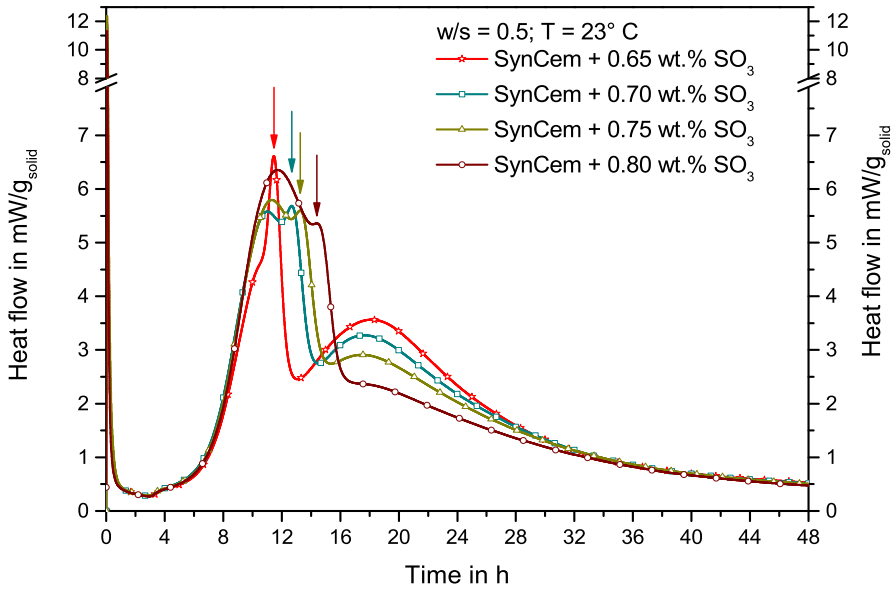

Fig. 4: Heat flow calorimetry of SynCem with SO_3 contents between 0.65 and 0.80 wt.% (on the dry cement). The arrows mark the main rate peak of the respective renewed aluminate reaction.

aluminate reaction (marked by the respective arrow) shifts into the acceleration stage of the silicate reaction. The silicate reaction seems to be tremendously disturbed, since the silicate reaction decelerates and reaccelerates from a lower rate level after the end of the sharp aluminate peak when the aluminate reaction is completed. With higher amounts of SO_3 in SynCem, the aluminate reaction is shifted to later times, but still results in interference with the silicate reaction, which reaccelerates afterwards. The later the silicate reaction is hampered, the lower the reacceleration of the silicate reaction. The silicate reaction in the SynCem containing 0.80 wt.% SO_3 is still affected, although the sulfate depletion peak occurs significantly later than the rate maximum.

Fig. 5 presents the mean values (at least two preparations, mostly three preparations) of the heat of hydration liberated within the first 48 h in the pastes shown in Fig. 3 and 4. It can be seen that all SynCem pastes reach significantly higher heats of hydration than the pure alite paste. Additionally, all SynCem pastes reach very similar heats of hydration. During the first 8 h of hydration, the path of all SynCem samples is essentially the same. After this, and earlier with a lower SO_3 content, a bend in the heat of hydration curves shows the aluminate reaction hampering the silicate reation, which reaccelerates afterwards. After 48 h all SynCem pastes reach about the same heat of hydration in spite of the different reaction paths between 8 and 35 h.

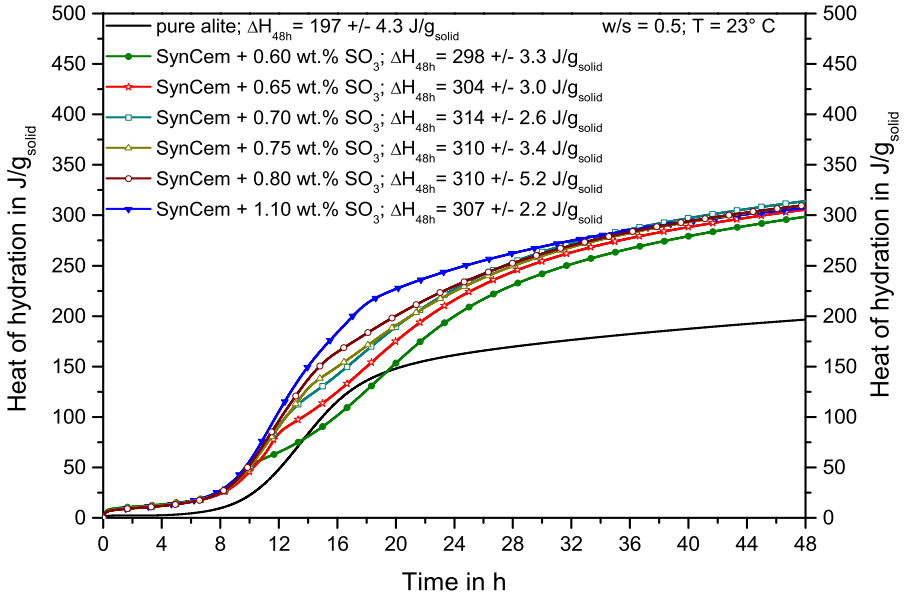

Fig. 5: Heat of hydration of pure alite and of SynCem with different SO_3 contents (on the dry cement).

7.7.4.2. Quantitative in-situ XRD

To get a better insight into the hydration process, the samples of 0.65 wt.% and 1.10 wt.% SO_3 have been examined with quantitative in-situ XRD.

7.7.4.2.1. SynCem with 0.65 wt.% SO_3

Not only is very accurate weighing and mixing necessary, but the exact point in time at which the aluminate reaction occurs is also very sensitive to temperature [25] and mixing conditions. Even though the laboratory conditions were controlled meticulously and the preparation was carried out carefully, the analyzed hydration reaction varied among the 5 independent measurements performed for SynCem with 0.65 wt.% SO_3. Table 4 presents the mean values of 5 independent measurements with 1 σ for the times directly after mixing and significantly after the aluminate reaction peak.

Fig. 6 presents the content of alite, portlandite, and C-S-H_{lro} in the SynCem paste with 0.65 wt.% SO_3 (on cement) over time. The alite content expected from the paste composition and the refinement of the dry alite can be found in the first diffractogram of the in-situ measurement as already found before in pure alite pastes [18, 42]. The alite content starts to decrease after 4-5 h. The phase content of alite shows three different slopes until 20 h of hydration: a faster decrease in content until around the point in time marked by line 2 (in Fig. 6), a lower slope between the times of line 2 and 3, and a higher slope after line 3. After 48 h, around 35 wt.% of alite has been dissolved. Portlandite precipitates starting at the same time that the alite dissolution starts. The period of lower phase-content change between the times of hydration marked by lines 2 and 3 in Fig. 6 can also be found in the increase of the portlandite and C-S-H_{lro} contents. C-S-H_{lro} can be detected after around 8.6 h (marked with line 1 in Fig. 6). Therefore, it can be detected significantly later than the dissolution of alite and precipitation of portlandite can be observed.

Within 46.5 h, 34.3 ± 1.5 wt.% alite in paste was dissolved (Table 4). Assuming C-S-H_{lro} to have a stoichiometry of $C_{1.7}SH_{2.6}$, the theoretically precipitating amount from alite dissolution of 30.4 wt.% was obtained within one standard deviation (29.7 ± 2.7 wt.% C-S-H_{lro}, Table 4). The portlandite phase content found is lower than expected theoretically (10.0 ± 2.1 wt.% instead of 14.5 wt.%). This is a typical problem in the XRD analysis of cementitious pastes, because portlandite forms large crystals. The spotiness resulting from this effect, in addition to the problem that the necessary statistic for powder XRD analysis is questionable for the portlandite refections, is calculated by preferred orientation to obtain a better fit of the diffractogram [18].

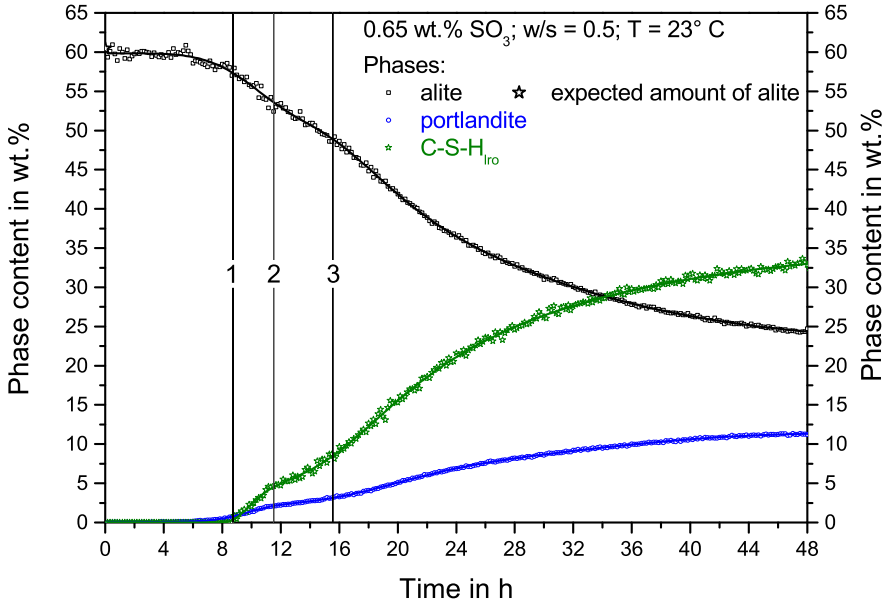

Fig. 6: Phase development of the silicate reaction in a hydrating paste of SynCem with 0.65 wt.% SO_3 (on cement). Data points and the fitted curves (section 7.7.3) are presented. Time line 1 represents the first time that C-S-H_{lro} can be detected, and time lines 2 and 3 visually separate different slopes in the phase contents over time.

Fig. 7 shows the phase developments in the aluminate reaction for the same paste. Bassanite could not be found in paste due to its fast dissolution [3, 12]. The anhydrite content in paste found in the first diffractograms is very close to the one expected to be in paste. It continuously decreases until about 4 to 5 h, after which time the anhydrite dissolves very quickly to a complete level. It can be seen that the C_3A content in paste is about 1.2 wt.% lower than expected for the paste composition and the refinement of the dry powder. This content of C_3A remains constant for about 10 h, after which it decreases very rapidly by about 1 wt.%. Afterwards, the C_3A content is about constant before it begins to decrease continuously. Ettringite precipitates until 11 h of hydration. Afterwards, around 0.6 wt.% ettringite dissolves again quite rapidly. The ettringite content then stays about constant and decreases very slowly during the last 15 h of the measurement. After about the same time as the C_3A dissolution is renewed, two AFm phases with different water contents start to precipitate. AFm-16H starts to precipitate directly after the fast dissolution of C_3A. After 46.5 h, about 84 wt.-% of the initially present C_3A has been dissolved (Table 4).

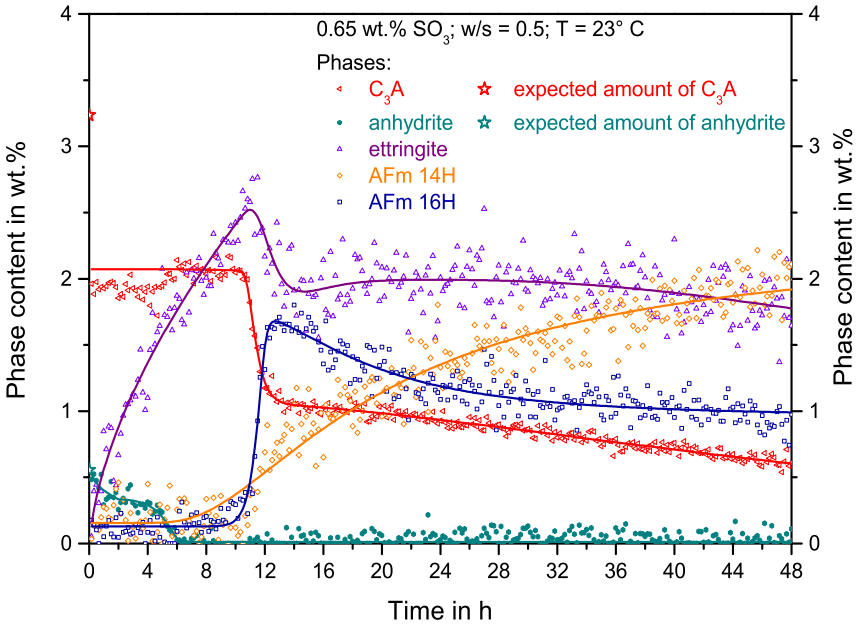

Fig. 7: Phase development of the aluminate reaction in a hydrating paste of SynCem with 0.65 wt.% SO_3 (on cement). Data points and the fitted curves (section 7.7.3) are presented.

Table 4: Phase content in paste at a specific time of hydration of SynCem with 0.65 wt.% SO_3 (0.43 wt.% SO_3 with respect to the paste) as a mean value with 1 σ of 5 independent in-situ XRD measurements. The values for 0 h refer to the value expected to be in paste. Bassanite was excluded from analysis because it is already dissolved in the first diffractogram taken after mixing.

Phase	Phase content in paste at a specific time of hydration in wt.%				
	0 h	0.2 h	24 h	46.5 h	$\Delta_{46.5\ h\ -\ 0\ h}$
alite	60.4	60.9 ± 1.6	36.0 ± 2.6	26.1 ± 1.5	- 34.3 ± 1.5
C_3A_{cubic}	3.2	1.9 ± 0.2	0.8 ± 0.2	0.5 ± 0.1	- 2.7 ± 0.1
anhydrite	0.56	0.4 ± 0.2	0.0 ± 0.1	0.0 ± 0.0	- 0.56
bassanite	0.17	-	-		- 0.17
C-S-H_{lro}	0	0.0 ± 0.1	21.0 ± 3.8	29.7 ± 2.7	+ 29.7 ± 2.7
portlandite	0	0.0 ± 0.1	6.1 ± 1.9	10.0 ± 2.1	+ 10.0 ± 2.1
ettringite	0	0.2 ± 0.2	2.0 ± 0.3	1.6 ± 0.3	+ 1.6 ± 0.3
AFM-14H	0	0.1 ± 0.1	1.0 ± 0.4	1.5 ± 0.4	+ 1.5 ± 0.4
AFm-16H	0	0.3 ± 0.1	0.7 ± 0.3	0.6 ± 0.3	+ 0.6 ± 0.3

7.7.4.2.2. SynCem with 1.10 wt.% SO_3

Fig. 8 shows the phase development of alite, portlandite, and C-S-H_{lro} in the SynCem paste with 1.1 wt.% SO_3 as mean value of 2 independent measurements with 1 σ. The amount of alite in paste directly after mixing is lower than the expected value. As the initial heat flow in the SynCem with 1.1 SO_3 is very similar to that of 0.65 wt.% SO_3 (Fig. 5), the lower alite content should result from the underdetermination of alite in the paste instead of already dissolved alite. In addition, it is known from earlier studies that the initial heat flow of pure alite paste is very low [6] (also shown in Fig. 3). The dissolution of alite and precipitation of portlandite and C-S-H_{lro} proceed in one reaction instead of three steps in SynCem with 0.65 wt.% SO_3 (Fig. 6). Within 46.5 h, 31.5 ± 0.4 wt.% alite in paste was dissolved, corresponding to the first alite content present in the paste (Table 5). Assuming the C-S-H_{lro} to have a stoichiometry of $C_{1.7}SH_{2.6}$, the theoretical precipitated amount of 27.9 wt.% was obtained within one standard deviation (27.0 ± 0.9 wt.% C-S-H_{lro}, Table 5). The portlandite phase content found is lower than expected theoretically (10.8 ± 0.4 wt.% instead of 13.3 wt.%).

Fig. 9 shows the development of the phases taking part in the aluminate reaction for the same paste. The anhydrite content in paste found in the first diffractograms is about 0.3 wt.% lower than that expected to be in paste. It is about constant for 2 h and decreases slowly afterwards. After 8.2 h, no anhydrite can be detected in the system. It can be seen that the C_3A content in paste is 1.0 wt.% lower than expected from the paste composition and the refinement of the dry powder. The phase content of C_3A remains constant for about 12.5 h, where it is reduced quite rapidly by about 1.4 wt.%. The C_3A hydration is thus still blocked for a significant time also in the SynCem containing 1.10 wt.% sulfate when the sulfate carrier is completely dissolved. After around 18 h, the C_3A content decreases continuously on low levels. In the SynCem paste with 1.10 wt.% SO_3, the renewed fast dissolution is not as rapid (4-5 h in the different experiments) as in the SynCem with 0.65 wt.% SO_3 (1.8-2 h in all 5 experiments). Ettringite increases very continously from the start of the hydration reaction to about 15 h. Afterwards, it dissolves again until it becomes about constant. AFm-14H starts to precipitate after about 13 h of hydration. After a relatively fast precipitation, AFm-14H keeps precipitating continuously.

We can summarize the consecutive events in the renewed acceleration of the aluminate reaction. We have a fast dissolution of C_3A, bassanite, and a part of the anhydrite in the initial period. Afterwards, while ettringite precipitates continuously anhydrite dissolves completely. After about 4 h after the diminution of anhydrite, C_3A dissolution is renewed. AFm-14H starts to precipitate 0.5 h later, in addition to the ongoing precipitating ettringite. After 15 h, the sulfate content available in the system is too low for further precipitation of ettringite; instead, a small part of ettringite dissolves again and AFm-14H is the only aluminate product resulting from further hydration.

After 46.5 h, about 88 wt.-% of the initially present C_3A has been dissolved (Table 5). The ettringite content after 46.5 h hydration is double that of the SynCem with 0.65 wt.% SO_3, while the content of AFm phases is only slightly higher in the SynCem with 1.10 SO_3 (2.7 instead of 2.1 wt.%).

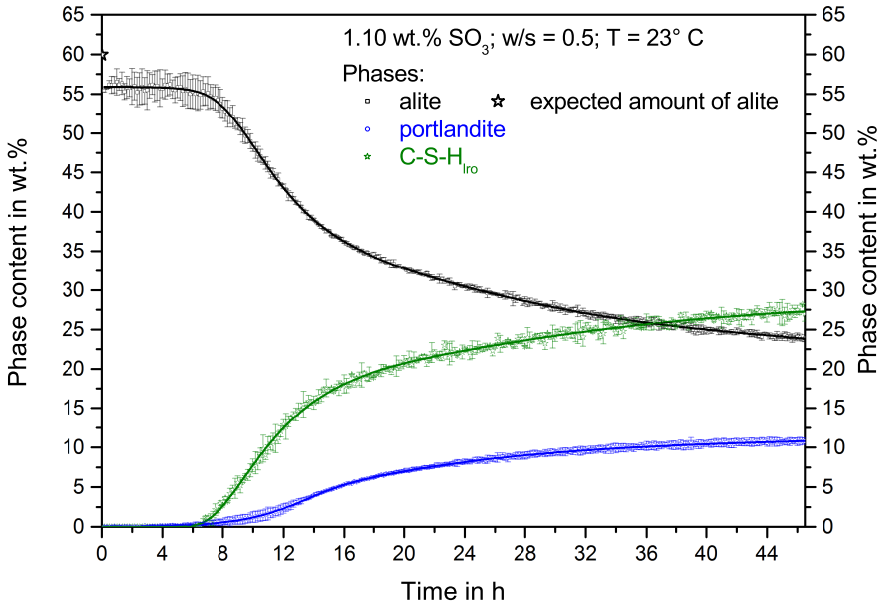

Fig. 8: Phase development of the silicate reaction in a hydrating paste of SynCem with 1.10 wt.% SO_3 (on cement). Data points and the fitted curves (section 7.7.3) are presented.

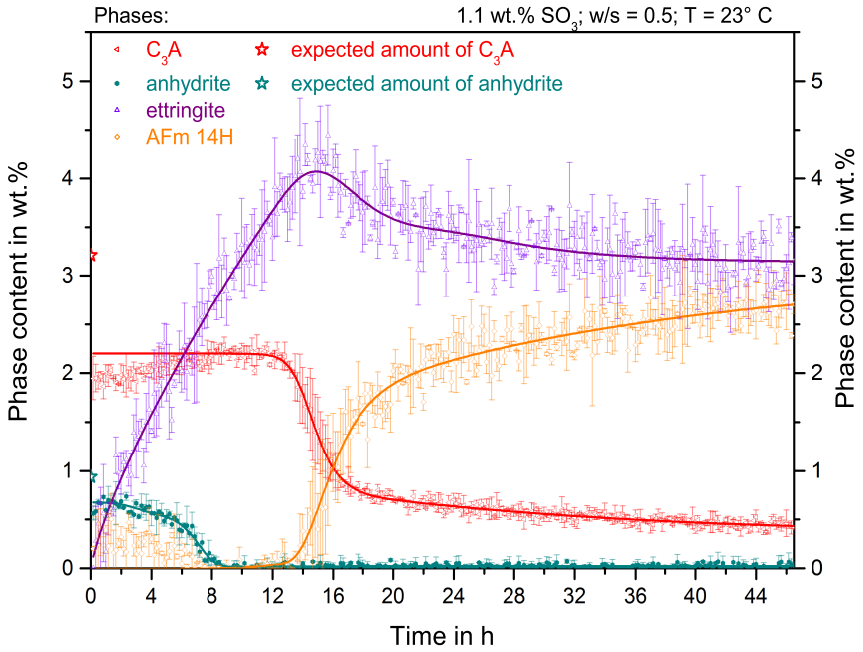

Fig. 9: Phase development of the aluminate reaction in a hydrating paste of SynCem with 1.10 wt.% SO_3 (on cement). Data points and the fitted curves (section 7.7.3) are presented.

Table 5: Phase content in paste at a specific time of hydration of SynCem with 1.10 wt.% (0.73 wt.% SO_3 with respect to the paste). as a mean value with 1 σ of 2 independent in-situ XRD measurements. The values for 0 h refer to the value expected to be in paste. Bassanite was excluded from analysis because it is already dissolved in the first diffractogram taken after mixing.

Phase	Phase content in paste at a specific time of hydration in wt.%				
	0 h	0.2 h	24 h	46.5h	$\Delta_{46.5\ h\ -\ 0\ h}$
alite	60.0	55.4 ± 0.2	30.5 ± 0.0	23.9 ± 0.4	-31.5 ± 0.4 (-0,2h value)
C_3A_{cubic}	3.2	2.0 ± 0.2	0.7 ± 0.1	0.4 ± 0.0	- 2.8 ± 0.0
anhydrite	0.94	0.6 ± 0.1	0.0 ± 0.0	0.0 ± 0.0	- 0.94
bassanite	0.29	-	-		- 0.29
C-S-H_{lro}	0	0.0 ± 0.0	22.5 ± 0.3	27.0 ± 0.9	+ 27.0 ± 0.9
portlandite	0	0.0 ± 0.0	8.2 ± 0.3	10.8 ± 0.4	+ 10.8 ± 0.4
ettringite	0	0.0 ± 0.0	3.5 ± 0.1	3.2 ± 0.2	+ 3.2 ± 0.2
AFm-14H	0	0.2 ± 0.0	2.4 ± 0.2	2.7 ± 0.1	+ 2.7 ± 0.1

7.7.4.3. Calculation of the heat flow from phase development

7.7.4.3.1. SynCem with 0.65 wt.% SO_3

The heat flow for the SynCem with 0.65 wt.% SO_3 was calculated from the quantitative phase development measured by XRD (Fig. 10). The first fast dissolution of C_3A (about 1.2 wt.% dissolved in the first minutes) and the dissolution of bassanite are not considered. Mainly the initial dissolution of C_3A causes the part of the initial heat flow not accounted for in Fig. 10. The heat flow during the induction period is caused by the precipitation of ettringite; the dissolution of anhydrite does not account for a significant heat flow. The silicate reaction as calculated from the alite dissolution proceeds in two steps. The heat flow during the acceleration of the main hydration period is mainly produced by silicate reaction. The heat during the sharp heat flow event is mainly produced by the dissolution of C_3A, with a minor contribution of the precipitation of AFm-16H. Underlying this, a high amount of heat is still produced during the decelerated course of the silicate reaction. The dissolution of ettringite is endothermic.

Fig. 11 compares the heat of hydration measured by heat flow calorimetry and calculated from in-situ XRD. The heat produced from the dissolution of C_3A in the first minutes is considered in the heat of hydration. That of bassanite is disregarded because it is negligibly small. It can be seen that the calculated and measured heats of hydration are very close to each other. A higher reaction degree in the second part of the silicate reaction in the in-situ XRD leads to a deviation of 20 J/g_{solid} from the calculated and measured heats of hydration. The heat production coming from aluminate reaction sums up to 34 J/g_{solid} until 46.5 h of hydration. That means that the silicate reaction provided 269 J/g_{solid} (286 J/g_{alite}) when the

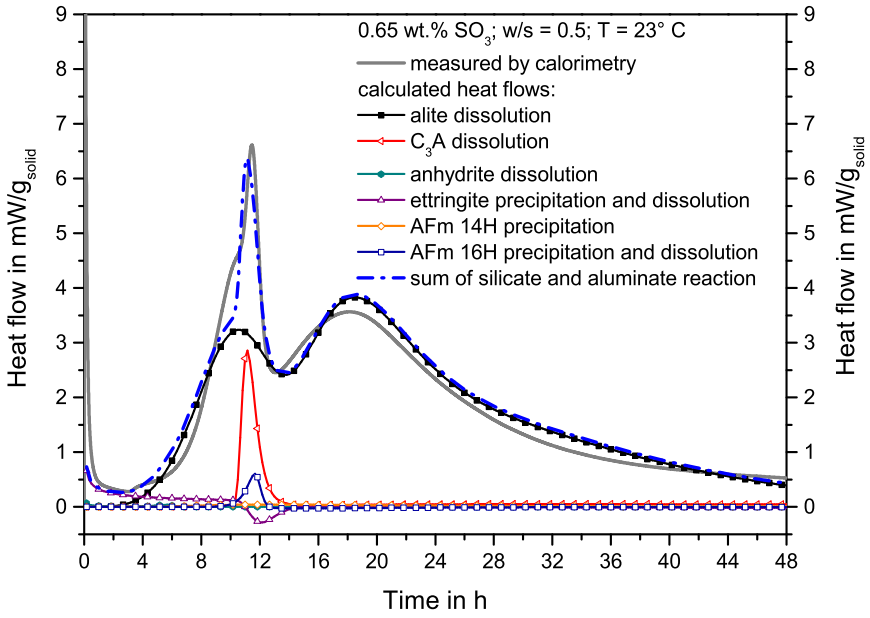

Fig. 10: Comparison of the heat flow measured by calorimetry and calculated from the phase development measured by XRD for SynCem with 0.65 wt.% SO_3.

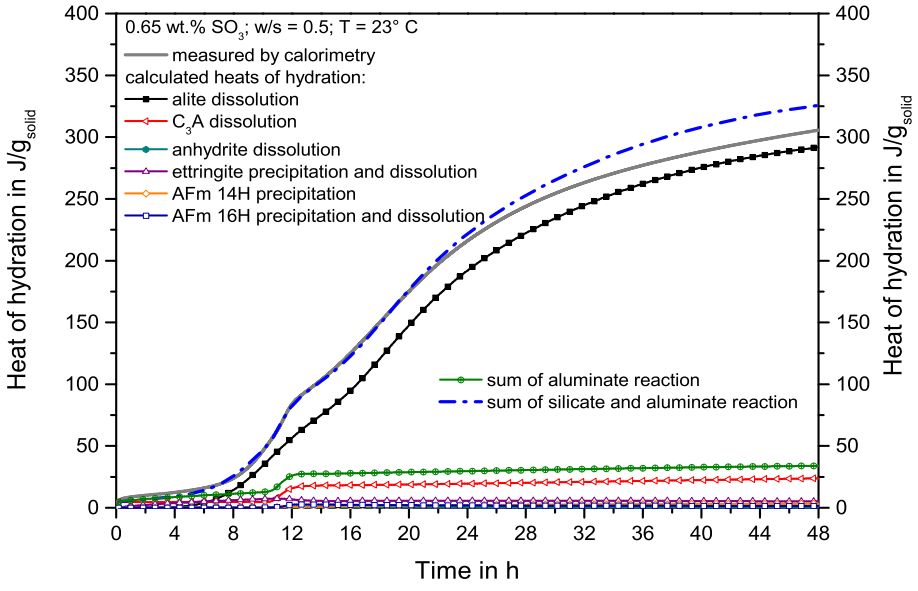

Fig. 11: Comparison of the heat of hydration measured by calorimetry and calculated from the phase development measured by XRD for SynCem with 0.65 wt.% SO_3.

aluminate reaction heat is subtracted from the measured heat of hydration (to overcome the slightly higher hydration degree for the single measurement of the in-situ XRD). This means that the alite reaction degree after 46.5 h is about 45 wt.% higher than in the pure alite paste (Fig. 5).

The comparison of the complete silicate reaction for SynCem with 0.65 wt.% SO_3 was calculated either from alite dissolution (1) or from portlandite precipitation (2) or C-S-H_{lro} precipitation (3) as measured by XRD is shown in Fig. 12. Two main features can be observed. The precipitation of C-S-H_{lro} starts significantly later than the dissolution of alite and the precipitation of portlandite. Afterwards, the heat flow calculated from C-S-H_{lro} precipitation results in a sharper increase and a higher first maximum than derived from the alite dissolution. In addition, after the reacceleration of the silicate reaction, the precipitation rate of C-S-H_{lro} is slightly higher than the alite dissolution rate until about 34 h of hydration when both reactions result in the same calculated heat flow.

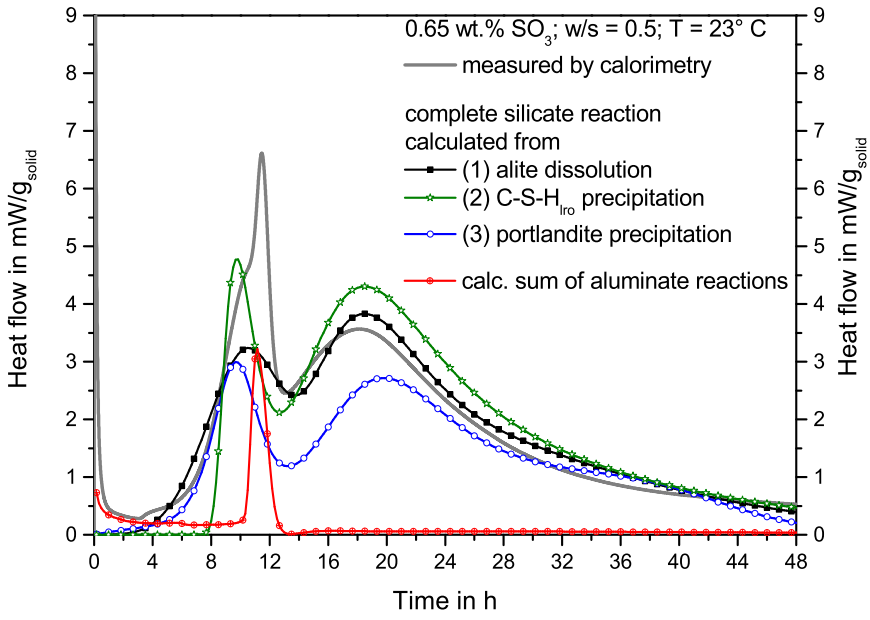

Fig. 12: Comparison of the heat flow measured by calorimetry and calculated from the development of the silicate phases measured by XRD.

7.7.4.3.2. SynCem with 1.10 wt.% SO_3

As in the other SynCem, the heat flow for the SynCem with 1.10 wt.% SO_3 (Fig. 13) during the induction period is caused by the precipitation of ettringite, since the dissolution of anhydrite does not account for a significant heat flow. The silicate reaction as calculated from the alite dissolution proceeds in one assymmetric peak, which is slightly too low. The heat flow during the main hydration period is produced by silicate reaction. The shoulder on the peak of the

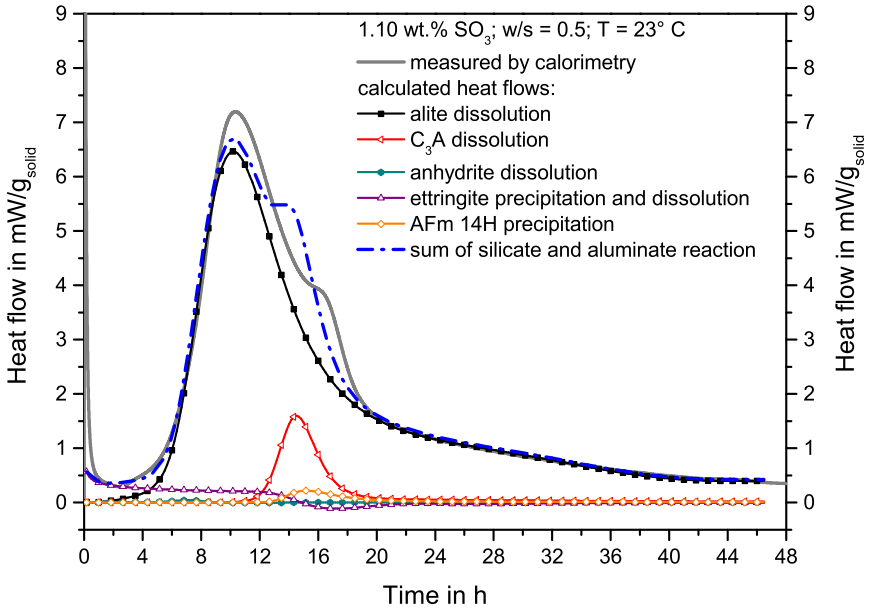

Fig. 13: Comparison of the heat flow measured by calorimetry and calculated from the phase development measured by XRD for SynCem with 1.10 wt.% SO_3.

decelerating silicate reaction is mainly produced by the dissolution of C_3A, with a small contribution of AFm-14H precipitation. It can be seen that the kinetics calculated from in-situ XRD are slightly enhanced in comparison to measured heat flow from calorimetry.

Fig. 14 compares the heat of hydration measured by heat flow calorimetry and calculated from in-situ XRD for the SynCem with 1.10 wt.% SO_3. The heat produced from the dissolution of C_3A in the first minutes is incorporated in the heat of hydration, that of bassanite is negligibly small. It can be seen that the calculcated and measured heats of hydration are very close to each other (deviation of 5 J/g_{solid} after 46.5 h). The heat production coming from aluminate reaction sum up to 42 J/g_{solid} until 46.5 h of hydration. Silicate reaction provided 268 J/g_{solid} (287 J/g_{alite}) when the aluminate reaction heat is subtracted from the measured heat of hydration. The silicate reaction degree is the same as in the SynCem with 0.65 wt.% SO_3 (about 43 % higher than in the pure alite paste in Fig. 5 after 46.5 h).

7.7.5. Discussion

7.7.5.1. Silicate reaction until the start of the acceleration period

C-S-H_{lro} precipitates later in time than portlandite formation or alite dissolution can be detected. Consistent with findings in pure alite pastes [6, 18], C-S-H precipitation starts later but accelerates faster than alite dissolution (Fig. 12). The presented results agree with the finding [18] that an XRD amorphous C-S-H has to be formed before the precipitation of C-S-H_{lro} and that C-S-H_{lro} precipitation is connected to the step in which crystalline alite

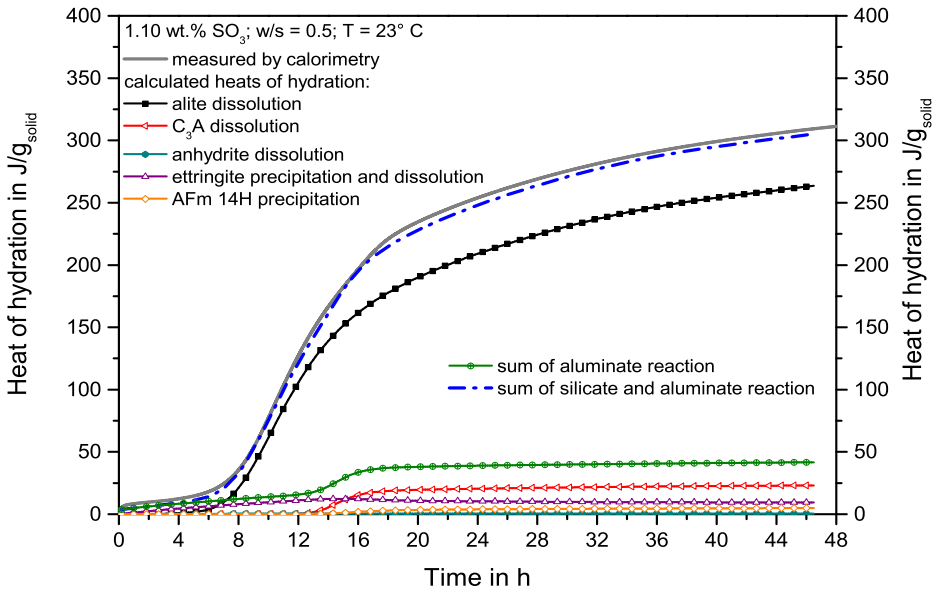

Fig. 14: Comparison of the heat of hydration measured by calorimetry and calculated from the phase development measured by XRD for SynCem with 1.10 wt.% SO_3.

begins to dissolve linearly with time (Fig. 6 and 8). C-S-H_{lro} is the metastable product in the early hydration of the silicate reaction, precipitating in the further hydration process. The already precipitated XRD amorphous C-S-H transforms into C-S-H_{lro} during the early hydration of alite, as the C-S-H content after 46.5 h corresponds very well to the value expected from alite dissolution. As discussed before [18], dimeric silicate tetrahedra are formed as soon as the acceleration period of the silicate reaction starts [16, 17]. The lasting presence of a monomeric silicate species associated with hydrogen in pastes during early hydration has been interpreted to mean that a two-step precipitation is always required for C-S-H [17]. The first step is the formation of an intermediate phase and the second step is the evolution into dimeric C-S-H. Recently, it has been shown that the amount of monomeric silicon tetrahedra associated with hydrogen should be in relation to the alite surface [43]. Their result seems to support the view that C-S-H_{lro} should consist of dimeric silicate species and can be formed directly from solution as soon as it has been precipitated in paste for the first time.

Therefore, we would state that it takes a while until a kind of C-S-H precipitates that is able to accelerate the hydration reaction. The precipitation of a dimeric kind of C-S-H should be able to start the acceleration of the silicate reaction, but the start of the linear dissolution of alite is associated with the precipitation of C-S-H_{lro}. This questions existing numerical models for alite hydration that start with a specific number of nuclei being present very soon after the mixing, which grow afterwards at constant rates in different directions [19, 44, 45]. Bullard et al. [15] pointed out recently that the assumption of constant rates for C-S-H precipitation leads to erroneous fitting parameters, as the C-S-H precipitation also follows a function of oversaturation. We want to add to this that the kind of C-S-H that precipitates is also very important for the ability to accelerate the hydration. Lothenbach & Nonat stated

that the high Ca concentrations in solution during the induction period probably are required to precipitate a C-S-H with a high Ca/Si ratio, which is observed in early OPC hydration [46]. This would explain why it takes time until the required kind of C-S-H can be precipitated for the first time in paste. Since the dissolution rate was shown to be significantly decreased with higher Ca concentrations in solution [7, 8], the silicate reaction proceeds very slowly, as observed, until the kind of C-S-H precipitates that is required for acceleration of the silicate reaction.

7.7.5.2. Aluminate reaction during the course of SynCem hydration reaction

The aluminate reaction proceeds very similarly for both SynCem with 0.65 and 1.10 wt.% SO_3 as analyzed by in-situ XRD (Fig. 7 and 9).

A fast dissolution of C_3A and bassanite takes place in the initial period. The former causes the main heat within the initial heat flow (Fig. 11 and 14 and [12]). During the induction period, the ongoing ettringite formation and the dissolution of sulfate carriers continue without further dissolution of C_3A [3, 12, 37], which reproduces the results of Hesse et al. [12]. Their suggestion [12] seems plausible that a XRD amorphous Al-containing phase has been precipitated, from which reservoir the further ettringite formation obtains the necessary Al. The ongoing ettringite formation leads to the higher heat flow in the induction period of the SynCem pastes in comparison to pure alite paste, as shown in Fig. 3, 10 and 13.

Anhydrite is dissolved completely in 4-5 h before the ettringite precipitation stops or the dissolution of C_3A is renewed. Unlike the results obtained in this study, previous studies of an OPC paste by Jansen et al. [3] and the model cement of Quennoz & Scrivener [26] showed that the C_3A dissolution restarted immediately after no available sulfate carrier was left in paste. In fact, a very small amount of sulfate carrier was still detected in both cases, but it did not prevent the further C_3A dissolution. Indeed, the behavior of the aluminate hydration in SynCem is comparable to the one in pure C_3A-gypsum pastes, as investigated by Minard et al. [4]. They also described a hydration step after the diminution of the sulfate carrier, where ettringite formation took place from sulfate from the pore solution before the renewed sharp C_3A dissolution and formation of AFm phases [4]. On the other hand, Quennoz & Scrivener [25] concluded that the sharp peak of C_3A dissolution and AFm phase precipitation in a C_3A – gypsum system would directly follow the diminution of gypsum in paste. The blockage of C_3A dissolution by sulfate ions was explained by Ca and/or sulfate ions adsorbing on C_3A surfaces and blocking reactive dissolution sites of C_3A [4]. The diminution of the crystalline sulfate carrier does not strictly imply that the solution cannot contain enough sulfate to prevent C_3A from dissolving. Obviously, enough sulfate is still in solution or on C_3A [4] or C-S-H [13, 26, 27, 47-49] surfaces to produce ettringite for another 4-5 h after the depletion of anhydrite.

No specific heat flow event for the dissolution of C_3A and an accelerated precipitation of ettringite after the diminution of the sulfate carrier could be observed in this study. This is different from cementitious pastes, where the renewed aluminate reaction is normally associated with the renewed and accelerated precipitation of ettringite [3, 12], and it is different from the model cement of [26]. Instead, only one significant heat flow event occurred, corresponding to the renewed dissolution of C_3A and, at first, coexistent precipitation of AFm phases and ettringite, and, after a short time, only precipitation of AFm

phases and a partial dissolution of ettringite. The anhydrite used in the present study is a very soluble one, due to the low gypsum dehydration temperature (380° C). Therefore, the combination of a readily soluble sulfate carrier with a C_3A with moderate reactivity leads to a system where only one significant heat flow event from the aluminate reaction after the initial heat flow can be detected.

The sulfate content in SynCem paste with 0.65 wt.% SO_3 is very low (0.43 wt.% SO_3 with respect to the paste). It is nominally sufficient for 2.5 wt.% ettringite when no AFm phase is present. From Fig. 7 it can be seen that slightly more ettringite is formed. It is known that ettringite forms solid solutions with OH^- and/or CO_3^{2-} [50]. The formation of AFm-16H and AFm-14H can fall back on approximately 0.14 wt.% SO_3 re-released by the conversion of ettringite within 48 h of hydration. With this amount, about 1.2 wt.% AFm-16H or AFm-14H of solely sulfate-containing AFm could be precipitated. With the systematic error in the quantitative analysis of the AFm phases (see section 7.3.4) it is possible but cannot be decided with certainty if significant amounts of OH^- and CO_3^{2-} are incorporated in the AFm phases (in sum 2.1 wt.%, Table 3).

The fast renewed dissolution of C_3A is accompanied by the precipitation of AFm phases as it was described by Quennoz & Scrivener for a second aluminate peak that occurred in their model cement [26]. In comparison of this study with the earlier work [26], this heat flow event was shifted to earlier times. This can be explained with the absolute SO_3 content in the paste. Although the C_3A/SO_3 ratio is slightly higher in our SynCem than in the model cement of [26], due to the comparably lower C_3A content, the absolute SO_3 content is lower in the case of the studied SynCem. The retardation of the aluminate reaction is linked to the amount of sulfate in solution and to the surface of C_3A [4]. As obviously not all sulfate is needed to block the C_3A surface from further reaction (as ettringite keeps precipitating), more sulfate in the system will lead to a later occurrence of the renewed aluminate reaction.

Except for the number of AFm phases precipitating, the only difference in the SynCem with 0.65 and 1.10 wt.% SO_3 is the intensity and sharpness of the heat flow event attributed to the dissolution of C_3A. In the lower sulfated SynCem, the renewed C_3A dissolution is faster and decelerates significantly earlier (1.8-2 h instead of 4-5 h, respectively) although in both SynCem pastes the same C_3A content is left after 46.5 h (Table 4 and 5). Quennoz and Scrivener attributed the finding that aluminate reactions were broader the later they occurred to the available space for the reaction [26]. Another reason could be that a later aluminate reaction occurs when more sulfate is in the paste. According to Minard et al. [4], the renewed dissolution of C_3A is associated with no more sulfate on C_3A reactive surface sites. The lower the sulfate content in paste is, the faster the C_3A blockage will disappear completely and the more reactive surface of C_3A is present, making a faster and more distinct reaction possible. Consequently, it is not necessarily the lack of space that leads to broader hydration reactions at later times.

After the renewed aluminate hydration event is over, a slowly and continuously ongoing precipitation of AFm phases and the dissolution of C_3A can be detected (Fig. 7 and 9). Minard et al. [4] described the transformation from already precipitated ettringite to AFm phases to be a very slow process. This is also found in this study, except for a short period following the renewed C_3A dissolution when the demand for sulfate is very high due to the fast C_3A dissolution.

During the complete hydration of SynCem, there is thus always an aluminate reaction proceeding from the first sharp initial dissolution until the end of the experiments.

7.7.5.3. Interaction of aluminate and silicate reaction

We could observe that the silicate reaction is extremely disturbed when the reaccelerated aluminate reaction occurs during the main hydration period of the silicate reaction. This is also the case when it occurs after the main peak of the silicate reaction (Fig. 4), which is normally considered to be a feature of a properly sulfated system. In the SynCem with 0.65 wt.% SO_3, the precipitation of C-S-H_{lro} and portlandite and the dissolution of alite show a period of slower reaction in the middle of two faster reactions. The heat flow calculated from this proves that the aluminate reaction is the reason for the lower rates of the silicate reaction. The higher the sulfate content in the SynCem, the later the interference of the silicate reaction takes place (Fig. 4). However, in all cases from 0.65 to 0.80 wt.% SO_3, the silicate reaction reaccelerates after the interfering aluminate reaction is deaccelerated and proceeds on low levels.

7.7.5.3.1. Discussion of the silicate hydration mechanisms

7.7.5.3.1.1. If C-S-H formation is not rate-determining

If the total hydration process depended on a complex dissolution process of alite, as suggested by Nicoleau & Nonat [23, 24], then the dissolution rate would depend on three main features: the saturation index [7, 8, 11], the development of the alite surface area due to a complex dissolution process [14], and the presence of inhibitating ions [9, 11, 51].

Taking the hydration reaction of the SynCem with 0.65 wt.% SO_3 to test this, it must be answered in particular if one of these factors is able to reduce the alite dissolution and increase it afterwards again, restarting from a lower dissolution rate.

It is certainly not plausible that the reactive alite surface area decreases and then increases again during the main hydration period.

The precipitation of AFm phases is not likely to increase the ion concentration of Ca in solution but rather would reduce it because of the need for a Ca source together with the amorphous aluminate phase. This would lead to a higher undersaturation with respect to alite and should therefore not decrease the alite dissolution but enhance it. Thus the only way to decrease the undersaturation for alite (without the reason of a decelerated C-S-H precipitation) would be that the possible lowered Ca concentration would be overcompensated by an affected Si concentration in solution. The degree of undersaturation could decrease as a lower amount of C-S-H is precipitating, but this in turn would mean that the acceleration of the silicate system would depend on C-S-H formation.

It has been experimentally shown that Al in solution can lead to a significant decrease of alite dissolution rates [9, 11, 51]. In spite of this, a sudden Al inhibition of the alite surfaces seems unlikely, as it will be demonstrated that sufficiently available Al should also be available before this point in time (section 7.7.5.3.1.2). In addition, a dissolution blockage due to Al on reactive surface sites is not really convincing for the less steep reacceleration of the silicate reaction after the deceleration of the renewed aluminate reaction.

It was shown by Nicoleau that the adsorption of Al ions on silicate surfaces is pH dependent, having a huge effect at lower pHs (11,7 and 12) and only a small effect at higher pHs (12.7 and 13) [9]. It is not expected, that the pH of the SynCem hydrating is significantly below 12.7 at the point in time when the alite dissolution decelerates for the first time. Consequently, the effect of Al on the dissolution rate of alite should be marginal at this stage of hydration. Additionally, Nicoleau et al. showed that the inhibiting effect of Al on C_3S should be caused by the formation of covalent bonds between Al ions and silicate on the C_3S surface [9]. They showed that this covalent bonding is not a totally reversible process (when changing the pH). Thus an existing blockage of the surface should persist after the hydration reaction reaccelerates. It could be argued that exactly this happens, because the slope of the reacceleration of the alite dissolution is slightly lower than that of the first acceleration, and the level of the dissolution rate is lower than at the first maximum of silicate hydration (Fig. 12). However, Nicoleau et al. [9] showed that not only was the dissolution rate reduced at the same pH when more Al was in solution but the reaction turnover was reduced as well. The total reaction degrees of the different SynCem pastes are very similar (Fig. 5), and the hydration degree of the silicate reaction was calculated for the SynCems with 0.65 and 1.10 wt.% SO_3 to be equal (286 and 287 J/g_{alite}, respectively). If an Al bonding to the silicate surface took place and reduced the dissolution rate, it is unlikely that it would not change the reaction degree until the alite reaction proceeded on low levels.

7.7.5.3.1.2. If C-S-H formation is rate-determining

It has been suggested that the delayed and less steep acceleration of the undersulfated system is caused by Al ions left from the early aluminate reaction [26, 52]. It has also been suggested that Al inhibition of the silicate hydration causes the precipitation of C-A-S-H phases instead of C-S-H if Al is in solution [52-54]. C-A-S-H is supposed not to be able to act as a substrate for C-S-H. This would therefore slow down the silicate reaction (even for very low amounts of Al from alite dissolution) [53, 54].

The reaccelerated silicate reaction is comparably delayed in the differently sulfated SynCem pastes (Fig. 3 and 4). The question therefore arises whether the further reaccelerated alite reaction (with a less steep reacceleration) during the time after the aluminate reaction has interfered with the silicate reaction in the SynCem with 0.65 wt.% sulfate can be explained by the effect of C-S-H poisoning.

In all experiments where the Al-inhibiting effect on C-S-H precipitation has been assumed to occur, it has been reported that the time required to form a C-S-H capable of serving as a substrate for C-S-H precipitation is prolonged [53, 54]. In contrast to their experiments in our SynCem, C-S-H_{lro}, the kind of C-S-H that is the product required to accelerate the silicate reaction, is already present in the paste before the silicate reaction reaccelerates. Therefore, it is improbable that a higher Al content, which was supposed by [52] to result from the change of the buffering system from sulfate carrier-ettringite-portlandite to ettringite-AFm phase-portlandite without a sulfate carrier, would lead to a delay in alite hydration in the SynCem in the way proposed.

Nevertheless, Al in solution leads to the precipitation of C-A-S-H phases instead of C-S-H, depending on the Al concentration in solution [46]. At later times until the end of the induction period, this was never addressed as a reason for the deceleration of the C-S-H formation.

Begarin et al. showed that Al in solution decreased before the hydration reaction started to accelerate [53]. It is therefore not a great leap to incorporate the Al in the C-S-H structure later on.

A minor uncertainty in rejecting of the Al-inhibiting effect of the C-S-H precipitation in the SynCem is that C-S-H is not "growing" in crystallite size like portlandite. It has been found before that the crystallite size of C-S-H_{lro} remains in very low dimensions throughout the hydration reaction [6, 18]. In the case of the SynCem, C-S-H mean coherently scattering sizes of 5.6 ± 0.7 nm (as Vol-IB) were calculated in the Rietveld refinements. Therefore, the "growth" of C-S-H is more of a continuous heterogeneous precipitation process of very small crystallites. If the effect that C-A-S-H phases cannot act as a substrate for the further precipitation of C-S-H is still present at this stage, it could indeed decelerate the hydration rate.

This effect can only occur, though, if the Al concentration in solution dramatically increases during the renewed C_3A dissolution. Taking into account the ongoing aluminate reaction, it seems that in spite of the sulfate present, more Al should be available in SynCem pastes than in pure alite paste. During initial dissolution of SynCem pastes, at least 1 wt.% C_3A is dissolved, which would be enough to form 4.6 wt.% ettringite within the first minutes of hydration (with 0.65 wt.% sulfate content in the SynCem only 2.3 wt.% ettringite could be produced nominally). However, the ettringite content in paste actually increases very slowly. At the point in time when C_3A starts its renewed dissolution, there is still Al from the initially dissolved C_3A in the system that is not incorporated in a crystalline aluminate hydrate phase, the Al set free from alite dissolution not even included. In the SynCem with 0.65 wt.% SO_3, even less Al is incorporated in crystalline hydrate phases at the time when C_3A dissolution reaccelerates in comparison to the SynCem with 1.10 wt.% SO_3.

Most of the Al in paste will probably be fixed to an amorphous aluminate phase as suggested by Hesse et al. [12]. However, the ongoing precipitation of ettringite, from the induction period until a short period after the time when the renewed C_3A dissolution starts, shows that the amorphous Al source provides reasonably available Al ions at least for the precipitation of ettringite. Since the precipitation of ettringite proceeds with ions from solution, this amorphous Al source continuously provides Al and therefore keeps Al in solution during the complete hydration process. This also strengthens the suggestion of Minard et al. [4] that Ca and/or sulfate on C_3A prevents further dissolution of C_3A, because a need for further Al at the time of the renewed acceleration of C_3A is not indicated.

Al could also be incorporated into C-S-H or TAH (third aluminate hydrate), an amorphous Al-containing phase [55] probably associated with C-S-H, as discussed further in [46]. If the Al inhibition of C-S-H nuclei is a significant problem, both incorporations of Al should not lead to the higher silicate hydration rates detected before the sulfate depletion peak in the SynCem. Al could also be adsorbed on alite surfaces as found by Nicoleau et al. [9]. If this effect is present in SynCem, it should operate at lower pHs at the start of hydration. It is unlikely that the adsorption of Al on alite surfaces could significantly lower the amount of Al not bound to a crystalline hydrate phase in paste without affecting the acceleration of silicate hydration (which is very fast in SynCem in comparison to pure alite).

Taking into account the ongoing aluminate reaction, it seems that more Al should be available in SynCem pastes than in pure alite paste, in spite of the sulfate present. Therefore, if the amorphous Al phase suggested by Hesse et al. [12] does not need sulfate to precipitate, then there is no explanation why sulfate in SynCem should be able to enhance the acceleration

period of the silicate reaction if the accelerating effect would be only the binding of Al from solution. All this indicates that sulfate is able to accelerate alite hydration by another way than just binding Al in a hydrate phase.

This is in contradiction to Quennoz & Scrivener [26], who suggested that the alite hydration itself is slowed down by Al inhibition. Sulfate would remove Al from solution and therefore prevent the inhibiting effect [26]. They demonstrated this by comparing alite and C_3S (without Al) hydration with and without the addition of gypsum. For the corresponding C_3S sample containing no Al, the reaction was not enhanced by gypsum addition [26]. On the other hand, their alite hydration accelerates faster than C_3S. Furthermore, with the addition of gypsum for both samples, the induction period was slightly prolonged. This effect occurred before with Brown et al. [56] for C_3S hydration with $CaSO_4$ in solution. It remains unclear why C_3S does not start earlier with its acceleration period than alite, in spite of having smaller particles (and no inhibiting Al ions) in it. And secondly, it is not clear if the enhancement of the hydration reaction that is attributed to the addition of sulfate to the system can lead to the same effect when the particle size distribution (PSD) of the powder is significantly smaller. We can therefore sum up that the effect of adding gypsum on alite hydration is not satisfyingly explained.

Nicoleau et al. showed that sulfate in solution is also able to decelerate alite hydration due to the adsorption of sulfate on dissolving alite surface area [9, 51]. On the other hand, Nicoleau suggested that sulfate in solution would lead to a decrease in the Ca activity in solution due to the aqueous $CaSO_4^0$ species and would therefore lead to a more undersaturated solution which is resulting in the acceleration of alite dissolution [51]. In the SynCem system used in this study, sulfate is introduced by calcium sulfates and not by sodium sulfate as added by [51]. Therefore, the presence of $CaSO_4^0$ in solution should not be able to reduce the Ca activity in solution in the same way. Assuming a congruent dissolution of anhydrite, Ca and sulfate are delivered in stochiometric amounts to the solution. Therefore, with respect to alite, the sulfate in SynCem should not be able to change the undersaturation degree in the way described.

The ability of C-S-H to adsorb sulfate is well known [13, 26, 27, 47-49]. It is not totally implausible that the adsorption of sulfate could change the precipitation and/or aggregation of the colloidal C-S-H, because the surface of nano-sized C-S-H is very large and certainly has a huge impact on the formation of new C-S-H nuclei on C-S-H (or on aggregation of new C-S-H on preexisting ones). An effect of surface charge from the adsorption of sulfate on C-S-H (which might also depend on the crystallographic orientation of the C-S-H surface) could indeed change the aggregation of C-S-H without significantly changing the C-S-H structure itself. For example, it was suggested by Mota et al. [49] that the adsorption of sulfate has an impact on C-S-H precipitation by promoting a repulsion of C-S-H needles formed due to the repulsion of adsorbed sulfate ions in contrast to a promotion of converging C-S-H needles without sulfate in solution.

In light of the results of this study though, it is improbable that a change in C-S-H precipitation could account for the higher reaction degree of alite in SynCem pastes in comparison with pure alite paste. First of all, although the ongoing ettringite formation after the diminution of crystalline sulfate carrier suggests that some sulfate could be adsorbed on C-S-H surfaces in the first hours of hydration, the amount of adsorbed sulfate on C-S-H surfaces should be low, as the sulfate content in all SynCems is very low in respect to available Al in paste. At the end

of the precipitation of ettringite and after the renewed aluminate reaction has taken place, it is very unlikely that significant amounts of sulfate are still adsorbed on C-S-H surfaces. Therefore, if a different C-S-H precipitation mode were responsible for the higher reaction turnover, it would be expected that the total reaction turnover of different SynCem pastes would differ in relation to the point where it is highly probable that no sulfate is adsorbed on C-S-H surfaces any more. Nevertheless, the same heat of hydration can be observed for all SynCem pastes after 48 h (Fig. 5).

This suggests that the higher reaction turnover of alite in the SynCem pastes in comparison to pure alite paste is caused by a mechanism that takes place in the first hours of hydration. On this time scale, the reaction of all SynCems is very similar (Fig. 3 and 4).

7.7.5.3.2. Proposed mechanism leading to the reacceleration of the silicate reaction and the previous deceleration

Apart from the often proposed Al inhibition of the reaction, there is another possibility that could affect the precipitation of C-S-H. A slowly proceeding aluminate reaction occurs during the reacceleration of the silicate reaction after the sharp aluminate reaction has come to an end. AFm phases continuously precipitate while C_3A and ettringite are slowly dissolved (Fig. 7 and 9). It has been shown before [57] that the different zeta potentials of silicates and ettringite would make a coagulation of C-S-H and ettringite or a precipitation of ettringite on alite surface very likely. When the measured zeta potential of AFm phases [58] is included, which was found to be less positive than that of ettringte (but still positive in comparision to the negative silicate surfaces), the continuously precipitating AFm phases could coagulate with the C-S-H [46, 55] and occupy C-S-H surface area that is therefore not available as substrate for further C-S-H precipitation.

The phase development of C-S-H_{lro} indicates that as soon as C-S-H_{lro} is present, only C-S-H_{lro} precipitates in the further hydration (Fig. 12 and Fig. 5 in [18]). This makes it likely that further C-S-H_{lro} precipitates on the surface of already precipitated C-S-H_{lro}. In addition, Nicoleau stated that with addition of 1 wt.% C-S-H seeds, freshly precipitated C-S-H only forms on C-S-H seeds, and alite surfaces remain free of C-S-H [59]. Therefore, if C-S-H precipitation is rate-limiting in the acceleration period, the coagulation of AFm phases and C-S-H could lead to the consumption of C-S-H surface area by AFm phases. The consumed surfaces therefore are not available for further C-S-H precipitation. Thus the precipitation of C-S-H in the hydration process after the renewed aluminate reaction peak is retarded in comparison to the pure alite paste, where no AFm phases precipitate continuously over time. This is because a part of the precipitated C-S-H surface is always blocked from the ongoing AFm precipitation. This results in a slower acceleration of C-S-H precipitation and leads to a less intense but broader accelerating hydration.

This process could also explain the interference of the reaccelerated aluminate reaction in the silicate hydration process. Firstly ettringite precipitates from the aluminate reaction together with AFm phases, and then AFm phases precipitate alone. The fast precipitation of those phases could significantly reduce the surface available for further C-S-H precipitation by blocking C-S-H surfaces. If C-S-H surface area is rate-limiting in the acceleration period of silicate hydration, the decrease in surface could lead to exactly the observed effects (Fig. 4). The precipitation of C-S-H is reduced after the end of the fast AFm precipitation, due to

blocked C-S-H surfaces. Afterwards, the C-S-H surface area can be increased again starting from the C-S-H surface area that is still available, accelerating the silicate reaction again.

7.7.5.3.3. What determines the final deceleration of the main silicate reaction?

It could be shown that the silicate reaction reaccelerates after the interference of the aluminate reaction is over. The question remains, what determines whether the silicate reaction is finally decelerated or if it is able to accelerate again. In this study, one alite with one PSD was used. As all studied SynCems achieved about the same reaction degree after 48 h, the question remains, if the determining factor for the degree of reaction lies within the PSD of the alite used or in the reaction mechanisms.

As Costoya [60] showed, the degree of reaction strongly depends on the PSD of alite used with a higher reaction degree for smaller particle sizes. This means that the hydration reaction will proceed as long as a specific part of alite depending on its particle size (before the hydration) is consumed, while the reason for this is still not so obvious. However, this cannot explain why the reaction degree after 48 h is significantly lower for pure alite without addition of an aluminate system (Fig. 5), than for alite in SynCem pastes, where the only difference is the presence of the aluminate reaction.

The hydration degree in the early hydration also depends, e.g., on temperature [28, 42, 61, 62], which is associated with an accelerated hydration reaction (and higher reaction turnover) for higher temperatures. It is also well known that the addition of several seeding materials from C-S-H seeds [63] to nano-$CaCO_3$ [64], nano-TiO_2 [65], or mesopourous carbon [66] accelerates the hydration kinetics and the reaction turnover of alite. Therefore, apart from the alite "powder intrinsic" reaction turnover, there is also an effect from hydration regimes such as temperature or seeding materials on the turnover of alite hydration.

Recently, the idea that the silicate reaction transition from acceleration to deceleration would be caused by diffusion processes is questioned by the finding that the apparent activation energy for alite hydration determined by Thomas [67] was found not to change from the main hydration period to a degree of hydration of 65 %. Garrault et al. [22] suggested that also the decrease of alite dissolution could cause the deceleration period. In the analysis of mechanically activated alite pastes, it could be shown that the start of the deceleration period was linked to the disappearance of small alite particles [6]. Nicoleau & Nonat [23, 24] very convincingly showed that alite dissolution should be responsible for the deceleration period, since they found the pore solution to decrease in ions as the deceleration period begins. This was also shown by Bullard et al. [15] to occur in simulations. Bullard et al. [15] suggested that the transition from the acceleration to deceleration period could be caused by reduced dissolvable alite surface due to the precipitation of C-S-H. On the other hand, an effect of dissolution at the beginning of the hydration on the alite surface as proposed by Sobolkina et al. [65] could also lead to the effect of different reaction degrees for different reaction rates. It was proposed that if more alite were dissolved in a paste to achieve similar Ca contents in a pore solution neccessary to start the hydration, the accelerated alite dissolution would cause the alite surface to increase at the start of hydration in line with the dissolution step theory [7], which proposes that a higher undersaturation leads to the opening of dissolution pits. Therefore, the available surface for the dissolution of alite would be enhanced for higher

undersaturated systems. A consecutive step retreat mechanism of the etch pits formed at the start of hydration could therefore lead to a higher available alite surface, which could enhance the hydration turnover in the end.

At the end of section 7.7.5.3.1.2, it was suggested that a mechanism that takes place in the first hours of the hydration should cause the higher reaction turnover of alite in the SynCems in comparison to pure alite pastes. On this time scale, the reaction of all SynCems proceeds very similar (Fig. 3 and 4), while the different SynCem pastes show very different hydration kinetics afterwards.

When we take a closer look at SynCem pastes in comparison to pure alite paste, it is clear that the aluminate reaction has to cause the differences in the reaction degree in some way. The aluminate reaction in SynCem paste in the first hour of hydration leads to the dissolution of C_3A and sulfate carriers and to the precipitation of ettringite and probably an amorphous aluminate phase. In section 7.7.5.3.1.2, it was shown that it is not likely that only the reduction of Al in solution by sulfate in the system led to the observed features. It has also been shown that it is not plausible that a change in C-S-H precipitation due to sulfate adsorption could lead to the higher reaction turnover in comparison to pure alite paste but to the same reaction turnover after 48 h for all SynCem pastes.

One explanation for the different reaction turnovers of alite in pure alite and SynCem pastes could be that the first precipitating, very fine (nano-)ettringite could be a seeding material for C-S-H. Due to the different zeta potentials of C-S-H and ettringite [57], it seems to be a good material for this purpose. This very fine ettringite might even provide a more preferable surface for heterogenous nucleation of C-S-H than the alite surface. Therefore, the seeding of this just precipitated, very fine ettringite could lead to a faster precipitation of XRD amorphous C-S-H and thus to a faster dissolution of alite at the very beginning of the hydration reaction. This could lead to a higher number of activated etch pits and to an increase in the reactive alite surface area at the beginning of the hydration reaction.

Additionally, this leads to a higher extent of the C-S-H reactive surface area. Therefore, when the XRD amorphous C-S-H evolves to dimeric C-S-H and to C-S-H_{lro}, the greater extent of the reactive surface area leads to the steeper acceleration of the silicate reaction in SynCem pastes in comparison to pure alite paste.

Since the alite surface area seems to be the determining factor for when the alite hydration enters the deceleration period, a higher reactive surface area of alite will lead to a higher degree of hydration for alite in SynCem pastes than in pure alite paste. The assumption that available alite surface is the reason for the transition from an acceleration to deceleration period also provides an explanation for the results of Costoya [60]. Since smaller particles have a higher surface-to-volume ratio, alites with smaller particle sizes will react to a higher degree during the main hydration period.

The seeding effect of the very fine (nano-)ettringite can also explain the results of experiments adding gypsum to alite or C_3S [26]. With alite and gypsum, a small ettringite formation will follow depending on the Al content in alite, which will not happen in the case of C_3S.

For the reaccelerating silicate reaction, this means that the reaction rate will increase again and additional C-S-H surface area can be produced as long as the alite surface area is high enough to release sufficient ions into the solution. If the alite surface area cannot supply

enough material to reaccelerate the hydration rate (as in the SynCem with 0.8 wt.% SO_3, Fig. 4), then the silicate reaction will continuously decrease after the interference by the aluminate reaction.

7.7.5.3.4. An additional peak of aluminate reaction vs. reaccelerated silicate reaction

Quennoz & Scrivener [26] described a third peak corresponding to an aluminate reaction, perhaps caused by a secondary growth of AFm phases after space filling. They did not find any dissolution or precipitation of products but only a sensitivity of this peak to the w/s ratio (Fig. 11 in [26]). They found that the second aluminate reaction peak (corresponding to the dissolution of C_3A and the change in reaction product from ettringite to AFm phases) was higher with an increasing w/s ratio while the third peak became very weak. In light of the interaction between the silicate and aluminate reaction shown in this study, another interesting effect is shown in Fig. 11 in [26]. The silicate reaction in the model cement [26] was less intense with higher w/s ratios. Before the final deceleration of the silicate reaction to the ongoing slow reaction regime, the aluminate reaction with AFm phases as reaction products proceeds very intensely. It is therefore plausible that this rapid AFm precipitation would be able to interfere with the silicate reaction, which would reaccelerate after the end of the second aluminate peak. It has been demonstrated before that the hydration degree of alite is not really affected by the w/s ratio [42, 68]. The SynCem pastes in the present study reach the same degree of hydration after 48 h (Fig. 5) - even for sightly different sulfate contents, using the same alite with the same PSD. This can be observed, although the silicate reaction reaccelerates to completely different hydration times and therefore to different degrees of hydration. Taking this into account, it is plausible that the third peak observed by [26] represents the residual silicate reaction that reaccelerates after the end of the aluminate reaction rather than another aluminate reaction peak.

7.7.6. Conclusions

The aluminate reaction in a cement paste can significantly interfere with the silicate reaction when the sulfate content of a cement paste is correspondingly low. After the C_3A surfaces are released from sulfate, blocking the C_3A, the silicate reaction decelerates and reaccelerates afterwards due to the reaccelerated aluminate reaction. In spite of different hydration times at the start of the interference of the aluminate reaction, the degree of hydration is comparable for all SynCem pastes studied after 48 h. Although the same reaction degree is achieved, it is clear that from a technical point of view, the silicate reaction and thus the development of strength will be significantly different within the 48 h.

The aluminate reaction inside the SynCem paste was found to begin with the short initial dissolution of C_3A, total bassanite, and a small amount of anhydrite. Afterwards, ettringite precipitation and anhydrite dissolution continuously proceeded throughout the different stages of the silicate reaction. The renewed dissolution of C_3A was found to take place significantly later than the disappearance of crystalline sulfate carriers, which can be explained by the adsorption of sulfate on C_3A and C-S-H surfaces, which is only slowly removed again. In our study, the renewed C_3A dissolution first led to the simultaneous precipitation of ettringite and AFm phases until obviously no sulfate is left in solution and ettringite partly dissolves to

form AFm phases. After the deceleration, this reaction continued on low levels during the further hydration. In this way, an aluminate reaction could be detected during the whole hydration reaction. The probable existence of an XRD amorphous Al-reservoir in paste [12] was addressed.

The experimental data of the SynCem pastes as well as of alite pastes before [6, 18] showed that C-S-H precipitates as colloidal material with very small crystallite sizes. The metastable kind of C-S-H during the early hydration is C-S-H_{lro}. This C-S-H_{lro} starts to precipitate as soon as the phase content of alite decreases linearly with time. Before this point in time, XRD amorphous C-S-H precipitates, which probably evolves from first containing only monomeric silicate tetrahedra to containing dimeric ones after the end of the induction period. After C-S-H_{lro} is present in the system, the further reaction product is C-S-H_{lro} and the prior XRD amorphous C-S-H seems to completely evolve to C-S-H_{lro}.

The mechanisms of the Al inhibition of the silicate reaction, both for the C-S-H precipitation and for the alite dissolution proposed in the literature, are found to be unlikely to be able to account for the experimental results observed in this study.

It is suggested that the aluminate reaction is able to interfere with the silicate reaction by reducing the C-S-H_{lro} surface area available for the precipitation of new C-S-H_{lro} due to the precipitation of AFm phases that coagulate with C-S-H as illustrated in Fig. 15. This can explain the decrease in the silicate reaction rate when the aluminate reaction interferes with it. Because the aluminate reaction was still proceeding on low levels, it can also explain the less steep reacceleration of the silicate reaction after the renewed aluminate reaction took place.

The final deceleration of the silicate reaction results from the reduction of accessible and available alite surface area during the course of hydration, which at some point in time is not able to satisfy the supply of ions demanded by the acceleration of the reaction due to increasing C-S-H surface area.

The higher reaction degree of alite in SynCem paste in comparison with pure alite paste is suggested to be caused by the acceleration of alite dissolution at the very start of hydration due to a seeding effect of initially precipitated, very fine (nano-)ettringite. As a result, a greater number of etch pits could be opened, which increases the available alite surface for hydration reaction. Since the transition to the deceleration period seems to be connected to the available alite surface, the deceleration shifted to later times. In addition, the seeding effect of the very fine ettringite can explain the enhanced reaction rates when comparing pure alite hydration and the hydration of alite in the presence of an aluminate reaction. Due to the larger available surface on which to precipitate C-S-H, more C-S-H reactive surface area is available and thus the reaction proceeds at higher rates.

This suggests that in an OPC system, the interaction of the aluminate and the silicate reaction at the very beginning of the hydration provides an intrinsic seeding for C-S-H precipitation.

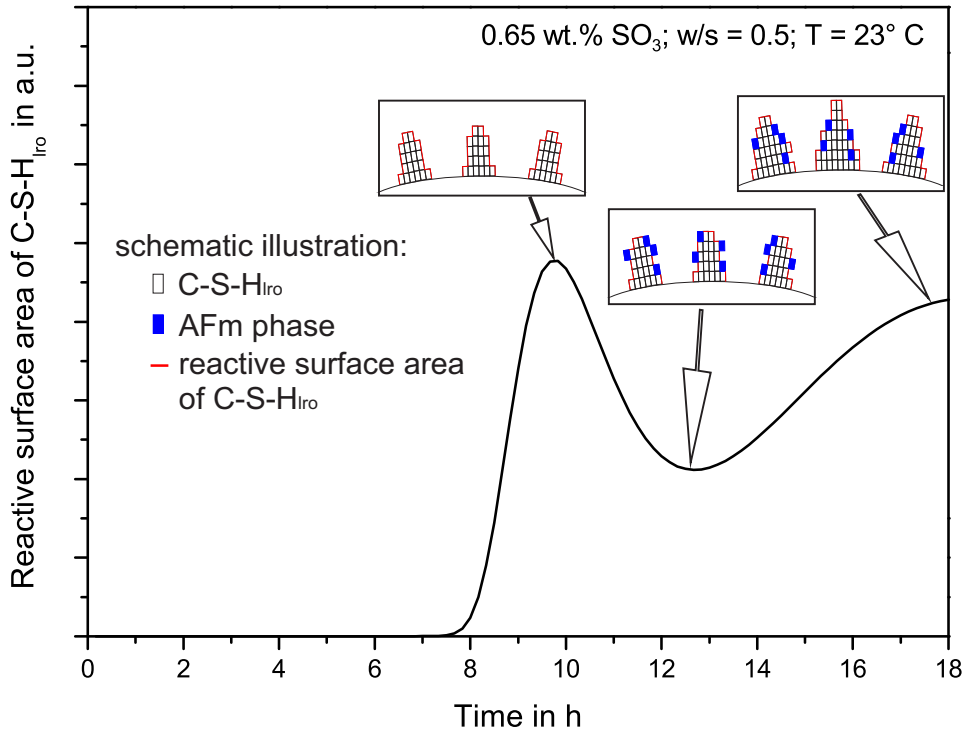

Fig. 15: Development of the reactive surface area of C-S-H_{lro} under the simplification of a constant surface precipitation rate of C-S-H_{lro} in arbitrary units together with a schematic illustration. Due to the precipitation of AFm phases, the reactive surface area of C-S-H_{lro} decreases between about 9.5 and 12.5 h. Afterwards, the reactive surface area increases again and thereby accelerates the hydration rate.

7.7.7. Acknowledgement

The authors would like to thank Christian Abe for measuring the particle size distributions.

7.7.8. References

[1] W. Lerch, The influence of gypsum on the hydration and properties of Portland cement pastes, American Society for Testing Materials, Proceedings 46 (1946).

[2] J. W. Bullard, H. J. Jennings, R. A. Livingston, A. Nonat, G. W. Scherer, J. S. Schweitzer, K. L. Scrivener, J. J. Thomas, Mechanisms of cement hydration, Cement Concr. Res. 41 (2011) 1208-1223.

[3] D. Jansen, F. Goetz-Neunhoeffer, C. Stabler, J. Neubauer, A remastered external standard method applied to the quantification of early OPC hydration, Cem. Concr. Res. 41 (2011) 602–608.

[4] H. Minard, S. Garrault, L. Renaud, A. Nonat, Mechanisms and parameters controlling the tricalcium aluminate reactivity in the presence of gypsum, Cement Concr. Res. 37 (2007) 1418-1426.

[5] R. W. Brown, R. Franz, G. Frohnsdorff, H. F. W. Taylor, Analyses of the aqueous phase during early C3S hydration, Cement Concr. Res. 14 (1984) 257-262.

[6] S. T. Bergold, F. Goetz-Neunhoeffer, J. Neubauer, Mechanically activated alite: New insights into alite hydration, Cement Concr. Res. 76 (2015) 202-201.

[7] P. Juilland, E. Gallucci, R. Flatt, K. Scrivener, Dissolution theory applied to the induction period in alite hydration, Cement Concr. Res. 40 (2010) 831-844.

[8] L. Nicoleau, A. Nonat, D. Perry, The di- and tricalcium silicate dissolution, Cement Concr. Res. 47 (2013) 14-30.

[9] L. Nicoleau, E. Schreiner, A. Nonat, Ion-specific effects influencing the dissolution of tricalcium silicate, Cement Concr. Res. 59 (2014) 118-138.

[10] P. Juilland, E. Gallucci, Morpho-topological investigation of the mechanisms and kinetic regimes of alite hydration, Cement Concr. Res. 76 (2015) 180-191.

[11] P. Suraneni, R. J. Flatt, Use of micro-reactors to obtain new insights into the factors influencing tricalcium silicate dissolution, Cement Concr. Res. 78 Part B (2015) 208-215.

[12] C. Hesse, F. Goetz-Neunhoeffer, J. Neubauer, A new approach in quantitative in-situ XRD of cement pastes: Correlation of heat flow curves with early hydration reactions, Cement Concr. Res. 41 (2011) 123-128.

[13] K. L. Scrivener, P. Juilland, P. J. M. Monteiro, Advances in understanding hydration of Portland cement, Cement Concr. Res. 78 Part A (2015) 38-56.

[14] L. Nicoleau, M. A. Bertolim, Analytical model for the alite (C_3S) dissolution topography, J. Am. Ceram. Soc. doi:10.1111/jace.13647.

[15] J. W. Bullard, G. W. Scherer, J. J. Thomas, Time dependent driving forces and the kinetics of tricalicum silicate hydration, Cement Concr. Res. 76 (2014) 26-34.

[16] S. A. Rodger, G. W. Groves, N. J. Clayden, C. M. Dobson, Hydration of Tricalcium Silicate followed by ^{29}Si NMR with cross-polarization, J. Am. Ceram. Soc. 71 (1988) 91-96.

[17] F. Bellmann, D. Damidot, B. Möser, J. Skibsted, Improved evidence for the existence of an intermediate phase during hydration of tricalicum silicate, Cement Concr. Res. 40 (2010) 875-884.

[18] S.T. Bergold, F. Goetz-Neunhoeffer, J. Neubauer, Quantitative analysis of C–S–H in hydrating alite pastes by in-situ XRD, Cement Concr. Res. 53 (2013) 119–126.

[19] S. Garrault, A. Nonat, Hydrated layer formation on tricalcium and dicalicum silicate surfaces: Experimental study and numerical simulations, Langmuir 17 (2001) 8131-8138.

[20] S. Bishnoi, K. L. Scrivener, Studying nucleation and growth kinetics of alite hydration using μic, Cement Concr. Res. 39 (2009) 849-860.

[21] E. Masoero, J. J. Thomas, H. M. Jennings, A reaction zone hypothesis for the effects of particle size and water-to-cement ratio on the early hydration kinetics of C_3S, J. Am. Ceram. Soc. 97 (2014) 967-975.

[22] S. Garrault, L. Nicoleau, A. Nonat, Tricalcium silicate hydration modeling and numerical simulations, Proceeding of CONMOD 10 (2010) 91-94.

[23] L. Nicoleau, The C_3S dissolution, a determining kinetic factor during hydration? ICCC, Beijing 2015.

[24] L. Nicoleau, A. Nonat, A new view on the kinetics of tricalcium silicate hydration, submitted to Cement Concr. Res.

[25] A. Quennoz, K. L. Scrivener, Hydration of C_3A-gypsum systems, Cement Concr. Res. 42 (2012) 1032-1041.

[26] A. Quennoz, K. L. Scrivener, Interactions between alite and C_3A-gypsum hydrations in model cements, Cement Concr. Res. 44 (2013) 46-54.

[27] E. Gallucci, P. Mathur, K. Scrivener, Microstructural development of early age hydration shells around cement grains, Cement Concr. Res. 40 (2010) 4-13.

[28] C. Hesse, Der Reaktionsverlauf der frühen Hydratation von Portlandzement in Relation zur Temperatur, Doktorarbeit, Friedrich-Alexander-Universität Erlangen-Nürnberg, 2009

[29] B.H. O'Connor, M.D. Raven, Application of the Rietveld refinement procedure in assaying powdered mixtures, Powder Diffr. 3 (1) (1988) 2–6.

[30] A.G. De La Torre, S. Bruque, J. Campo, M.A.G. Aranda, The superstructure of C_3S from synchrotron and neutron powder diffraction and its role in quantitative phase analyses, Cem. Concr. Res. 32 (2002) 1347–1356.

[31] P. Mondal, J. W. Jeffery, The crystal structure of tricalcium aluminate, $Ca_3Al_2O_6$, Acta Cryst. B31 (1975) 689-697.

[32] C. Bezou, A. Nonat, J.-C. Mutin, A. Norlund Christensen, M.S. Lehmann, Investigation of the crystal structure of γ-$CaSO_4$, $CaSO_4$.0.5 H_2O, and $CaSO_4$.0.6 H_2O by powder diffraction methods, J. Solid State Chem. 117 (1) (1995) 165-176.

[33] A. Kirfel, G. Will Charge density in anhydrite, $CaSO_4$, from X-ray and neutron diffraction measurements, Acta. Cryst. B36 (1980) 2881-2890.

[34] F. Goetz-Neunhoeffer, J. Neubauer, Refined ettringite ($Ca_6Al_2(SO_4)_3(OH)_{12}.26H_2O$) structure for quantitative diffraction analysis, Powder Diffr. 21 (1) (2006) 4-11.

[35] W.R. Busing, H.A. Levy, Neutron diffraction study of calcium hydroxide, J. Chem. Phys. 26 (3) (1957) 563–568.

[36] Allmann, R., Refinement of the hybrid layer structure $[Ca_2Al(OH)_6]^+ \cdot [1/2SO_4 \cdot 3H_2O]^-$, Neues Jb. Mineral. Monat. (1977) 136-144.

[37] D. Jansen, F. Goetz-Neunhoeffer, B. Lothenbach, J. Neubauer, The early hydration of Ordinary Portland Cement (OPC): an approach comparing measured heat flow with calculated heat flow from QXRD, Cem. Concr. Res. 42 (2012) 134–138.

[38] D. Ectors, J. Neubauer, F. Goetz-Neunhoeffer, The hydration of synthetic brownmillerite in presence of low Ca-sulfate content and calcite monitored by quantitative in-situ-XRD and heat flow calorimetry, Cem. Concr. Res. 54 (2013) 61–68.

[39] M. Wojdyr, Fityk: a general-purpose peak fitting program, J. Appl. Crystallogr. 43 (2010) 1126–1128.

[40] T. Matschei, B. Lothenbach, F. P. Glasser, Thermodynamic properties of Portland cement hydrates in the system CaO-Al_2O_3-SiO_2-$CaSO_4$-$CaCO_3$-H_2O, Cement Concr. Res. 37 (2007) 1379-1410.

[41] K. Fuji, W. Kondo, Estimation of thermochemical data for calcium silicate hydrate (C-S-H), J. Am. Ceram. Soc. 66 (1983) C-220–C-221.

[42] D. Jansen, S. T. Bergold, F. Goetz-Neunhoeffer, J. Neubauer, The hydration of alite: a time resolved quantitative X-ray diffraction approach using G-factor method compared with heat release, J. Appl. Crystallogr. 44 (2011) 895-901.

[43] E. Pustovgar, J.-B. d'Espinose, M. Palacios, A. Andreev, R. Sangodkar, R., B. Chmelka, R. J. Flatt, Revealing the steps of tricalcium silicate hydration, Proceedings of the ICCC, 1130-FP-SN450, Beijing 2015.

[44] J. J. Thomas, A new approach modeling the nucleation and growth kinetics of tricalcium silicate hydration, J. Am. Ceram. Soc. 90 (2007) 3282-3288.

[45] L. Nicoleau, Accelerated growth of calcium silicate hydrates: Experiments and simulations, Cement Concr. Res. 41 (2011) 1139-1348.

[46] B. Lothenbach, A. Nonat, Calcium silicate hydrates: Solid and liquid phase composition, Cement Concr. Res. 78 Part A (2015) 57-70.

[47] L. Divet, R. Randriambololona, Delayed ettringite formation: Effect of temperature and basicity on the interaction of sulphate and C-S-H phase, Cement Concr. Res. 28 (1998) 357-363.

[48] Y. Fu, P. Xie, P, Gu, J. J. Beaudoin, Effect of temperature on sulphate adsorption/desorption by tricalcium silicate hydrates, Cement Concr. Res. 24 (1994) 1428-1432.

[49] B. Mota, T. Matschei, K. Scrivener, The influence of sodium salts and gypsum on alite hydration, Cement Concr. Res. 75 (2015) 53-65.

[50] H. Poellmann, H.-J. Kuzel, R. Wenda, Solid solution of ettringites. Part I: Incorporation of OH^- and CO_3^{2-} in $3CaO.Al_2O_3.3CaSO_4.32H_2O$, Cement Concr. Res. 20 (1990) 941-947.

[51] L. Nicoleau, A. Nonat, The solubility of C_3S and its related factors, ICCC, Beijing 2015. October 2015

[52] T. Matschei, M. Costoya, A contribution to an improved understanding of the hydration kinetics of OPC, Tagungsbericht ibausil, Weimar 2012, 1-0276 – 1-0285.

[53] F. Begarin, S. Garrault, A. Nonat, L. Nicoleau, Hydration of alite containing aluminum, Adv. Appl. Ceram. 110 (2011) 127-130.

[54] S. Garrault, A. Nonat, Y. Sallier, L. Nicoleau, On the origin of the dormant period of cement hydration, ICCC, Madrid 2011.

[55] M. D. Andersen, H. J. Jakobsen, J. Skibsted, A new aluminum-hydrate species in hydrated Portland cements characterized by ^{27}Al and ^{29}Si MAS NMR spectroscopy, Cement Concr. Res. 36 (2006) 3-17.

[56] P. W. Brown, C. L. Harner, E. J. Prosen, The effect of inorganic salts on tricalcium silicate hydration, Cement and Concr. Res. 16 (1985) 17-22.

[57] A. Zingg, F. Winnefeld, L. Holzer, J. Pakusch, S. Becker, L. Gauckler, Adsorption of polyelectrolytes and its influence on the rheology, zeta potential, and microstructure of various cement and hydrate phases, J. Colloid Interface Sci. 323 (2008) 301-302.

[58] J. Plank, C. Hirsch, Impact of zeta potential of early cement hydration phases on superplasticizer adsorption, Cement Concr. Res. 37 (2007) 537-542.

[59] L. Nicoleau, Personal Communication, Nov. 2015.

[60] M. M. Costoya Fernandez, Effect of particle size on the hydration kinetics and microstructural development of tricalicum silicate, PhD thesis, Ecole Polytechnique Federale De Lausanne, 2008.

[61] I. Odler, J. Skalny, Hydration of tricalcium silicate at elevated temperatures, J. Appl. Chem. Biotechnol. 23 (1973) 661-667.

[62] S.T. Bergold, D. Jansen, S. Dittrich, F. Goetz-Neunhoeffer, J. Neubauer, Development of C-S-H during the early hydration of alite with water at different temperatures: direct quantification by in-situ XRD, GDCh-Monographie 45 (Tagung Bauchemie, 2012), 91–96.

[63] J. J. Thomas, H. M. Jennings, J. J. Chen, Influence of nucleation seeding on the hydration mechanisms of tricalcium silicate and cement, J. Phys. Chem. C 113 (2009) 4327-4334.

[64] T. Sato, F. Diallo, Seeding effect of nano-$CaCO_3$ on the hydration of tricalicum silicate, Transport. Res. Rec. 2141 (2010) 61-67.

[65] B. Yeon Lee, K. E. Kurtis, Influence of TiO_2 nanoparticles on early C_3S hydration, J. Am. Ceram. Soc. 93 (2010) 3399-3405.

[66] A. Sobolkina, V. Mechtcherine, S. T. Bergold, J. Neubauer, C. Bellmann, V. Khavrusa, S. Oswald, A. Leonhardt, W. Reschetilowski, Effect of carbon-based materials on the early hydration of tricalcium silicate, J. Am. Ceram. Soc., accepted for publication, doi: 10.1111/jace.14187.

[67] J.J. Thomas, The instantaneous apparent activation energy of cement hydration measured using a novel calorimetry-based method, J. Am. Ceram. Soc. 95 (2012) 3291-3296.

[68] D. M. Kirby, J. J. Biernacki, The effect of water-to-cement ratio on the hydration kinetics of tricalcium silicates cements: Testing the two-step hydration hypothesis, Cement Concr. Res. 42 (2012) 1147-1156.

8. Appendix

A list of all publications prepared during the PhD time is given in chronological order.

2016:

Professional Journals:

- S.T. Bergold, F. Goetz-Neunhoeffer, and J. Neubauer, Mechanically activated alite: 2. Influence of the drying technique on reactivity and its indications for the kinetics of alite hydration, submitted to Cement Concr. Res. on 17th of February 2016.

- S.T. Bergold, F. Goetz-Neunhoeffer, J. Neubauer, Hydration at the edge: Changing the balance between silicate and aluminate reaction in a synthetic cement system, submitted to Cement Concr. Res. on 26th of January 2016.

- Sobolkina, V. Mechtcherine, S.T. Bergold, J. Neubauer, C. Bellmann, V. Khavrusa, S. Oswald, A. Leonhardt, W. Reschetilowski, Effect of carbon-based materials on the early hydration of tricalcium silicate, J. Am. Ceram. Soc., accepted for publication, doi: 10.1111/jace.14187.

2015:

Professional Journals:

- S.T. Bergold, F. Goetz-Neunhoeffer, J. Neubauer, Mechanically activated alite: New insights into alite hydration, Cement Concr. Res. 76 (2015) 202-201.

2014:

Abstract in Conference Proceedings:

- S.T. Bergold, F. Goetz-Neunhoeffer, J. Neubauer, The development of C-S-H during hydration of mechanically activated alite: New insights into alite hydration by fastening the cement hydration, GDCh Monographie 48 (Tagung Bauchemie 2014) 238.

2013:

Professional Journals:

- S.T. Bergold, F. Goetz-Neunhoeffer, J. Neubauer, Quantitative analysis of C–S–H in hydrating alite pastes by in-situ XRD, Cement Concr. Res. 53 (2013) 119–126.

2012:

Conference Proceedings:

- S.T. Bergold, D. Jansen, S. Dittrich, F. Goetz-Neunhoeffer, J. Neubauer, Development of C-S-H during the early hydration of alite with water at different temperatures: direct quantification by in-situ XRD, GDCh-Monographie 45 (Tagung Bauchemie, 2012) 91–96.

- S.T. Bergold, F. Goetz-Neunhoeffer, J. Neubauer, In-situ XRD phase analysis of the early hydration of alite: time resolved quantification of the poorly crystalline C-S-H gel, Tagungsbericht ibausil, Weimar (2012) 1-0261 - 1-0267.

2011:

Professional Journals:

- D. Jansen, S.T. Bergold, F. Goetz-Neunhoeffer, J. Neubauer, The hydration of alite: a time resolved quantitative X-ray diffraction approach using G-factor method compared with heat release, J. Appl. Crystallogr. 44 (5) (2011) 895-901.

Conference Proceedings:

- S.T. Bergold, D. Jansen, F. Goetz-Neunhoeffer, J. Neubauer, Vergleich von Wärmeflusskalorimetrie und quantitativer in-situ XRD nach der G-Faktor Methode am Beispiel der Hydratation von Alit, GDCh-Monographie 44 (Tagung Bauchemie 2011) 165-170.

- S.T. Bergold, M. Göbbels, Combined study of phase relations by X-ray diffractometry / Rietveld & EPMA in the system MnO_x-Al_2O_3-SiO_2-MgO, Z. Kristallogr., Proceedings 1 (2011) 449-454.

Abstract in Conference Proceedings:

- S.T. Bergold, D. Jansen, F. Goetz-Neunhoeffer, J. Neubauer, Time resolved in-situ XRD analysis of the evolution of C-S-H gel during the early hydration of alite with water, Conference Proceedings DMG/DKG Tagung, Salzburg, 2011.